Doctoral Thesis

博士論文

Carbonization of Non-recyclable Poly(Ethylene) Terephthalate for the Production of Carbon-based Material – A Sustainable Approach for the Realization of Domestic PET Recycling

（リサイクル不能廃ポリエチレンテレフタレートの炭化による炭素材料の生産 – 持続可能な国内循環型 PET リサイクルの実現へ）

ジェニファー　チャー　ウィー　ファン

Carbonization of Non-recyclable Poly(Ethylene) Terephthalate for the Production of Carbon-based Material – A Sustainable Approach for the Realization of Domestic PET Recycling

（リサイクル不能廃ポリエチレンテレフタレートの炭化による
炭素材料の生産
– 持続可能な国内循環型 PET リサイクルの実現へ）

By
Jennifer Chia Wee Fern

A dissertation submitted to
The Graduate School of Frontier Sciences, The University of Tokyo
in partial fulfillment of the requirements for the degree of Doctor of Philosophy

Dissertation Examination Committee:
Associate Professor Teppei Nunoura
Professor Yoshito Oshima
Professor Shigeru Tabeta
Lecturer Makoto Akizuki
Lecturer Jun Nakatani

Department of Environment Systems
The Graduate School of Frontier Sciences
The University of Tokyo, Japan

2021 January

Abstract

The global waste PET treatment has been highly dependent on exporting of waste PET to recycling sites situated in developing countries, which had caused dire environmental problems including terrestrial and marine pollution. The reason for this dependency is due to the lack of domestic recycling facilities in the exporting countries as a result of expensive and inconvenient treatment of non-recyclable PET. This study identified the issues of current waste PET treatments and initiated carbonization as an alternative treatment method. The main objectives of this study is to provide a new method for the effective utilization of non-recyclable PET through the "waste-treats-waste" approach by (i) studying the fundamental experimental investigation and the mechanism of char formation of carbonization of PET, (ii) studying the applicability of the process on non-recyclable PET in the state closest to the "real-world", and (iii) studying the gas adsorption ability of activated char obtained from PET carbonization.

Carbonization was chosen as the method for treatment of non-recyclable PET due to the valorization of waste PET and its potential of producing valuable carbon-based materials for various applications. The carbonization process of PET was studied comprehensively by conducting experimental studies in a laboratory scale batch reactor under varying conditions and conducting thorough analysis on the char, wax and gaseous product obtained from each operating parameter in variance. Findings showed that the physical properties of feedstock did not affect the product composition and char characteristics due to the singularity of the polymer in feedstock, which proves the advantages of carbonization of PET as a treatment method for feedstock with physical irregularity. Complete carbonization of PET was obtained at 400-480°C to produce char with high carbon content. Based on the experimental results, the phase behavior of PET carbonization and the mechanism of char formation were clarified to reveal the decomposition of PET in which the release of CO due to decarbonylation leads to the formation of char whereas the release of CO_2 due to decarboxylation leads to the formation of aromatic compounds in wax.

The applicability of carbonization on feedstocks in the state closest to the "real-world" was studied, in which UV degraded PET, colored PET and multilayer PET were chosen

as the study target due to the inapplicability of current recycling technologies to treat these materials. UV degraded PET was prepared based on the accelerated weathering test method and carbonization experiments were conducted in constant operating parameters. Results showed increasing fixed-carbon yield when PET was exposed to UV degradation. Carbonization of the colored PET showed slight decrease in fixed-carbon yield compared to clear PET due to the presence of colorant additives whereas carbonization of multilayer PET showed no apparent change in char yield and fixed-carbon yield in char. The findings indicated the potential benefits and applicability of carbonization on non-recyclable PET.

In order to evaluate the performance of non-recyclable PET through the "waste-treats-waste" approach, char obtained from PET carbonization was activated using the conventional physical activation method to determine its CO_2 adsorption ability. Findings showed that the maximum CO_2 uptake in equilibrium and CO_2 separation ability from stream of the activated char was comparable to commercial adsorbents and that temperature change had little to no effects on the adsorption of CO_2 on the adsorbent. All experimental findings were summarized, and assessment based on the energy consumption and CO_2 emission were conducted in order to determine the feasibility of PET carbonization in the realization of domestic circulation of waste PET. Results concluded that replacement of incineration with carbonization resulted in drastic cut in annual CO_2 emission without causing a drastic decrease in economic value, which further affirms the advantage of carbonization in the treatment of waste PET.

This study was able to effectively treat non-recyclable PET by overcoming the issues of current treatments through carbonization to produce valuable carbon material, in addition to understanding the mechanism of char formation and evaluate the applicability of carbonized product through the "waste-treats-waste" approach. The outcomes of this study will be highly beneficial for the development of new materials from waste to encourage the improvement of the material value of other plastic wastes as a solution for the global plastic problems.

Acknowledgement

First and foremost, I would like to express my deepest gratitude to my supervisor, Associate Professor Teppei Nunoura for giving me the opportunity to work under him and for all the guidance, encouragement and patience throughout this research. His drive and passion for science have motivated me throughout the three years of my doctorate research. Thank you for teaching me the importance of pushing beyond my limits and believing in my abilities.

I would like to express my sincere gratitude to the thesis committee members, Professor Yoshito Oshima, Professor Shigeru Tabeta, Lecturer Makoto Akizuki and Lecturer Jun Nakatani for taking the time and accepting the offer as my thesis committee members. I am very grateful for all the critical comments, insightful opinions, and fruitful discussions during and after the dissertation defense.

I would also like to extend great appreciation to Assistant Professor Osamu Sawai for not only providing the guidance and assistance in my research, but also sharing his wide knowledge and experience in the scientific community. Thank you for teaching me the importance of critical thinking and effective communication in research life.

I would also like to take the opportunity to acknowledge Associate Professor Junichiro Otomo from the University of Tokyo, Department of Environment Systems for the permission of usage and technical assistance in BET/BJH analyzation; Ph.D. Haru Sakashita and Ph.D. Yoshihisa Asano from the University of Tokyo, Department of Applied Chemistry for their technical supports in CHN/O/S analyzation and FT/IR analyzation; Assistant Professor Takeshi Yajima and Ph.D. Daisuke Hamane from the University of Tokyo, Institute for Solid State Physics for their technical supports in XRD analyzation and SEM/EDX analyzation; Associate Professor Mitsunori Iwataki and Ms. Lum Wai Mun from the University of Tokyo, Department of Aquatic Bioscience for the permission of usage and their technical assistance in microscopic analysis; Professor Tadahisa Iwata and Mr. Yusuke Matsumoto from the University of Tokyo, Department of Biomaterials Sciences for the permission of usage and their technical supports in the tensile test.

I am forever indebted to Honjo International Scholarship Foundation, HISF, founded by Mr. Masanori Honjo and current president, Mr. Hachiro Honjo for providing the three year fully funded financial support, which has been a great honor to be a HISF scholar. The HISF has created an excellent and supportive community. The HISF staffs, Mr. Koichi Matsumoto, Ms. Itsuko Kawashima and Mr. Rajeeb Shrestha have provided me much with emotional support and great advice during this journey.

I would like to express my appreciation to Professor Kenichi Tonokura, Professor Tomochika Tokunaga, Associate Professor Junichiro Otomo, Professor Takeshi Iimoto, Associate Professor Tomohiko Ihara and all faculty members of the University of Tokyo, Graduate School of Frontier Sciences, Department of Environment Systems for their continual guidance and support in this program. Their expertise and advice in various fields of studies have given me a wide insight on the significance of my research. Special thanks to the department secretory, Ms. Miho Miyazaki and laboratory secretory, Ms. Sawako Sato for their assistance and advice throughout the years.

A great appreciation to my seniors, Ph.D. Disni Sanjeewani Gamlath Gamaralalage, Ph.D. Liu Jiaqi and Ph.D. Sakambari Padhi for not only being the best seniors I have ever met, but also the friendships, advice and encouragements throughout the years. Your presence has been a great support for me. I would also like to thank my fellow friends and doctors-to-be: Masudur Rahman, Vazquez Santiago Jairo, Ortiz Corrales Julian Andres, Igarashi Yu, Norazira Abdu Rahman, Xuan Truong Trinh, Diane Valenzuela Gubatanga and Lum Wai Mun. Your friendships have given me motivation and morale support throughout this journey.

Finally, I would like to express my deepest and heartiest thanks to my parents, Mr. Chia Ju Eng and Mdm. Ong Bao Jen, my brother and his wife, Mr. Andrew Chia Chun Guan and Dr. Chai Soo Mun, my best friend and sister, Ms. Yvonne Chia Wee Yee, my beautiful niece, Kelsey Chia Yue Sze, and my husband, Mr. Keita Yamasaki for the endless encouragement, love and care. You guys are the sole reason for my existence.

Table of contents

Abstract i

Acknowledgement iii

List of Figures xi

List of Tables xx

Nomenclature and Units xxiv

Abbreviations xxviii

Chapter 1: Introduction

1.1 Background and essentials of the research 1

1.2 Objectives of this study 2

1.3 Structure of the dissertation 4

Chapter 2: The challenges for domestic circulation of PET bottle recycling

2.1 Introduction 9

2.2 Plastic waste generation and environmental impacts 9

2.2.1 Global plastic generation 9

2.2.2 Types of plastics and their uses 10

2.2.3 Management of plastic wastes 12

2.2.4 Terrestrial and marine pollution due to plastic wastes 14

2.3 PET bottle recycling and the current issues 16

2.3.1 Conventional PET bottle recycling 16

2.3.2 Global dependency of China's PET bottle recycling factories 18

2.3.3 Global response to China's ban on plastic waste imports 18

2.3.4 Domestic circulation of PET recycling in Japan 21

2.3.5 Challenges and improvements 22

2.4 Carbonization of PET: Challenges and limitations of current technologies 23

2.4.1 Tertiary recycling of PET 23

2.4.2 Carbonization of PET 24

2.4.3 Mechanism of PET carbonization 29

2.5 Waste PET-derived activated carbon and its uses 31

2.5.1 Activation of carbon 31

2.5.2 Utilization of waste PET-derived activated carbon 31
2.5.3 Carbon capture through waste PET-derived activated carbon 33
2.5.4 Domestic PET recycling with carbon capture 33
2.6 Chapter summary 36
Chapter 3: Experimental methodology
3.1 Materials and reagents 37
3.1.1 Types of feedstock 37
3.1.2 Preparation of UV degraded PET 38
3.1.3 Reagents 40
3.2 Carbonization experiment 41
3.2.1 Reactor set-up 41
3.2.2 Experimental procedure 42
3.3 Activation experiment 43
3.3.1 Reactor set-up 43
3.3.2 Experimental procedure 43
3.4 Analysis of feedstock and product 44
3.4.1 Sample analysis 44
3.4.2 Solid product analysis 44
3.4.3 Wax product analysis 47
3.4.4 Gas product analysis 47
3.5 Gas adsorption experiment 49
3.5.1 Adsorption isotherm measurement 49
3.5.2 Breakthrough experiments 49
Chapter 4: Effect of parameters on carbonization of PET
4.1 Introduction 51
4.2 Effect of feedstock variance on carbonization of PET 52
4.2.1 Experimental set-up and feedstock preparation 52
4.2.2 Results and discussion 53
4.2.3 Conclusions: Effect of feedstock variance on carbonization of PET 56
4.3 Effect of operating conditions on carbonization of PET 57
4.3.1 Experimental set-up 57

4.3.2 Results and discussion 58
4.3.3 Conclusions: Effect of operating conditions on carbonization of PET 76
4.4 Effect of steam as medium on carbonization of PET 77
4.4.1 Experimental set-up and feedstock preparation 77
4.4.2 Results and discussion 78
4.4.3 Conclusions: Effect of steam as medium on carbonization of PET 88
4.5 Chapter summary 89
Chapter 5: Mechanism of char formation based on carbonized product
5.1 Introduction 91
5.2 Theory of thermal degradation of PET from past researchers 92
5.3 Phase behavior based on the van Krevelen diagram 94
5.3.1 Background 94
5.3.2 Results and discussion 94
5.4 Degree of cross-linking, $X_{cross\text{-}link}$, indicator for char formation 96
5.4.1 Theory of cross-linking 96
5.4.2 Derivation and assumptions of equations 96
5.4.3 Distribution of $X_{cross\text{-}link}$ in char and wax 100
5.5 Chapter summary 103
Chapter 6: Effect of contaminants in non-recyclable PET on carbonized product
6.1 Introduction 105
6.2 Effect of UV degraded PET on carbonized product 106
6.2.1 Background of UV degradation on PET 106
6.2.2 Mechanism of UV degradation of PET 106
6.2.3 Preparation of sample 108
6.2.4 Characteristics of UV degraded PET 108
6.2.5 Carbonization of UV degraded PET 114
6.2.6 Conclusions: Effect of UV degraded PET on carbonized product 122
6.3 Effects of colored and multilayer PET on carbonized product 123

6.3.1 Background of colored and multilayer PET 123
6.3.2 Preparation and characterization of feedstock 125
6.3.3 Carbonization of colored PET 127
6.3.4 Carbonization of multilayer PET 130
6.3.5 Effect of cobalt oxide on carbonized product 137
6.3.6 Conclusions: Effects of colored and multilayer PET on carbonized product 138
6.4 Chapter summary 140
Chapter 7: Gas adsorption study of activated char
7.1 Introduction 141
7.2 Activation of char and surface properties 142
7.2.1 Experimental procedures and materials 142
7.2.2 Results and discussion 142
7.2.3 Conclusions: Activation of char and surface properties 144
7.3 Static adsorption study 146
7.3.1 Experimental set-up 146
7.3.2 Equations and expressions 146
7.3.3 Results and discussion 148
7.3.4 Conclusions: Static adsorption study 164
7.4 Dynamic adsorption study 165
7.4.1 Background of breakthrough curve 165
7.4.2 Experimental set-up 166
7.4.3 Results and discussion 166
7.4.4 Conclusions: Dynamic adsorption study 170
7.5 Model of breakthrough curve 171
7.5.1 Background of modelling 171
7.5.2 Model for breakthrough curves 171
7.5.3 Results and discussion 174
7.5.4 Conclusions: Model of breakthrough curve 178
7.6 Chapter summary 179
Chapter 8: Assessment of carbon emission and cost estimation
8.1 Introduction 181

8.2 Carbon emission and cost estimation of various operations 182
8.2.1 Material flow of PET bottles in Japan 182
8.2.2 Collection and transport operations 182
8.2.3 CO_2 emission and cost estimation from incineration with and without energy recovery 184
8.2.4 CO_2 emission and cost estimation from conventional recycling 185
8.2.5 CO_2 emission and cost estimation from carbonization reactor 186
8.2.6 CO_2 emission and cost estimation from carbon capture 192
8.2.7 Landfill 194
8.2.8 Conclusions: CO_2 emission and cost estimation of various operations 194
8.3 Life cycle assessment 195
8.3.1 Introduction 195
8.3.2 Evaluated scenarios 195
8.3.3 Results of LCA assessment 198
8.3.4 Conclusions: Life cycle assessment 208
8.4 Additional assessment based on relating variables 209
8.4.1 Background 209
8.4.2 Assessment based on varying parameters 209
8.4.3 Conclusions: Additional assessment based on relating variables 216
8.5 Chapter summary 217
Chapter 9: Conclusions and recommendations
9.1 Conclusions 219
9.2 Recommendations for future work 223
References 225
Appendix A. – Rank of bale 260
Appendix B. – Derivation of equation for average intensity of exposure 262
Appendix C. – Decomposition profile of PET 265
Appendix D. – Temperature distribution of reactor in equilibrium 266
Appendix E – Reproducibility of carbonization experiment 268
Appendix F. – Statistical analysis 270

Appendix G. – Verification of oxygen barrier layer 275
Appendix H. – Initial and maintenance cost of operations 279
Appendix I. – List of inventories 281
Appendix J. – Safety note 285

List of Figures

Figure 1-1:	Structure of the dissertation.	7
Figure 2-1:	Global plastic production in 2018.	9
Figure 2-2:	Examples of plastic waste and their consequent lifetime to naturally decompose.	11
Figure 2-3:	Waste management hierarchy.	12
Figure 2-4:	Various approaches for recycling of plastic waste.	13
Figure 2-5:	Global ocean clean-up result reported by Ocean Conservancy and estimated weight distribution of the top 10 reported ocean plastic wastes.	15
Figure 2-6:	Main processes in a conventional PET bottle recycling.	17
Figure 2-7:	Amount of export PET flakes from Japan categorized by different countries.	20
Figure 2-8:	Estimated recycling flow of PET bottles from collection to regeneration in Japan in 2018.	21
Figure 2-9:	Molecular mass growth processes to PAH through H_2 abstraction-C_2H_2 addition.	29
Figure 2-10:	Schematic illustration of turbostratic and graphitic carbon structures.	30
Figure 2-11:	Schematic of the domestic PET recycling with carbon reduction and integrated biomass power plant.	34
Figure 3-1:	Types of commercial bottles used.	38
Figure 3-2:	Types of feedstock treatment.	38
Figure 3-3:	Schematic diagram of accelerated weathering test.	38
Figure 3-4:	Experimental set-up of carbonization system.	41
Figure 3-5:	Photo of carbonization system.	42
Figure 3-6:	Experimental set-up of activation operation.	43
Figure 3-7:	Experimental set-up for gas adsorption experiments.	50
Figure 4-1:	Study scheme of Chapter 4 to investigate the effects of operating parameters.	51

Figure 4-2:	Photo of char and wax obtained from PET carbonization at 400-480°C and 120 min.	53
Figure 4-3:	Composition of product after carbonization of PET with variance in bottle thickness, bottle type/shape and feedstock treatment.	55
Figure 4-4:	Proximate value of char obtained from PET carbonization with variance in bottle thickness, bottle type/shape and feedstock treatment.	55
Figure 4-5:	Composition of char, wax and gas for operations under different temperatures at constant holding time of 120 min.	58
Figure 4-6:	Photo of char obtained from PET carbonization at 320-400°C and 400-480°C at constant holding time 120 min.	59
Figure 4-7:	Proximate value of char obtained from PET carbonization at 320-400°C, 360-440°C and 400-480°C at constant holding time 120 min.	61
Figure 4-8:	Overlay of FT/IR spectra of char obtained from different operating temperatures.	63
Figure 4-9:	GC/MS spectra of wax product obtained from different operating temperatures at 320-400°C, 360-440°C and 400-480°C with constant holding time.	65
Figure 4-10:	Gas composition of gaseous products obtained from PET carbonization at 320-400°C, 360-440°C and 400-480°C at constant holding time 120 min	67
Figure 4-11:	Hydrocarbon composition of gaseous products obtained from PET carbonization at 320-400°C, 360-440°C and 400-480°C at constant holding time.	67
Figure 4-12:	Composition of char, wax and gas for operations under different holding times, at constant temperatures of 360-440°C and 400-480°C.	69

Figure 4-13:	Proximate value of char obtained from operations under different holding times, at constant temperatures of 360-440°C and 400-480°C.	69
Figure 4-14:	Overlay of FT/IR spectra of char obtained from different holding times at 60 min, 120 min and 240 min with constant operating temperature at 400-480°C.	71
Figure 4-15:	GC/MS spectra of wax product obtained from different holding times, at constant temperature of 400-480°C.	73
Figure 4-16:	Gas composition of gaseous products obtained from PET carbonization under different holding times, at constant temperatures of 360-440°C and 400-480°C.	75
Figure 4-17:	Hydrocarbon composition of gaseous products obtained from PET carbonization under different holding time, at constant temperature of 360-440°C and 400-480°C	75
Figure 4-18:	Schematic layout of autoclave batch reactor for carbonization under steam medium.	77
Figure 4-19:	Composition of char, wax and gas for operations under different water to feedstock ratios at constant holding time of 120 min.	79
Figure 4-20:	SEM images of char surface obtained from carbonization of PET at nitrogen and steam medium.	79
Figure 4-21:	Proximate value of char obtained from PET carbonization under different water to feedstock ratios at constant holding time of 120 min.	81
Figure 4-22:	FT/IR spectra of char obtained from PET carbonization under water to feedstock ratios 0.25:1 and 0.5:1.	81
Figure 4-23:	Composition of wax obtained using HPLC analysis from carbonization of PET under different water to feedstock ratios.	83
Figure 4-24:	Composition of gaseous product obtained from PET carbonization under different water to feedstock ratios.	83

Figure 4-25:	Composition of char, wax and gas for operations under different holding times, under constant water to feedstock ratio and temperature.	85
Figure 4-26:	Proximate value of char and the fixed-carbon yield for operations under different holding times, constant water to feedstock ratio and temperature.	85
Figure 4-27:	FT/IR spectra of char obtained from PET carbonization under holding times 120 min and 240 min.	87
Figure 4-28:	Composition of wax obtained using HPLC analysis from carbonization of PET under steam condition at different holding times.	87
Figure 4-29:	Composition of gaseous product obtained from PET carbonization under steam condition at different holding times.	87
Figure 5-1:	Study scheme of Chapter 5 to investigate the mechanism of char formation based on carbonized product.	91
Figure 5-2:	PET and its most likely thermal cleavage mechanisms to various products.	92
Figure 5-3:	Proposed degradation pathways in the pyrolysis process of model compound PET.	93
Figure 5-4:	van Krevelen diagram of wood-derived char.	94
Figure 5-5:	Relationship between atomic H/C and atomic O/C of char and wax.	95
Figure 5-6:	Simplified degradation pathways in the pyrolysis process of model compound PET.	97
Figure 5-7:	Relationship between CO_2 and CO obtained from PET carbonization.	98
Figure 5-8:	Relationship between $X_{cross\text{-}link}$ and temperature change of PET carbonization under different holding time.	99
Figure 5-9:	Relationship between $X_{cross\text{-}link}$ and the dimensionless ratio of carbonyl groups for char obtained from PET carbonization.	100

Figure 5-10: Phase transition of PET carbonization. 100
Figure 5-11: Relationship between $X_{cross\text{-}link(CO)}$ and X_c; and the relationship between $X_{cross\text{-}link(CO_2)}$ and $X_{w.}$ 102
Figure 6-1: Study scheme of Chapter 6 to investigate the effects of contaminants in PET on carbonized product. 105
Figure 6-2: Chemical reactions undergone by PET during UV exposure leading to carboxyl end-groups. 107
Figure 6-3: Magnified surface morphology of PET. 109
Figure 6-4: FT/IR spectra of raw PET, 0.2-year accelerated weathering and 8.6-year accelerated weathering. 109
Figure 6-5: Photo of strain test using EZ test and PET after strain test. 110
Figure 6-6: Magnified surface morphology of teared edge of PET from tensile test. 111
Figure 6-7: Formation of crack and craze during tensile stress. 111
Figure 6-8: Stress-strain curves for raw PET and PET exposed to 8.6-year accelerated weathering. 113
Figure 6-9: Relationship between the amount of UV degradation on the stress at break of PET. 113
Figure 6-10: Composition of product obtained from carbonization of PET exposed to different accelerated weathering tests. 115
Figure 6-11: Composition of gaseous products obtained from carbonization of PET exposed to different accelerated weathering tests. 117
Figure 6-12: Hydrocarbon composition of gaseous products obtained from carbonization of PET exposed to different accelerated weathering tests. 117
Figure 6-13: Relationship between CO_2 and CO obtained from carbonization of PET without exposure and PET with UV exposure. 119
Figure 6-14: Comparison of carbonization of PET without UV exposure and carbonization of PET with UV exposure using student's t-test. 121

Figure 6-15:	Chemical structure of phthalocyanine and anthraquinone.	123
Figure 6-16:	Separated layers of commercial PET bottle sample.	125
Figure 6-17:	FT/IR spectra of layers of commercial PET bottle samples.	127
Figure 6-18:	Comparison of product distribution and fixed-carbon yield obtained from carbonization of clear PET layer, outer PET and inner PET.	129
Figure 6-19:	Comparison of gas composition obtained from carbonization of clear PET layer, outer PET and inner PET.	129
Figure 6-20:	Product distribution obtained from carbonization of single PET layer and mixture of PET and OBL of different added mass percentage.	130
Figure 6-21:	FT/IR spectra of char obtained from carbonization of PET and mixture of PET and OBL of different mass percentage.	131
Figure 6-22:	XRD pattern of leftover ash.	132
Figure 6-23:	Graphical representation of the GC/MS analysis.	135
Figure 6-24:	Overall gas composition and hydrocarbon composition of gaseous product obtained from carbonization.	136
Figure 6-25:	Comparison of product distribution and gas composition obtained from carbonization of single PET layer, PET with 8 wt% OBL and PET with 1 wt% cobalt oxide.	138
Figure 7-1:	Study scheme of Chapter 7 to investigate the gas adsorption characteristics and gas adsorption capacity of activated char.	141
Figure 7-2:	Surface magnification of char and activated char, PET-AC.	143
Figure 7-3:	Adsorption isotherm and pore size distribution of PET-AC, AC-GH2x and zeolite 5A.	145
Figure 7-4:	IUPAC classification of hysteresis loop corresponding to pore shapes.	145
Figure 7-5:	Amount of CO_2 and N_2 adsorbed and Henry's plot during single gas component adsorption isotherm measurements at 20°C and 35°C.	149

Figure 7-6: Amount of CO_2 and N_2 adsorbed and selectivity of gas components during binary gas component adsorption isotherm measurements at 35°C, 20 CO_2-vol% (N_2 balance). 151

Figure 7-7: Amount of CO_2, CO, CH_4 and N_2 adsorbed and selectivity of the gas components during multiple gas component adsorption isotherm measurements at 35°C, 20 CO_2-vol%, 20 CO-vol%, 20 CH_4-vol% (N_2 balance). 153

Figure 7-8: Isosteres for adsorption of CO_2 on PET-AC, AC-GH2x and zeolite 5A. 155

Figure 7-9: Experimental and predicted adsorption isotherms based on the Langmuir isotherm model and Scatchard plots for PET-AC, AC-GH2x and zeolite 5A, respectively at 20°C and 35°C. 159

Figure 7-10: Adsorption mechanism of PET-AC proposed based on adsorption equilibrium. 163

Figure 7-11: A typical breakthrough curve of gas adsorbed onto adsorbent. 165

Figure 7-12: Breakthrough curves of binary gas components using PET-AC, AC-GH2x and zeolite 5A at 35°C, 20 CO_2-vol% (N_2 balance). 167

Figure 7-13: Breakthrough curves of multiple gas components using PET-AC, AC-GH2x and zeolite 5A at 35°C, 20 CO_2-vol%, 20 CO-vol%, 20 CH_4-vol% (N_2 balance). 169

Figure 7-14: Schematic diagram of the fixed-bed adsorption used in this study. 171

Figure 7-15: Comparison of experimental results and mathematical model of breakthrough curves of PET-AC, AC-GH2x and zeolite 5A for binary gas component and multiple gas component at 35°C. 175

Figure 8-1:	Study scheme of Chapter 8 to investigate the feasibility of carbonization in the overall treatment of PET based on the assessment of carbon emission and cost estimation.	181
Figure 8-2:	Material flow of PET bottles from collection to recycling in Japan.	183
Figure 8-3:	Transportation of waste PET from collection sites to transport station before sent to recycling or incineration facilities.	182
Figure 8-4:	Heat balance diagram of reactor.	186
Figure 8-5:	A proposal for PET carbonization facility for mass treatment.	189
Figure 8-6:	Mass and energy balance of wax and gas from PET carbonization.	190
Figure 8-7:	Theoretical system boundaries for the case assessment of material recycling, carbonization, incineration and landfill based on the avoided burden approach.	196
Figure 8-8:	Simplified scenarios for incineration (with and without energy recovery), mechanical recycling, carbonization and landfill with their consecutive inventories.	197
Figure 8-9:	CO_2 emission of the evaluated scenarios based on the avoided burden approach LCI analysis.	199
Figure 8-10:	Net profit of the evaluated scenarios based on the avoided burden approach LCI analysis.	200
Figure 8-11:	Estimation of CO_2 emission and reduction from different cases.	201
Figure 8-12:	Comparison of CO_2 emitted and net profit of operation for Case 1 and Case 2, respectively.	204
Figure 8-13:	Annual CO_2 emission and annual profit of operation for Case 3.	207
Figure 8-14:	Annual CO_2 emission and annual profit of Case 2 in which carbonization of PET is conducted under varying temperatures.	211

Figure 8-15:	Annual CO_2 emission and annual profit of Case 2 in which carbonization of PET is conducted in the presence of cobalt oxide.	213
Figure 8-16:	Annual CO_2 emission and annual profit of Case 3 in which carbonization of PET is conducted under varying temperatures.	215
Figure A-1:	A segment from Classification Standard of PET bottle.	261
Figure A-2:	PET bottle bale characterized based on the Classification Standard.	261
Figure B-1:	Cross-section of PET bottle from source of UV.	262
Figure C-1:	Decomposition profile of PET.	265
Figure D-1:	Temperature distribution of reactor in equilibrium.	266
Figure D-2:	Cross-section of reactor	267
Figure E-1:	Composition of product and fixed-carbon yield of char after carbonization of PET from the same starting feedstock type and feedstock treatment.	268
Figure G-1:	FT/IR spectra of MXD6 nylon from Standard Test Piece and compared with middle layer.	277
Figure G-2:	FT/IR spectra of MXD6 from previous researches and compared with this study.	278

List of Tables

Table 2-1:	Estimated weight of targeted items.	16
Table 2-2:	Operating conditions and product composition of thermal degradation of PET from past researches.	28
Table 2-3:	Past researches on the uses of activated carbon derived from waste PET.	32
Table 3-1:	Label of feedstock used for each chapter.	37
Table 3-2:	Summary of accelerated weathering test expressed in total hours in UV exposure and total years in accelerated weathering.	40
Table 3-3:	Experimental parameters used for static adsorption experiments and dynamic adsorption experiments.	50
Table 4-1:	Parameters used in determining the effect of feedstock on carbonization.	52
Table 4-2:	Label of feedstock with variance in bottle thickness, bottle type/shape and feedstock treatment.	52
Table 4-3:	Elemental composition of char obtained from PET carbonization with variance in bottle thickness, bottle type/shape and feedstock treatment.	55
Table 4-4:	Parameters used in determining the effects of operating temperature and holding time on PET carbonization.	57
Table 4-5:	Elemental composition of char obtained from PET carbonization at 320-400°C, 360-440°C and 400-480°C at constant holding time 120 min.	61
Table 4-6:	A summary of the absorption bands and the corresponding vibrational modes from FT/IR spectrum of PET.	63
Table 4-7:	Elemental composition of wax residue obtained from PET carbonization at 320-400°C, 360-440°C and 400-480°C at constant holding time 120 min.	64

Table 4-8:	Ultimate value of char obtained from operations under different holding times, at constant temperatures of 360-440°C and 400-480°C.	71
Table 4-9:	Ultimate value of wax obtained from operations under different holding times, at constant temperatures of 360-440°C and 400-480°C.	72
Table 4-10:	Parameters used in determining the effects of reaction medium and holding time on PET carbonization.	77
Table 4-11:	Elemental composition of char obtained from PET carbonization under different water to feedstock ratios at constant holding time of 120 min.	81
Table 4-12:	Elemental composition of char obtained from PET carbonization different holding times, under constant water to feedstock ratio and temperature.	85
Table 6-1:	Results of one sample t-test for the fixed-carbon yield.	115
Table 6-2:	Results of one sample t-test for total ethane and ethylene produced.	118
Table 6-3:	Results of t-test for independent samples for Control and UV.	121
Table 6-4:	Major types of oxygen barrier used in multilayer PET bottles.	124
Table 6-5:	Elemental composition of separated layers of commercial PET bottle samples.	126
Table 6-6:	Characteristics of wax obtained from carbonization of clear PET layer, outer PET layer and inner PET layer.	129
Table 6-7:	Characteristics of char obtained from carbonization of PET and mixture of PET and OBL of different added mass percentage.	132
Table 6-8:	Characteristics of wax obtained from carbonization of PET and mixture of PET and OBL of different mass fractions.	133
Table 6-9:	GC/MS analysis results of the wax obtained from carbonization of single PET layer and PET with OBL of different added mass percentage.	134

Table 7-1:	Comparison of elemental composition of char obtained from PET carbonization and PET-AC obtained after activation of char.	143
Table 7-2:	Specific surface areas, total pore volumes and geometric mean radius of the adsorbents estimated from N_2 adsorption/desorption isotherm method.	145
Table 7-3:	Fitting parameters of Langmuir model for adsorption isotherm of pure CO_2.	160
Table 7-4:	Summary of breakthrough point, gas saturation point and amount of gas adsorbed.	167
Table 7-5:	Summary of breakthrough point, gas saturation point and amount of gas adsorbed.	169
Table 7-6:	Kinetic parameters of CO_2 on PET-AC, AC-GH2x, zeolite 5A obtained from the breakthrough curves.	177
Table 7-7:	Comparison of kinetic parameters of CO_2 on different adsorbents from different studies.	177
Table 8-1:	PET bottles collection rate, PET bottles recycling rate in domestic recycling factories, and PET bottles which are not domestically recycled.	183
Table 8-2:	List of inventories for conventional recycling.	185
Table 8-3:	Summary of empirical formulas and unit molecular weight.	187
Table 8-4:	Calculation of HHV of PET, char, wax and gas in unit kJ/mol.	187
Table 8-5:	Calculation for CO_2 emission from combustion of gas and wax.	191
Table 8-6:	Summary of CO_2 adsorption properties for Zeolite 13X and PET-derived activated carbon.	193
Table 8-7:	Total energy and CO_2 emission from combustion of gas and wax.	212
Table 8-8:	Demand and supply of PET-derived activated carbon for Case 3.	215

Table D-1:	List of equations fitted to the temperature distribution of reactor in equilibrium and calculated average temperatures of each temperature setting.	266
Table E-1:	Descriptive statistics of char yield and volatile matter of char for the same starting feedstocks.	269
Table F-1:	Descriptive statistics of char yield, volatile matter of char and carbon content of char for feedstocks with label A-E.	271
Table G-1:	Elemental composition of middle layer, sample from Standard Test Piece and the ideal elemental composition of MXD6 nylon based on the chemical composition	275
Table G-2:	Ideal CHN composition of MXD6, Nylon-6 and Nylon-66 based on their chemical compositions	276
Table H-1:	Summary of operation and maintenance costs for a conventional waste incineration facility.	279
Table H-2:	Summary of operation and maintenance costs for a conventional PET recycling facility.	279
Table H-3:	Summary of operation and maintenance costs for an assumed carbonization facility.	280
Table H-4:	Summary of operation and maintenance costs for an assumed PSA facility.	280
Table I-1:	Summary of inventories for CO_2 emission and cost estimation of various operations.	281

Nomenclature and Units

$\%Ash$	[%]	Ash content
A	[m^2]	Surface area of reactor jacket
A_b	[m^2]	Cross-sectional area of fixed-bed
a_v	[m^2/ m^3]	Surface area to volume ratio
b	[MPa^{-1}]	Langmuir isotherm equation parameter
b_i	[MPa^{-1}]	Binding energy of adsorbate to the adsorbent at different regions in the adsorption system
$\%C$	[%]	Carbon content
c	[mol/m^3]	Concentration of adsorbate in bulk fluid
c^*	[mol/m^3]	Concentration in equilibrium with average loading $\bar{q}$ in stream
c_e	[mol/m^3]	Amount of gas adsorbed at equilibrium
c_F	[mol/m^3]	Final concentration of adsorbate in bulk fluid
$C{=}O/C{=}O_0$	[-]	Dimensionless ratio of the amount of carbonyl groups in char
D_e	[m^2/s]	Effective diffusivity
d	[m]	Distance of the center of PET bottle from light source
d_w	[mm]	Wall thickness of PET bottle
ΔF	[kJ/mol]	Change of surface energy of adsorbent due to adsorption
$\%fC$	[%]	Fixed carbon content
$\%H$	[%]	Hydrogen content
HHV	[MJ/kg]	Higher heating value
ΔH^0	[kJ/mol]	Standard enthalpy
H^0	[kJ]	Total enthalpy of a closed adsorption system
h_a	[kJ/mol]	Molar enthalpy of adsorbed molecules
h_g	[kJ/mol]	Molar enthalpy of gas
I	[W/m^2]	Intensity of light source
K	[-]	Adsorption equilibrium constant

K_H	[-]	Henry coefficient
k	[s^{-1}]	Overall mass-transfer coefficient
k_c	[m/s]	External mass-transfer coefficient
ΔL	[m]	Change in length of adsorbent particle due to expansion or compression
L_0	[m]	Original length of adsorbent particle at ambient pressure and temperature
M_w	[g/mol]	Molecular weight
m	[kg]	Mass of adsorbent in the adsorbent tank
$\%N$	[%]	Nitrogen content
N	[-]	Number of domestic factories
n	[mol]	Amount of gas adsorbed in mol
n_i	[mol]	Amount of gas species, i adsorbed in mol
$\%O$	[%]	Oxygen content
P	[MPa]	Pressure
P_e	[MPa]	Pressure in equilibrium
q	[mol/kg]	Adsorbed amount
$\bar{q}$	[mol/m^3]	Adsorbed amount per adsorbent volume in stream
q^*	[mol/m^3]	Adsorbate loading in equilibrium with the solute concentration in stream
q^0	[kJ/mol]	Isosteric heat of adsorption
q_e	[mol/kg]	Equilibrium adsorption capacity
$q_{e,i}$	[mol/kg]	Equilibrium adsorption capacity of gas species, i
q_m	[mol/kg]	Maximum amount adsorbed
$q_{m,i}$	[mol/kg]	Maximum amount adsorbed of gas species, i
R	[m^3Pa/molK]	Gas constant
Re	[-]	Reynolds number
R_{CR}	[-]	Ratio of carbonization facility to recycling factory
R_{PR}	[-]	Ratio of PSA system to recycling factory
R_p	[m]	Adsorbent radius

r	[m]	Radius of PET bottle
ΔS^0	[kJ/molK]	Standard entropy
$S_{A/B}$	[-]	Adsorption selectivity
Sc_i	[-]	Schmidt number
Sh	[-]	Sherwood number
T	[°C] or [K]	Temperature
T_s	[°C]	Surface temperature of reactor jacket
t	[s]	Time
t_b	[min]	Breakthrough point
t_s	[min]	Saturation point
Δt	[s]	Differential time duration
u	[m/s]	Interstitial (inlet) velocity
$\%VM$	[%]	Volatile matter content
$X_{cross\text{-}link}$	[wt%]	Degree of cross-linking
$X_{cross\text{-}link}(CO)$	[wt%]	Degree of cross-linking in terms of CO
$X_{cross\text{-}link}(CO_2)$	[wt%]	Degree of cross-linking in terms of CO_2
X_c	[wt%]	Degree of decarbonylation
X_w	[wt%]	Degree of decarboxylation
x_A	[-]	Mole fraction of species A in the adsorbed phase
x_B	[-]	Mole fraction of species B in the adsorbed phase
y_A	[-]	Mole fraction of species A in the bulk phase
y_B	[-]	Mole fraction of species B in the bulk phase
y_{char}	[%]	Yield of char
y_{fC}	[%]	Fixed-carbon yield
y_{CO}	[wt%]	Yield of CO
y_{CO_2}	[wt%]	Yield of CO_2
y_{wax}	[%]	Yield of wax
z	[m]	Length of adsorption bed
Δz	[m]	Differential adsorption bed length

ε	[-]	Emissivity factor
ε_b	[-]	Bed porosity
ξ	[-]	Dimensionless distance coordinate
λ	[mol/kJ]	Constant with relation to the material properties of adsorbent
λ_m	[W/m^2]	Heat transfer coefficient of insulation jacket
σ	[W/m^{2}K^4]	Stefan-Boltzmann constant
τ	[-]	Dimensionless time coordinate
τ_b	[-]	Dimensionless CO_2 breakthrough time
τ_s	[-]	Dimensionless CO_2 saturation time

Abbreviation

PET-AC	Activated char from PET
ANOVA	Analysis of variance
BJH	Barret-Joyner-Halenda
BtoB	Bottle-to-Bottle
BtoF	Bottle-to-Fiber
BET	Brunauer-Emmett-Teller
CCS	Carbon Capture and Sequestration
CCU	Carbon Capture and Utilization
AC-GH2x	Commercial activated carbon
EVOH	Ethylene and vinyl alcohol
FT/IR	Fourier transform infrared spectroscopy
ATR-FT/IR	Fourier transform infrared spectroscopy by attenuated total reflection
GC/MS	Gas chromatograph mass spectroscopy
GC/FID	Gas chromatograph with flame ionization detector
GC/TCD	Gas chromatograph with thermal conductivity detector
HPLC	High performance liquid chromatograph
HDPE	High-density polyethylene
LDF	Linear driving force
LDPE	Low-density polyethylene
MS	Mean of squares
OBL	Oxygen barrier layer
PET	Poly(Ethylene) Terephthalate
PAH	Polycyclic Aromatic Hydrocarbon
PP	Polypropylene
PS	Polystyrene
PSA	Pressure Swing Adsorption
PVC	Polyvinyl chloride
REF	Reference
RQ	Research Question

SEM	Scanning electron microscope
STEL	Short-term exposure limit
SS	Sum of Squares
TPA	Terephthalic acid
TWA	Time-weighted average
UV	Ultraviolet
UVA	Ultraviolet A
VSA	Vacuum Swing Adsorption
XRD	X-ray diffraction analysis

This page intentionally left blank.

Chapter 1: Introduction

1.1 Background and essentials of the research

The global PET bottle recycling is highly dependent on overseas factories, especially factories situated in China (Brooks et al., 2018). However, in 2018, China refused to import plastic waste, PET bottles included, due to environmental concerns. In response to the sudden ban, PET bottles are now being relocated to Southeast Asian countries, which had caused environmental problems including terrestrial and marine pollution, and health impacts due to the insufficient recycling capability of these countries (Parker, 2018). As a result, stricter regulation and import bans have been implemented, which prevents the export of PET bottles to other countries (Wang et al., 2020). It is now evident that exporting countries needs to decrease its dependency of overseas recycling factories and that domestic circulation of PET bottle recycling in exporting countries needs to be reinforced to ensure the sustainability of PET bottles.

The fact that domestic recycling industry in exporting countries are facing challenges such as expensive labor, vast land usage, and inability to provide cheap energy and water supply led to the dependency on overseas recycling factories. Another main reason for the diminishing PET recycling business in exporting countries is the treatment of non-recyclable PET bottles (Terazono and Oguchi, 2019).

Non-recyclable PET bottles include bottles with colored pigments, UV degraded bottles, bottles with multilayer structure and bottles with impurities on the surface. They are difficult to purify and separate; therefore, usually disposed of as combustible waste, thus causing the loss of profit in the recycling industry (NAPCOR, 2018). Incentives need to be taken to improve the material value of waste PET in order to boost up profit in the domestic recycling industry which leads to the decrease of dependency on exporting waste bottles to other countries.

In addition to non-recyclable PET bottles, items manufactured from post-recycled PET are often not recyclable. In most cases, PET bottles are downcycled into polyester fibers, sheet and molded product through conventional material recycling. Post-recycled PET is used to manufacture plastic items such as disposable cups, clothing

wear, cushion, carpeting, etc. For example, it takes approximately 10 PET bottles to produce the total fibers needed to make a T-shirt (American Chemistry Council, Inc., 2020). However, due to additives such as coloring and reinforcing agents, items produced from post-recycled PET are difficult to be recycled and are usually left for incineration or landfill.

Given the limitation of conventional recycling methods, non-conventional recycling methods should be reconsidered for the efficient recycling of waste PET. For one, carbonization should be considered as a new approach to improve the material quality of non-recyclable PET. Carbonization, or slow pyrolysis, is the thermal process for conversion of organic material to produce carbon-rich material known as char. Carbonization is widely used for solid waste treatment due to the temperature range sufficient for sterilization of waste, simplicity of the method, ease for bulk treatment and low energy input compared to thermal recycling. Char is a valuable precursor for activated carbon due to the high carbon content and absence of mineral matter.

Despite the numbers of researches on pyrolysis and carbonization of PET available, the inconsistency in temperature, residence time and reactor type indicate the complexity of carbonization process of PET for char formation and should be investigated in depth in order to obtain the conditions suitable for carbonization of PET for high char formation. Furthermore, current research lacks information concerning the mechanism of char formation from PET carbonization. In addition to the carbonization of non-recyclable PET, the effects of structural change due to long-term exposure of UV light and the effects of dye pigment in the PET structure on the carbonization products are not known.

1.2 Objectives of this study

The ultimate objective of this research is to improve the material value of non-recyclable PET for the realization of domestic circular economy for PET recycling through carbonization of PET followed by activation into activated carbon as an effective adsorbent for carbon dioxide. Japan was chosen as the country of study due

to the high collection rate of post-consumed PET but high dependency on overseas recycling, thus exhibiting high potential for the realization of domestic PET recycling.

The current study aims to resolve five research questions (RQs):

(RQ1:) What are the conditions needed for high char formation?

(RQ2:) What is the mechanism for char formation?

(RQ3:) How applicable is the method to actual feedstock?

(RQ4:) How efficient is the method for carbon capture and sequestration?

(RQ5:) Is carbonization a potential method for treatment of non-recyclable PET?

These unresolved problems motivated this research and it has five objectives:

1) To investigate the effects of operating parameters, namely feedstock properties, reaction medium, temperature and residence time, on the carbonization of commercial clear PET as model feedstock in a laboratory scale batch reactor.
2) To clarify the mechanism of char formation based on the product composition and properties to predict the extent of carbonization at specified conditions.
3) To investigate the effects of carbonization of non-recyclable PET (UV degraded PET, colored PET and multilayer structured PET) on the product composition, namely char yield.
4) To conduct activation of char and to study the gas adsorption ability of product in order to evaluate the capacity of carbon dioxide adsorption.
5) To assess the contribution of this process to the environment in terms of energy consumption and carbon dioxide emission.

The contribution of this work is to provide a new method for the effective utilization of non-recyclable PET through the "waste-treats-waste" approach, a method of developing new materials from waste for the purpose of solving environmental concerns. This will help mitigate the dependency of thermal treatment, leading to the decrease of greenhouse gas emission and also prevent illegal dumping of plastic wastes which consequently contributes to solving microplastic pollution. The clarification of the carbonized products and the study of the carbonization process are expected to significantly contribute to the understanding of char formation, which

includes improving the char yield of product composition for the future development of efficient carbon utilization technologies. This study will potentially become an incentive to encourage the improvement of the material value of other plastic wastes as a solution for the global plastic problems.

1.3 Structure of the dissertation

The scope of this research covers the fundamental experimental investigation on PET carbonization, the clarification of char formation mechanisms, the effect of non-recyclable PET on the carbonized product and the investigation of gas adsorption properties of activated char and the assessment of environmental and economic aspects. The overall structure of this dissertation is shown in **Figure 1-1**.

Chapter 1 contains the general information in brief, background of the research and the essentials of this research, where the current situation and problems of PET bottle recycling are highlighted. Information of carbonization reaction is briefly introduced in Chapter 1. Research objectives are explained under 5 specified objectives.

Chapter 2 provides the intensive insight of the global plastic waste generation, its impacts on the environment, the current PET bottle recycling technologies and the current issues of PET recycling. This chapter also gives an in-depth review on the fundamental knowledge of carbonization of PET, its current challenges, the potential utilization of carbonized product as activated carbon and the prospects of the method.

Chapter 3 introduces all consumed materials, experimental methodologies and analytical methodologies applied in the study for each sub-section in detail. Procedures of carbonization reaction, activation reaction and gas adsorption experiment are explained including schematic diagrams. Chapter 3 is referred for the other chapters for describing the methodology applied in each chapter. All analytical procedures followed in the study are also explained. This chapter provides information that is vital as a guidance for the follow up of future research of current study.

Chapter 4 is the experimental investigation under controlled conditions. The step of investigation is described. This chapter focuses on effects of feedstock variance, operating temperature, holding time and reaction medium on carbonization performance. The effects of each parameter on the properties and characteristics of carbonized product were also studied in depth and reported.

Chapter 5 describes the reactions and char formation mechanisms involved in the process based on theory and experimental results obtained from Chapter 4, specifically, through the visualization of reaction pathways using the van Krevelen diagram and proposing a new theory of cross-linking behavior. In this chapter, the derivation of equations was presented, and the cross-linking analysis based on the experimental results was conducted.

Chapter 6 is the extension of experimental investigation of Chapter 4 using feedstock in the state closest to the "real-world" feedstock, namely feedstock with dye pigments, UV degraded feedstock and feedstock with multilayered structure. This chapter focuses on the effects of the "real-world" feedstock on carbonization performance and the properties of product composition.

Chapter 7 is the experimental activation of char products obtained from Chapter 4 under controlled conditions. This chapter focuses on the adsorption studies of different types of gas components in order to determine the adsorption capacity and selectivity of the activated char. This chapter reports the char surface properties before and after activation, the CO_2 adsorption isotherm of activated char based on the bench-scale static adsorption method, and the CO_2 breakthrough curves of activated char were obtained based on the bench-scaled dynamic adsorption method. A simple mathematical model was applied to predict the CO_2 breakthrough curves and to obtain the overall mass-transfer coefficient and effective diffusivity.

Chapter 8 focuses on the contribution of carbonization as an alternative method for treatment of non-recyclable PET to the environment based on estimations of energy consumption and CO_2 emission of the PET recycling system through a simple

estimation study. The results in Chapter 4 and 7 were applied to estimate the theoretical expense and energy consumption for an assumed industrial scale carbonization facility. The economic assessment and CO_2 emission estimation were conducted based on the life-cycle assessment method. This chapter also described the boundary conditions and limitations such as maximum capacity of the processes.

Finally, **Chapter 9** shows the overall conclusions of the present study. The recommendations for the future studies were provided by considering the overall outcomes of the studies from this research.

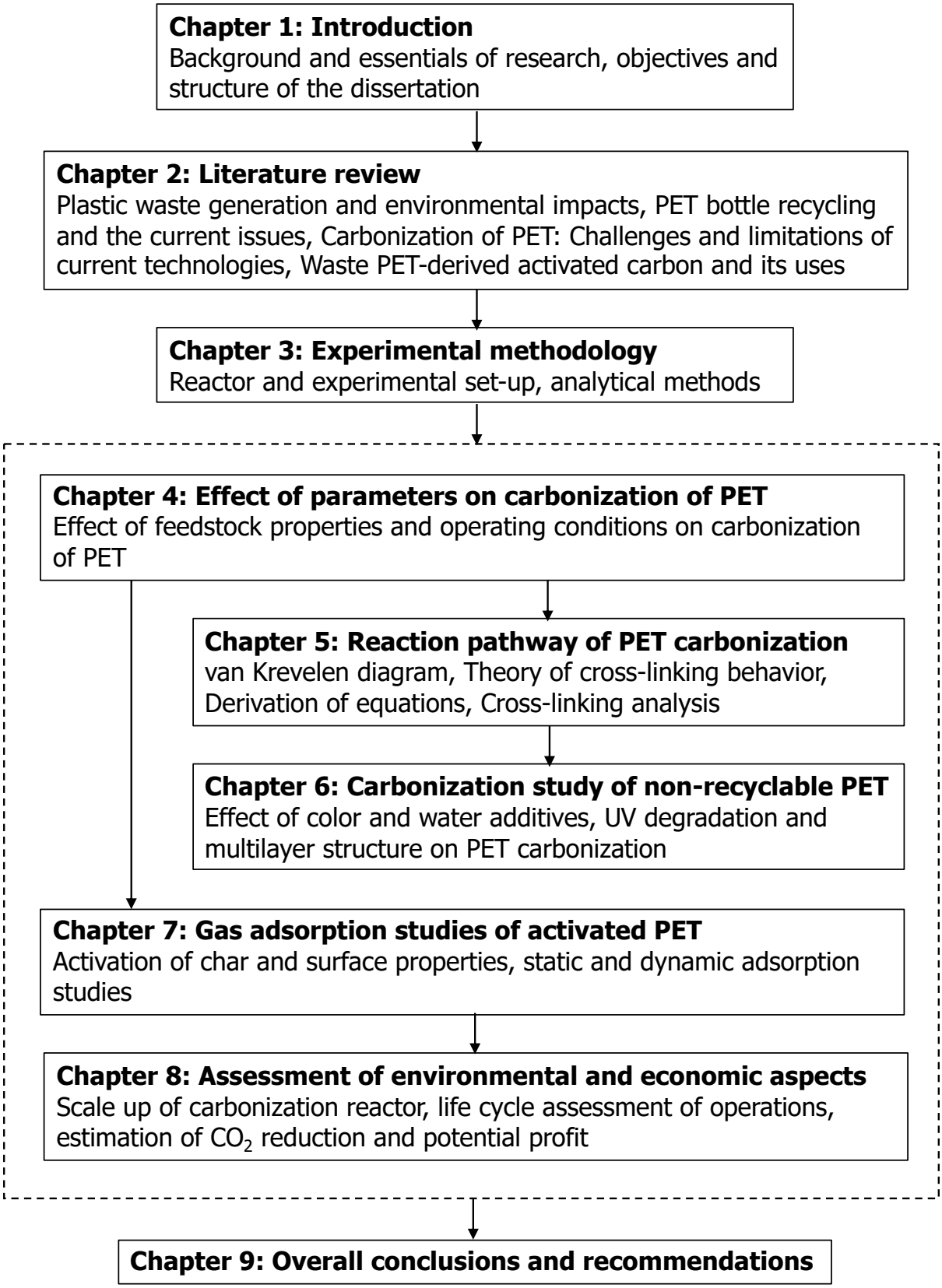

Figure 1-1: Structure of the dissertation.

This page intentionally left blank.

Chapter 2: The challenges for domestic circulation of PET bottle recycling

2.1 Introduction

In waste management, four basic approaches: reduce, reuse, recycle of material and recover of energy are used in order to control environmental impacts. However, current issues involving plastic pollution have yet to be resolved despite the available management and waste flow of plastic. This chapter gives an insight on the current plastic waste problem, types of approaches for plastic waste management, the current technologies of recycling PET bottles and their limitations. This chapter also describes the process carbonization, as a new approach for managing non-recyclable PET through utilization of the carbon product, the potential and limitation of the process.

2.2 Plastic waste generation and the environmental impacts

2.2.1 Global plastic generation

Plastic products have substituted materials such as paper and wood in various manufacturing industries because of their advantages including high durability, light weight, high insulation properties, low cost and ease of mass production. As shown in **Figure 2-1**, the annual production of plastics globally reached 359 million tons by 2018. Asia accounts for more than half of the plastic production, where China is the largest plastic producer (30%), followed by North America (18%), Europe (17%) and the rest of Asia (17%). Japan is producing 4% of the global plastic product. Overall, annual growth rate of the world's plastic production is approximately 4%.

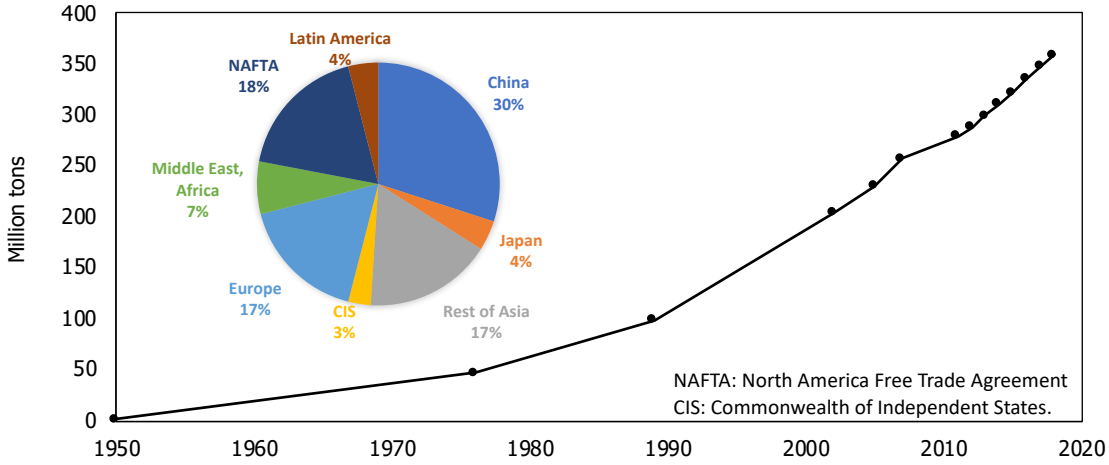

Figure 2-1: Global plastic production in 2018 (Plasticseurope, 2019).

2.2.2 Types of plastics and their uses

The main types of plastic products are low-density polyethylene (LDPE), high-density polyethylene (HDPE), polypropylene (PP), poly(ethylene) terephthalate (PET), polyvinyl chloride (PVC) and polystyrene (PS).

LDPE is made from the monomer ethylene with density range of 917-930 kg/m^3 (Malpass, 2010). LDPE is mainly used to make thin film products such as product packaging, grocery bags, agricultural film etc. LDPE has the lowest tensile strength and durability compared to other plastics on the current market.

HDPE is also made of the monomer ethylene with higher degree of branching compared to LDPE. HDPE has a density range of 930-970 kg/m^3 (Malpass, 2010), therefore is slightly more durable and stretchable than LDPE. It is widely used in manufacturing ropes, fishing nets, toys and liquid packaging.

PP is made of the monomer propylene with density range of 895-920 kg/m^3 (Tripathi, 2001). It is durable, flexible, heat and acid resistant, and is used to make laboratory equipment, automotive parts, medical devices and food containers.

PET consists of polymerized units of the monomer ethylene terephthalate, with repeating ($C_{10}H_8O_4$) units. It has high transparency and durability; and is non-toxic, therefore, widely used in beverage and food packaging. Density of PET is 1380 kg/m^3, which makes mechanical separation such as froth floatation difficult (Zhao et al., 2018a).

PVC consists of polymerized units of the monomer vinyl chloride and has the highest durability and heat resistance properties compared to all plastic products and is widely used in building construction and automotive interiors (Chanda and Roy, 2006). PVC comes in two basic forms: rigid (density range 1300-1450 kg/m^3) and flexible (1100-1350 kg/m^3).

PS is made of monomer styrene with density range 960-1050 kg/m^3 (Scheirs and Duane, 2003). PS is heat resilient and light weight and is widely used in food packaging, construction and medical appliances.

According to the World Wide Fund (WWF, 2018), plastic waste takes hundreds of years to naturally decompose. **Figure 2-2** shows the examples of plastic waste and their consequent lifetime in the nature. Plastic bags and disposable coffee cups made up of LDPE take approximately 20 to 30 years to decompose. The decomposition time increase to 200 years for plastic straws made up of PP, 400 years for plastic rings made up of HDPE and 450 years for plastic cup lids made up of PS. It takes 500 years for coffee pods and plastic bottles made up of PET to decompose naturally. The WWF also estimated that the annual production of waste plastic for an individual is roughly 130 kg, in which approximately 30 kg of the waste plastic ends up in the ocean. Measures need to be taken to minimize the amount of plastic wastes from entering the terrestrial and marine environment which will cause inevitable damage to the ecosystem.

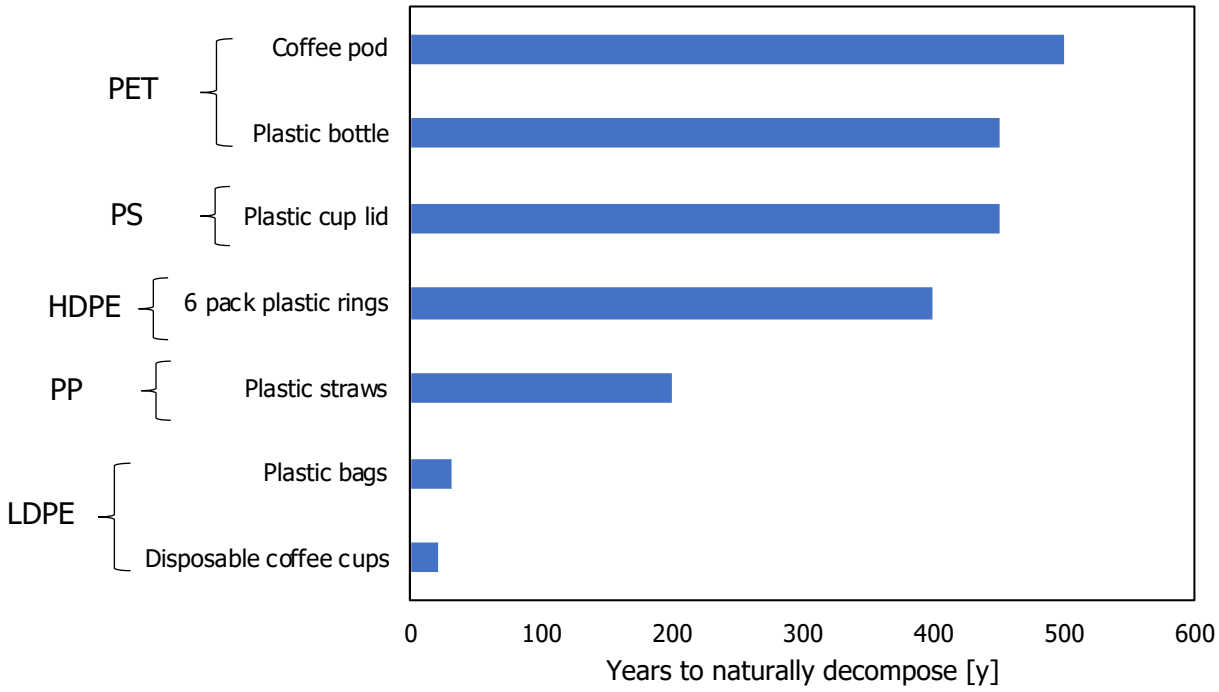

Figure 2-2: Examples of plastic waste and their consequent lifetime to naturally decompose (WWF, 2018).

2.2.3 Management of plastic wastes

Figure 2-3 shows the waste management hierarchy enacted by the United States Environmental Protection Agency for the purpose of focusing industry, government and the public on source reduction rather than treatment and disposal. In the order from the most preferable waste management methods to the least preferable waste management methods, is source reduction, recycling, energy recovery, treatment (without energy recovery) and disposal or landfill.

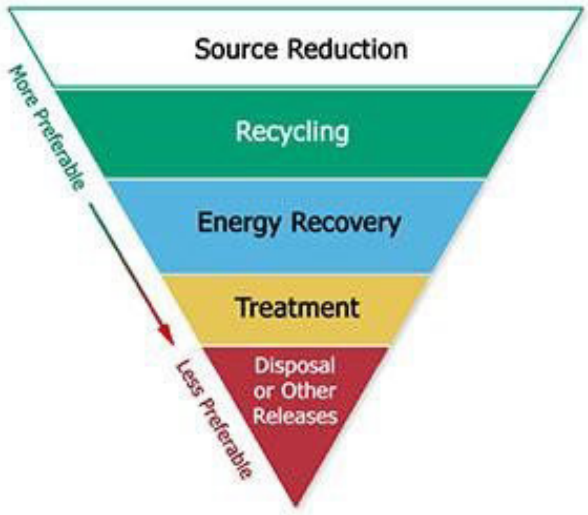

Figure 2-3: Waste management hierarchy (EPA, 2011).

In the management of plastic waste, Prata et al. (2019) also stated that reducing plastic litter inputs by source-reduction and proper management of plastic waste are vital solutions to restore the oceans. However, the continual increase of plastic production and consumption indicates that there is still lack of public awareness in the importance of reducing plastic litter and management of plastic waste still needs improvements to completely tackle terrestrial and ocean pollution. On the other hand, landfill of plastic waste is generally considered to be the least desired approach in plastic waste management (Zhu et al., 2016a; Chirayil et al., 2019) due to the potential of leachate and waste accumulation in both terrestrial and marine environment. As a result, recycling of plastic waste is currently the most frequently used approach in the management of waste plastic.

There are four main approaches for recycling of plastic wastes as shown in **Figure 2-4**. They are primary, secondary, tertiary and quaternary recycling (ASTM, 2000). Primary, secondary and quaternary recycling are the well-established, currently available conventional recycling methods, whereas tertiary recycling is the new or less conventional method in the recycling industry.

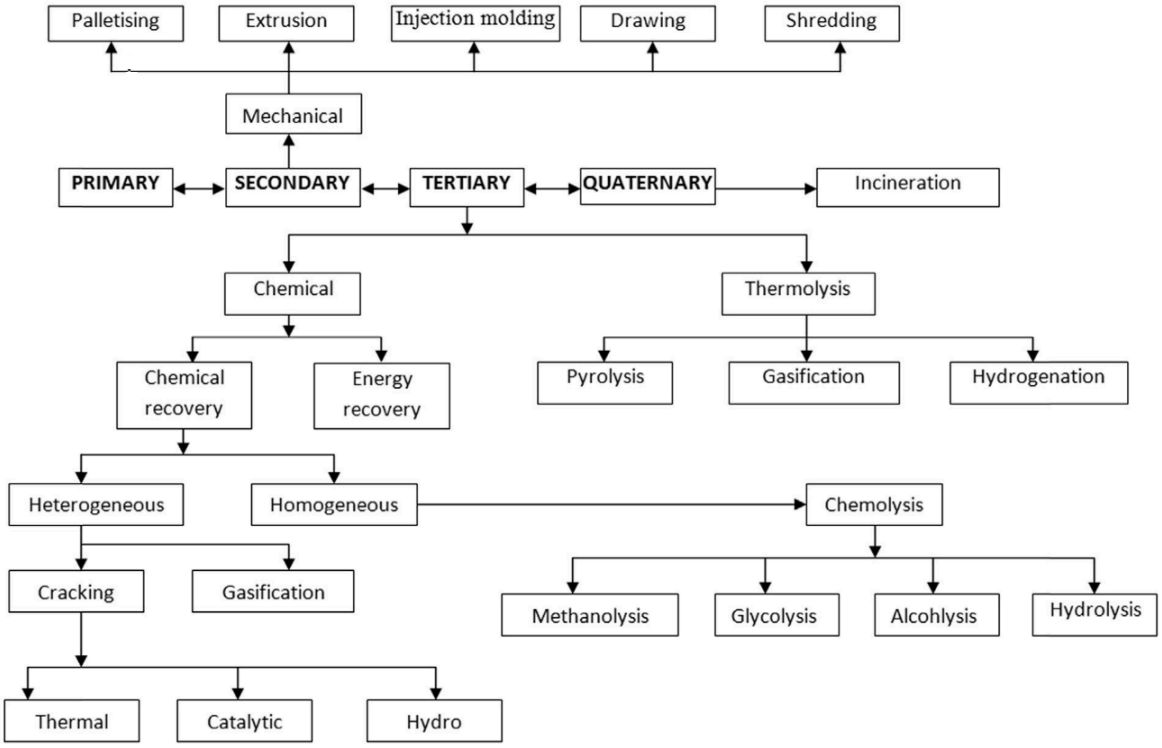

Figure 2-4: Various approaches for recycling of plastic waste (Singh et al., 2017).

Conventional recycling methods

Primary recycling is the recycling of clean, uncontaminated, single-type waste, and it remains the most popular due to the simplicity and low cost of operation. However, one of the biggest challenges of primary recycling is the selection and segregation of wastes. Therefore, unused plastic products, or factory rejects are the most common feedstock in primary recycling. Products converted from waste plastic is expected to have performance level comparable to that of original products made from virgin plastics. (Al-Salem et al., 2009)

Secondary recycling is the conversion of waste plastics into product having less demanding performance requirements than the original material. For example, PET

bottles are recycled into fibers and sheets with less durability to be used as new plastic product. Primary and secondary recycling is directly related to reducing the cost and environmental impacts of production and extraction of natural resources.

Quaternary recycling is the incineration of a plastic to reclaim heat energy, in which some scientists do not consider this method of approach as recycling. (Kumar et al., 2011; Lamberti et al., 2020)

Non-conventional recycling methods

The non-conventional recycling methods in tertiary recycling include pyrolysis, cracking, gasification and chemolysis. Chemical and thermal recycling are the main approaches of the available tertiary recycling technologies. In chemical recycling, chemolysis and gasification have been studied to extract raw materials and fuel gas (Hahladakis et al., 2020). In thermal recycling, pyrolysis or carbonization have been studied mainly for the extraction of oil product.

Despite the numbers of available solutions and alternatives, plastic waste problem is yet to be resolved and has been causing harm to the ecosystem.

2.2.4 Terrestrial and marine pollution due to plastic wastes

The plastic waste in the marine ecosystem has led to the newly emerging issue of microplastic. Since the recent 10 years, scientists are focusing on the source of microplastic emissions and their characterization.

Wagner et al. (2014) had estimated that approximately 80% of the marine plastics originate from inland sources and are emitted by rivers to the oceans. Karbalaei et al. (2018) had also stated that a wide range of microplastics are found in terrestrial ecosystems owing to a plethora of anthropogenic activities. Under environmental conditions, larger plastic items degrade to microplastics, fragments defined to be smaller than 5 mm in diameter (Thompson et al., 2004). Microplastics are of special concern due to the increase in bioaccumulation potential with decreasing fragment size. Microplastics may be ingested by various organisms of different sizes ranging

from plankton to fish, followed by fish to birds and mammals, and accumulate throughout the food web (Wright et al., 2013). The ingested microplastics will cause contamination due to chemical additives and organic pollutants, leading to negative impacts on the public health (Oehlmann et al., 2009; Bakir at al., 2012). Avery-Gomm et al. (2019) had pressed on the importance of reducing waste generation at land-based source and that the current waste management system needs to be improved.

A global voluntary ocean clean-up association, Ocean Conservancy (2019) has reported the quantity of ocean wastes collected in a global scale as seen in **Figure 2-5**. Based on the report, the top 5 ocean plastic waste collected were cigarette butts, plastic food wrapper, beverage PET bottle, plastic straw and beverage bottle cap. Based on the reported numbers, the weight of each ocean plastic waste was estimated and the weight distribution is shown in the same figure. Based on the results, beverage PET bottle, with average weight of 26 g per bottle, accounted for more than 50% of the total plastic waste found in the ocean. Note that the items are calculated based on the reported weight as shown in **Table 2-1**.

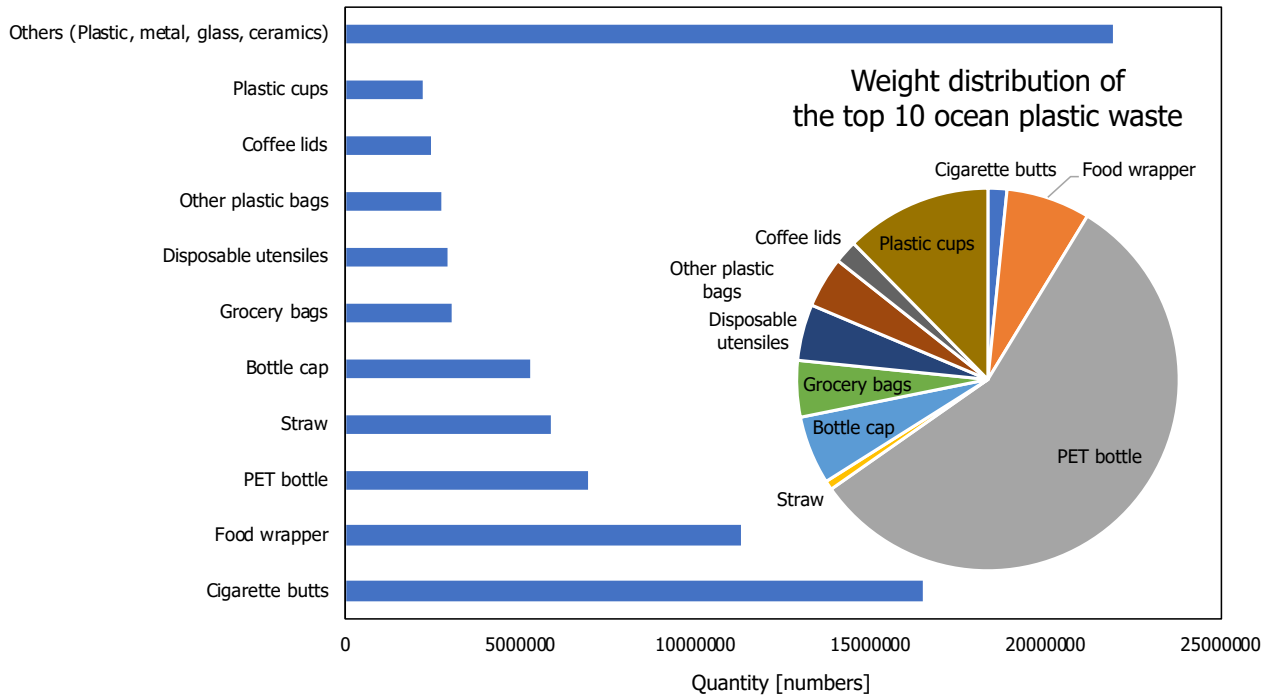

Figure 2-5: Global ocean clean-up result reported by Ocean Conservancy (2019) and estimated weight distribution of the top 10 reported ocean plastic wastes.

Table 2-1: Estimated weight of targeted items.

Items	Weight	Reference/Notes
Cigarette butt	0.31 g	Slaughter et al. (2011)
Food wrapper*	5.0 g	-
Beverage bottle (500 mL)	18.71 g	Islam et al. (2018)
Straw	0.42 g	Borenstein (2018)
Bottle cap	2.62 g	Current study
Grocery bag	5.0 g	EPA (2011)
Plastic utensil	5.2 g	BKS Plastics Ltd. (2020)
Other plastic bag*	5.0 g	-
Coffee Lid	3.23 g	Rodden (2010)
Plastic cup	18.0 g	Knox (2019)

*Estimated using the weight of grocery bag.

Based on the data presented, beverage bottles or PET bottles make up more than half of the total weight of the top 10 plastic waste found in the ocean. This has led to serious marine pollution due to the long span PET bottles need to degrade naturally. The current management of waste PET bottles needs to be studied in depth in order to determine the issues of current waste PET bottle management and find a suitable solution to the problem.

2.3 PET bottle recycling and the current issues

2.3.1 Conventional PET bottle recycling

In conventional recycling of PET bottles, PET bottles undergo separation and cleaning process as shown in **Figure 2-6** to obtain processed products in the form of flakes or pallets. The separation process includes separating materials other than PET such as vinyl chloride bottles and colored bottles followed by intensive cleaning process to remove any foreign contamination from entering the recycling process. This is to ensure the high-quality production of recycled PET materials. Flakes are obtained after thorough cleaning and drying process while pellets are formed by melt granulation of flakes. Flakes and pallets are used as raw materials in the manufacturing of new plastic products such as fabrics and plastic sheets. In conventional material recycling

processes, it is inevitable that frequent recycling of PET will decrease the quality of PET resin due to contamination by additive compounds and degradation of PET polymer chains. The complete removal of contamination and intensive quality check is essential to produce new plastic products, especially for processes like the Bottle-to-Bottle (BtoB) mechanical recycling, a process in which waste PET bottles are recycled into new bottles. Bottle-to-Fiber (BtoF) mechanical recycling, on the other hand, is the conventional material recycling approach of waste PET bottles.

Pellets obtained from recycling PET bottle are popular raw material for manufacturing various plastic products. However, among the PET bottles collected, colored PET bottles and bottles with visible surface damage due to natural weathering are considered to be a nuisance among recyclers due to the limited end use of the material (Hahladakis et al., 2020). For example, in the manufacture of fabric for clothing or fillers for bedding items, mixing of small traces of colored fibers will largely decrease the trading value of the item (Kojima, 2018). On the other hand, bottles with visible surface damage will decrease the quality of PET resin due to the degradation of PET polymer chains (Venkatachalam et al., 2012). In the separation line of most recycling factories, recyclers will separate and remove colored PET bottles and bottles with visible surface damage before entering the pulverization process. And these rejected PET bottles will either be incinerated or disposed in landfills.

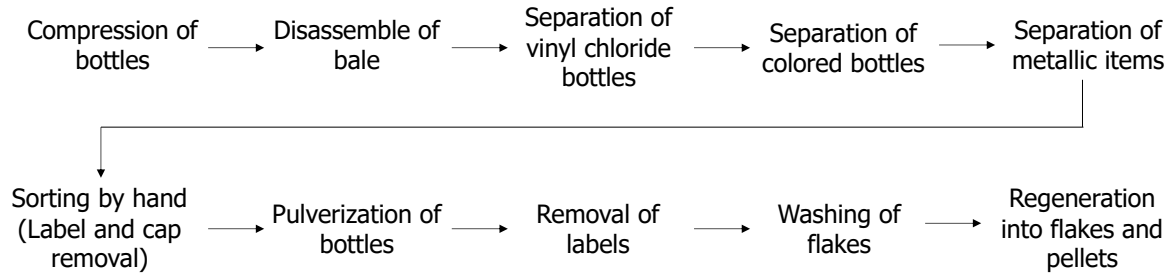

Figure 2-6: Main processes in a conventional PET bottle recycling.

2.3.2 Global dependency of China's PET bottle recycling factories

Waste PET bottles are recognized as one potential source of resource supply to the modern society compared to other plastic wastes due to the singularity of the material. PET recycling created businesses for various entities in the global trading market, where one of the largest PET recycling businesses was focused in China (Velis, 2014). China needs affordable post-consumer PET products over expensive virgin PET resin in order to be recycled into new plastic products to meet the increasing demand for plastic products. On the other hand, bottle exporters such as Japan, America, Canada and some European countries needed exporting destination in which countries with lower environmental standard is preferred to export the countries' PET wastes (Furfari, 2016; Huang et al., 2020). And conveniently, China provided the necessities for PET recycling and resource utilization due to the ability of the country to provide cheap labor, inexpensive energy and water source, and also vast land usage (Hoornweg et al., 2005). For decades, exporting countries have been over-dependent on exporting their PET waste to China (Naustdalslid, 2014; Qi et al., 2016). For instance, Japan has reported a high recycling rate of 84.5% for PET bottles in 2017. However, out of 500 thousand tons of PET bottles recycled, approximately 201 thousand tons of PET bottle were sent to overseas recycling factory for recycling, where most of the recycling factories were situated in China. An overturn event in 2018, China refused to import plastic wastes, PET bottles included, due to environmental concerns (Brooks et al., 2018). In response to the sudden ban on import of plastic wastes, plastic wastes in exporting countries stockpiled due to the lack of ability to treat plastic wastes locally. As a result of saturation of local recycling and collecting sites, rich countries are now facing major problems in managing their plastic wastes (Wang et al., 2019).

2.3.3 Global response to China's ban on plastic waste imports

On December 31, 2018, China had implemented new policies for import restriction of plastic waste, including plastic scraps from daily life to promote the effective use of environmental-friendly resource and to improve the solid waste management for the prevention of environmental pollution that would consequently affect the health of people in China (Ministry of Ecology and Environment, 2018). One of the factors for the change in policy was reported to be due to the detection of foreign contaminants

in plastic scraps by the custom officials in China that may pose a danger to the public health and also the detection of use of false import permits by illegal importers (Japan-China Environment Service Center, 2017).

This restriction has prevented countries from exporting any waste PET bottle to China, even if the bottles are processed, separated and cleaned properly. Although China restricted the import of flakes and bales, the import of processed plastic material such as pellets is still permitted. As a result, bottle collectors and flake processors migrated their material to countries in East Asia and Southeast Asia to be processed into pellets before importing them back into China. Morita and Hayashi (2018) confirmed that the route for trading plastic scraps and material recycling transitioned from route between Japan and China to route between Japan and China via Southeast Asian countries.

In response to the transition of recycling route, authorities in Southeast Asian countries warned on the sudden increase of plastic waste import, including PET bottles along with increasing numbers of illegal plastic waste recycling plants (The Edge Malaysia, 2019). However, countries such as Thailand and Malaysia have temporarily halted the import of waste PET bottle due to concerns over the environmental issues related to possible illegal dumping of low quality and non-recyclable PET bottles.

Some countries have taken measures to reduce plastic waste production and improve domestic recycling towards circular economy solutions. For example, in Germany, a new law that focuses on reducing packaging waste was enforced to reach a target of 70% reusable beverage packaging. In France, a penalty system for non-recyclable plastic will be introduced and only recycled plastic will be used for packaging by 2025.

However, others have maintained their stance in exporting plastic waste and shifted to export plastic waste to other countries. In the UK, China's ban on plastic waste has forced the country to shift its waste export to other Asian countries, especially Malaysia and Indonesia. (Wang et al., 2019). For the US, exportation of plastic wastes has also shifted from China to Malaysia and Thailand.

In Japan, as of now, export destinations have shifted from China to Southeast Asian countries such as Malaysia and Vietnam (**Figure 2-7**). It is inevitable to say that Japan has reached the maximum capacity of recycling their own waste, not just PET bottles but also other plastic scraps. An official statement was made by the Japanese authorities to permit municipals to incinerate plastic scraps, including PET bottles due to the accumulation of the waste as a temporary measure to curb the increase volume of plastic waste (The Containers and Packaging Recycling Law, 2019; Mainichishinbun, 2019). This could cause potential harm to the environment due to the increase of CO_2 emission from incinerators.

Furthermore, regulations are now in place for the trade of mixed plastic scrap between countries, as agreed in the latest Basel Convention signed by over 180 countries, thus further reducing the ability to export plastic waste and increasing the need for local solutions. Countries are now facing challenges to prevent, minimize and properly manage plastic waste for the benefit of the environment and human health, and needs to be conducted through domestic circular economy. The development of a domestic circular economy will ensure the reduction of production of new plastics and the replacement of virgin resin using recycled resin, which will ultimately lead to the prevention of plastic pollution in addition to curbing CO_2 and greenhouse gas emissions (Avery-Gomm, 2019). Incentives need to be taken to shift PET bottle recycling to domestic circulation.

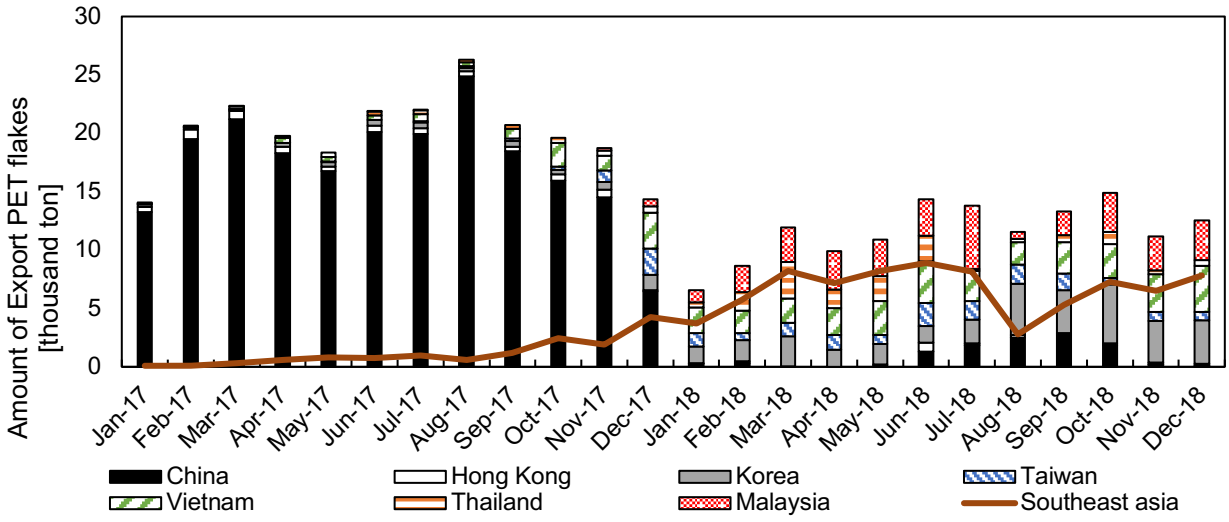

Figure 2-7: Amount of export PET flakes from Japan categorized by different countries (The Council for PET bottle recycling, 2019).

2.3.4 Domestic circulation of PET recycling in Japan

As mentioned, waste PET bottles are the most highly demanded resource and it is high time that countries should secure the resource and provide the most efficient and reliable recycling system in the nation without relying on other counties through the domestic circulation of PET. This section gives an insight on Japan's unique PET bottle recycling system.

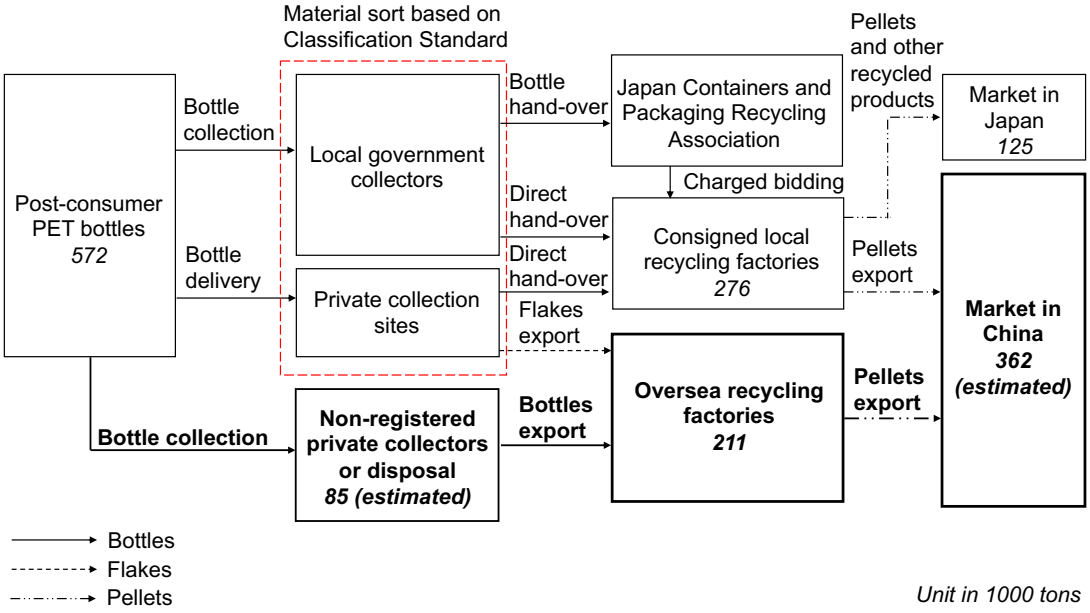

Figure 2-8: Estimated recycling flow of PET bottles from collection to regeneration in Japan in 2018 (The Council for PET Bottle Recycling, 2019).

In Japan local municipalities and private collectors each play vital parts in recycling PET bottles. Based on the data collected by the Council for PET Bottle Recycling in 2018, an estimated material flow of PET bottle is summarized in **Figure 2-8**. Note that the mass balance was not conserved due to the weight which may include labels and caps of the bottles. Total post-consumer PET bottles were estimated to be 572 kton based on the collection rate. Bottles collected by both local municipals and private collectors were sorted based on the Classification Standard (refer to **Appendix A**) and handed over to local recycling factories either handed directly or handed through the Japan Containers and Packaging Recycling Association, a government-designated organization to consign a specified recycler to conduct recycling of designated PET bottles. The total amount of PET bottles exported was unclear, however, was estimated to be 85 thousand tons. Approximately 74% of PET bottles recycled either

overseas or locally were estimated to be sent to China as raw material due to the high demand of plastic products.

One of the reasons that some bottles are not collected by registered designated bodies is that PET bottles disposed in public places such as convenience stores and public trash bins near vending machines are not separated and cleaned properly, thus losing its recycling value (Takahasi et al., 2013). To avoid loss and extra payment for proper treatment, some entities turn to hand over these PET bottles to non-registered private collectors. These non-registered collectors will then send the PET bottles to overseas recycling factories through unknown route to make profit, thus resulting in the environmental pollution of the import country (Terazono and Oguchi, 2019).

2.3.5 Challenges and improvements

In Japan, domestic circulation of PET recycling should be reviewed and reinforced in order to improve the current PET bottle recycling system. A major problem in the conventional recycling system that needs to be addressed is the lack of proper treatment of non-recyclable PET. Non-recyclable PET such as colored bottles, dirty bottles and bottles exposed to UV degradation have no recycle value and are usually processed as waste in Japan (Terazono et al., 2011). Since Japan has very limited landfill, normally, thermal management treatment or exportation to other countries are expected for non-recyclable PET. Incinerating non-recyclable PET are cost and energy intensive, not to mention causing environmental impact due to emission of toxic Polycyclic Aromatic Hydrocarbon, PAH gases (4000 μg-PAH/g for 1 g of PET incinerated, Zhou et al., 2015) and greenhouse gases. Exportation of bottles to other countries will cause leachate to the terrestrial and marine environment. Development for a better and more appropriate method for processing non-recyclable PET is still needed to improve the recycling routes of both recyclable and non-recyclable PET.

Given the limitation of conventional recycling methods, non-conventional recycling methods should be reconsidered for the efficient recycling of waste PET. For one, carbonization should be considered as a new approach to improve the material quality of non-recyclable PET.

2.4 Carbonization of PET: Challenges and limitations of current technologies

2.4.1 Tertiary recycling of PET

Tertiary recycling is usually used to convert plastic wastes into smaller molecules, usually liquid or gases. Here, an advanced thermo-chemical treatment method, namely pyrolysis will be discussed (Al-Salem et al., 2017).

Pyrolysis is defined as the process where thermal degradation of long chain organic materials occurs in inert atmospheres. Products of pyrolysis are typically categorized as gases, tars or wax, and char. Tar or wax is a mixture of aromatic hydrocarbons with molecular weight greater than benzene. The production of combustible gases or oil with high calorific values through pyrolysis adds advantage to the reduction of landfilling of plastic wastes. (Yoshioka et al., 2004; Anuar Sharuddin et al., 2016).

Pyrolysis of PET has been studied widely by various scientists (Vouvoudi and Dimitris, 2019; Ding et al., 2020). For one, Cepeliogullar and Putun (2013) have explored the potential of PET in pyrolysis process to produce liquid oil, known as wax using fixed-bed reactor at 500°C with continuous flow of nitrogen gas. It was reported that the wax and gaseous product were the main product of PET pyrolysis. The main component of wax, benzoic acid was a general sublime with deteriorated fuel quality that clogs pipes and heat exchanger, thus resulting in serious problems in industrial scale (Wan Ho, 2015; Anuar Sharuddin et al., 2017). Furthermore, the high oxygen content in PET attributes to the high CO_2 formation during pyrolysis, thus decreasing the heating value of combustible gas. Compared to its plastic counterparts such as PE or PP which can be effectively converted into high quality pyrolysis liquid oil (Williams and Slaney, 2007; Rehan et al., 2017; Sogancioglu et al., 2017), pyrolysis and liquefaction of PET produced mainly gaseous products consisting of carbon dioxide and carbon monoxide, wax with high corrosive properties and low fuel quality, and solid residue.

Up till now, solid residue, or also known as char, from PET pyrolysis is considered a by-product which can only be utilized as alternative fuel source. However, most recent studies have reported the potential of producing carbon-based materials from PET for various applications (Djahed et al., 2016; Moura et al., 2018; Wen et al., 2019). Despite the recent trend of the numbers of possibilities of utilizing char, solid product from pyrolysis has yet to be explored intensively. The process of producing char through pyrolysis, also known as carbonization, will be discussed.

2.4.2 Carbonization of PET

Carbonization, or slow pyrolysis is the thermal process for conversion of organic material to produce carbon material, or better known as char, which can be used as reductant in metallurgical processes, soil amendment and precursor of active carbon (Skreiberg et al., 2018). The carbon products include amorphous carbons, also known as non-graphitic carbon, and graphitic carbon (Zhuo and Levendis, 2014; Zhou et al., 2020; Chen et al., 2020). Different from pyrolysis, the primary target product of carbonization is char whereas liquid and gaseous products are defined as by-products.

The char yield and extent of carbonization is largely dependent on the feedstock properties and operating conditions. Operational factors include type of reactor, residence time, temperature and pressure of operation, and experimental conditions such as heating rate of the process.

Types of reactor

There are numbers of studies on the thermal degradation study of plastic materials conducted using lab or pilot scale reactors such as the fluidized bed reactors, fixed bed reactors, batch and semi-batch reactors, and conical spouted bed reactors. Mostly pyrolysis studies have intensively focused on the extraction of oil and non-condensable gas (Blazsó et al., 2002; Saha et al., 2008; Hujuri et al., 2010; Kaminsky and Kim, 1999; Kaminsky et al., 2004). Micropyrolyzers and thermogravimetric analysers (TGA) are usually used for laboratory-scale pyrolysis studies to determine the decomposition behavior and kinetic parameters of plastics (Blazsó et al., 2002; Saha et al., 2008; Hujuri et al., 2010). On the other hand, medium to large scale plants such as the

fluidized bed units are used to study the feasibility of the pyrolysis process on plastic material for the implementation of method in industrial scale (Kaminsky and Kim, 1999; Kaminsky et al., 2004).

On the other hand, batch reactors have been reported as non-cost effective as the frequent charging of the feedstock is required, increasing labor cost of the process (Fogler, 2010). Although batch reactors can suffer from various set-backs such as cost energy requirements and feedstock supply, batch reactors have been used to a great extent in lab-scale applications, since they are usually easier to design and operate. Furthermore, they enable to work with samples with variance in sample types and particle sizes, which are closer conditions to those of potential industrial applications.

Residence time

The residence time of the feedstock material in the reactor is one of the main governing factors that affect carbonization. Al-Salem and Lettieri (2010) and Ludlow-Palafox and Chase (2001) both reported that during HDPE thermal degradation in TGA setups, longer residence time resulted in the increase of non-condensable gases. On the other hand, according to Onwudili et al. (2009), the effect of residence time on the degradation of LDPE and PS was studied and it was observed that long residence time was sufficient for secondary reactions to occur and crack oil for gas and char production. Overall, residence time is one important factor in the carbonization process of plastic materials.

Temperature

Temperature controls the main decomposition behavior of plastic material (Al-Salem et al., 2017). Temperature is an important operating parameter as it is highly associated with the cracking reaction of the polymer where the carbon molecule bonds dissociate and volatilize from the surface of the polymer (López et al., 2011). Westerhout et al. (1997) had studied thermal degradation process on various polymers such as PE, PP and PS and reported that at higher temperatures the influence of product concentration, polymer type and residence time on product distribution were insignificant compared to the influence of temperature. Scott et al.

(1990) conducted thermal degradation process of PVC, PS and PE and observed that at temperatures lower than 700°C the major part of the product yielded was solid, whereas at higher temperatures the main product was gas. The degradation profile of material based on the TGA analysis is often used in determining the suitable operating temperature of thermal degradation process of materials.

Reaction medium

Carbonization or pyrolysis process is normally conducted in nitrogen atmosphere (Vivero et al., 2005; Encinar and González, 2008; Çit et al., 2010; Dimitrov et al., 2013; Cepeliogullar and Putun, 2013; Fakhrhoseini and Dastanian, 2013; Ko et al., 2014). This is due to the reasons that nitrogen is an inert and conductive medium in the reaction which leads to less energy input requirement as compared to other gases such as CO_2 and CO (Huang et al., 2018). On the other hand, pyrolysis reaction in steam medium had been reported to produce promising carbon adsorbents due to the high penetration of steam into the carbon structure, which leads to the formation of micropores in the adsorbents (Warhurst et al., 1997; Alkhatib et al., 2011; Lam et al., 2019). This suggests the potential of formation of adsorbents with high porosity from PET through carbonization using steam medium. However, this is in contradiction with the fact that pyrolysis in steam atmosphere leads to higher oil yield (lower char yield) of PET due to the progression of hydrolysis reaction (Kumagai et al., 2014; 2015). Clarification and comparison of characteristics of char products obtained through carbonization using nitrogen and steam medium is needed.

Pressure

Pressure of reactor is often altered in the thermal degradation of polymer for the gasification process. It has been reported in the past that the average molecular weight of the gaseous products decreases along with the increase in operating pressure (Murata et al., 2004). Most research on carbonization are conducted at atmospheric pressure to avoid secondary cracking of char and wax which leads to the gasification of product. Antal's group (Mok and Antal, 1983; Antal et al., 2000; Wang et al., 2011;), however, had intensively studied the effect of pressure on pyrolysis product, and had discussed that high yields of char were obtained when pyrolysis of

biomass feedstock was conducted at elevated pressure in a closed vessel. Maintaining the pressure in the closed vessel is a vital factor for the formation of char in carbonization.

Heating rate

In most cases of thermal degradation of plastic material, as the heating rate increases, the yield of char and the yield of wax decrease whereas the yield of gases increases (Encinar and González, 2008; Fakhrhoseini and Dastanian, 2013; Ko et al., 2014). One of the reasons is the fact that higher heating rate increases the degradation process of feedstock, resulting in the increased production of gaseous product. Yield of char can be maximized by conducting carbonization at low heating rates.

Table 2-2 lists the reviews from past researches on the operating conditions and product composition of PET pyrolysis. These studies were carried out using TGA and/or electric furnace where external heat was provided throughout the process under controlled heating rate and temperature.

Based on the past researches, low heating rate evidently contributes to the high yield of char compared with other operating parameters. Despite the numbers of researches on pyrolysis and carbonization of PET available, the inconsistency in reaction medium, temperature, residence time and reactor type indicate the complexity of carbonization process of PET for char formation. In addition, as far as what had been reviewed, the effects of these parameters on char characteristics are not available. Therefore, it is of great interest to investigate the conditions suitable for carbonization of PET for high char formation and the properties of char produced.

Table 2-2: Operating conditions and product composition of thermal degradation of PET from past researches.

Reactor Type	Tempe-rature [°C]	Heating Rate [°C /min]	Product Composition [wt%]	REF
TGA, nitrogen flow	600	3	Char: 18	Vivero et al. (2005)
TGA, nitrogen flow	800	5 10 15 20	Char: 9.37; Wax: 39.02; Gas: 51.61 Char: 8.28; Wax: 35.40; Gas: 56.32 Char: 5.75; Wax: 29.71; Gas: 64.54 Char: 5.63; Wax: 29.16; Gas: 65.21	Encinar and González (2008)
TGA, nitrogen gas flow	600	5	Char: 12.0	Dimitrov et al. (2013)
TGA, nitrogen flow	850	3 5 8	Char: 24 Char: 22 Char: 21	Ko et al. (2014)
Fixed bed reactor, nitrogen flow	400 500 600 700	10	Char: 13; Wax: 62; Gas: 25 Char: 7; Wax: 65; Gas: 28 Char: 5; Wax: 60; Gas: 35 Char: 5; Wax: 50; Gas: 45	Çit et al. (2010)
Fixed bed reactor, nitrogen flow	500	10	Char: ≅0; Wax: 23.1; Gas: 76.9	Cepelioglu llar and Putun (2013)
Fixed bed reactor, nitrogen flow	500	6 8 10 12 14	Char: 9.0; Wax: 38.9; Gas: 52.1 Char: 8.1; Wax: 34.2; Gas: 57.7 Char: 7.5; Wax: 32.1; Gas: 60.2 Char: 6.6; Wax: 30.3; Gas: 63.1 Char: 5.7; Wax: 29.2; Gas: 65.1	Fakhrhos eini and Dastanian (2013)

Note that liquid product, tar and other condensable volatiles are all defined as wax

2.4.3 Mechanism of PET carbonization

In the formation of char, several processes are included. They are (a) cross-linking, (b) aromatization, (c) fusion of aromatics, (d) turbostratic char formation and (e) graphitization.

In cross-linking, H_2O molecule forms from the scission of OH group from the feedstock. For example, in the pyrolysis of cellulose (Chaiwat et al., 2009), H_2O molecule produced by dehydration forms cross-linking in the cellulose structure at approximately 300ºC.

Aromatization is the fusion of aliphatic carbons to form polycyclic aromatic hydrocarbons. The formation of char through aromatization is complex and usually conducted in the presence of catalysts. An example of method for aromatization is the Diels-Alder reaction.

In fusion of aromatics, light aromatic compound can combine directly with H_2 abstraction-C_2H_2 addition to produce PAH. An example of fusion of aromatics is shown in **Figure 2-9**, where benzene phenyl is converted to pyrene through the H_2 abstraction-C_2H_2 addition.

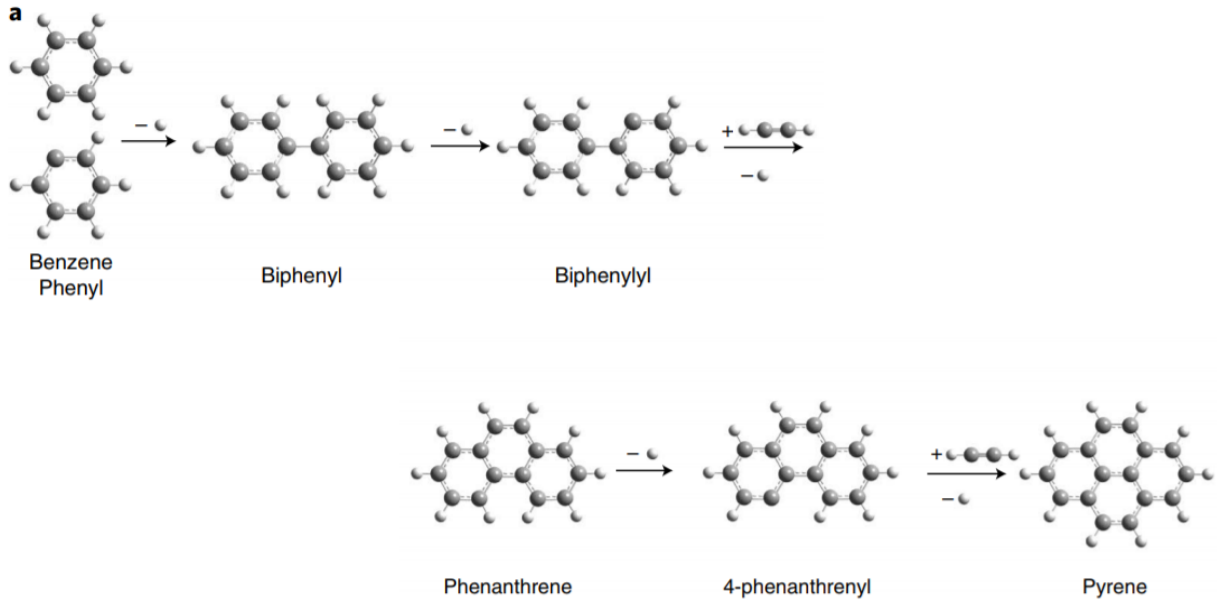

Figure 2-9: Molecular mass growth processes to PAH through H_2 abstraction-C_2H_2 addition (Zhao et al., 2018b).

Turbostratic and graphitic carbon structures are shown in **Figure 2-10**. Turbostratic char refers to incomplete process of graphitization, where solid spheroids appear in the molten carbonaceous material, typically at 500-700ºC (Dasgupta and Sathiyamoorthy, 2013; Schimmelpfennig and Glaser, 2001). Most of the char formed during combustion of polymeric materials is reported to have similar traits to the turbostratic char.

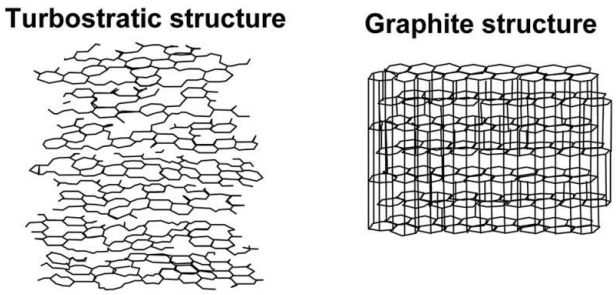

Figure 2-10: Schematic illustration of turbostratic and graphitic carbon structures (Adapted from Dasgupta and Sathiyamoorthy, 2013).

Aromatic rings are the building blocks from which char is produced. Feedstock with large numbers of aromatic rings will give a high char yield (van Krevelen, 1975). Thermal decomposition of materials usually begins with the elimination of small molecules (H_2O, CO_2, CO, CH_4) to form unsaturation in the feedstock chain, which can lead to cross-linking (Kovarskaya et al., 1975), and subsequently, progression of carbonization.

In the case of PET, it is often described as a polymer that undergoes random chain scission and volatilization of low molecular weight fragments such as benzoic acid, acetaldehyde, CO, CO_2, ethylene and methane. The theory and product of thermal degradation of PET are discussion in several studies (Çit et al., 2007, 2010; Brems et al., 2011; Dimitrov et al., 2013). However, up till today, there are no clarification on the structure of the char product, or the subsequent carbonization mechanism to form char. The study of the carbonization process of PET is vital for the understanding of char formation from thermal decomposition of PET in order to improve the yield of char for the development of efficient carbon utilization technologies.

2.5 Waste PET-derived activated carbon and its uses

2.5.1 Activation of carbon

Basically, there are two main steps for the preparation and manufacture of activated carbon, firstly, the carbonization of carbonaceous material at approximately 800°C in the absence of oxygen to obtain solids with high carbon content, followed by the activation of the carbonized product (char), which is either physical or chemical.

Physical activation is a two-step process which involves the carbonization of a carbonaceous material followed by the activation of the resulting char at elevated temperature in the presence of suitable oxidizing gases such as CO_2, steam, air or their mixtures. CO_2 is usually used as the activation gas due to the reasons that it is clean, easy to handle and it facilitates control of the activation process due to the slow reaction rate at temperatures around 800°C (Zhang et al., 2014). However, most researchers reported that the activated carbons produced by physical activation did not have satisfactory characteristics in order to be used as adsorbents or as filters (Haykiri-Acma et al., 2005; Ioannidou and Zabaniotou, 2007).

In the chemical activation process, the carbonization and activation steps are usually carried out simultaneously. The precursor mixed with chemical activating agents, as dehydrating agents and oxidants followed by pyrolyzing/activating of the material. Chemical activation offers several advantages since it is carried out in a single step, combining carbonization and activation, performed at lower temperatures and therefore resulting in the development of a better porous structure, although there are reported environmental concerns of using the chemical agents for activation.

2.5.2 Utilization of waste PET-derived activated carbon

Up until recently, char derived from PET carbonization has been reported to have high potential of producing carbon-based materials for various applications (Djahed et al., 2016; Wen et al., 2019; Moura et al., 2018). For one, researchers worldwide have been focusing on the "waste-treats-waste" method, a novel approach for the development of new materials from waste for the purpose of solving environmental

concerns. **Table 2-3** shows the most recent studies in chronological order that have described the uses of activated carbon derived from waste PET.

Table 2-3: Past researches on the uses of activated carbon derived from waste PET.

Precursor	Activation method	Target adsorbate/absorbate	REF
Waste PET bottle	KOH activation	Methylene blue dye from aqueous solution	Djahed et al. (2016)
Waste PET bottle	KOH activation Steam activation	p-nitrophenol and Fe(III) from aqueous solution	Mendoza-Carrasco et al. (2016)
Char from PET carbonization	N/A	Methylene blue and acid blue 25	El Essawy et al. (2017)
Char from PET carbonization	CO_2 activation	Cephalexin from aqueous solution	Rai and Singh (2018)
Waste PET powder	$ZnCl_2$ activation K_2CO_3 activation	Methylene blue and victoria blue B dye from aqueous solution	De Castro et al. (2018)
Char from PET carbonization	CO_2 activation	CO_2 from flue gas	Moura et al. (2018)
Char from PET carbonization	KOH activation	CO_2 from flue gas	Kaur et al. (2019a,b)

The production of activated carbon from waste PET is most advantageous in terms of low to zero cost of the raw material. The valorization of waste PET is also beneficial in terms of providing a new usage to the waste and omitting the need for costly conventional treatment (Coelho et al., 2011; Singh et al., 2017; Wang et al., 2019). In addition to providing an alternative usage to the material, producing activated carbon from waste PET can consequently provide better waste treatment method with contrast to the conventional waste treatment method which includes landfilling and thermal treatment. This is highly attractive as an incentive to solve environmental problems caused by plastic waste.

2.5.3 Carbon capture through waste PET-derived activated carbon

The production of carbon-based adsorbents from char derived from PET carbonization is highly promising for the separation of CO_2 from gas source due to the high content of carbon and negligible ash content in its chemical structure (Mendoza-Carrasco et al., 2016). Owing to their hydrophobic nature, carbon-based materials are not strongly affected by moisture compared to alumina-silicate based adsorbents such as zeolites (Xu et al., 2013).

CO_2 capture from power plants is considered a leading candidate for helping mitigate global climate change caused by anthropogenic CO_2 emissions. This can be achieved through cyclic adsorption in fixed beds, or also known as Pressure Swing Adsorption (PSA), which is now a relatively mature technology, and is advantageous in terms of flexibility to be retrofitted to any CO_2 source given the optimization of adsorption column to ensure acceptable energy demand and cost (Shen et al., 2012; Bui et al., 2018). PSA process consists of numbers of cycle steps – adsorption, co- and counter-current pressurization, co- and counter-current depressurization, purge, etc. (Kuroda et al., 2018), which enables the selective separation of components from gas stream onto an adsorbent at elevated pressure and desorption at low pressure (Aaron and Tsouris, 2005; Ho et al., 2008; Li et al., 2011).

Utilization of carbon-based adsorbents from char derived from PET carbonization is highly beneficial in terms of cost reduction in the manufacturing of adsorbents, which is essential for the realization of highly efficient, low-cost and wide usage of PSA system for CO_2 capture.

2.5.4 Domestic PET recycling with carbon capture

Figure 2-11 shows the schematic of the domestic PET recycling with carbon reduction and integrated biomass power plant proposed in this study. In the proposed ideal design, biomass power plant with energy recovery from waste plastic is integrated with PET recycling plant in order to maximize the efficiency of energy usage and carbon capture capability, in addition to minimize transportation frequency of plastic waste (PE, PP, PS and PET). PET recycling plant, which recycles PET into new

plastic product will be incorporated with carbonization and activation plant to produce activated carbon from non-recyclable PET. This allows the treatment of all collected PET wastes and prevents any possible outflow of PET waste from the system. PSA system is proposed for post-combustion CO_2 capture in this study due to the maturity of the technology and the capability of utilizing waste PET-derived activated carbon produced in this cycle. The exhausted activated carbon is sent to permanent storage in order to minimize the emission of carbon into the atmosphere.

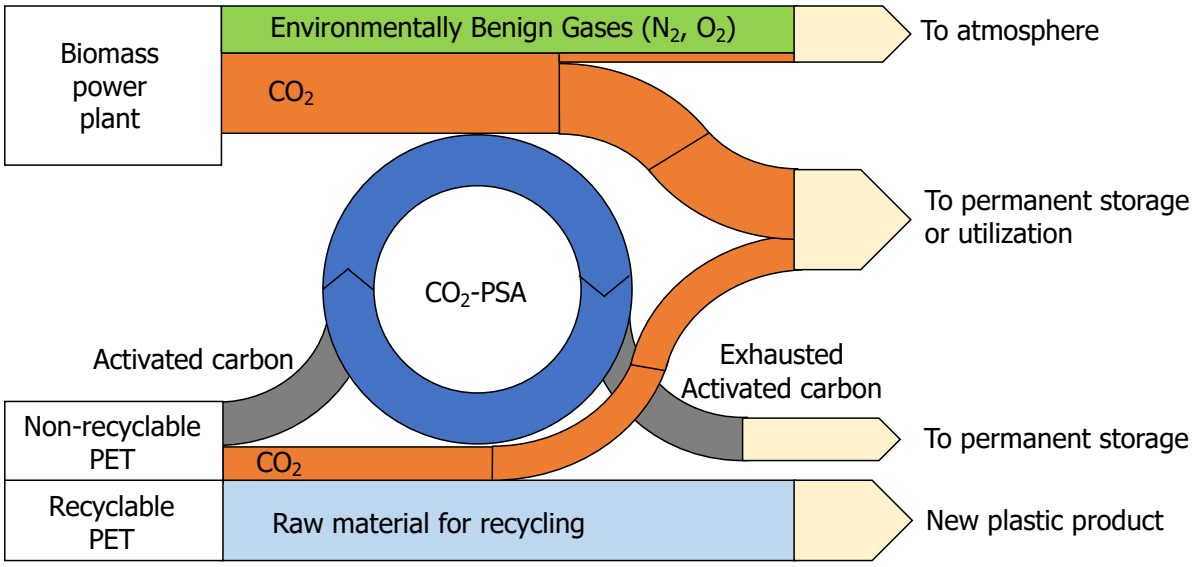

Figure 2-11: Schematic of the domestic PET recycling with carbon reduction and integrated biomass power plant.

In most cases, industries and policy makers are hesitant to increase installment of carbon capture facilities due to the general perspective of perceiving captured CO_2 as having negative economic value. In fact, captured CO_2 can be used for various positive-value applications though the approach known as CO_2 capture and utilization (CCU) (Aresta and Dibenedetto, 2010; Li et al., 2016a,b). There are numbers of facilities that utilize CO_2 for various applications including food and beverage industry and some in chemical production for example urea and methanol (GCCSI, 2017a). Other CO_2 utilization includes mineral carbonation, cultivation of crops and algae (GCCSI, 2016) and industrial processes such as fertilizer production, ammonia production and ethylene glycol plants. CO_2 is also a popular, non-toxic solvent for extraction (Peters et al., 2011). CO_2 utilization is a potential resource conservation

strategy, in which the captured CO_2 displaces fresh CO_2 that would otherwise have to be extracted from natural sources (Bruhn et al., 2016).

Carbon Capture and Sequestration (CCS) or Carbon Capture and Utilization (CCU) plays an important role in decarbonizing the industry sector in order to meet the climate change commitment of limiting warming to less than 2°C, based on the 21st Conference of Parties (COP21) or the Paris Agreement, which had set a reduction target of 60% for CO_2 emissions (UNFCCC, 2016). Numbers of integrated assessment models have been conducted and conclude that CCS or CCU is vital to the long-term solution of climate change. Although there are currently only 37 CCS projects at various stages in the Americas, Europe, Middle East and Asia-Pacific (GCCSI, 2017b), these numbers of projects are expected to increase due to the speculation of implementation for carbon taxes and economic incentives under the principle of the polluter pays in a global scale (Grimaud and Rouge, 2014). These incentives are expected to add increased financial value to the domestic PET recycling and carbon capture cycle proposed in this study.

2.6 Chapter summary

This chapter highlights the continuing plastic waste problem and the resulting pollution to the ecosystem despite the numbers of available solutions and alternatives. Based on previous studies and data provided by scientific and non-governmental community, marine pollution due to waste PET bottle is a drastic matter and it is clear that the current management of waste PET bottles needs to be improved and domestic circulation of PET recycling needs to be reinforced in order to ensure the sustainability of PET usage and improve the marine and terrestrial environment. A major problem in the conventional PET recycling system is addressed – that is, the lack of proper treatment of non-recyclable PET. Subsequently, carbonization of PET was suggested as a new approach to improve the material quality of non-recyclable PET and the overall PET recycling system. Carbonization – a thermal degradation process, similar to pyrolysis for the production of carbon-based material was reviewed in depth. The operating parameters of different plastic materials including type of reactor, residence time, temperature and pressure of operation and heating rate of the process based on previous studies were studied and summarized. It is known that low heating rate and using batch type reactor (sealed reactor) contributes to the high yield of char. However, due to the inconsistency of available researches, the effects of feedstock properties, residence time and temperature on char formation are unknown. Furthermore, the effects of the operating parameters on the properties of char and the mechanism of char formation are not well understood. Moreover, so far, there are no researches on the carbonization of the real feedstock, that is, non-recyclable PET such as colored PET and UV degraded material. Therefore, the experimental work was conducted in this study to determine the product distribution and properties of product, and to clarify the mechanism of char formation in PET carbonization.

The final section of this chapter summarized the potential of waste PET-derived activated carbon from most recent studies. The utilization of waste PET-derived activated carbon was focused in the carbon capture using PSA system. The section gives an insight on the possibility of developing current method for the realization of domestic PET recycling with negative CO_2 emission from environmental, social and economic aspect.

Chapter 3: Experimental methodology

This chapter describes the experimental equipment and procedures for carbonization, activation and gas adsorption experiment. The fundamental analysis of feedstock and products from the process (char, wax and gas) are also included in this chapter.

3.1 Materials and reagents

3.1.1 Types of feedstock

Feedstock used in this study consisted of commercial PET bottle with variance in structure, color and feedstock preparation. **Table 3-1** lists the label, description and treatment of feedstock. Carbonated drink bottle was employed in this study as a representative material which is closest and most abundant material in PET bottle recycling. The representative material was treated with various methods such as UV exposure to imitate the waste material in the "real-world". The details of feedstock preparation and characterization are further explained in Chapter 6.

Table 3-1: Label of feedstock used for each chapter.

Chapter	Description	Feedstock treatment
4	Carbonated Drink bottle, Asahi Soft Drinks Co., Ltd.	Minimal treatment
	Drink bottle, Coca-Cola Central Japan Co., Ltd.	Minimal treatment
	Mineral Water bottle, Suntory Beverage & Food Ltd.	Minimal treatment
	Carbonated Drink bottle, Asahi Soft Drinks Co., Ltd.	Compressed into small bulk
	Carbonated Drink bottle, Asahi Soft Drinks Co., Ltd.	Cut in uniform pieces
6	Carbonated Drink bottle, Asahi Soft Drinks Co., Ltd.	Minimal treatment
	Carbonated Drink bottle, Asahi Soft Drinks Co., Ltd.	UV exposure, Minimal treatment
	Carbonated Drink bottle, Nestlé Waters Co., Ltd.	Separation of layer, Compressed into small bulk

(a) Carbonated Drink bottle, Asahi Soft Drinks Co., Ltd. (d_w = 0.40 mm)

(b) Carbonated Drink bottle, Coca-Cola Central Japan Co., Ltd (d_w = 0.40 mm)

(c) Mineral Water bottle, Suntory Beverage & Food Ltd (d_w = 0.15 mm)

(d) Carbonated Drink bottle, Nestlé Waters Co., Ltd. (d_w = N/A)

Figure 3-1: Types of commercial bottles used (d_w denotes as wall thickness).

Minimal treatment

Compressed into small bulk

Cut into uniform pieces

Figure 3-2: Types of feedstock treatment.

3.1.2 Preparation of UV degraded PET

For the preparation of UV degraded PET, accelerated weathering test was conducted based on the ASTM D 4329-05 (ASTM, 2005) using 500 mL commercial PET bottles as shown in **Figure 3-3**.

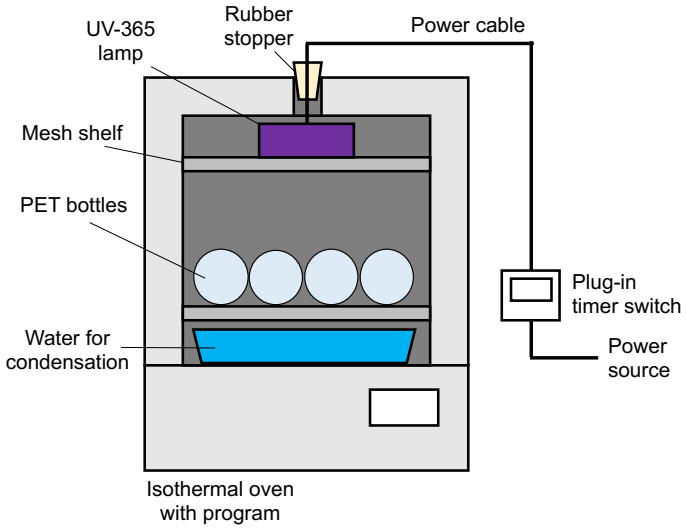

Figure 3-3: Schematic diagram of accelerated weathering test.

A UVA lamp (18.2 W/m^2 at 365 nm) was placed inside a test chamber which was filled with hot vapor of water. PET bottles were exposed to repeated cycles of 8 hr exposure to UV radiation at 60ºC followed by 4 hr water condensation at 50ºC. Note that radiant dosage for 1 year accelerated weathering was calculated based on the annual mean UV exposure in Japan which was reported to be 9111 kJ/m^2 in 2018 (CGER/NIESS, 2018). The following assumptions are considered to determine the total years for natural weathering of PET:

(i) The annual mean UV radiant exposure (UVA: 315-400 nm) in Tsukuba, Japan for 2018 reported by Center for Global Environment Research, National Institute for Environmental Studies (CGER/NIESS, 2018) is 9111 kJ/m^2.

(ii) The irradiance is controlled at a narrow wavelength range using a UVA-365 lamp with artificial weathering test being conducted at 18.2 W/m^2 at 5 cm at 365 nm.

(iii) Variation due to time-of-day, seasonal change and geographical variations are neglected for ease of calculation.

Based on the fundamental principle that UV intensity and distance from light source follow the inverse square law, the intensity of exposure by UVA-365 lamp (18.2 W/m^2 at 0.05 m) can be expressed as

$$I = \frac{0.0455}{r^2} \tag{3-1}$$

Therefore, the average intensity of exposure from UVA-365 lamp to the surface of PET can be expressed as

$$Average\ intensity\ of\ exposure = \frac{\int_0^{2\theta} I\ d\theta}{\int_0^{2\theta} d\theta} = \frac{0.0455}{d^2 - r^2} \tag{3-2}$$

, where d is the distance of the center of PET bottle from light source whereas r is the radius of PET bottle. Detailed derivation of equation is presented in **Appendix B**.

The accelerated weathering will then be calculated using the equation below, and **Table 3-2** shows the total UV exposure and total years in accelerated weathering.

$$\frac{Average\ intensity\ of\ exposure\ by\ UVA}{Annual\ mean\ UV\ radiant\ exposure\ (Tsukuba)} = \frac{Accelerated\ weathering\ in\ days}{Days\ in\ a\ year} \quad (3\text{-}3)$$

Table 3-2: Summary of accelerated weathering test expressed in total hours in UV exposure and total years in accelerated weathering.

Distance of sample from UVA lamp*	Total UV exposure	Accelerated weathering	Label
[m]	[hours]	[years]	
0.084 – 0.15	144	0.21	UV0.2
0.084 – 0.15	416	0.59	UV0.6
0.084 – 0.15	1640	2.34	UV2.3
0.025 – 0.091	528	4.17	UV4.2
0.025 – 0.091	816	6.45	UV6.5
0.025 – 0.091	1088	8.60	UV8.6

*Measured from the top surface to the bottom surface of bottle.

3.1.3 Reagents

For sampling and analysis, acetonitrile (HPLC standard), benzoic acid, acetophenone, benzene, toluene, biphenyl and fluorene, all obtained from Fujifilm Wako Co., Japan were used in present study. Ultrapure water was prepared from Direct-Q 3UV water purification system (Merck Ltd.).

For comparison study in the gas adsorption experiment, commercial activated carbon (AC-GH2x, Osaka Gas Chemicals Co. Ltd., Japan) and zeolite (Zeolite 5A, Fujifilm Wako Co., Japan) were prepared. AC-GH2x is steam activated charcoal made from coconut shell. Zeolite 5A is an alkali metal aluminosilicate with calcium form of A crystal structure. All adsorbents were kept at dry condition at 373 K.

Gas components used in this study were CO_2 (99.5%), N_2 (99.99%), CO_2-N_2 (20 CO_2-vol%, N_2 balance), and CO_2-CO-CH_4 (20 CO_2-vol%, 20 CO-vol%, 20 CH_4-vol%, N_2 balance), in which all were provided by Suzuki Shokan Co., Ltd., Japan.

3.2 Carbonization experiment

3.2.1 Reactor set-up

Experimental study focuses on carbonization of feedstock in laboratory-scale reactor. The carbonization system is shown in **Figure 3-4** and **Figure 3-5**. The reactor was employed to investigate the effects of operating parameters in Chapter 4 and to investigate the effects of different feedstock in Chapter 6.

The autoclave reactor with inner volume of 1.95 L was made of stainless steel (SUS316). The reactor was equipped with an inlet for N_2 displacement and an outlet for gaseous products. The outlet was connected to a heat exchanger followed by a gas-liquid separator, back pressure regulator and to a gas bag for collection of gaseous products. A ceramic crucible (φ90) to hold the feedstock was placed inside the reactor. A band heater was supplied with 200 V, providing maximum heating power of 2.6 kW. Two type-K thermocouples were installed, where the thermocouples were positioned at the center and at the outer wall of the autoclave reactor. Maximum temperature is preset as 500°C for outer wall as safety measures. Pressure transducer (Keyence AP-10S) was equipped to measure the reactor pressure. The autoclave reactor was covered with heat resistant jacket for insulation. According to the safety regulation, the autoclave reactor can withstand pressure up to 10 MPa, which covers for the safety operating limits of this study.

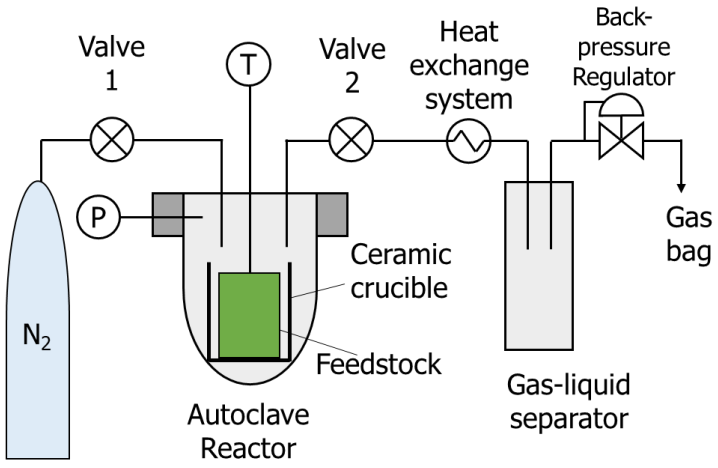

Figure 3-4: Experimental set-up of carbonization system.

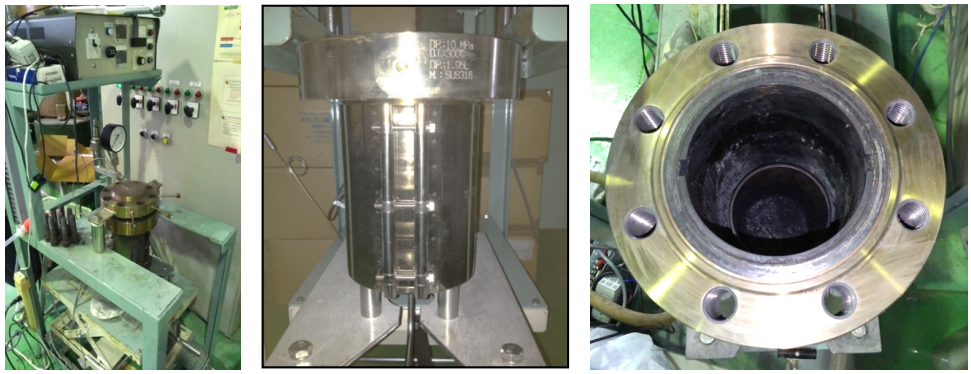

Figure 3-5: Photo of carbonization system.

3.2.2 Experimental procedure

Experimental operations for PET carbonization were conducted as follows. Batch mode runs (Valve 1 and 2 closed) were initiated by heating the reactor from room temperature to set temperature under heating rate of 1ºC/min. After reaching the set temperature, the condition was kept constant until the predefined time. Note that holding time was set to start when temperature reaches the set temperature. Parameter selection was based on the decomposition profile of PET as shown in **Appendix C**. In this study, three experimental points were taken for the temperature ranges of 320-400°C as low operating temperature, 360-440°C as moderate operating temperature, and 400-480°C as high operating temperature. The operating temperatures are expressed in the temperature range between the inner reactor and the band heater. For example, 400-480°C indicates the target temperature of reactor to reach 400°C using a band heater set at 480°C. The temperature distribution of the inner reactor in equilibrium is shown in **Appendix D**. After the reaction, gaseous products were collected in aluminum gas bags (GL Sciences Inc., Japan) while wax was collected from the gas-liquid separator. Char was collected from the reactor after cooling overnight. Char and wax were weighed and stored in airtight containers before subjected to analyzation. Mass of gas was calculated based on the reactor pressure and composition in the gaseous product. Note that wax was taken as the balance from char and gas due to the large amount of residual wax that was solidified in the pipes of the reactor. For char, calorific value, ultimate and proximate analysis, FT/IR spectra were obtained. For wax, calorific value and ultimate analysis were obtained, while GC/MS and HPLC analysis were used for qualification and quantification of the compounds. Gaseous products were analyzed using GC/TCD and GC/FID.

3.3 Activation experiment

3.3.1 Reactor set-up

The experimental equipment for physical activation of char is shown in **Figure 3-6**. The experimental set-up was fabricated using Swagelok fittings (SUS316, Swagelok Co., Japan) and leak proof tested. The experimental set-up was placed in a muffled furnace (NEW-2C, Hayashi Denko Co. Ltd, Japan), and connected to the gas supply chain. The carrier gas used were pure N_2 (99.99%, 47 L) and CO_2 (99.5%, 40 L), both provided by Suzuki Shokan Co., Ltd., Japan. Char used for activation was obtained from carbonization under condition reported in Chapter 4.

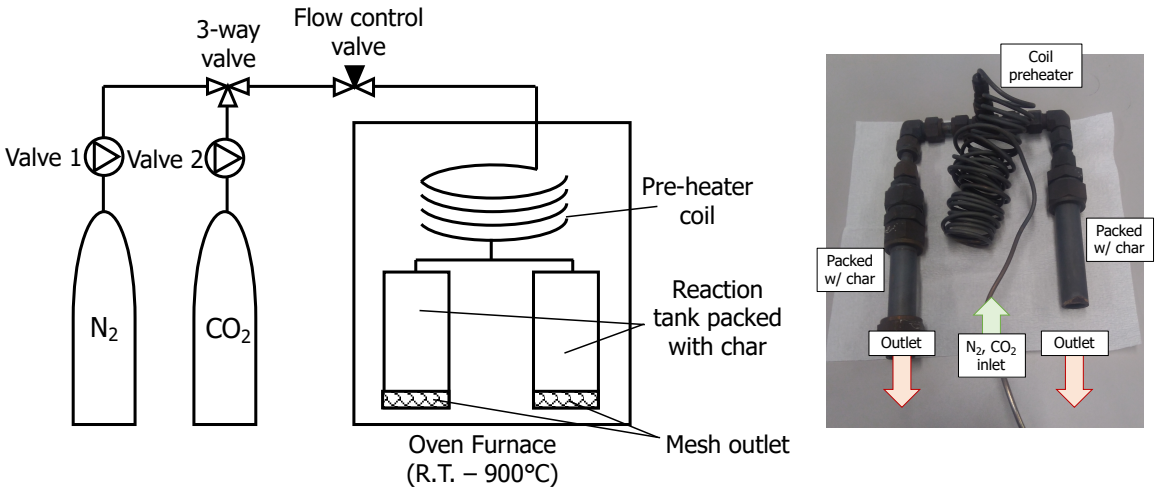

Figure 3-6: Experimental set-up of activation operation.

3.3.2 Experimental procedure

The furnace was heated up from room temperature to 900ºC in 100 mL/min-STP N_2 flow. After reaching 900ºC, N_2 was replaced with CO_2 at flow of 100 mL/min-STP to allow burn-off of char for 120 min. The yield of activated char after burn-off was calculated. The change in CHN composition was also analyzed. Surface properties of activated char was analyzed through the BET/BJH method and morphology changes was observed through SEM analyzation. Activated char obtained were applied in consequent gas adsorption experiment.

3.4 Analysis of feedstock and product

3.4.1 Sample analysis

3.4.1.1 Fourier transform infrared spectroscopy

Infrared spectroscopy by attenuated total reflection, ATR-FT/IR (FT/IR-6800, Jasco, Japan) was conducted for the structural analysis of sample surface. The analysis was conducted in the Department of Applied Chemistry, the University of Tokyo.

3.4.1.2 Microscopic analysis

Surface of PET with variance in UV exposure was examined using a Zeiss Axioskop 2 (Carl Zeiss, Germany) microscope to observe the formation of microcracks formed due to UV degradation. The analysis was conducted in the Laboratory of Aquatic Biology and Environmental Science, the University of Tokyo.

3.4.1.3 Tensile test

Tensile strength was obtained using an EZ test tensile tester (Shimadzu, Japan) to determine the extent of degradation of PET. The analysis was conducted in the Laboratory of Polymeric Materials, the University of Tokyo. Tensile test was conducted by applying force to sample with both ends clamped in fixed position and pulled slowly at constant extension rate until it breaks. Based on the extent of stretching, the force-extension curve was plotted, where properties such as yield stress, elongation of the material at yield, stress at break and elongation at break were determined.

3.4.2 Solid product analysis

3.4.2.1 Proximate analysis

Proximate analysis is conducted to the determination of moisture, ash, volatile matter and fixed carbon in char. The analysis follows the standard method for analysis of coal and coke, ASTM D271-46 (ASTM, 1970). In the preparatory step, char was crushed using a grinder to pass through an 840 μm sieve. The moisture of char was determined by placing 5 g of char contained in a porcelain crucible into an isothermal oven heated at 105ºC for 1.5 hr. The percentage of moisture in the char was calculated and used to obtain other results at dry basis. After drying, the porcelain crucible containing the dried char was placed in a muffle furnace at room temperature and heated to 750ºC

for 2 hours. The porcelain crucible with the remains from char was then placed to cool in desiccator and weighed to obtain the percentage of ash.

On the other hand, the volatile matter was determined by placing 1 g of dried char contained in a sealed porcelain crucible into a heated furnace chamber at 950ºC for 7 min. After heating, the crucible was removed from the furnace and cooled in a desiccator. The loss of weight is the volatile matter.

The fixed carbon content was calculated by difference as below equation.

$$\%fC = 100 - \%VM - \%Ash(Char) \quad (3\text{-}4)$$

, where $\%fC$: fixed carbon content; $\%VM$: volatile matter content; $\%Ash(Char)$: ash content in char. The fixed carbon content is presented on ash-free basis, whereas others are reported in whole dry sample basis. The representation of char yield is often misleading because the chemical composition of char is not defined. As a response, fixed-carbon yield of char was calculated based on the equation, which was defined by Antal et al. (2000), given as

$$y_{fC} = y_{char}\left(\frac{\%fC}{100 - \%Ash(feedstock)}\right) \quad (3\text{-}5)$$

, where y_{fC}: fixed-carbon yield; y_{char}: yield of char; $\%Ash(feedstock)$: ash content in feedstock. In many cases, fixed-carbon yield is a more significant parameter to indicate the carbonization efficiency because the parameter represents the efficiency realized by the pyrolytic conversion of ash-free organic matter in the feedstock into a relatively pure, ash-free carbon (Antal and Gronli, 2003).

3.4.2.2 Ultimate analysis

Ultimate analysis was conducted through an Elemental Analyzer (CE-440F, Sci Globe, Japan) to obtain the elemental composition in the Department of Applied Chemistry, the University of Tokyo. Approximately 2 mg of sample dried overnight were placed in an alumina crucible, sealed lightly and fixed into the auto sampler. The equipment was operated at 980ºC for the combustion oven and 620ºC for the reduction oven. Calibration of equipment was conducted using Acetanilide to give 71.09% Carbon, 6.71% Hydrogen, 10.36% Nitrogen and 11.84% Oxygen.

3.4.2.3 Heating value analysis

The higher heating value (HHV) of the product was determined using a calorimeter (1013-J, Yoshida Seisakusho Co., Ltd.). The calorimeter was based on ASTM D271-46 and was equipped with a combustion bomb, covered in a water-jacket kept at 25ºC to protect the calorimeter from atmospheric temporal change. Approximately 1 g of sample, dried overnight, was covered in tissue paper held up with ignition wire and was set in the combustion bomb. The combustion bomb was filled with oxygen to 2 MPa to allow sufficient burning of samples. Standardization of the equipment was conducted for each run by using a tablet of benzoic acid to give approximately 26.454 MJ/kg. The value obtained was recorded as the HHV. Note that HHV is calculated with the product of water being in liquid form while lower heating value (LHV) is calculated with the product of water being in vapor form.

3.4.2.4 Fourier transform infrared spectroscopy

Fourier transform infrared spectroscopy, FT/IR (FT/IR-6800, Jasco, Japan) was conducted for the structural analysis of solid surface. The analysis was conducted in the Department of Applied Chemistry, the University of Tokyo. Note that FT/IR using KBr method was used for char samples.

3.4.2.5 Scanning electron microscope

Scanning electron microscope, SEM (IT100SEM, JEOL Ltd., Japan) was used to investigate the surface morphology changes of char before and after activation. The analysis was conducted with the assistance of electron microscope laboratory of the Institute for Solid State Physics, the University of Tokyo.

3.4.2.6 Powder X-ray diffraction analysis

The chemical composition of ash was examined using XRD (SmartLab, Rigaku, Corp.). The instrument was conducted with the assistance of X-ray analysis laboratory of the Institute for Solid State Physics, the University of Tokyo. The analysis was carried out with a voltage of 40 kV, an electrical current of 30.0 mA, degree range of 10º to 90º, and the analysis rate of 4°/min.

3.4.2.7 BET/BJH analysis

The surface area, total pore volume, and pore size distribution of PET-AC were determined using a Belsorp-mini II device (MicrotracBEL, Japan) based on the Brunauer-Emmett-Teller (BET) and Barret-Joyner-Halenda (BJH) adsorption/desorption methods. The analysis was conducted in Otomo Laboratory, the University of Tokyo.

3.4.3 Wax product analysis

3.4.3.1 Ultimate analysis and heating value analysis

The ultimate value and HHV of wax were obtained with similar methods presented in char analysis.

3.4.3.2 Gas chromatography mass spectroscopy

For identification, the wax obtained was extracted using dichloromethane and analyzed using GC/MS (GC-2010; Shimadzu, Capillary Column: Aquatic, 60 m × 0.32 mm; GL Science) to identify the components. High purity helium was used as carrier gas (9 mL/min); the injector temperature was 180ºC with splitless injection of 1 µL; the temperature program for GC oven started at 40ºC holding for 2 min, then raised at 5ºC/min to 180ºC and held for 15 min. Peaks were identified by using NIST02 Mass Spectral Library (Shimadzu) of the GC/MS system.

3.4.3.3 High performance liquid chromatography

For quantification, wax was extracted using acetonitrile, filtered and analyzed through high-performance liquid chromatography (HPLC). The eluent (acetonitrile:deionized water=4:1) was delivered at a flowrate of 1.5 mL/min to an Inertsil ODS-3 column (GL Science) heated to 40ºC and detected at 254 nm using the UV detector (UV-2070; Jasco, Japan).

3.4.4 Gas product analysis

3.4.4.1 Gas chromatography with thermal conductivity detector

Gases were analyzed using gas chromatography with thermal conductivity detector, GC/TCD (GC-2014, Packed Column: Shincarbon ST, 4.0 m ×3 mm; Shimadzu, Japan).

Argon was supplied as the carrier gas at a flow rate of 30 mL/min. The analytical conditions were as follows: both injection part temperature and detection part temperature were set constant at 170ºC. Column temperature was held at 60ºC for 7 min and increased at the rate of 20ºC/min to 160ºC and held for 5 min. Data of retention time, peak area and percent of substance was printed out by Chromatopac integrator (Shimadzu C-R8A) connected to the gas chromatograph.

The GC/TCD was routinely calibrated for analysis of H_2, N_2, CO, CO_2 and CH_4 using standard gas mixture containing 20 CO_2-vol%, 15 CO-vol%, 4 CH_4-vol%, 6 H_2-vol% (balance N_2) provided by Tatsuoka Co., Ltd. Standard gas mixture was released into 250 mL aluminum gas bag with Teflon valve and port (GL Science, Japan) and the gas was drawn using a gas tight syringe (Sigma-Aldrich Co. Ltd).

3.4.4.2 Gas chromatography with flame ionization detector

Hydrocarbons were analyzed using gas chromatography with flame ionization detector, GC/FID (GC-2014, Packed Column: Shincarbon ST, 2.0 m ×3 mm; Shimadzu, Japan). Helium and hydrogen were supplied as carrier gas at a flow rate of 60 mL/min. The analytical conditions were as follows: injection part temperature was set constant at 230ºC and detection part temperature was set constant at 300ºC. Column temperature was held at 200ºC for 20 min and increased at the rate of 10ºC/min to 300ºC and held for 10 min. Data of retention time, peak area and percent of substance was printed out by Chromatopac integrator (Shimadzu C-R8A).

The GC/FID was routinely calibrated for analysis of CH_4, C_2H_4, C_2H_6, C_3H_6 and C_3H_8, using standard gas mixture containing 20 CO_2-vol%, 15 CO-vol%, 4 CH_4-vol%, 6 H_2-vol% (balance N_2) provided by Tatsuoka Co., Ltd. and canned gas mixture containing 1 vol% each for C_2H_4, C_2H_6, C_3H_8, C_3H_6, n-C_4H_{10} and iso-C_4H_{10} (balance N_2) provided by GL Science, Japan. Standard gas mixtures were released into 250 mL aluminum gas bags with Teflon valve and port (GL Science, Japan) and the gas were drawn using a gas tight syringe (Sigma-Aldrich Co. Ltd). Based on the gas composition and the gas yield from analysis, the HHV of gaseous product was calculated.

3.5 Gas adsorption experiment

3.5.1 Adsorption isotherm measurement

Figure 3-7a shows a static volumetric gas adsorption system which consisted of a pending tank and an adsorbent tank (SUS316, 0.15 L, Swagelok Co., Japan). The pending tank was equipped with an interchangeable gas inlet for argon gas and sample gas, and a vacuum channel for outgas. A mass flow controller (CMS9500, Azbil Co., Japan) was installed to control the flow of gas in between the pending tank and adsorbent tank. The adsorbent tank was packed with adsorbent and connected to an outgas channel. Both the tanks were equipped with type-K thermocouple (Sakaguchi E.H VOC Corp, Japan) and pressure indicator (AP-13S, Keyence Co., Japan), which were connected to a data logger (GS-4VT, Graphtec Co., Japan). A rotary vacuum pump (DAP-15, AS ONE Co., Japan) was used for the outgas channel to allow the regeneration of the spent adsorbents and evacuate any unwanted gas held by the adsorbent tank prior to the experiments. The system was assembled using Swagelok fittings and was tested to be leak proof. Prior to each run, the system was purged with argon gas before supply of sample gas. All experimental runs were operated at 20°C and 35°C. Operation was set to hold for 5 min after the mass flow controller indicates zero to allow sufficient time of system to achieve equilibrium gas adsorption.

3.5.2 Breakthrough experiments

Figure 3-7b shows a dynamic gas adsorption system. As opposed to the static gas adsorption system, the outlet of the adsorbent tank was connected to a back-pressure regulator to maintain the pressure in the system and provide constant outlet flow of gas. The outlet gas flow was monitored by a flow indicator which was connected to a three-way valve for gas collection. The effluent was collected in gas bags (GL sciences Inc., Japan) in between intervals and analyzed by GC/TCD. The pressure indicators, thermocouple and flow indicator were connected to a data logger to monitor the rate and amount of gaseous compound being transferred between the two tanks. The experimental parameters used to measure the breakthrough curves of sample gas were summarized in **Table 3-3**. Prior to each run, the system was purged with argon gas to allow the adjustment of gas flow rate and pressure in the adsorbent tank before the supply of sample gas. All experimental runs were operated at 20°C.

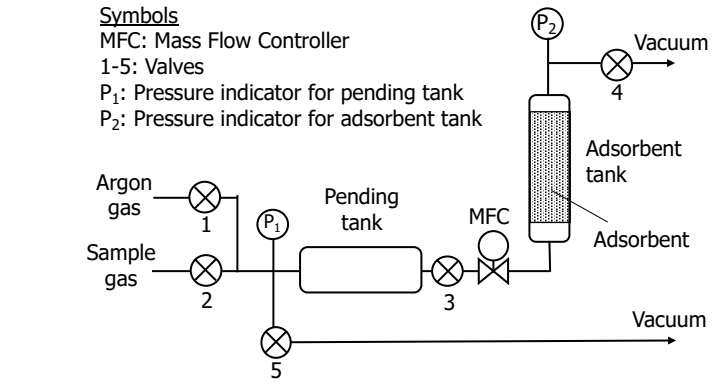

(a) Static adsorption system

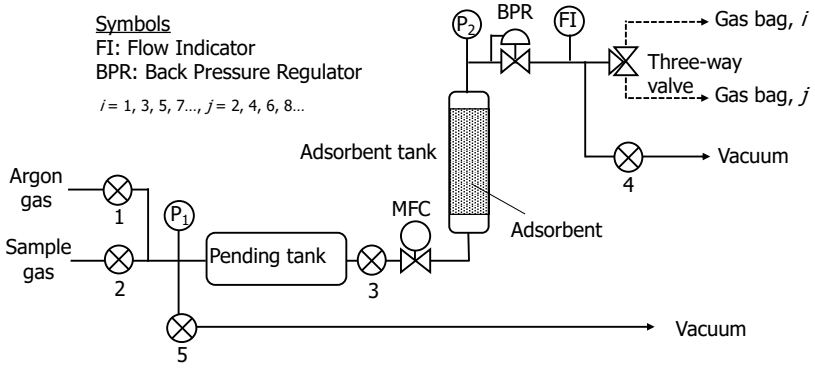

(b) Dynamic adsorption system

Figure 3-7: Experimental set-up for gas adsorption experiments.

Table 3-3: Experimental parameters used for static adsorption experiments and dynamic adsorption experiments.

Adsorbent		PET-AC	AC-GH2x	Zeolite 5A
Adsorbate partial pressure	MPa		0.1	
Adsorbate flow rate	mL/min		27	
Mass adsorbent	kg	6.83×10^{-3}	5.17×10^{-3}	6.43×10^{-3}
Bed height	m		0.15	
Bed volume	m^3		6.04×10^{-6}	
Bed porosity	-	0.435	0.571	0.102
Mean adsorbent diameter	m	1.25×10^{-3}	4.05×10^{-3}	4.75×10^{-3}
Bulk density	kg/m^3	1131	856	1065
Solid density	kg/m^3	2000[a]	2000[b]	1185[c]
Single gas component:			100 CO_2-vol% 100 N_2-vol%	
Binary gas component:			20 CO_2-vol% (N_2 balance)	
Multiple gas component:			20 CO_2-vol%, 20 CO-vol%, 20 CH_4-vol% (N_2 balance)	

[a]Determined using tap density method; [b]Patil et al. (2014); [c]Delgado et al. (2015)

Chapter 4: Effect of parameters on carbonization of PET

4.1 Introduction

Carbonization of PET is a complex process with multiple reactions occurring simultaneously. Thus, the process performance can be influenced by several parameters, and these parameters need to be manipulated in order to improve the efficiency of the process. Numerous studies of thermal degradation of plastic material had reported the increase of char yield due to the slow heating rate in the operation (Encinar and González, 2008; Fakhrhoseini and Dastanian, 2013; Ko et al., 2014). On the other hand, despite the numbers of researches on pyrolysis and carbonization of PET available, there has been inconsistency in reaction medium, temperature, residence time, feedstock and reactor type, thus indicating the complexity of the process for char formation. The aim of this chapter is to investigate the effects of operating parameters, namely feedstock treatment and properties, operating temperature, holding time and medium type on the products of carbonization. The main interest is on the effects of temperature, holding time and medium type on the char yield and its characteristics, which has been unclear and not reported in past studies. The experiments were carried out under controlled conditions according to the study scheme as shown in **Figure 4-1**.

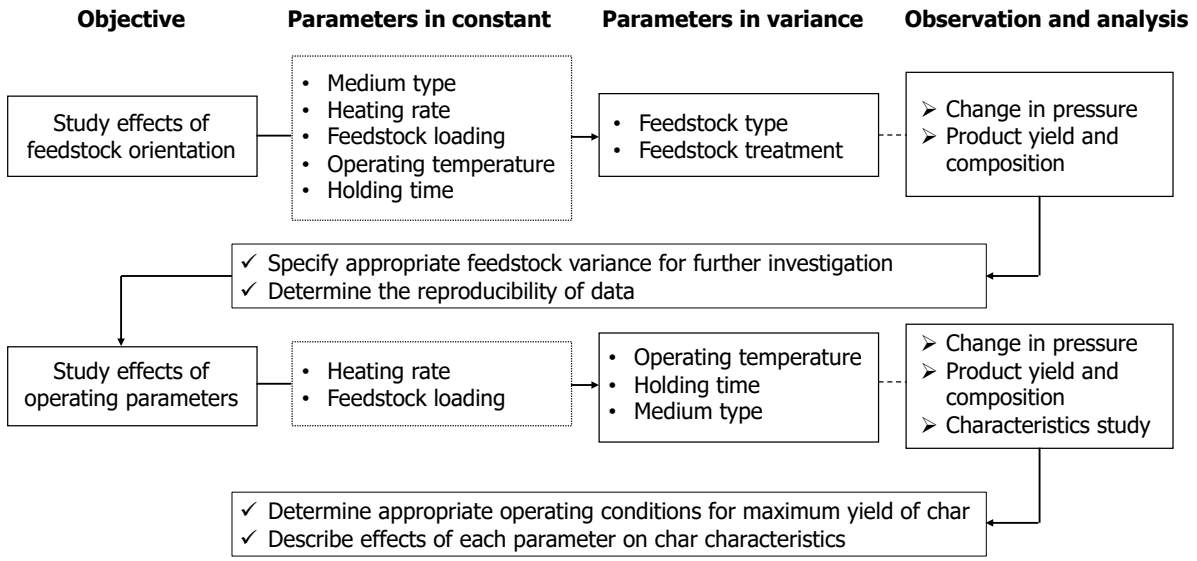

Figure 4-1: Study scheme of Chapter 4 to investigate the effects of operating parameters.

4.2 Effect of feedstock variance on carbonization of PET

A preliminary study was conducted to investigate the effects of feedstock variance on carbonization of PET. Different types and treatments of feedstock were prepared for carbonization under constant operating temperature and holding time. Prior to the study, a reproducibility test was conducted with same samples and constant operating conditions as reported in **Appendix E** which confirms the viability of current study.

4.2.1 Experimental set-up and feedstock preparation

The reactor configuration and experimental procedures are described in detail in Chapter 3. In this study, parameters in constant are as shown in **Table 4-1**. The variance in bottle thickness, bottle type/shape and feedstock treatment was studied. **Table 4-2** lists the label, description and treatment of feedstock.

Table 4-1: Parameters used in determining the effect of feedstock on carbonization.

Variables in operation	Units	Operating parameter
Medium type	[-]	Nitrogen displacement
Heating rate	[°C/min]	1.0
Feedstock loading	[g]	70-75
Operating temperature	[°C]	400-480
Holding time	[min]	120

Table 4-2: Label of feedstock with variance in bottle thickness, bottle type/shape and feedstock treatment.

Label	Description	Feedstock treatment
A	Carbonated Drink bottle, Asahi Soft Drinks Co., Ltd.	Minimal treatment
B	Carbonated Drink bottle, Coca-Cola Central Japan Co., Ltd.	Minimal treatment
C	Mineral Water bottle from Suntory Beverage & Food Limited	Minimal treatment
D	Carbonated Drink bottle, Asahi Soft Drinks Co., Ltd.	Compressed into small bulk
E	Carbonated Drink bottle, Asahi Soft Drinks Co., Ltd	Cut in uniform pieces

4.2.2 Results and discussion

4.2.2.1 Visual observation of product

Samples were carbonized using the parameters shown previously. Char, wax and gaseous products were obtained as the carbonized products. **Figure 4-2** shows the image of char and wax after operation at 400-480°C and 120 min. Char was collected in the crucible after the reactor was cooled overnight to room temperature. Char obtained from PET carbonization was hard and brittle, with no smell. On the other hand, wax was collected from the liquid-gas separation after the operation. Wax was soft and had pungent smell similar to gasoline during collection but hardened under exposure to low temperature at approximately 10°C.

(a) Char (b) Wax

Figure 4-2: Photo of char and wax obtained from PET carbonization at 400-480°C and 120 min.

4.2.2.2 Effects of feedstock variance on carbonized product

Product composition and char characteristics

Figure 4-3 shows the composition of product after carbonization of PET with variance in bottle thickness, bottle type/shape and feedstock treatment. The composition of product was obtained in the range as follows: Char 27.1-29.6%; Wax 36.5-41.3%; Gas 30.2-36.1%. Note that wax was taken as the balance from char and gas due to the large amount of residual wax that was solidified in the pipes of the reactor. Wax and gaseous product make up most of the product composition, which is the typical result from thermal decomposition of PET as shown in Table 2-2. (Encinar and González, 2008). However, in this study, the char obtained was higher than reported results (Encinar and González, 2008; Çit et al., 2010; Fakhrhoseini and

Dastanian, 2013). This is due to the reason that the heating rate in this study is set to operate at the lowest rate so far that has never been reported. When energy input is high, the polymer chains will be subjected to rapid chain scission, thus leading to rapid volatilization of gas and wax. When energy input is low, the chain scission occurs to form cross-linking before volatilization, thus leading to char formation. Overall, the product composition from the thermal decomposition of PET shows good consistency regardless of starting feedstock state.

Figure 4-4 shows the proximate value and fixed-carbon yield of char. The fixed-carbon content was 71.8±1.1% for char obtained from all operations, whereas overall fixed-carbon yield was 20.3±0.7%. Fixed-carbon content and fixed-carbon yield in char also showed good consistency regardless of initial feedstock treatment.

Table 4-3 shows the elemental distribution and calorific value of char, where %C refers to carbon content, %H refers to hydrogen content, %N refers to nitrogen content and %O refers to oxygen content. HHV was obtained using the methods described in Chapter 3. The elemental distribution of char obtained was as follows: %C 87.9±1.7%; %H 4.5±0.3%; %O 7.1±1.7%; and HHV 35.8±0.5 MJ/kg. The high carbon content in char indicates that PET was successfully carbonized. The high carbon content of char contributes to the high HHV which was obtained from analyzation of calorific value. Overall, it can be seen that the elemental distribution and calorific value (HHV) of char obtained from PET carbonization of different feedstock treatment showed good consistency. A simple statistical analysis based on the analysis of variance, ANOVA, was also reported in **Appendix F.1**, which further proves that there was no statistically significant difference between the data.

As a conclusion, the product composition of carbonized product and characteristics of char showed no evident changes regardless of the starting feedstock state. The good consistency in carbonization results may be due to the singularity of polymeric material of feedstock, where variance in bottle shapes, types and preparation methods did not alter the composition of polymers in the starting feedstock. Thus, carbonization of singular polymeric material, PET shows consistent carbonized product and properties.

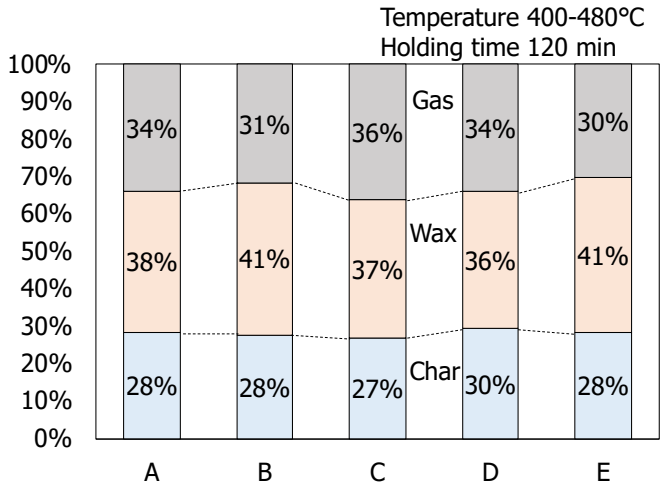

Figure 4-3: Composition of product after carbonization of PET with variance in bottle thickness, bottle type/shape and feedstock treatment.

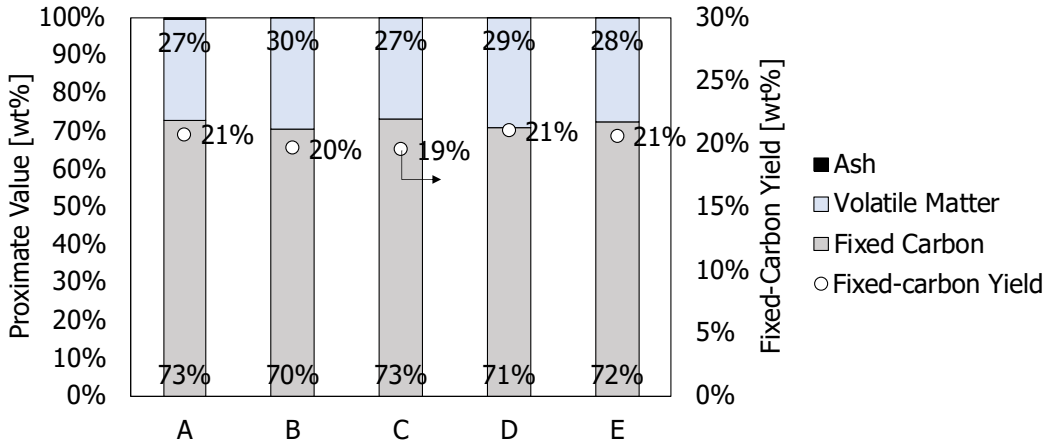

Figure 4-4: Proximate value of char obtained from PET carbonization with variance in bottle thickness, bottle type/shape and feedstock treatment.

Table 4-3: Elemental composition of char obtained from PET carbonization with variance in bottle thickness, bottle type/shape and feedstock treatment.

	Ultimate Analysis[a] [wt%]				HHV[a]
	C%	H%	N%	O%	[MJ/kg]
Raw PET (A)	61.8	4.0	0.3	33.9	23.61
A	89.3	4.4	0.4	5.8	35.69
B	87.3	4.3	0.3	8.1	35.54
C	89.5	5.0	0.4	5.1	36.58
D	85.4	4.3	1.1	9.2	35.69
E	87.9	4.2	0.4	7.5	35.40

[a]: Dry basis; Data obtained from CHN analysis had 0.3% error

4.2.3 Conclusions: Effect of feedstock variance on carbonization of PET

Based on the experimental results, the conclusions were drawn as follows:

1) Carbonization of PET was able to produce product composition and char characteristics with high consistency as demonstrated by the reproducibility test (**Appendix E**).
2) Feedstock size and initial treatment methods did not have distinct effect on the product composition and char characteristics due to the singularity of the polymer in feedstock.
3) Results are reproducible and produced similar product composition regardless of physical variance of feedstock due to the singularity of polymer in feedstock.

Considering the overall results, the feedstock will be prepared with minimal treatment for the ease of sample preparation in further studies. The influences of operating parameters were investigated in the next section.

4.3 Effect of operating conditions on carbonization of PET

Based on the preliminary study to investigate the effects of feedstock variance on carbonization of PET, physical properties of feedstock and sample preparation had no evident effects on the product yield and its properties. In this section, operating conditions were investigated to identify the product composition of char, wax and gas.

4.3.1 Experimental set-up

Clear PET bottle purchased from Asahi Soft Drinks Co., Ltd were prepared with minimal treatment. The experimental parameters are shown in **Table 4-4**, where parameter selection was based on the decomposition profile of PET. The parameters under variable are the operating temperature and holding time. Operating temperature was set to vary in the range of low heating temperature at 320-400°C, moderate heating temperature at 360-440°C and high heating temperature at 400-480°C. On the other hand, holding time was set to vary in the range of short holding time of 30 min to long holding time of 240 min. Analyzation methods are described in Chapter 3.

Table 4-4: Parameters used in determining the effects of operating temperature and holding time on PET carbonization.

Variables in operation	Units	Operating parameter			
Medium type	[-]	Nitrogen displacement			
Heating rate	[°C/min]	1.0			
Feedstock loading	[g]	70-75			
Operating temperature	[°C]	320-400		360-440	400-480
Holding time	[min]	30	60	120	240

4.3.2 Results and discussion

4.3.2.1 Effect of operating temperature on carbonized product

Product composition

Figure 4-5 shows the yield of char, wax and gas for operations under different temperatures at constant holding time of 120 min. Note that wax was taken as the balance from char and gas due to the large amount of residual wax that was solidified in the pipes of the reactor. In a series of temperature difference, char yield decreased from 93 wt% in low operating temperature of 320-400°C to 28 wt% in high operating temperature of 400-480°C. Wax yield increased from 6 wt% in low operating temperature of 320-400°C to 38 wt% in high operating temperature of 400-480°C. Gas yield increased from 1 wt% in low operating temperature of 320-400°C to 34 wt% in high operating temperature of 400-480°C. Further analyzation was conducted to determine the properties of product and to indicate the extent of carbonization.

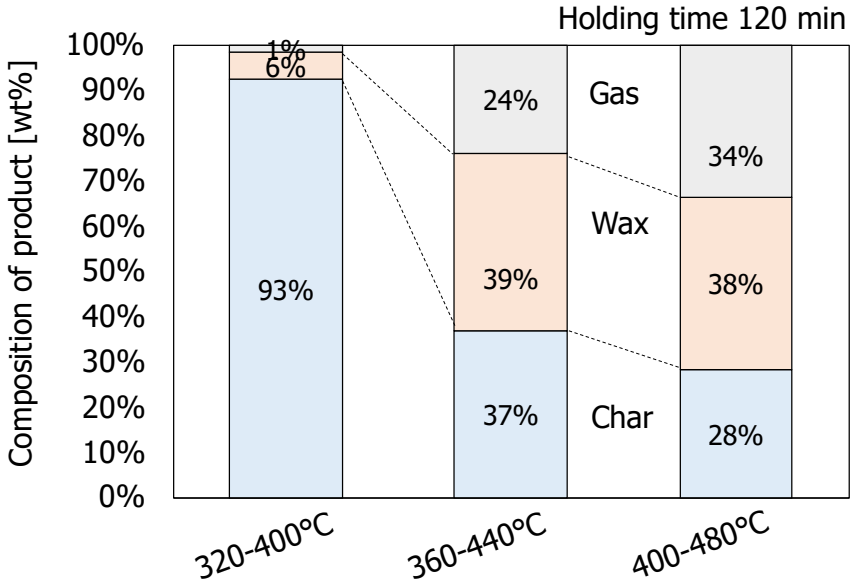

Figure 4-5: Composition of char, wax and gas for operations under different temperatures at constant holding time of 120 min.

Characteristics of char

Figure 4-6 shows the photo of char obtained from PET carbonization at low operating temperature of 320-400°C and high operating temperature of 400-480°C at constant holding time 120 min. From the physical appearance, it is evident that char obtained at 320-400°C did not undergo carbonization due to the low operating temperature. It was also recognized that carbonization of PET proceeded through a distinct melt phase during the operation despite the initial starting preparation of feedstock. The product also had a corrosive and pungent smell. On the other hand, char obtained at 400-480°C was brittle and hard. In addition, no fragment of raw PET was observed.

(a) 320-400°C (b) 400-480°C

Figure 4-6: Photo of char obtained from PET carbonization at 320-400°C and 400-480°C at constant holding time 120 min.

Figure 4-7 shows the proximate value of char and the fixed-carbon yield for each condition. From the results, it can be seen that char from all runs had little to almost no moisture and ash due to the low moisture and ash content in PET. However, the fixed carbon content increased rapidly compared to the original PET material with 6.4% to 8.6% for low operating temperature 320-400°C, 43.1% for moderate operating temperature 360-440°C and 72.6% for high operating temperature 400-480°C. The fixed-carbon yield was calculated to give 8.0% for low operating temperature 320-400°C, 16.0% for moderate operating temperature 360-440°C and 20.7% for high operating temperature 400-480°C.

Table 4-5 shows the elemental composition and the higher heating value of char for each condition. From the results, it can be seen that %C increased drastically from 61.8% of raw PET to 81.1% for char from moderate operating temperature 360-440°C and 89.3% for char from high operating temperature 400-480°C. In addition, evident decrease of %O can be seen for char from moderate operating temperature 360-440°C and high operating temperature 400-480°C. The HHV increased with increasing operating temperature due to the increase of carbon content in char.

From the results obtained, although low operating temperature 320-400°C gave the highest composition of char, further analyzation of proximate analysis and ultimate analysis suggested that most of the char was composed of highly volatile by-product due to low operating temperature. This explains the large mass fraction of volatile matter in char from low operating temperature 320-400°C, which was comparable to the raw PET. The high fixed carbon content and fixed-carbon yield of char from high operating temperature 400-480°C show that high temperature is favored for the carbonization of PET to produce char with low volatile matter and high fixed-carbon yield. A study by Aworn et al. (2008) reported that 17 to 25% of volatile matter in carbon material is suitable to achieve the highest surface area during activation, indicating that high operating temperature produces material appropriate for activation. In order to assess the extent of carbonization, FT/IR analyzation, a technique that provides information about chemical bonding and chemical composition of material, was conducted for char obtained from PET carbonization.

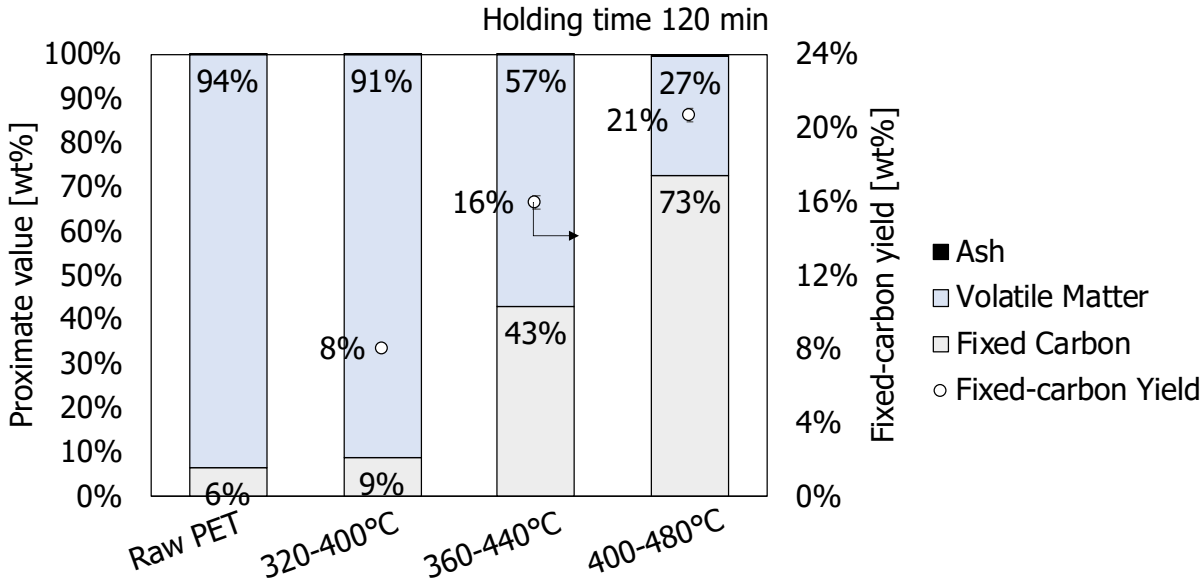

Figure 4-7: Proximate value of char obtained from PET carbonization at 320-400°C, 360-440°C and 400-480°C at constant holding time 120 min.

Table 4-5: Elemental composition of char obtained from PET carbonization at 320-400°C, 360-440°C and 400-480°C at constant holding time 120 min.

	Ultimate Analysis[a] [wt%]				HHV[a]
	C%	H%	N%	O%	[MJ/kg]
Raw PET	61.8	4.0	0.3	33.9	23.61
320-400°C	67.1	3.9	0.4	28.6	25.62
360-440°C	81.1	4.5	0.5	13.9	32.64
400-480°C	89.3	4.4	0.4	5.8	35.70

[a]:Dry basis; Data obtained from CHN analysis had 0.3% error.

The absorption bands and corresponding vibrational modes from FT/IR spectrum of PET samples are summarized in **Table 4-6**. The IR absorption spectrum of PET is as follows: The adsorption peak at wave number 2969 cm^{-1} (②) shows the asymmetry stretching of C-H of the methylene in ethylene glycol segment. Carbonyl group (C=O) is located at wave number 1730 cm^{-1} (④) and is one of the strongest IR absorption, making it most suitable for the indication of conversion of PET to char. The absorption peak at wave number 1577 cm^{-1} (⑤) shows the stretching vibration of phenyl ring (C=C) while absorption peak at wave number 1504 cm^{-1} (⑤) shows the bending vibration of phenyl ring (C=C). The absorption peaks at wave numbers 1453 cm^{-1} and 1342 cm^{-1} (⑥) show the bending and wagging vibration of methylene (C-H) in the ethylene glycol segment while absorption peak at wave number 1410 cm^{-1} (⑥) shows the stretching and bending vibration of C-C of aromatic skeleton. Absorption peak at 1240 cm^{-1} (⑦) shows the stretching vibration of C-O of carboxylic acid in terephthalate group. The absorption peak at 1096 cm^{-1} (⑧) shows the symmetric stretching vibration of C-O of ethylene glycol.

FT/IR spectra of char obtained from PET carbonization at 320-400°C, 360-440°C and 400-480°C at constant holding time 120 min are shown in **Figure 4-8**. From the results, it can be seen that char obtained from low operating temperature at 320-400°C shows similar FT/IR spectra as PET, indicating the lack of progression of carbonization reaction due to insufficient heat and energy supply, thus retaining most of the PET structure in the char residue. The increase of operating temperature shows rapid change in FT/IR spectra. In moderate operating temperature at 360-440°C, C=O and C-O of carboxylic group slightly retained in the structure (#④, #⑥ and #⑦) while no peak was shown for C-H of the methylene in ethylene glycol segment (#②). This explains the detection of CO, CO_2 and methane gas during gas analyzation, which will be discussed later in this section. Char obtained from PET carbonization at high operating temperature 400-480°C had little to almost no remaining structure of PET. From here on, char with no remaining structure of PET based on the FT/IR spectra as well as high fixed-carbon content ($\%fC$ > 70%) indicates the complete carbonization of PET.

Table 4-6: A summary of the absorption bands and the corresponding vibrational modes from FT/IR spectrum of PET.

#	Absorption bands (cm^{-1})	Bands for PET
①	3432	O-H group (hydroxyl)
②	3054, 2969, 2908	Asymmetrical stretch of C-H
③	2350	Axial symmetrical deformation of CO_2
④	1730	Stretching of C=O of carboxylic acid group
⑤	1577, 1504	Vibrations aromatic skeleton with stretching C=C
⑥	1453, 1410, 1342	Stretching of the C-O group deformation of the O-H group and bending/wagging vibration modes of the ethylene glycol segment
⑦	1240, 1124	Terephthalate group ($OOCC_6H_4$-COO)
⑧	1096, 1050	Methylene group and vibrations of the ester C-O bond
⑨	972, 872, 848	Aromatic rings, 1,2,4,5; Tetra replaced
⑩	1960, 795	Vibrations of adjacent 2 aromatic H in p-substituted compounds and aromatic bands
⑪	712	Interaction of polar ester groups and benzene rings

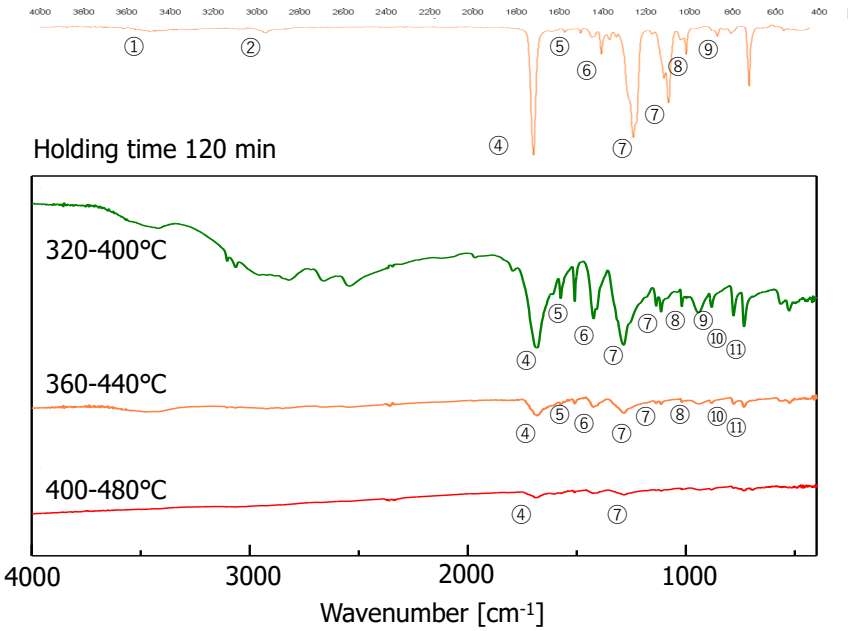

Figure 4-8: Overlay of FT/IR spectra of char obtained from different operating temperatures.

Characteristics of wax

Table 4-7 shows the ultimate value and the HHV of wax residue for each condition. It can be seen that %C, %H and %O for wax obtained from all three runs show the same composition; average 71.5% for %C, 5.6% for %H and 22.6% for %O. Based on the results obtained, it can be speculated that oxygen from PET polymer had volatilized to form oxygenated chemical compounds in the wax phase, as seen in the high concentration of %O in wax compared to char. One of the reasons for this is that in the thermal decomposition of PET, PET decomposes into 2 same radicals through the C-C homolytic cleavage to be converted into benzoic acid methyl ester, as detected in the wax with GC/MS. The high viscosity and solidification of wax at low temperature (<200°C) leads to complication of reactor operation due to the clogging of pipes and heat exchanger (Shioya et al., 2005; Wan Ho, 2015). However, the high HHV of wax may be applicable for use as fuel during the carbonization process, which was assessed and discussed further in Chapter 8.

Table 4-7: Elemental composition of wax residue obtained from PET carbonization at 320-400°C, 360-440°C and 400-480°C at constant holding time 120 min.

	Ultimate Analysis[a] [wt%]				HHV[a]
	C%	H%	N%	O%	[MJ/kg]
320-400°C	71.0	5.8	0.4	22.8	27.06
360-440°C	71.1	5.5	0.3	23.1	27.13
400-480°C	72.2	5.6	0.3	21.9	26.62

[a]:Dry basis; Data obtained from CHN analysis had 0.3% error.

Figure 4-9 shows the GC/MS spectra of wax product obtained from different operating temperatures at 320-400°C, 360-440°C and 400-480°C with constant holding time at 120 min. The main organic compounds of wax identified using GC/MS include aromatic compounds: benzene, toluene, ethylbenzene, p-xylene, biphenyl, fluorene; aromatic ketone: acetophenone, benzaldehyde; and carboxylic acids: benzoic acid, 4-methylbenzoic acid, 4-ethylbenzoic acid. It was observed that benzoic acid is the main component of wax. In addition, PAH compounds such as biphenyl and fluorene were detected for wax obtained from carbonization at higher temperatures.

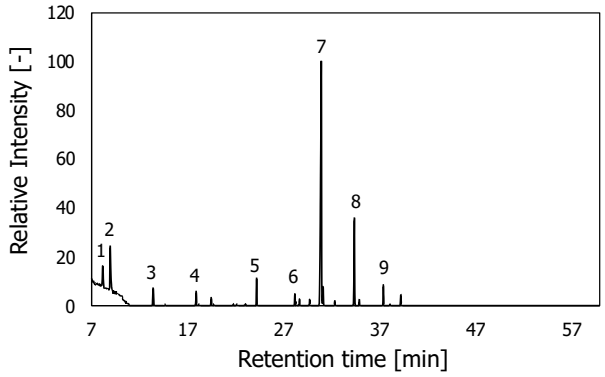

1. Benzene
2. Furan, 2,3-dihydro
3. Toluene
4. Ethylbenzene
5. Benzaldehyde
6. Benzaldehyde, 2-methyl-
7. Benzoic Acid
8. Benzoic acid, 4-methyl-
9. 4-Ethylbenzoic acid

(a) 320-400°C, 120 min

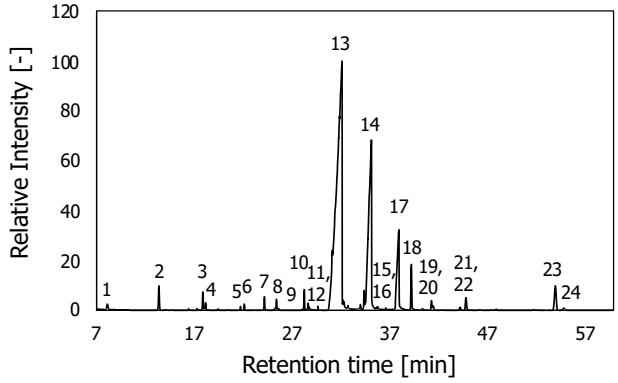

1. Benzene
2. Toluene
3. Ethylbenzene
4. p-Xylene
5. n-Propylbenzene
6. o-Ethylmethylbenzene
7. Benzaldehyde
8. Benzamide
9. 1-Phenyl-1,2-propanediol
10. Benzaldehyde, 4-methyl
11. Benzaldehyde, 4-methyl
12. o-Ethylphenol
13. Benzoic Acid
14. Benzoic Acid, 4-methyl
15. Naphthalene, 2-methyl
16. Naphthalene, 2-methyl
17. p-Ethylbenzoic acid
18. Biphenyl
19. Benzamide
20. Benzoic acid, 4-propyl-
21. 1,1′-Biphenyl, 4-methyl
22. 1,1′-Biphenyl, 4-methyl
23. Fluorene
24. 9H-Fluorene

(b) 360-440°C, 120 min

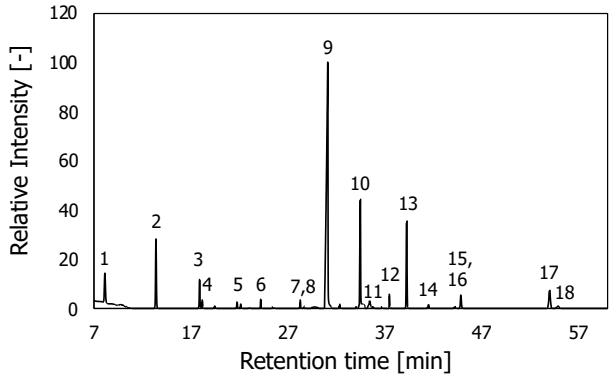

1. Benzene
2. Toluene
3. Ethylbenzene
4. p-Xylene
5. Acetophenone
6. Benzaldehyde
7. Acetophenone
8. Benzaldehyde, 4-methyl
9. Benzoic Acid
10. Benzoic acid,4-methyl
11. Naphthalene, 1-methyl
12. p-Ethylbenzoic acid
13. Biphenyl
14. Diphenylmethane
15. 1,1′-Biphenyl, 3-methyl
16. 1,1′-Biphenyl, 4-methyl
17. Fluorene
18. 9-Benzylfluorene

(c) 400-480°C, 120 min

Figure 4-9: GC/MS spectra of wax product obtained from different operating temperatures at 320-400°C, 360-440°C and 400-480°C with constant holding time.

Properties of gaseous product

Figure 4-10 shows the gas composition whereas **Figure 4-11** shows the hydrocarbon composition of gaseous products obtained from PET carbonization under operating temperatures 320-400°C, 360-440°C and 400-480°C at constant holding time 120 min, respectively. Note that the unit is in grams of gaseous component per grams of initial feedstock.

Comparing the composition of gas collected for low operating temperature at 320-400°C to high operating temperature at 400-480°C, it was observed that the total gas collected increased with increasing operating temperature. For low operating temperature at 320-400°C, little to almost no gas was emitted due to the lack of decomposition of feedstock. For all runs, CO_2 makes up the most gas emitted, followed by CO. In all cases, little to almost no hydrogen was detected.

In the case of hydrocarbons emitted, it can be seen that total hydrocarbon was approximately 4.0 wt% for moderate operating temperature at 360-440°C and 3.8 wt% for high operating temperature at 400-480°C. One interesting finding about this result is that the composition of methane, ethylene and ethane was completely different for gaseous products obtained from moderate operating temperature at 360-440°C and high operating temperature at 400-480°C. For moderate operating temperature at 360-440°C, ethylene makes up most of the total hydrocarbons emitted, with 3.0 wt% ethylene, followed by 0.9 wt% methane and 0.1 wt% ethane. On the other hand, for high operating temperature at 400-480°C, methane makes up most of the total hydrocarbons emitted, with 2.1 wt% methane, 1.3 wt% of ethylene and 0.4 wt% of ethane. This indicates the progression of thermal cracking of hydrocarbons C2 and above to methane at high operating temperature.

Overall, the progression of carbonization of PET leads to the production of CO_2 and CO, which makes up most of the gas emitted.

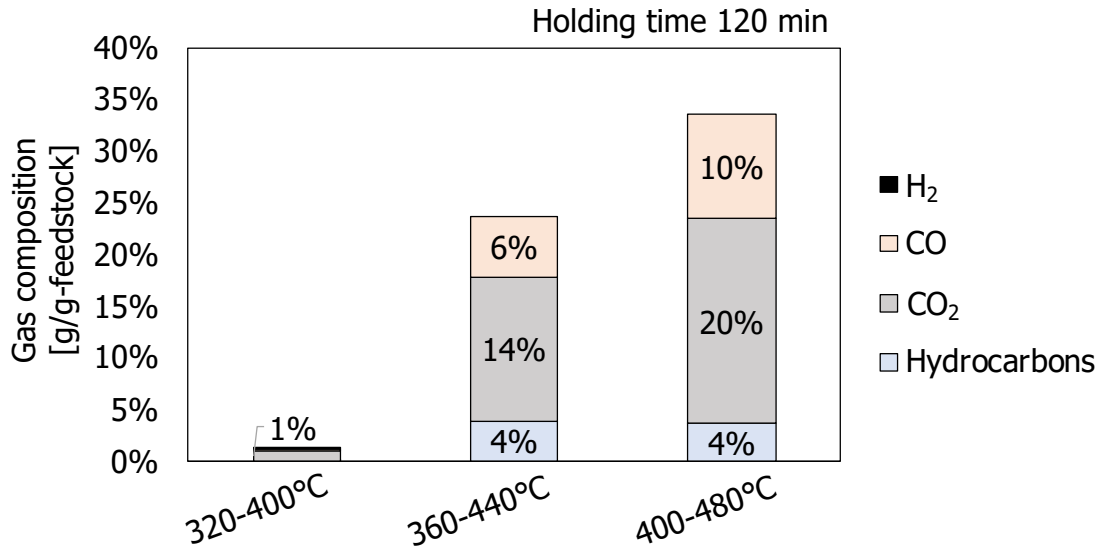

Figure 4-10: Gas composition of gaseous products obtained from PET carbonization at 320-400°C, 360-440°C and 400-480°C at constant holding time 120 min.

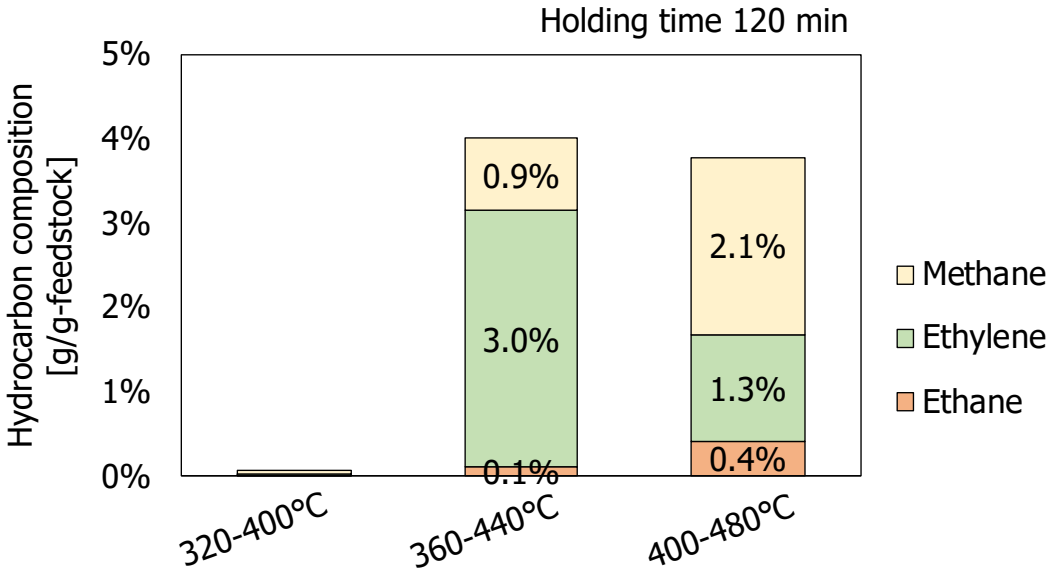

Figure 4-11: Hydrocarbon composition of gaseous products obtained from PET carbonization at 320-400°C, 360-440°C and 400-480°C at constant holding time.

4.3.3.2 Effect of holding time on carbonized product

Product composition

Figure 4-12 shows the composition yield of char, wax and gas for operations under different holding times at constant temperature of 360-440°C and 400-480°C. Note that wax was taken as the balance from char and gas due to the large amount of residual wax that was solidified in the pipes of the reactor. In a series of different holding time at moderate operating temperature 360-440°C, char yield was obtained as follows: 37 wt% at holding time 120 min and 34 wt% at holding time 240 min. On the other hand, in a series of different holding time at high operating temperature 400-480°C, char yield was obtained in the range 28-30 wt% for all holding time. No evident difference for the composition of product was observed under different holding time for both operating temperatures.

Characteristics of char

Figure 4-13 shows the proximate value of char and the fixed-carbon yield for operations under different holding times, at moderate operating temperature of 360-440°C and high operating temperature of 400-480°C. Similar to previous findings, char from all runs had little to almost no moisture and ash. At moderate operating temperature of 360-440°C, increase of fixed carbon content and consequent decrease of volatile matter was observed when holding time was prolonged. This indicates that under moderate operating temperature, the heat supply was insufficient at holding time 120 min and carbonization progressed during increased holding time. As a result, fixed-carbon yield increased from 16 wt% to 18 wt%. On the other hand, at high operating temperature of 400-480°C, slight increase in fixed carbon content whereas slight decrease in volatile matter was observed. However, the fixed-carbon yield showed no evident changes and was approximately 21 wt% for all runs. This indicates that, at high operating temperature, carbonization was complete at holding time as short as 30 min and increase of holding time had no evident effect on the composition of product.

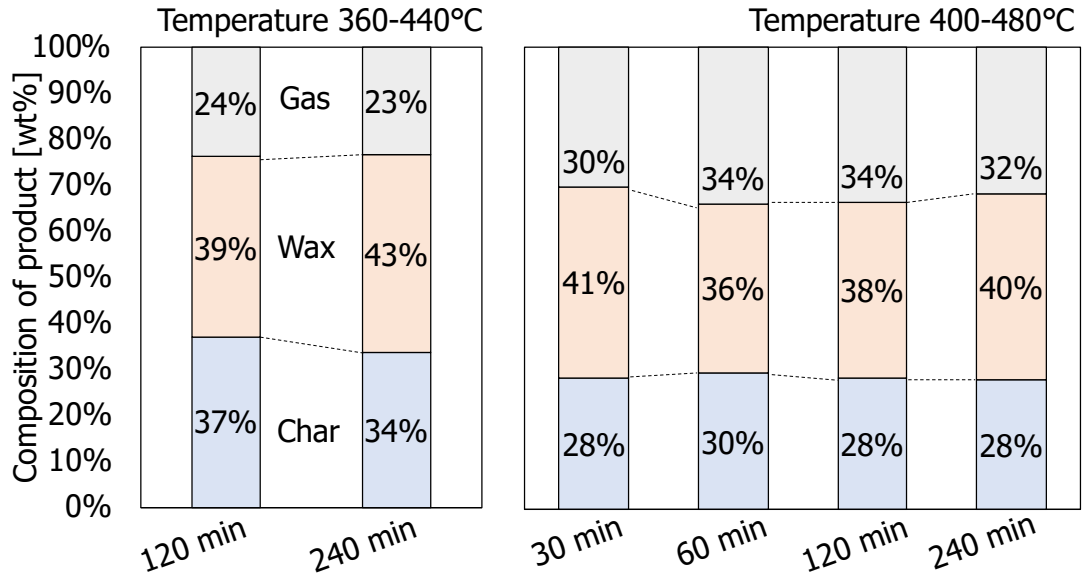

Figure 4-12: Composition of char, wax and gas for operations under different holding times, at constant temperatures of 360-440°C and 400-480°C.

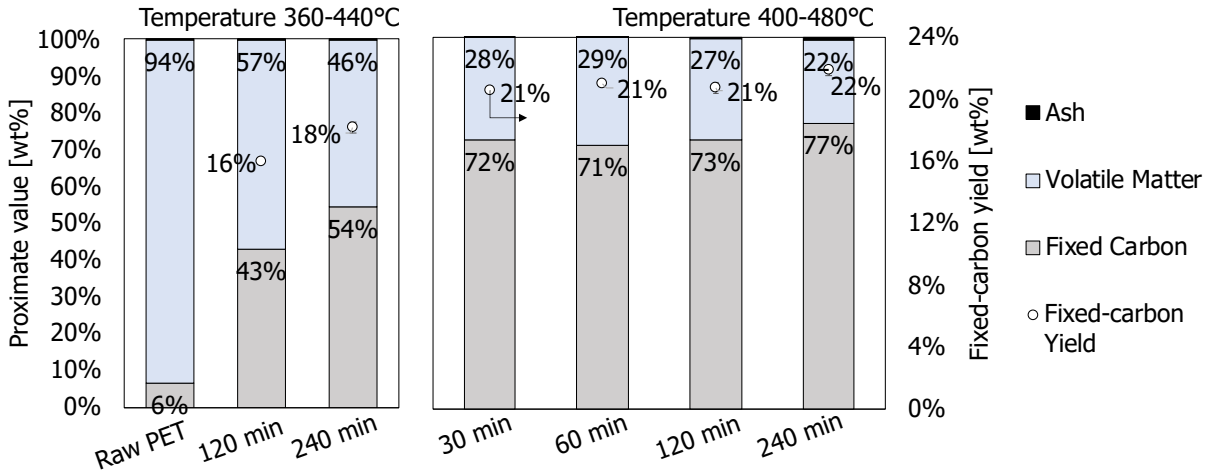

Figure 4-13: Proximate value of char obtained from operations under different holding times, at constant temperatures of 360-440°C and 400-480°C.

Table 4-8 shows the elemental composition and the HHV of char for each condition. At moderate operating temperature of 360-440°C, continual increase of %C from 75.5 wt% at 120 min to 81.1 wt% at 240 min was observed. Inversely, continual decrease of %O from 20.2 wt% at 120 min to 13.9 wt% at 240 min was observed. %H had no evident changes. The HHV increased with increasing %C and decreasing %O. This indicates that under moderate operating temperature, the carbonization process continues to progress at prolonged holding time until carbonization is completed. At high operating temperature of 400-480°C, it was observed that %C drastically increased from 61.8 wt% of raw PET to 87.9 wt% at 30 min, followed by slight increase to reach 90.6% at 240 min. Inversely, %O drastically decreased from 33.9 wt% of raw PET to 7.5 wt% at 30 min, followed by slight decrease to reach 4.6 wt% at 240 min. The minimum %O was observed for char obtained from 400-480°C at holding time 240 min, with corresponding maximum measured HHV of 36.20 MJ/kg. The results further confirm that, at high operating temperature, complete carbonization was achieved at holding time as short as 30 min to obtain high carbon content char and increase of holding time had no evident effect on the composition of product obtained.

Figure 4-14 shows the FT/IR spectra of char obtained from PET carbonization at high operating temperature of 400-480°C at holding time of 60 min, 120 min and 240 min. From the results, slight peaks for vibration of C-H of the methylene in ethylene glycol segment (#②) and interaction C-H of benzene ring and ester group (#⑪) was observed for char obtained at holding time 60 min. For chars obtained at holding time 120 min and 240 min, functional groups of PET were not detected. Although char with high carbon content was produced at holding time as short as 30 min, increasing holding time of operation produces char with no functional groups detected on the surface.

Overall, as for the carbonization at 400-480°C, increasing the retention time of operation had no significant effect on the char yield, indicating the complete carbonization of feedstock at the early stage of the operation at holding time as short as 30 min.

Table 4-8: Ultimate value of char obtained from operations under different holding times, at constant temperatures of 360-440°C and 400-480°C.

	Ultimate Analysis[a] [wt%]				HHV[a]
	C%	H%	N%	O%	[MJ/kg]
Raw PET	61.8	4.0	0.3	33.9	23.61
360-440°C					
120 min	75.5	4.0	0.3	20.2	28.94
240 min	81.1	4.5	0.5	13.9	32.64
400-480°C					
30 min	87.9	4.2	0.4	7.5	35.40
60 min	88.4	4.4	0.5	6.7	35.85
120 min	89.3	4.4	0.4	5.8	35.69
240 min	90.6	4.2	0.6	4.6	36.20

[a]:Dry basis; Data obtained from CHN analysis had 0.3% error.

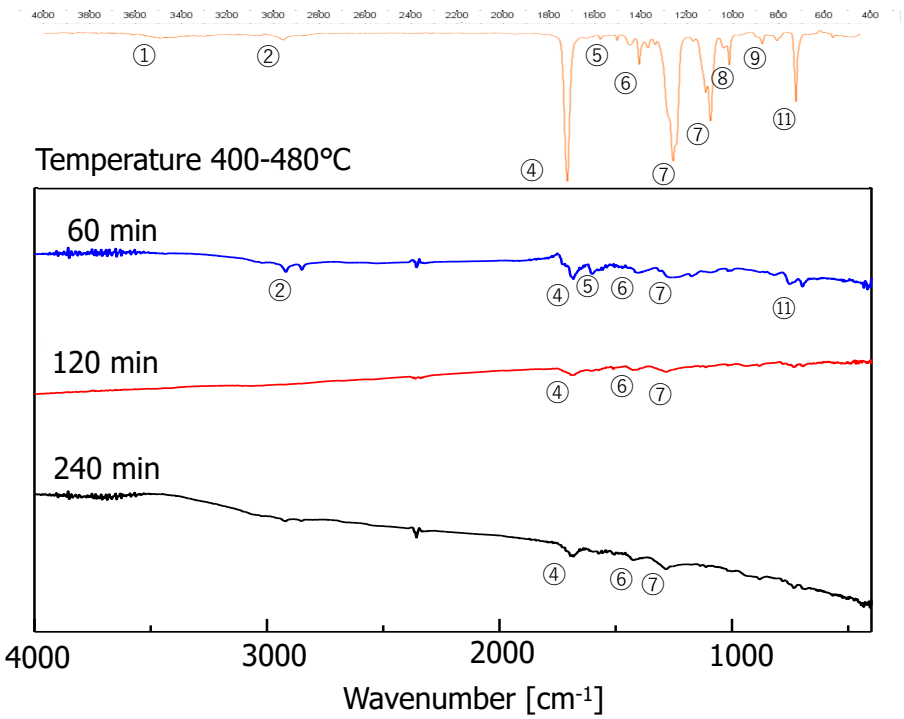

Figure 4-14: Overlay of FT/IR spectra of char obtained from different holding times at 60 min, 120 min and 240 min with constant operating temperature at 400-480°C.

Characteristics of wax

Table 4-9 shows the elemental composition and the HHV of wax obtained from operations under different holding time, at constant temperature of 360-440°C and 400-480°C. The %C, %H and %O for wax obtained from all operation were approximately constant, ranging from 61.9 wt% to 72.2 wt% for %C, 4.6 wt% to 5.8 wt% for %H, and 21.9 wt% to 33.1 wt% for %O. Additionally, the HHV of wax measured was high, indicating the possibility of usage of wax as fuel. From the results, it is evident that the increase of holding time did not affect the composition and yield of wax.

Table 4-9: Ultimate value of wax obtained from operations under different holding times, at constant temperatures of 360-440°C and 400-480°C.

	Ultimate Analysis[a] [wt%]				HHV[a]
	C%	H%	N%	O%	[MJ/kg]
360-440°C					
120 min	71.1	5.5	0.3	23.1	27.13
240 min	70.1	5.3	0.3	24.3	28.15
400-480°C					
30 min	69.9	5.2	0.4	24.5	28.74
60 min	71.1	5.4	0.3	23.2	26.77
120 min	72.2	5.6	0.3	21.9	27.62
240 min	61.9	4.6	0.3	33.1	22.53

[a]:Dry basis; Data obtained from CHN analysis had 0.3% error.

Figure 4-15 shows the GC/MS spectra of wax product obtained from different operating temperature at 320-400°C, 360-440°C and 400-480°C with constant holding time at 120 min. The main organic compounds of wax identified did not differ much from that of section 4.3.2.1. This indicates that prolongation of holding time does not largely affect the product of wax.

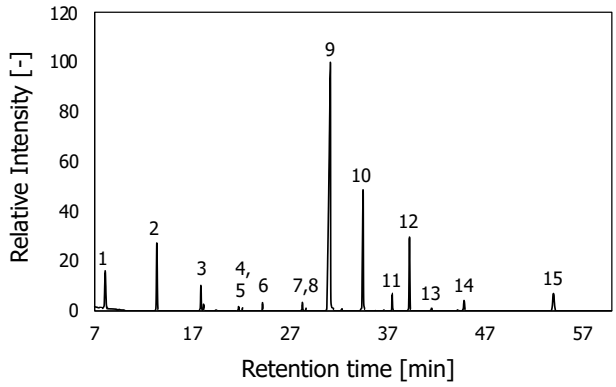

1. Benzene
2. Toluene
3. p-Xylene
4. n-Propylbenzene
5. Acetophenone
6. Benzaldehyde
7. Acetophenone
8. Benzaldehyde, 4-methyl-
9. Benzoic acid
10. Benzoic acid, 4-methyl-
11. 4-Ethylbenzoic acid
12. Biphenyl
13. Diphenylmethane
14. 1,1′-Biphenyl, 4-methyl-
15. Fluorene

(a) 60 min

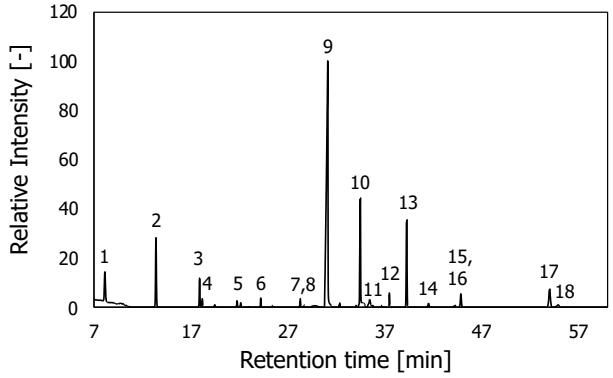

1. Benzene
2. Toluene
3. Ethylbenzene
4. p-Xylene
5. Acetophenone
6. Benzaldehyde
7. Acetophenone
8. Benzaldehyde, 4-methyl
9. Benzoic Acid
10. Benzoic acid,4-methyl
11. Naphthalene, 1-methyl
12. p-Ethylbenzoic acid
13. Biphenyl
14. Diphenylmethane
15. 1,1′-Biphenyl, 3-methyl
16. 1,1′-Biphenyl, 4-methyl
17. Fluorene
18. 9-Benzylfluorene

(b) 120 min

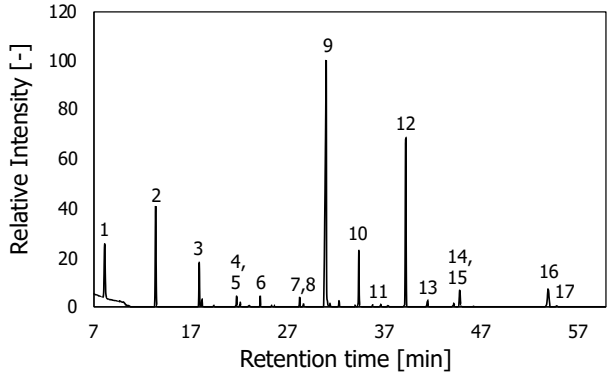

1. Benzene
2. Toluene
3. Ethylbenzene
4. Benzene, propyl
5. Acetophenone
6. Benzaldehyde
7. Acetophenone
8. Benzaldehyde, 4-methyl
9. Benzoic Acid
10. Benzoic acid,4-methyl
11. Naphthalene, 1-methyl
12. Biphenyl
13. Diphenylmethane
14. 1,1′-Biphenyl, 3-methyl
15. 1,1′-Biphenyl, 4-methyl
16. Fluorene
17. 9-Benzylfluorene

(c) 240 min

Figure 4-15: GC/MS spectra of wax product obtained from different holding times, at constant temperature of 400-480°C.

Properties of gaseous product

Figure 4-16 shows the gas composition whereas **Figure 4-17** shows the hydrocarbon composition of gaseous products obtained from PET carbonization under different holding times, at constant temperature of 360-440°C and 400-480°C, respectively. Note that the unit is in grams of gaseous component per grams of initial feedstock. At moderate operating temperature of 360-440°C, the composition of gas collected remained unchanged when holding time was prolonged, where CO_2 makes up the most gas emitted, followed by CO and hydrocarbons. No hydrogen was detected. On the other hand, the total gas collected was higher at high operating temperature of 400-480°C, and the composition of gas collected remained constant when holding time was prolonged. Similarly, no hydrogen was detected.

In the case of hydrocarbons emitted, at moderate operating temperature of 360-440°C, total hydrocarbons were the highest at approximately 4.0 wt% at holding time 120 min, where ethylene was the main composition of hydrocarbons. At prolonged holding time of 240 min, evident decrease of ethylene and increase of methane were observed. This indicates that, with prolonged holding time, thermal cracking of C2 hydrocarbons and above has progressed. The final product of thermal cracking of C2 hydrocarbons and above was not confirmed. However, it was speculated that the thermal cracking of C2 hydrocarbons and above reacted with low molecular weight volatile fragments, and that formation of methane was dominant with the progression of reaction. At high operating temperature of 400-440°C, composition of hydrocarbon showed no evident changes under prolonged holding time, where methane was the main component, followed by ethylene and ethane.

Based on the overall results obtained, the relationship between thermal cracking of hydrocarbons and char formation was unclear. In other words, despite the increased formation of methane from ethylene with prolonged retention time, there was no significant increase of char. Therefore, based on the current findings, thermal cracking of hydrocarbons might only have little to no contribution to the deposition of carbon on solid surface for aromatic formation of char.

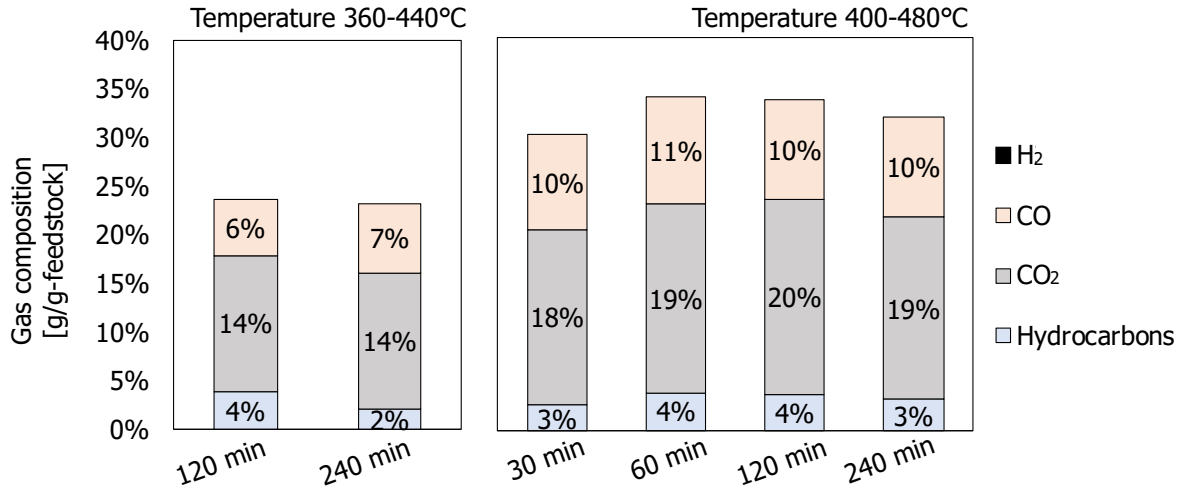

Figure 4-16: Gas composition of gaseous products obtained from PET carbonization under different holding times, at constant temperatures of 360-440°C and 400-480°C.

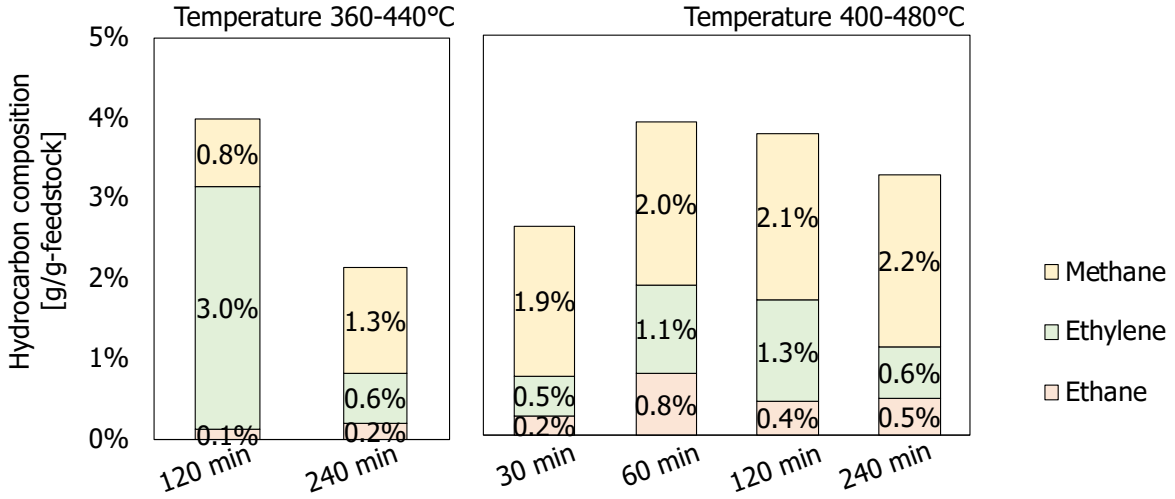

Figure 4-17: Hydrocarbon composition of gaseous products obtained from PET carbonization under different holding times, at constant temperatures of 360-440°C and 400-480°C.

4.3.3 Conclusions: Effect of operating conditions on carbonization of PET

The effects of operating temperature on carbonization of PET were studied and based on the experimental results, the conclusions were drawn as follows:

1) Carbonization of PET at operating temperature as high as 400-480°C produced char with high carbon content.
2) PET proceeded through a distinct melt phase during the operation, and char produced was brittle and hard whereas wax produced hardens at low temperature.
3) CO and CO_2 were the main components of gaseous product of PET carbonization.
4) Char with high carbon content showed no remaining structure of PET based on the FT/IR spectra.
5) Complete carbonization of PET was described to produce high fixed-carbon content ($\%fC$ > 70%) char with no remaining structure of PET.

The effects of holding time on carbonization of PET were studied and summarized as follows:

1) At moderate operating temperature (360-440°C), carbonization of PET progressed with increasing holding time from 120 min to 240 min, indicating the progress of carbonization.
2) At high operating temperature (400-480°C), increasing of holding time above 30 min had no evident effect on the composition and characteristics of char, wax and gaseous product.
3) Prolongation of holding time of operation had no evident effect on the product composition once the carbonization was complete.

4.4 Effect of steam as medium on carbonization of PET

In this study, experiments in steam condition were conducted. Water was chosen as the added solvent in this study due to the condition of the "real-world" feedstock, in which water residue is often found in the insides of waste PET bottles. The findings of this section determine the necessity to dry the feedstock prior to carbonization.

4.4.1 Experimental set-up and feedstock preparation

Clear PET bottles purchased from Asahi Soft Drinks Co., Ltd were prepared with minimal treatment. Here, deionized water was introduced into the carbonization system at the initial stage of the experiment to be heated into steam. Water was supplied in the ceramic crucible and was in direct contact with the feed sample as shown in **Figure 4-18** before heated up to desired temperature. **Table 4-10** shows the detailed experimental conditions. Analyzation methods are described in detail in Chapter 3.

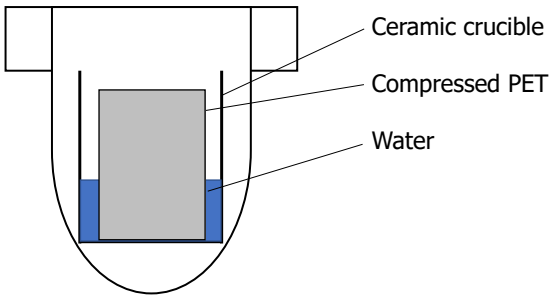

Figure 4-18: Schematic layout of autoclave batch reactor for carbonization under steam medium.

Table 4-10: Parameters used in determining the effects of reaction medium and holding time on PET carbonization.

Variables in operation	Units	Operating parameter			
Medium type	[-]	Water heated to steam			
Heating rate	[°C/min]	1.0			
Feedstock loading	[g]	70-75			
Water to feedstock ratio	[wt%]	0.12:1	0.25:1		0.5:1
Operating temperature	[°C]	400-480			
Holding time	[min]	30	60	120	240

4.4.2 Results and discussion

4.4.2.1 Effect of water to feedstock ratio on carbonized product

Product composition

Figure 4-19 shows the composition yield of char, wax and gas for operations under different water to feedstock ratio at constant holding time of 120 min. Note that wax was taken as the balance from char and gas due to the large amount of residual wax that was solidified in the pipes of the reactor. Also, the results of carbonization at nitrogen medium, 400-480°C and holding time of 120 min from section 4.3.2 was used as comparison data for water to feedstock ratio 0:1. In a series of water to feedstock ratio, it can be seen that composition of product differed in the presence of steam. Char yield exhibited sharp decrease when water was introduced into the reaction, however, it gradually increased with increasing water to feedstock ratio. It is well noted that gas yield decreased drastically whereas wax composition increased when water was introduced into the carbonization reaction.

Characteristics of char

Figure 4-20 shows the magnification using SEM of char surface obtained from carbonization of PET at nitrogen and steam medium (water:feedstock=0.25:1) at operating temperature of 400-480°C and holding time 120 min. From the surface observations, it is evident that there are large differences of surface morphology of char carbonized at nitrogen medium compared to steam medium. Char produced under nitrogen condition shows flaky surface close to ceramic material. This explains the brittle nature and glassy appearance of char produced under this condition. Additionally, the distinctive shape of char may have been due to the rapid volatilization of volatile matter (gas/wax), leaving carbon residue in the form of char. On the other hand, char produced under steam condition showed aggregation of fiber-like or needle-like particles, similar to woody biomass. The reason for the needle-like structure in char may be due to the hydrolysis of PET when steam was present in the reaction.

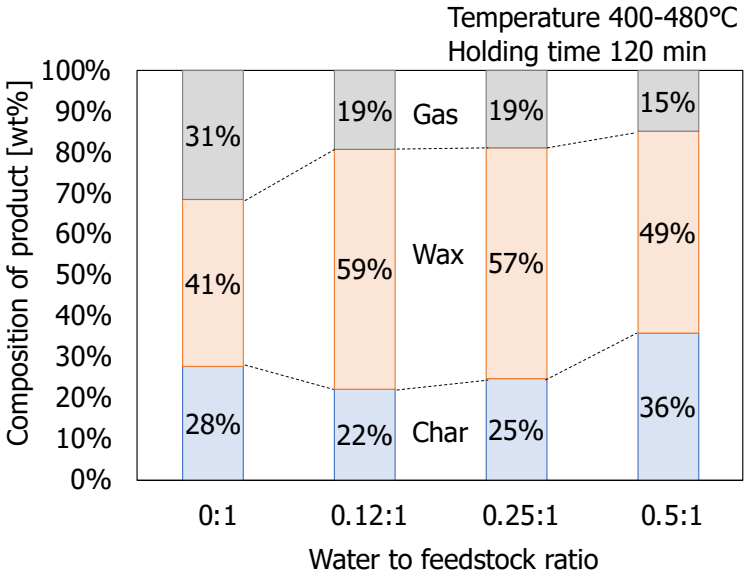

Figure 4-19: Composition of char, wax and gas for operations under different water to feedstock ratios at constant holding time of 120 min.

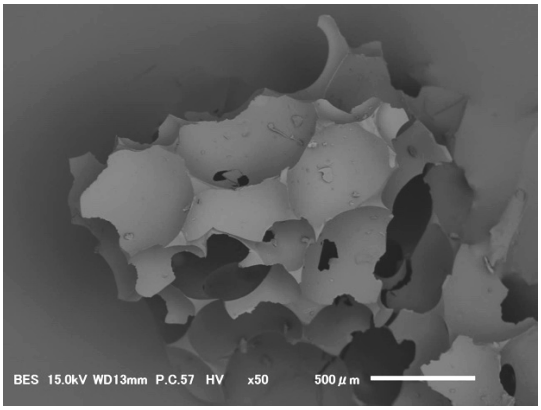

(a) Nitrogen (x50)

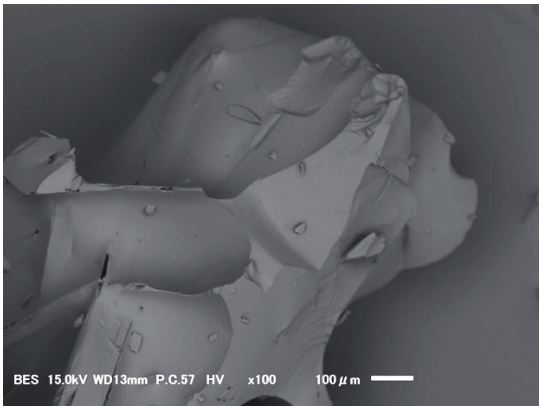

(b) Nitrogen (x100)

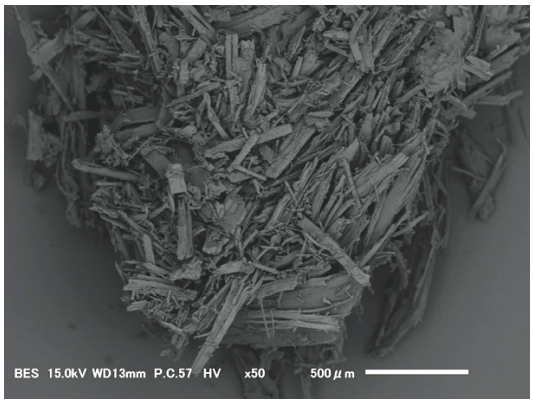

(c) Steam (x50)

(water:feedstock=0.25:1)

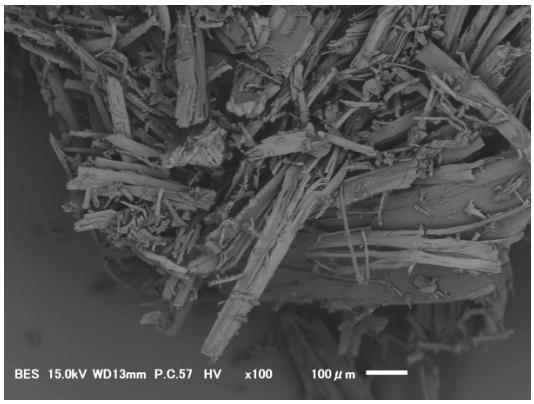

(d) Steam (x100)

(water:feedstock=0.25:1)

Figure 4-20: SEM images of char surface obtained from carbonization of PET at (a,b) nitrogen and (c,d) steam medium.

Figure 4-21 shows the proximate value of char and the fixed-carbon yield for each condition. Char obtained from all operating conditions had little to almost no moisture, indicating the hydrophobicity of the material. However, compared to carbonization of PET under nitrogen displacement, conducting experiment with steam drastically increased the volatile matter of char. As a result, the fixed-carbon yield sharply decreased from 20.7 wt% at nitrogen condition to 4.9 wt% at water to feedstock ratio 0.5:1. The presence of steam during pyrolysis was reported to significantly increase the hydrolysis reaction of PET to produce low molecular weight volatile compounds such as terephthalic acid and benzoic acid (Grause et al., 2004; Diaz-Silvarrey et al., 2018). It is now speculated that the PET hydrolysis is the main factor for the hindrance of progress of carbonization, thus forming char with high volatile matter.

Table 4-11 shows the elemental composition and the higher heating value of char for each condition. It was observed that HHV of char decreased with increasing water to feedstock ratio. The presence of steam in the operation led to the lack of carbonization due to the progression of hydrolysis, thus forming char with high volatile matter. As a result, the high %O and %H content led to the decrease of HHV of char.

FT/IR analyzation was conducted for char obtained from PET carbonization under water to feedstock 0.25:1 and 0.5:1 in order to assess the extent of carbonization as shown in **Figure 4-22**. Unlike the FT/IR spectra of char obtained from nitrogen condition, FT/IR spectra of char obtained from steam condition showed similar FT/IR spectra as raw PET, even though the carbonized char showed blackish carbon residue. This indicates that in the presence of steam, hydrolysis reaction was dominant so that the chemical structures of PET retain in the char. This explains the high volatile content and high oxygen content of char.

As a summary, carbonization of PET in the presence of steam hinders the progression of carbonization due to the dominance of hydrolysis reaction, thus producing char with high volatile content, in addition to retaining most of the chemical structures of PET in char.

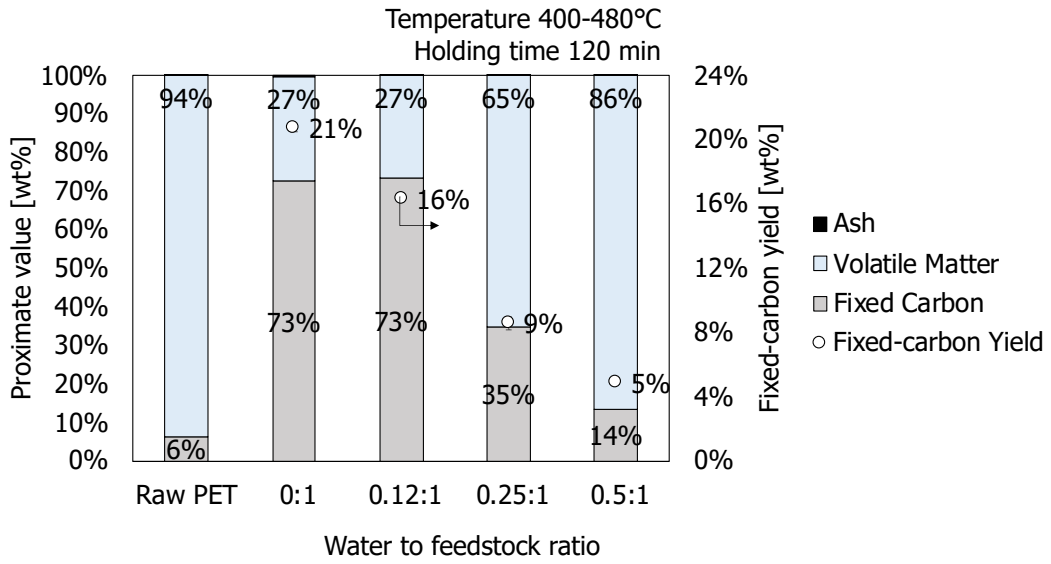

Figure 4-21: Proximate value of char obtained from PET carbonization under different water to feedstock ratios at constant holding time of 120 min.

Table 4-11: Elemental composition of char obtained from PET carbonization under different water to feedstock ratios at constant holding time of 120 min.

	Ultimate Analysis[a] [wt%]				HHV[a]
	C%	H%	N%	O%	[MJ/kg]
Raw PET	61.8	4.0	0.3	33.9	23.61
0:1	89.3	4.4	0.4	5.8	35.69
0.12:1	90.7	4.4	1.1	3.8	36.19
0.25:1	73.1	4.0	0.3	22.6	28.22
0.5:1	63.0	3.8	0.3	32.9	23.38

[a]:Dry basis; Data obtained from CHN analysis had 0.3% error.

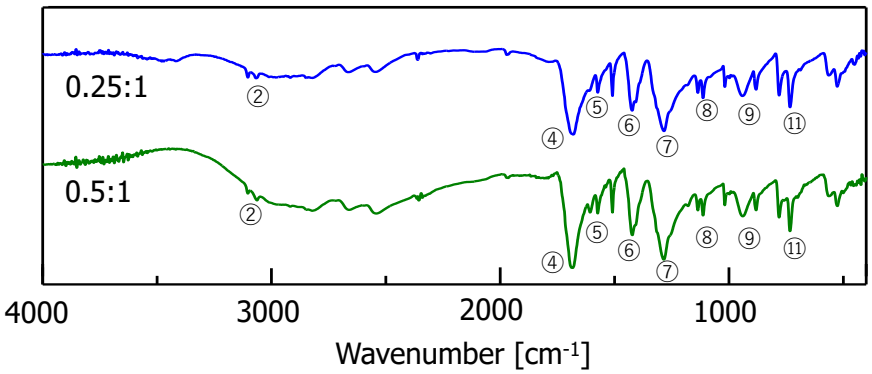

Figure 4-22: FT/IR spectra of char obtained from PET carbonization under water to feedstock ratios 0.25:1 and 0.5:1.

Characteristics of wax

GC/MS results of wax obtained from carbonization in steam medium showed no distinct difference from that of carbonization in nitrogen medium; that is benzoic acid, 4-methylbenzoic acid (p-toluic acid), biphenyl and fluorene were mostly detected. In order to examine the extent of hydrolysis of PET in the presence of steam, HPLC analysis of wax was conducted and presented in **Figure 4-23**.

High composition of benzoic acid was obtained during carbonization of PET in steam condition. This further affirms the effect of steam which led to the hydrolysis reaction of PET during carbonization. Yoshioka's group (Kumagai et al., 2013; 2014; 2015) has intensively studied the effects of steam on the decomposition of PET. For one, Kumagai et al. (2013) had studied the dominance between pyrolysis and hydrolysis reaction during thermal degradation of PET with gas flow at different steam concentration. They presented the schemes of pyrolysis and hydrolysis reactions as:

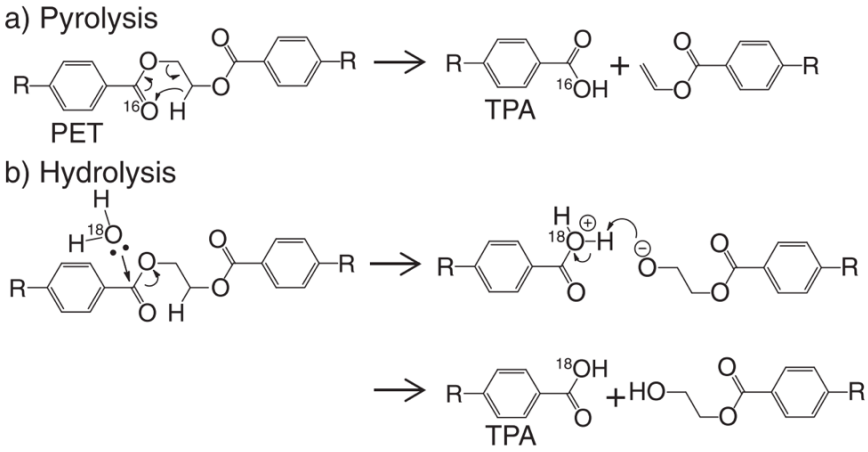

They reported that, by using an ^{18}O-labeled steam atmosphere ($H_2{}^{18}O$) at 100 vol% steam concentration and 400°C, PET was decomposed in which 74% of the ester bonds were pyrolyzed while 26% were hydrolyzed (Kumagai et al., 2013). In addition, terephthalic acid (TPA) was the main product of the steam reaction. This differs from current result, in which benzoic acid was the main product. One of the reasons is that Kumagai et al. (2013) had conducted their experiments in an open flow reactor with rapid heating rate, while current study was conducted in a closed batch reactor with slow heating rate of 1°C/min. It is speculated that the slow heating rate and closed system of current study led to the further decomposition of terephthalic acid to form low molecular weight volatile compound, that is benzoic acid. On the other hand, in a

flow reactor, terephthalic acid formation is highly associated with the C-O scission in the ester bond and also C-C bond in the PET structure. Therefore, the rapid thermal decomposition occurs to form terephthalic acid, and due to the rapid gas flow, terephthalic acid did not undergo demethanation to form methane and benzene.

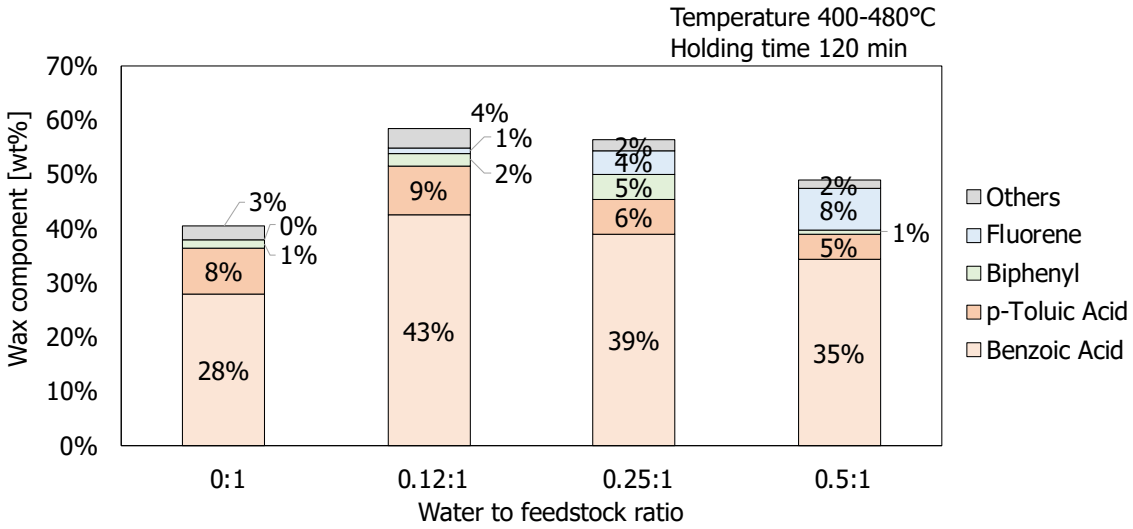

Figure 4-23: Composition of wax obtained using HPLC analysis from carbonization of PET under different water to feedstock ratios.

Properties of Gaseous Product

Figure 4-24 shows the composition of gaseous product obtained from PET carbonization under different water to feedstock ratio. The composition of CO and CO_2 decreased when steam was present in the system. It is highly speculated that the presence of steam may have prevented the rapid scission of C-O bonds in the ester group of PET to form CO and CO_2, which instead, led to the progression of benzoic acid production, leading to the decrease of CO and CO_2.

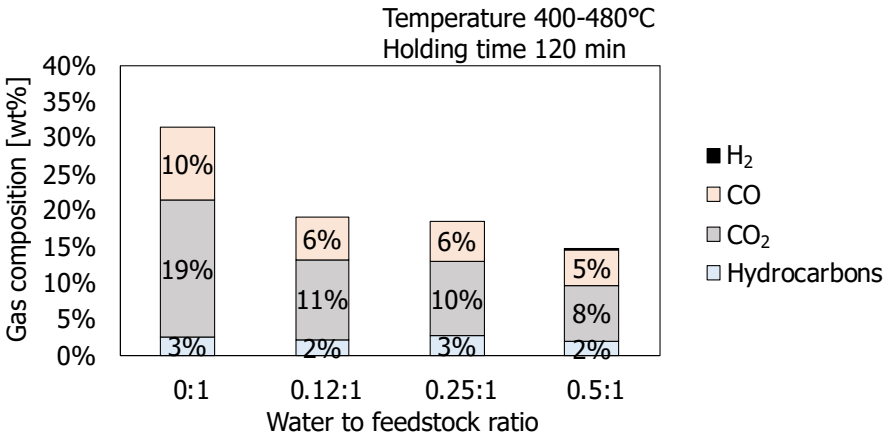

Figure 4-24: Composition of gaseous product obtained from PET carbonization under different water to feedstock ratios.

4.4.2.2 Effect of holding time under constant water to feedstock ratio

Product composition

Figure 4-25 shows the composition yield of char, wax and gas for operations conducted at different holding times under constant water to feedstock ratio of 0.25:1. Note that wax was taken as the balance from char and gas due to the large amount of residual wax that was solidified in the pipes of the reactor. It is well noted that increase of wax yield whereas decrease of char yield was evident during the increase of holding time when water was introduced into the carbonization reaction.

Characteristics of char

Figure 4-26 shows the proximate value of char and the fixed-carbon yield for operations under different holding times, under constant water to feedstock ratio of 0.25:1 at constant temperature of 400-480°C. It was observed that during carbonization under steam condition, increase of holding time led to the increase of fixed carbon content. As reported by Kumagai et al. (2013), hydrolysis and pyrolysis reaction progressed simultaneously during the thermal decomposition of PET in the presence of steam. In current case, it was speculated that hydrolysis reaction was dominant over carbonization (or pyrolysis) reaction in a closed batch reactor. Therefore, the presence of steam led to the hydrolysis of PET to produce benzoic acid, and consequently hindered the progression of carbonization. However, prolongation of holding time contributed to the progression of carbonization process, thus increasing the fixed carbon content of char, and consequently increased the fixed-carbon yield.

Table 4-12 shows the elemental composition and the HHV of char for each condition. It was observed that HHV of char increased with holding time due to the increasing carbon content of char when holding time was prolonged.

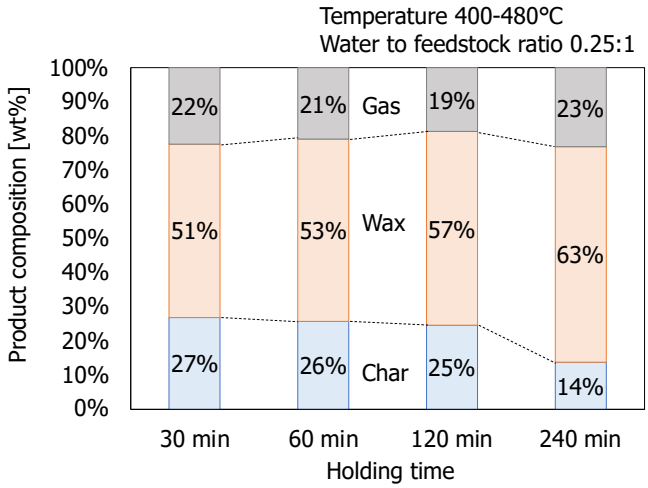

Figure 4-25: Composition of char, wax and gas for operations under different holding times, under constant water to feedstock ratio and temperature.

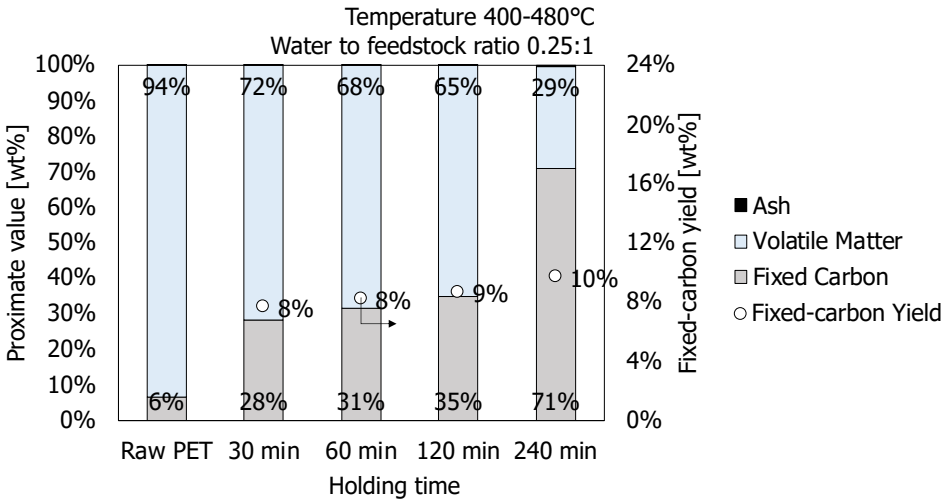

Figure 4-26: Proximate value of char and the fixed-carbon yield for operations under different holding times, constant water to feedstock ratio and temperature.

Table 4-12: Elemental composition of char obtained from PET carbonization different holding times, under constant water to feedstock ratio and temperature.

	Ultimate Analysis[a] [wt%]				HHV[a] [MJ/kg]
	C%	H%	N%	O%	
Raw PET	61.8	4.0	0.3	33.9	23.61
30 min	68.9	3.9	0.3	26.9	25.19
60 min	70.8	4.2	0.3	24.7	25.92
120 min	73.1	4.0	0.3	22.6	28.22
240 min	89.6	4.4	0.4	5.6	35.69

[a]:Dry basis; Data obtained from CHN analysis had 0.3% error.

FT/IR analyzation was conducted for char obtained from PET carbonization under holding time 120 min and 240 min at constant water to feedstock 0.25:1 as shown in **Figure 4-27**. For FT/IR spectra of char obtained from carbonization under steam condition at 120 min, FT/IR spectrum was similar to that of raw PET, indicating the incomplete carbonization of PET. However, with prolonged holding time of 240 min, it was observed that little to almost no remaining structure of PET was obtained, thus indicating the complete carbonization of char. This result agrees well with the results obtained from proximate analyzation and ultimate analyzation. Although presence of steam hindered the progression of carbonization, under prolonged reaction time, carbonization of PET progressed to form high fixed-carbon yield char with high carbon content.

Characteristics of wax

Figure 4-28 shows the composition of wax obtained using HPLC analysis from carbonization of PET under steam condition at different holding time. Similarly, with reference to the composition of wax from carbonization under nitrogen condition, benzoic acid, p-toluic acid, biphenyl and fluorene were the main components detected and quantified. Based on the results, high composition of benzoic acid was obtained in wax during carbonization of PET under steam condition. Under prolonged holding time, composition of benzoic acid increased from 35 wt% at 30 min holding time to 54 wt% at 240 min holding time, indicating the progress of hydrolysis reaction in the wax phase.

Properties of Gaseous Product

Figure 4-29 shows the composition of gaseous product obtained from PET carbonization under steam condition at different holding time. Similarly, CO and CO_2 are the main components of gaseous product under steam condition and prolongation of holding time had no evident effect on the gaseous product.

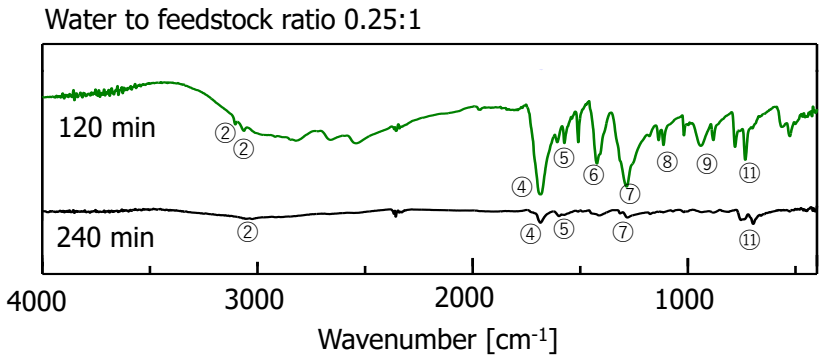

Figure 4-27: FT/IR spectra of char obtained from PET carbonization under holding times 120 min and 240 min.

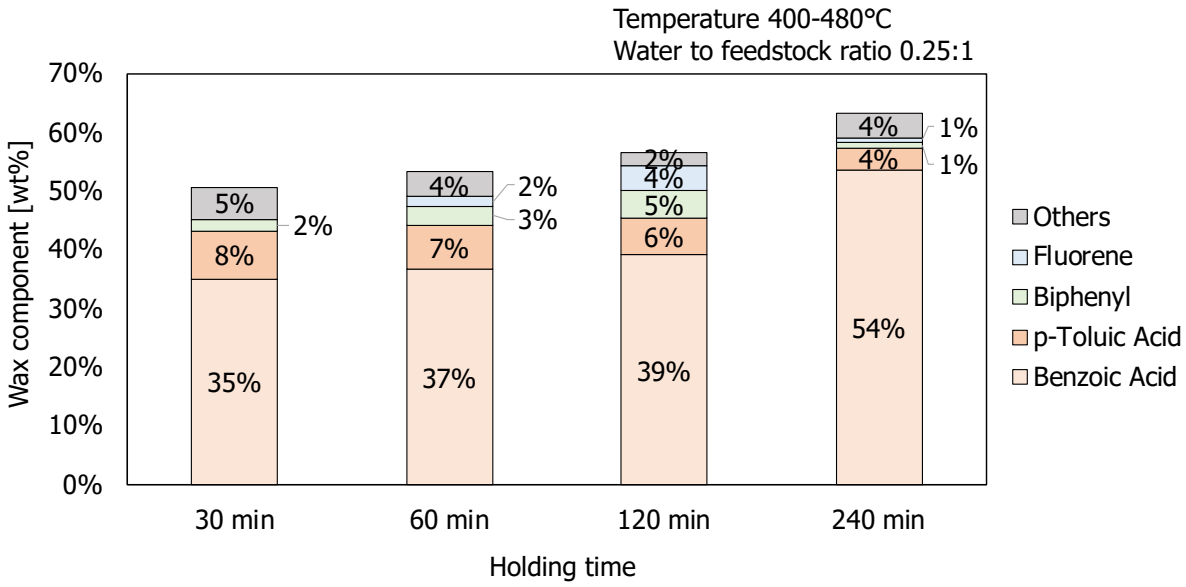

Figure 4-28: Composition of wax obtained using HPLC analysis from carbonization of PET under steam condition at different holding times.

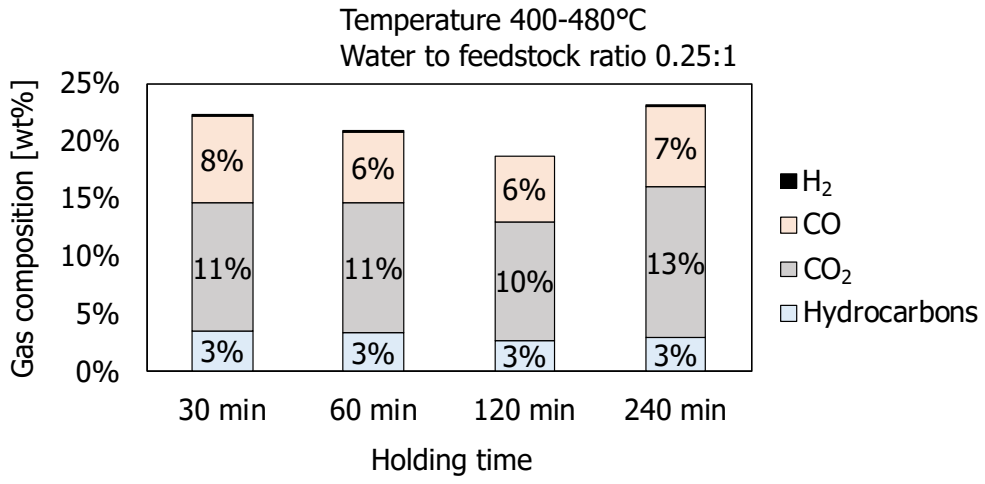

Figure 4-29: Composition of gaseous product obtained from PET carbonization under steam condition at different holding times.

4.4.3 Conclusions: Effect of steam as medium on carbonization of PET

The effects of water to feedstock ratio on carbonization of PET were studied and based on the experimental results, the conclusions were drawn as follows:

1) Gas yield decreased drastically whereas wax composition increased at increasing water to feedstock ratio.
2) Char produced under steam condition showed aggregation of fiber-like or needle-like particles when steam was present in the reaction.
3) Fixed-carbon yield of char sharply decreased in the presence of steam due to the hydrolysis reaction of PET to produce low molecular weight volatile compounds such as terephthalic acid and benzoic acid.
4) High composition of benzoic acid in wax while low composition of CO and CO_2 in gaseous product were obtained during carbonization of PET in steam condition.

The effects of holding time on carbonization of PET in the presence of steam were studied and summarized as follows:

1) Prolongation of holding time of operation under steam condition led to the decrease of char yield and increase of wax yield.
2) Hydrolysis reaction was dominant over carbonization reaction in the presence of steam. Therefore, prolonged reaction time is required for the progression of carbonization to produce char with high carbon content.

4.5 Chapter summary

In this chapter, the effects of operating parameters, namely feedstock treatment and properties, operating temperature, holding time and medium type on the products of carbonization were investigated. The effects of temperature, holding time and medium type on the char yield and its characteristics were studied in depth and summarized.

Firstly, the effects of feedstock variance on carbonization of PET were investigated by carbonizing different types and treatments of feedstock under constant operating conditions. Results demonstrated that feedstock size and treatment method had no evident effects on the product composition and char characteristics due to the singularity of the polymer in feedstock. The results also showed reproducibility and no statistically significant difference regardless of feedstock types from different bottle makers. Therefore, it was evident that physical properties of feedstock and sample preparation had no evident effects on the carbonized product.

Next, the effects of operating temperature and holding time were investigated to identify and characterize the product of PET carbonization. Carbonization of PET at 400-480°C produced char with high carbon content due to the complete carbonization of feedstock and holding time of operation had no evident effect on the product composition once the carbonization was complete. Results also showed that CO and CO_2 are the main components of gaseous product of PET carbonization.

Finally, the effects of steam as medium on carbonization of PET were investigated. Under steam condition, char with low fixed carbon content was produced due to the progress of hydrolysis reaction which hindered the carbonization reaction. Based on the morphological observation, char obtained from carbonization under nitrogen and steam condition showed distinct structures, indicating the difference in decomposition reaction. Carbonization of PET under steam condition did not contribute to the production of carbonaceous product with porous structure, rather, char produced under steam condition showed aggregation of fiber-like or needle-like particles.

This page intentionally left blank.

Chapter 5: Mechanism of char formation based on carbonized product

5.1 Introduction

Previous chapter showed the fundamental studies of carbonization and provided results for carbonized product obtained from all phases. However, the thermal degradation reaction of polymer involves multiple series of complex reaction pathways and the formation of char has not been clarified. In this chapter, the phase behavior of PET carbonization and the mechanism of char formation was studied in detail by utilizing the results obtained from the previous chapter. The mechanism study for char formation aims to significantly contribute to the understanding of char formation from thermal decomposition of polymer and to better understand the carbonization operation, which includes improving the char yield of PET carbonization for the future development of efficient carbon utilization technologies. The detailed study scheme and method of approach are shown in **Figure 5-1**. Firstly, the van Krevelen diagram was applied to identify the reaction pathways of phase changes during carbonization of PET. Then, a study on the analysis of cross-linking behavior was conducted to identify the relationship between parameters and variables based on the experimental operation.

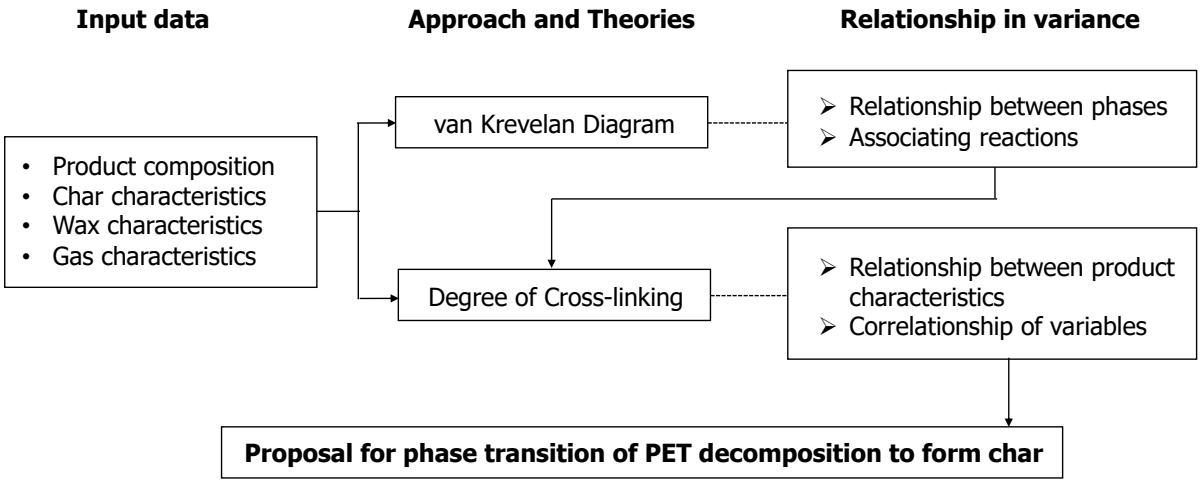

Figure 5-1: Study scheme of Chapter 5 to investigate the mechanism of char formation based on carbonized product.

5.2 Theory of thermal degradation of PET from past researches

In early studies, the theory of thermal degradation of PET was studied and proposed by various scientists. Çit et al. (2007; 2010) conducted thermal degradation of PET reagent to study the effect of temperature at range of 400-700°C, and based on the product yield and structure of decomposition products, they had suggested that PET degradation occurs through primary and secondary degradation. Primary degradation of PET is highly associated with the random scission of ester link to form carboxylic acid and olefinic end groups. On the other hand, secondary degradation is associated with the rapid production of low molecular weight volatile compounds such as benzoic acid, acetaldehyde, CO, CO_2, ethylene and methane.

Similarly, Brems et al. (2011) had explained that among the thermally weak linkages, the C-O bonds along the polymer chains of the ester group are most likely to be subjected to thermal cleavage with further degradation to phthalic and benzoic acid, and possibly to benzene and CO_2 release as shown in **Figure 5-2**.

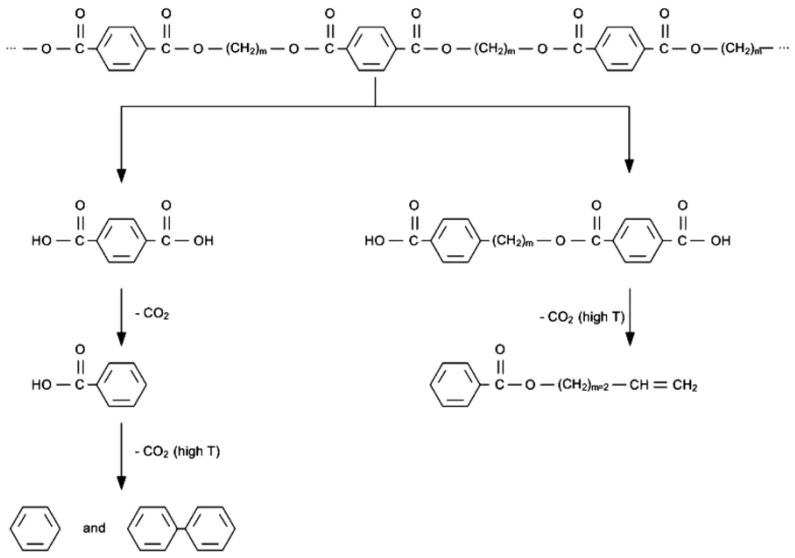

Figure 5-2: PET and its most likely thermal cleavage mechanisms to various products (Brems et al., 2011).

Dimitrov et al. (2013) had also suggested a decomposition mechanism based on the products obtained from the thermal decomposition of PET samples at 400°C. They argued that pyrolysis of PET in acidic medium at 400°C leads to the decomposition of PET to form vinyloxycarbonyl benzoic acid, benzoic acid, and acetaldehyde/CO_2.

Huang et al. (2018) used density functional theory methods to calculate the bond dissociation enthalpies of PET and proposed a possible pathway for the thermal degradation of PET as shown in **Figure 5-3**. Based on their findings, PET can decompose into two same radicals through the C-C homolytic cleavage, and the radical can be further converted into benzoic acid methyl ester (Pathway 1). PET can also decompose into various radicals through the C-O homolytic cleavage, and these radicals can further decompose into various products such as CO_2, CO, benzene, benzoic acid, acetophenone, 1-hydroxyl ethyl benzoate, vinyl benzoate (Pathway 2 & Pathway 3).

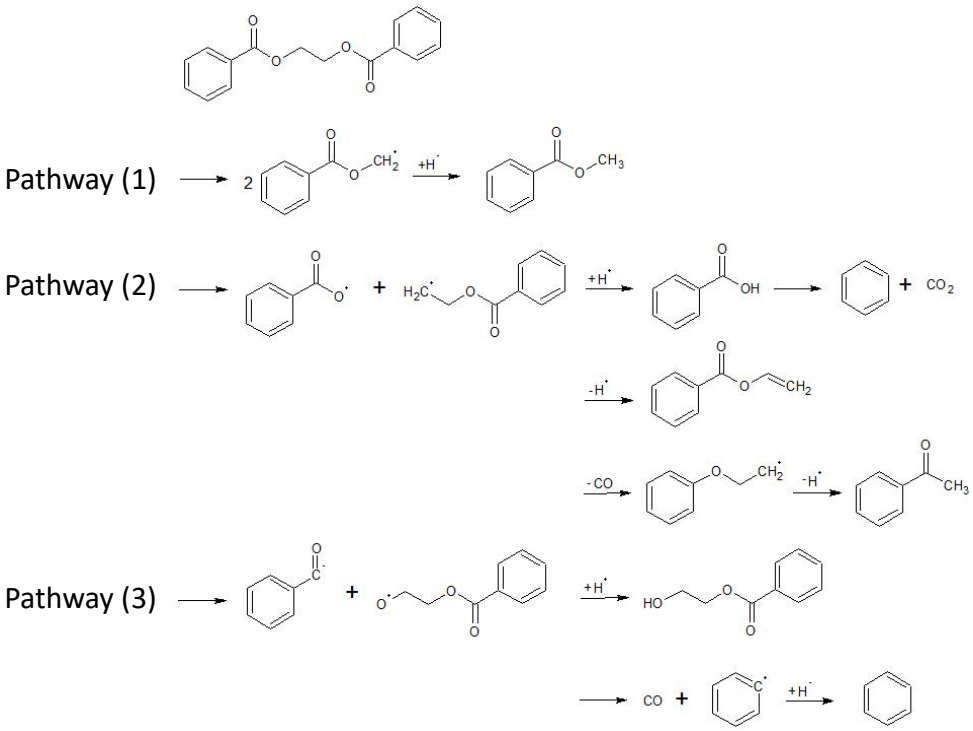

Figure 5-3: Proposed degradation pathways in the pyrolysis process of model compound PET (Huang et al., 2018).

Based on the mentioned, PET degradation occurs through the cleavage of thermally weak linkages along the ester group of the polymer to form low molecular weight fragments. However, based on the reviewed researches, so far, there are no available studies on the mechanism or degradation pathways of PET to form char during carbonization. The results and findings in this chapter aim to mend the research gaps and provide clarification to the mechanism of formation of char.

5.3 Phase behavior based on the van Krevelen diagram

5.3.1 Background

The van Krevelen diagram was developed in the 1950s, as a graphical representation of macroelemental ratios to evaluate the origin and chemical evolution of petroleum and kerogen samples (van Krevelen, 1950). The diagram represents the relationship between atomic O/C and atomic H/C ratios of organic compounds (Tang and Bacon, 1964; Bacon and Tang, 1964). It has become an important tool for characterizing organic matter extending well beyond petrochemical applications and has been used in numerous studies to elucidate chemical reactions (Berge et al., 2011; Wilk et al., 2019). **Figure 5-4** shows the condensation of woody biomass to coal during torrefaction shown by the van Krevelen diagram.

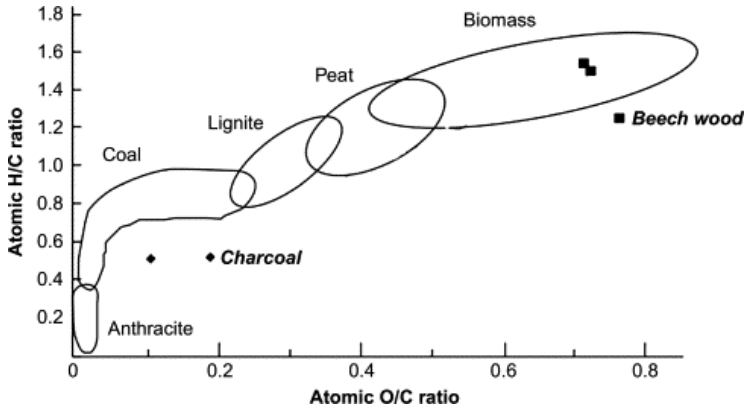

Figure 5-4: van Krevelen diagram of wood-derived char (Heidenreich, 2016).

5.3.2 Results and discussion

Figure 5-5 shows the relationship between atomic H/C and O/C of solid (char) and wax plotted based on the van Krevelen diagram. The elemental composition of char and wax from Chapter 4 was used to obtain atomic H/C ratio and O/C ratio. The solid arrow, dotted arrow, dashed arrow and split arrow represent the decarboxylation, decarbonylation, dehydration and demethanation processes, respectively. Decarboxylation and decarbonylation are chemical reactions where carboxyl group from a compound is removed to release carbon dioxide molecule and carbon monoxide molecule, respectively (Ehlers et al., 1969; Santillan-Jimenez and Crocker, 2012; Lu et al., 2013). Dehydration reaction associates with the removal of water molecule from a compound, while demethanation involves the conversion of methane to COx through dehydrogenation (Schnitzer and Hoffman, 1965; van Krevelen, 1984).

Based on the results, solid phase was obtained in the orange region whereas wax was obtained in the yellow region. It is evident that rapid decomposition of PET occurred through decarbonylation to form char and decarboxylation to form wax. In the solid phase, PET decomposes to form char with high fixed-carbon yield under high temperature, as shown by the red indicators. The chars obtained from complete carbonization in the plot are in similar position to those associated with bituminous and lignite coals (Heidenreich et al., 2016). Char obtained in this region was recorded to have high calorific value (approximately 35.8 MJ/kg) compared to the calorific value of raw PET (approximately 23.6 MJ/kg) due to the high carbon content and high aromaticity of product (McBeath et al. 2011; Wiedemeier et al., 2015). In the wax phase, PET decomposed to form wax with high atomic H/C and O/C ratio. As a summary, the van Krevelen diagram shows the decomposition pathway of PET as accordingly: first, PET undergoes decarbonylation and decarboxylation to produce solid and wax, respectively due to rapid thermal decomposition. In solid phase, C=O group dissociates from the PET structure to form high carbon content char. In wax phase, wax with high oxygen and hydrogen content forms.

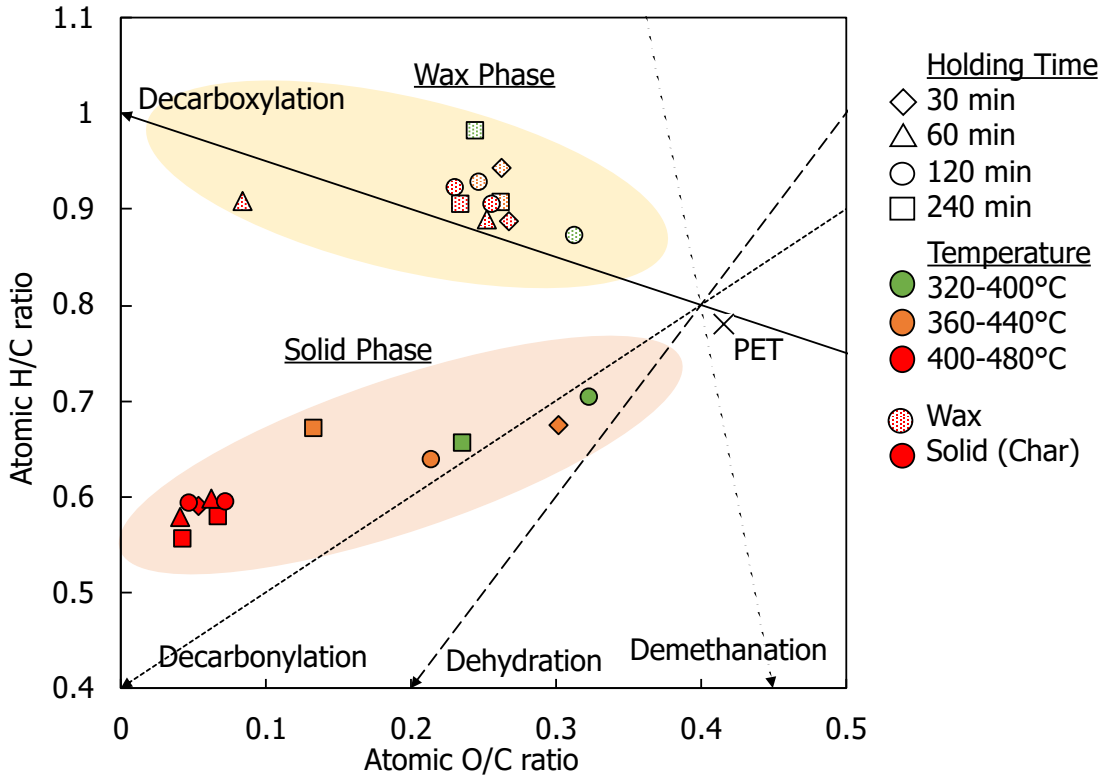

Figure 5-5: Relationship between atomic H/C and atomic O/C of char and wax.

5.4 Degree of cross-linking, $X_{cross\text{-}link}$, indicator for char formation

5.4.1 Theory of cross-linking

Cross-linking has been widely studied as the most important reaction for the formation of char (Zhang et al., 2019). Levchik (2000) had first discussed the cross-linking reaction during the thermal decomposition of polymers, where aromatic cross-linking usually begins with the elimination of small molecules (H_2O, CO_2, CO, CH_4). The elimination of low molecular weight volatile matter leads to the formation of unsaturation in the polymer chain which subsequently leads to cross-linking. Chaiwat et al. (2008; 2009) had intensively reported the behavior of cross-linking reaction during cellulose pyrolysis through investigating the relationship between pyrolysis behavior and cross-linking formation in cellulose. Based on their findings, the dehydration reaction is highly associated with the formation of char, where formation of one water molecule from two molecules of -OH group contributes to the formation of cross-linking in the cellulose structure. On the other hand, Marongiu et al. (2003) and Mehl et al. (2004) had reported the behavior of cross-linking reactions during PVC pyrolysis. It was reported that dehydrochlorination to form HCl leads to the condensation of polyacrylic aromatic hydrocarbon, thus leading to the formation of benzene, naphthalene and phenanthrene. They had further confirmed this relation through quantitative analysis of chloride bond, where the release of chlorine leads to the cyclization and cross-linking reaction in the polyene molecules to form alkyl aromatic hydrocarbons and char residues. Yang et al. (2000) have discussed that in the case of thermal decomposition of polymer, polymer having side groups has higher chemical reactivity in which the chemical structure of the polymer changes through intra- and interchain reaction in the side groups, resulting in cross-linking reaction. Based on past researches, the theory of cross-linking in PET was intensively studied.

5.4.2 Derivation and assumptions of equations

5.4.2.1 The relationship between CO_2 and CO

Firstly, it was assumed that in the case of PET decomposition, scission of C-O bond leads to cross-linking reaction to form char. Based on the degradation pathway of PET presented by Huang et al. (2018), the thermal decomposition mechanism and pathway of PET is simplified as **Figure 5-6**.

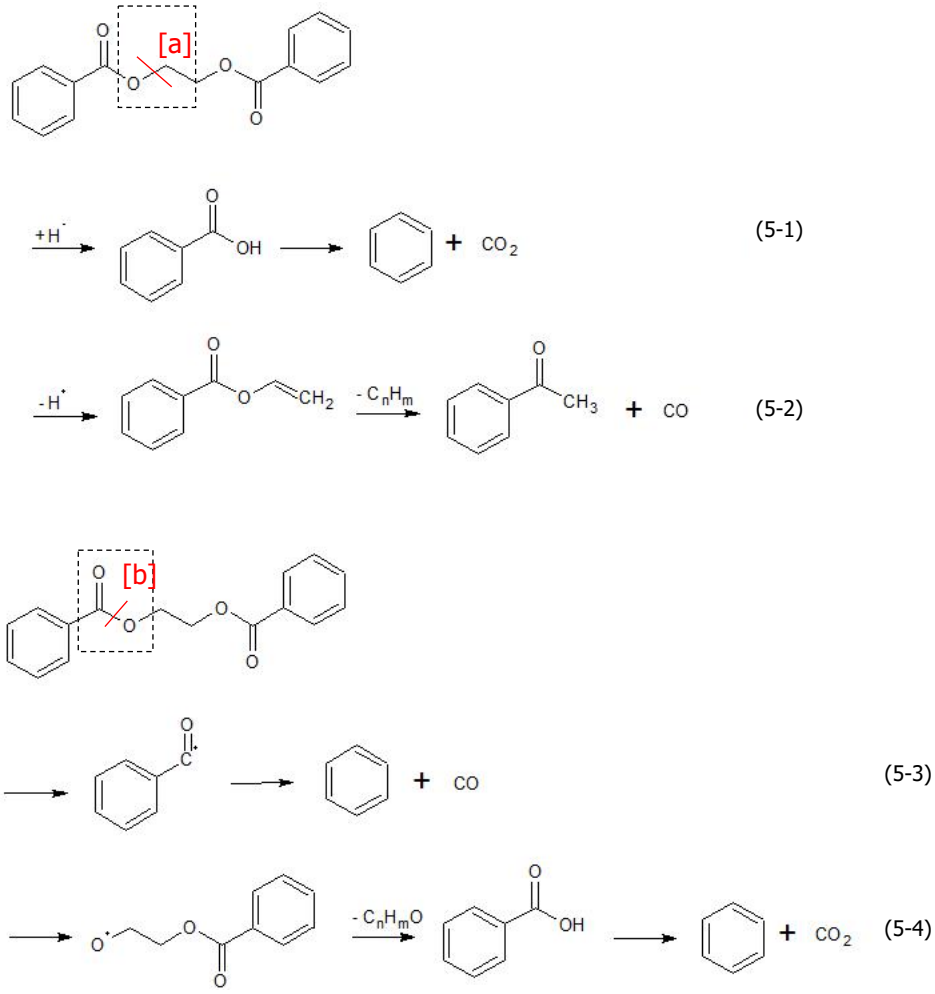

Figure 5-6: Simplified degradation pathways in the pyrolysis process of model compound PET.

Pathways (5-1) and (5-2) were derived from C-O bond scission at site [a] of the ester group to form benzene, acetophenone, CO and CO_2, whereas pathways (5-3) and (5-4) were derived from C-O bond scission at site [b] of the ester group to form benzene, CO and CO_2. This can be confirmed from the high CO and CO_2 yield that was detected in the gaseous product. Based on both pathways, 1 molecule of CO and 1 molecule of CO_2 are formed per 1 PET monomer due to the scission of C-O bond. Also, based on both pathways, benzoic acid is the intermediate compound during the decomposition reaction. Here, it was assumed that scission of C-O bond to release CO and CO_2 leads to the formation of char. Consequently, the highest yield of CO and CO_2 is denoted as

$$\frac{1\ molecule\ of\ CO + 1\ molecule\ of\ CO_2}{1\ PET\ monomer} = \frac{28 + 44}{192} = 37.5\ wt\% \qquad (5\text{-}5)$$

Next, the relationship between CO_2 and CO produced from carbonization operations in terms of mol/mol-monomer was plotted as shown in **Figure 5-7**. The statistical significance of the relationship between CO_2 produced and CO produced was also proven and reported in **Appendix F.2**. Based on the results, there is a significant correlation between the CO_2 produced and CO produced. Therefore, it can be deduced that the thermal degradation of PET produces CO and CO_2 with a molar ratio nearly equal to 1:1, indicating that 1 mol of CO_2 is produced per 1 mol CO. Additionally, both CO and CO_2 produced are shown to be under 1.0 mol/mol-feedstock for all experimental conditions. This indicates that thermal decomposition of 1 PET monomer produces no more than 1 molecule of CO and 1 molecule of CO_2.

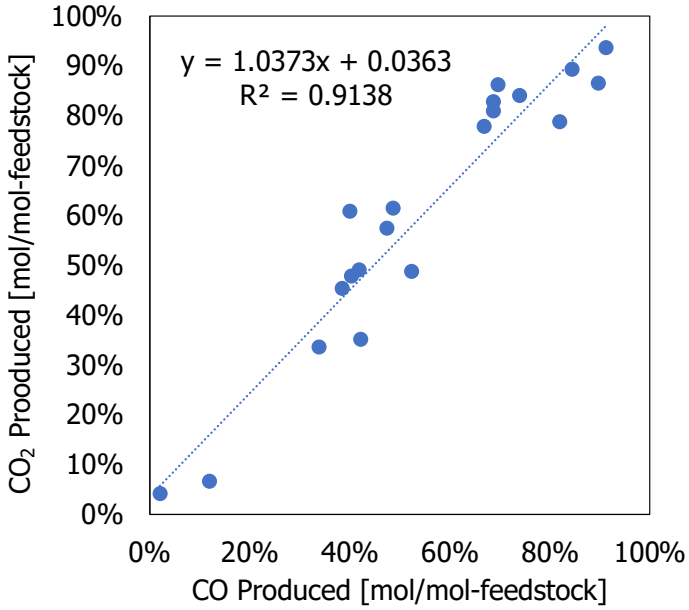

Figure 5-7: Relationship between CO_2 and CO obtained from PET carbonization.

5.4.2.2 Degree of cross-linking, $X_{cross\text{-}link}$ as a function of CO and CO_2

Based on the assumptions that (i) maximum 1 molecule CO and 1 molecule CO_2 can be produced from 1 PET monomer; and (ii) CO and CO_2 produced by scission of C-O bond form cross-linking in the PET structure during carbonization, the degree of cross-linking in PET carbonization $X_{cross\text{-}link}$ was now defined as a function of CO and CO_2, as

$$X_{cross\text{-}link} = \frac{Yield\ of\ CO\ [g/g\text{-}feedstock] + Yield\ of\ CO_2 [g/g\text{-}feedstock]}{Maximum\ yield\ of\ CO\ +\ Maximum\ yield\ of\ CO_2} = \frac{y_{CO} + y_{CO_2}}{0.375} \quad (5\text{-}6)$$

Here, the relationship between $X_{cross\text{-}link}$ and dependent parameters was considered for further understanding of char formation mechanism. **Figure 5-8** shows $X_{cross\text{-}link}$ plotted with increasing holding time under different operating temperature. It was observed that $X_{cross\text{-}link}$ was low under low operating temperature and increases under increasing holding time, while $X_{cross\text{-}link}$ was relatively high at the start of holding time under higher operating temperature at 400-480ºC, reaching the maximum $X_{cross\text{-}link}$ of 80% at 60 min. The results confirmed that cross-linking reaction to form char proceeds at higher operating temperature, and that increasing the holding time promotes the cross-linking in PET for char formation. Note that $X_{cross\text{-}link}$ was over 50% when the holding time was 0 min at 400-480°C, due to the holding time of operation which was set to start when the temperature had reached the set temperature. At 400-480°C, the holding time was set to start at the time when a fraction of the feedstock had decomposed, therefore, the drastic increase of CO and CO_2 can be seen at holding time 0 min, resulting in $X_{cross\text{-}link}$ over 50% at the start of reaction.

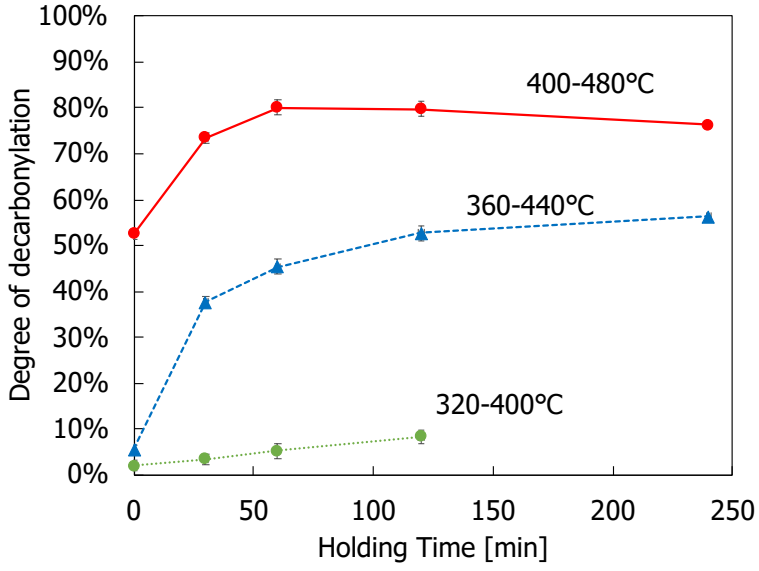

Figure 5-8: Relationship between $X_{cross\text{-}link}$ and temperature change of PET carbonization under different holding time.

Figure 5-9 shows the relationship between $X_{cross\text{-}link}$ and the dimensionless ratio of the amount of carbonyl groups in char to that in feedstock, $C{=}O/C{=}O_0$. Note that this ratio was obtained by taking C=O as the absorbance of peak at 1700 cm^{-1} from the FT/IR spectra of char and $C{=}O_0$ as that of raw PET. The statistical significance of the

relationship between $C=O/C=O_0$ and $X_{cross\text{-}link}$ was also proven and reported in **Appendix F.3**. Based on the results, there is a significant correlation between $C=O/C=O_0$ and $X_{cross\text{-}link}$. Therefore, it can be deduced that $C=O/C=O_0$ decreased with increasing $X_{cross\text{-}link}$. This shows that loss of C=O in the PET structure led to the formation of CO and CO_2. In other words, this suggests that cross-linking formation in char was highly related to the loss of C=O in the PET structure.

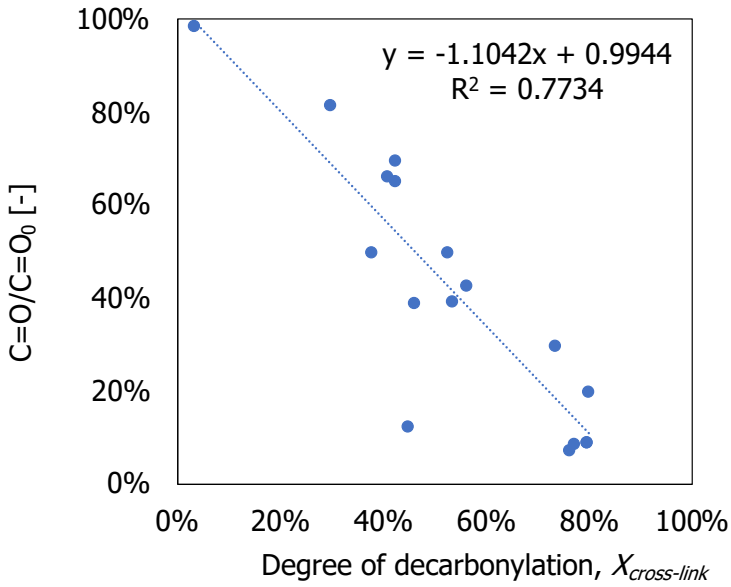

Figure 5-9: Relationship between $X_{cross\text{-}link}$ and the dimensionless ratio of carbonyl groups for char obtained from PET carbonization.

5.4.3 Distribution of $X_{cross\text{-}link}$ in char and wax

To this point, the degree of cross-linking during carbonization of PET was defined to be $X_{cross\text{-}link}$ as a function of CO and CO_2. However, in order to further clarify the mechanism of carbonization of PET, it is necessary to analyze the ratio of cross-linking structure distributed in both char and wax. **Figure 5-10** suggests the possible phase transition of PET during carbonization.

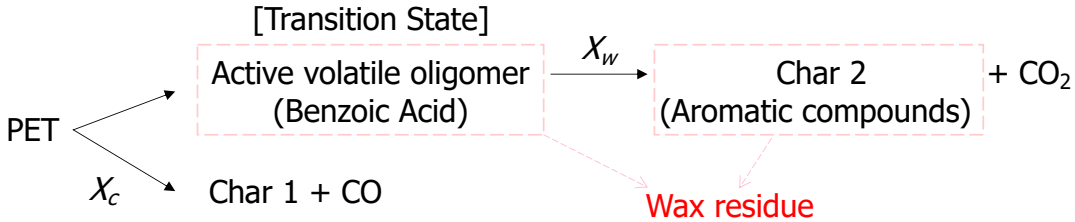

Figure 5-10: Phase transition of PET carbonization.

Based on this, it can be assumed that char residue denoted as Char 1 is a result of cross-linking reaction due to the release of CO during decarbonylation. The degree of cross-linking in terms of CO, $X_{cross\text{-}link}$(CO) is newly expressed as

$$X_{cross\text{-}link}(CO) = \frac{Yield\ of\ CO\ [g/g\text{-}feedstock]}{Maximum\ yield\ of\ CO\ +\ Maximum\ yield\ of\ CO_2} = \frac{y_{CO}}{0.375} \quad (5\text{-}7)$$

On the other hand, the rapid decomposition of PET also resulted in the production of active volatile oligomer which was in transition state. Here, the composition of active volatile oligomer was unknown, however, it is assumed to mainly compose of benzoic acid, as discussed in the previous section. Active volatile oligomer was a result of volatilization due to high operating temperature. As the reaction progressed, the active volatile oligomer decomposed through decarboxylation to release CO_2 and formed decomposition product which was collected as wax at the end of the operation. Here, the decomposition product of active volatile oligomer is denoted as Char 2, which is mainly composed of aromatic compounds such as benzene, acetophenone, and biphenyl as reported in Chapter 4. Based on this, the degree of cross-linking in terms of CO_2, $X_{cross\text{-}link}$(CO_2) is newly expressed as

$$X_{cross\text{-}link}(CO_2) = \frac{Yield\ of\ CO_2\ [g/g\text{-}feedstock]}{Maximum\ yield\ of\ CO + Maximum\ yield\ of\ CO_2} = \frac{y_{CO_2}}{0.375} \quad (5\text{-}8)$$

Here, two newly defined parameters, degree of decarbonylation to form Char 1, X_c, and degree of decarboxylation to form Char 2, X_w are presented as:

$$\begin{aligned} &Degree\ of\ Decarbonylation, X_c \\ &=\ C{=}O\ loss\ in\ PET\ \times Char\ yield\ [wt\%] \\ &= \left(1 - \frac{C{=}O}{C{=}O_0}\right) \times y_{char} \end{aligned} \quad (5\text{-}9)$$

$$\begin{aligned} &Degree\ of\ Decarboxylation, X_w \\ &= Decomposition\ of\ Benzoic\ acid \times\ Wax\ yield\ [wt\%] \\ &= \left(1 - \frac{BA[g]}{BA_0[g]}\right) \times y_{wax} \end{aligned} \quad (5\text{-}10)$$

, where X_c is defined as the loss of the amount of carbonyl group in PET contained in char, whereas X_w is defined as the decomposition of benzoic acid contained in wax. Note that BA_0 is assumed as the mass of wax used during HPLC analyzation.

Based on the newly defined equations, the relationship between the degree of cross-linking in terms of CO, $X_{cross\text{-}link(CO)}$ and the degree of decarbonylation, X_c; and the relationship between degree of cross-linking in terms of CO_2, $X_{cross\text{-}link(CO_2)}$ and the degree of decarboxylation, X_w are plotted as shown in **Figure 5-11**. As seen from the results, good linear relationships between X_c and $X_{cross\text{-}link(CO)}$; and X_w and $X_{cross\text{-}link(CO_2)}$ were observed. This indicates that the decarbonylation reaction to release CO is highly associated with the formation of cross-linking to form char in the solid residue, whereas the decarboxylation reaction to release CO_2 is highly associated with the formation of cross-linking to form aromatic compound in the wax residue. The statistical significance of the relationships was proven and reported in **Appendix F.4**.

For further investigation, wax collected from carbonization of PET at 400-480°C, 120 min was set as feedstock and a pyrolytic reaction under the operating condition as described in Chapter 3 for carbonization at 400-480°C, 120 min was repeated. It was observed that the white fluffy wax turned into blackish liquified tar. On the other hand, no CO could be detected while only CO_2 was produced in the operation, indicating the decomposition of wax produces CO_2 to form aromatic compounds and carbon (tar) which confirms the validity of equations.

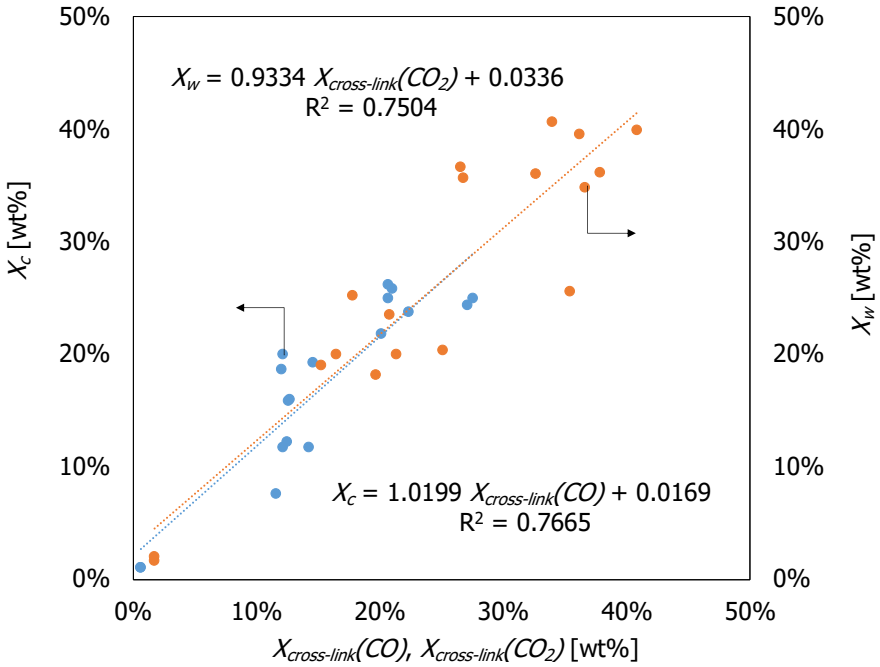

Figure 5-11: Relationship between $X_{cross\text{-}link(CO)}$ and X_c; and the relationship between $X_{cross\text{-}link(CO_2)}$ and X_w.

5.5 Chapter Summary

In this chapter, the phase behavior of PET carbonization was investigated, and the mechanism of char formation was clarified based on the results obtained from carbonization of PET in the previous chapter.

Firstly, the van Krevelen diagram was applied to identify the reaction pathways of phase changes during carbonization of PET. It was observed that, during carbonization, PET undergoes decarbonylation to produce char and decarboxylation to form wax due to rapid thermal decomposition. It was clear that in solid phase, C=O group dissociates from PET structure to form high carbon content char, whereas in wax phase, wax with high oxygen and hydrogen content forms.

Next, a study on the analysis of cross-linking behavior was conducted to identify the relationship between parameters and variables based on the experimental operation. A new parameter index, the degree of cross-linking, $X_{cross\text{-}link}$ was proposed to investigate the cross-linking behavior in char. Results showed that the release of CO and CO_2 due to the scission of C-O bond leads to the formation of char in solid residue. Further investigation on the distribution of cross-linking behavior in char and wax confirmed the release of CO due to decarbonylation to form char while the release of CO_2 due to decarboxylation to form aromatic compounds in wax. Overall, the degree of cross-linking was proven to be a suitable indicator for the formation of char during PET carbonization.

This chapter had provided valuable results and findings which contributed to mending of the research gaps and provided clarification to the mechanism of formation of char. The mechanism study for char formation is expected to significantly contribute on better understanding of the carbonization operation, which includes improving the yield of char of PET carbonization for the future development of efficient carbon utilization technologies.

This page intentionally left blank.

Chapter 6: Effect of contaminants in non-recyclable PET on carbonized product

6.1 Introduction

The major factor affecting the suitability of PET for recycling is the level and nature of contaminants present. There are strict requirements for PET to be reprocessed, which include dye content, yellowing index, metal content and PVC content (Awaja and Dumitru, 2005). Contamination of PET is the major cause of deterioration of its physical and chemical structure during re-processing. It is vital to minimize the amount of contaminants in order to ensure the quality of recycled PET (Giannotta et al., 1994; Pawlak et al., 2000; Welle, 2011). The main contaminants include water, coloring contaminants, acetaldehyde, PVC and polyolefins. In the case of water contamination, water reduces molecular weight of PET during PET recycling through hydrolysis reaction as has been described in Chapter 4. However, proper drying during the recycling process helps prevent water contamination. Fragments of colored bottles and printed ink labels cause undesirable contamination during processing. Therefore, colored bottles are sorted before the recycling process to reduce coloring contaminants. On the other hand, PET degradation reactions lead to molecular weight loss, yellowing reactions and production of acetaldehyde, which decreases the quality of recycled PET. Collected PET which does not satisfy the conditions for recycling usually ends up in incineration. This chapter focuses on colored PET, multilayer PET and PET exposed to UV degradation. Study scheme is shown in **Figure 6-1**.

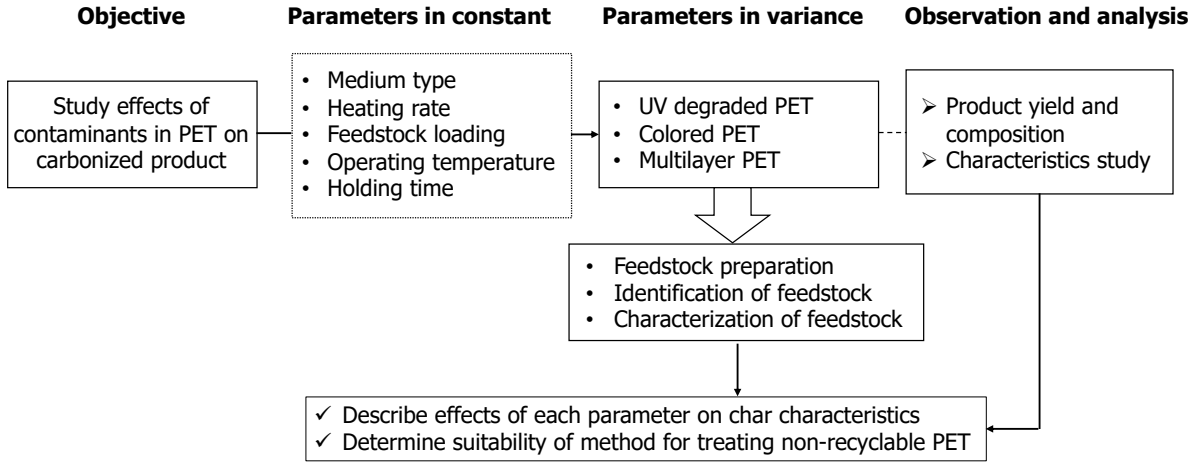

Figure 6-1: Study scheme of Chapter 6 to investigate the effects of contaminants in PET on carbonized product.

6.2 Effect of UV degraded PET on carbonized product

6.2.1 Background of UV degradation on PET

The solar spectrum reaching the earth's surface is in the range from 290 nm to 3000 nm with a composition of 8.3% of ultraviolet, 42.3% of visible light and 49.4% of infrared light (EPA, 2012). The wavelength of light which has the most harmful effect on polymers is in the 290 to 400 nm range of the UV spectrum. Although UV light makes up only approximately 8% of sunlight reaching the surface of earth, it is responsible for most material damage that are exposed to the outdoor environment. In the case of PET, UV exposure leads to the photolysis of PET molecule, which is the breaking of chemical bonds in the polymer chains that subsequently causes a large decrease in molecular weight. The chain scission process in PET will result in serious deterioration in mechanical properties of PET products. UV degradation on PET is observed and reported in PET bottles collected in marine environment (Ioakeimidis et al., 2016) and terrestrial environment (Furusawa, 2019), in addition to PET products such as pails and textiles used in outdoor environment (Davis and Sims, 1983). Degraded PET material becomes a problem in the recycling industry due to the deterioration in mechanical property and decreased molecular weight. For fibers and films produced from PET exposed to UV degradation, the materials tend to lose their elasticity, are brittle and break easily (Ranby and Rabek, 1975; Mascia, 1974; Pappas and Winslow, 1981).

6.2.2 Mechanism of UV degradation of PET

Waste PET bottles exposed to long-term UV degradation are not suitable for material recycling to produce films and fibers. The reason for this is that photodegradation of PET causes chain scission by analogues of Norrish types I and II reaction of the ester group (Pearce et al., 1983), where the formation of carboxylic group by Norrish type II is dominant over Norrish type I in the UV degradation of PET (Al-Azzawi, 2015). As shown in **Figure 6-2**, the Norrish type II pathway, through a six-member ring transition state due to sufficient UV radiation, leads to the scission of C-O of the ester group in the main chain of the polymer to form carboxyl end-groups. The generation of carboxyl end-groups is the main cause for the loss of mechanical strength of the polymer.

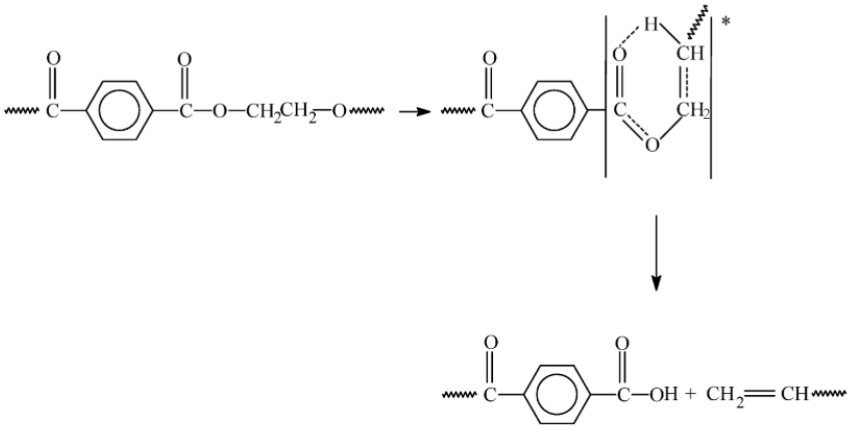

Figure 6-2: Chemical reactions undergone by PET during UV exposure leading to carboxyl end-groups (Adapted from Fechine et al., 2004).

On the other hand, for the thermal decomposition mechanism of PET, Huang et al. (2018) had calculated the thermal decomposition mechanism of PET polymers and proposed a possible pathway for the thermal degradation of model compound PET as shown in Figure 5-3 in Chapter 5. With reference to Figure 5-3, pathways (2) and (3) had been studied in depth in the previous chapter, where it was suggested that the release of CO is highly associated with char formation in the solid phase whereas the release of CO_2 is highly associated with formation of aromatic compound in the wax phase. However, pathway (1), which is the thermal decomposition of PET into 2 same radicals through the C-C homolytic cleavage to be converted into benzoic acid methyl ester has yet to be discussed in depth. It is highly expected that the scission of C-C bond in pathway (1) leads to the volatilization of aromatic compounds as collected in the form wax, and that the scission of C-C bond leads to the formation of methane and low ethylene or ethane yield in the gas product. In other words, when PET polymer is exposed to UV radiation to an extent, it is expected that in the carbonization reaction, char yield is higher whereas wax yield is lower than the carbonization of non-exposed PET due to the increased carboxylic end-group in the main polymer structure. In addition, due to the absence of C-C homolytic cleavage, higher ethylene/ethane yield and lower methane yield are expected in the gaseous products of carbonization of UV degraded PET.

As a summary, the following hypotheses were suggested:

(i) Higher char yield and lower wax yield are expected in the carbonization of UV degraded PET;

(ii) Higher CO_2 yield than CO (in unit mol/mol-feedstock) are expected due to the increase of carboxylic end-group in the main polymer structure;

(iii) Higher ethylene/ethane yield and lower methane yield due to the decrease of C-C homolytic cleavage during thermal decomposition of PET.

In order to investigate these hypotheses, thorough sample preparation and carbonization of UV degraded PET were conducted. Therefore, the aim of this study is to investigate the influence of the extent of UV degradation of PET on the properties of product obtained from carbonization. PET bottles were exposed in a weathering chamber for various intervals, and then analyzed and monitored for surface change. The PET samples were then carbonized to obtain products for discussion.

6.2.3 Preparation of sample

UV degraded PET was prepared using the accelerated weathering test method as described in Chapter 3. Infrared spectroscopy by attenuated total reflection (ATR-FT/IR), microscopic analysis and tensile test were conducted to determine the extent of UV degradation of PET. For tensile test, the stress at break was determined and compared.

6.2.4 Characteristics of UV degraded PET

Figure 6-3 shows the magnified surface morphology of PET without UV irradiation, PET with 0.2-year accelerated weathering and PET with 8.6-year accelerated weathering. From the figure, uniform surface structure of PET without UV irradiation can be seen. However, slight distortion on the surface can be seen for PET exposed to 0.2-year accelerated weathering. The distortion of surface structure was more evident in PET exposed to 8.6-year accelerated weathering.

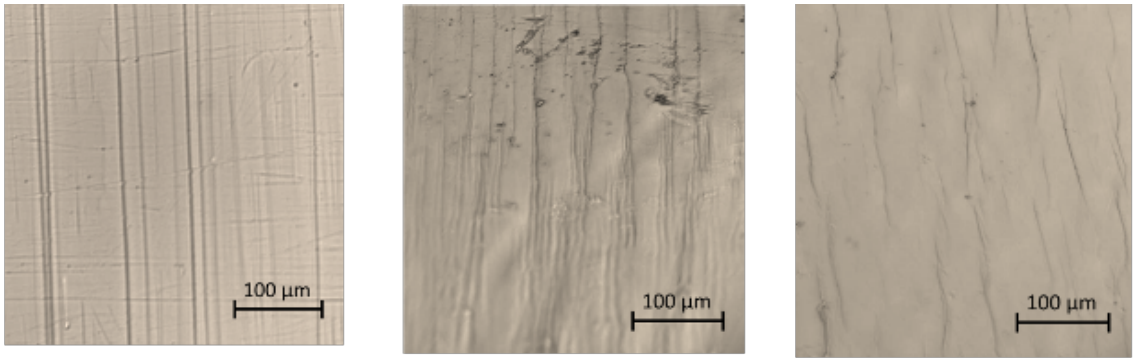

(a) Raw PET (b) PET with 0.2-year accelerated weathering (c) PET with 8.6-year accelerated weathering

Figure 6-3: Magnified surface morphology of PET.

Figure 6-4 shows the FT/IR spectra of PET samples around 1700 cm^{-1} which indicates the absorption band of C=O stretching in the carboxylic acid group of PET structure. The absorption intensity increased with increasing accelerated weathering. This is due to the formation of carboxylic acid group (-COOH) through Norrish II which consequently magnified the intensity of absorption band of C=O. This confirms that degradation of PET occurred due to chain scission in PET.

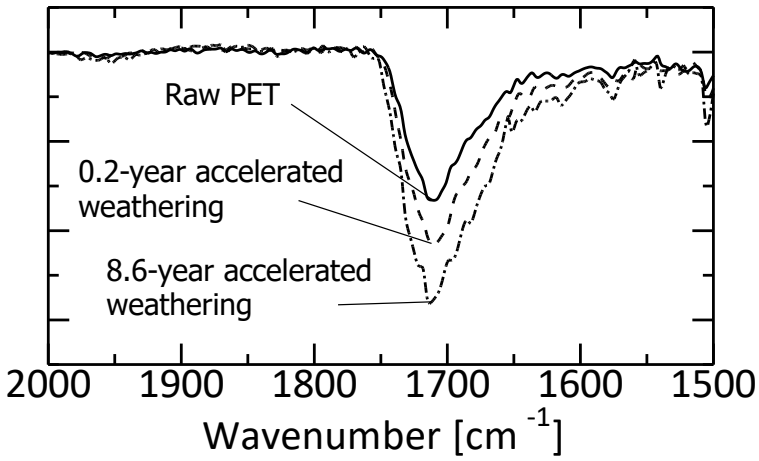

Figure 6-4: FT/IR spectra of raw PET, 0.2-year accelerated weathering and 8.6-year accelerated weathering.

Tensile test was conducted for PET samples and **Figure 6-5** shows the breakage of PET strip before the material was fully elongated. In addition to the fracture of material, PET strip was dissasociated into multiple layers during the tensile test. The edge of the breakage was also observed using a microscopic analysis.

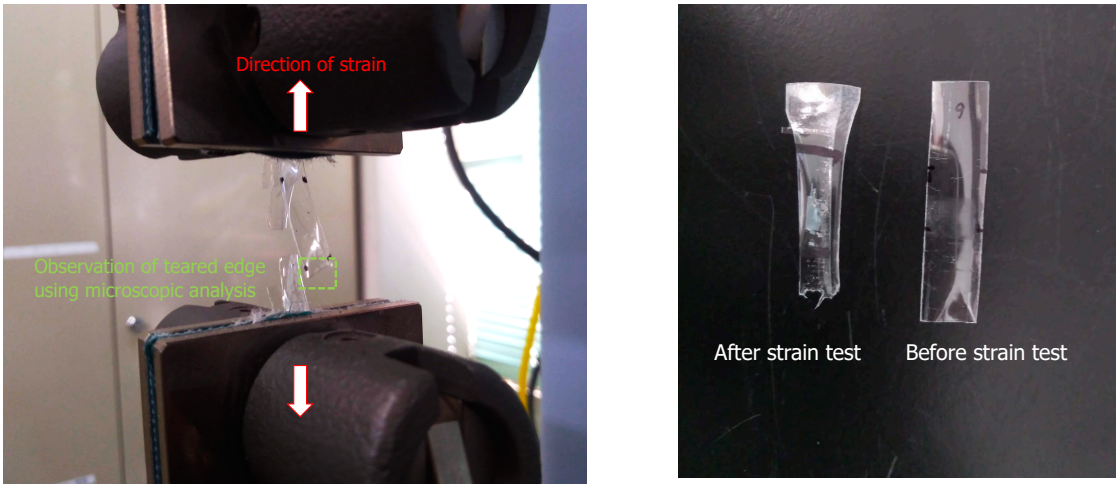

(a) Strain test using EZ test (b) Appearance of PET after strain test

Figure 6-5: Photo of strain test using EZ test and PET after strain test.

Figure 6-6 shows the magnified surface morphology of teared edge of PET from tensile test. It was observed that there was no evident sign of pits on the surface of raw PET whereas wide and deep cracks in both vertical and horizontal direction existed on the surface of accelerated weathering samples. When PET is exposed with UV radiation, chain scission in the polymer occurs, leading to shorter chain lengths and formation of microvoids or microcracks on the surface. The microvoids are also the reason for the discoloration of PET bottle. When tensile stress is applied, the polymer stretches and orientates in a very localized area, thus widening the microvoids and forming a craze. The oriented chains will continue to stretch until reaching break point, thus creating voids which elongated in the normal direction to the applied stress as shown in **Figure 6-7**. The voids will grow until cracks are formed to leading to failure (tearing of material).

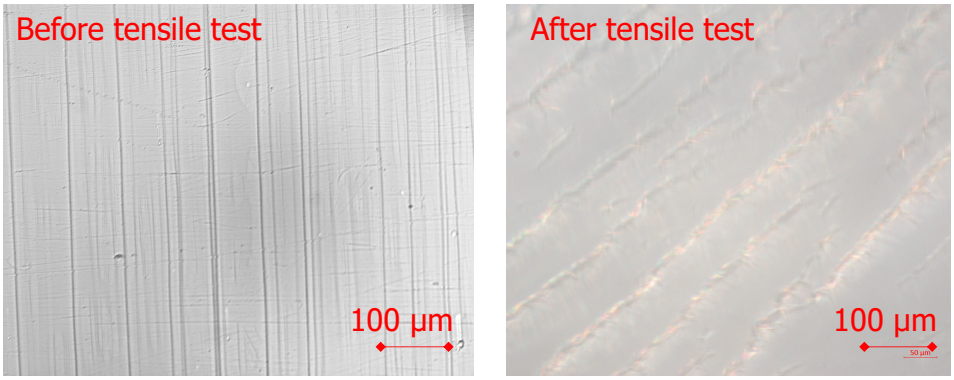

(a) Raw PET

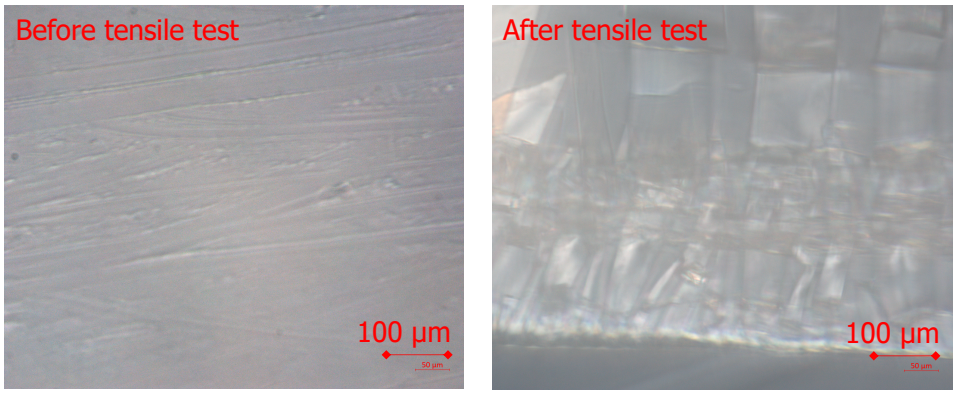

(b) PET after 8.6-year accelerated weathering

Figure 6-6: Magnified surface morphology of teared edge of PET from tensile test.

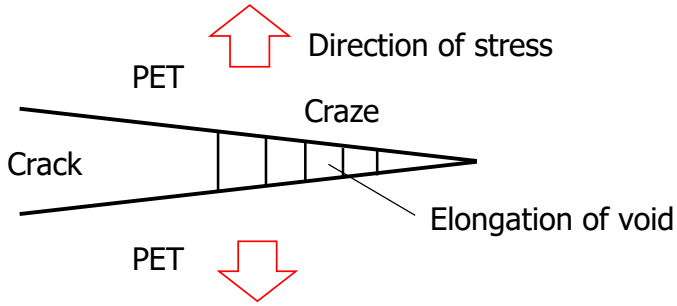

Figure 6-7: Formation of crack and craze during tensile stress (Al-Azzawi, 2015).

Figure 6-8 shows the stress-strain curves for raw PET and PET exposed to 8.6-year accelerated weathering. As seen from the results, the strain, which is the ability of material to deform plastically under tensile stress before fracture, decreased when PET was exposed to UV degradation.

Figure 6-9 shows the relationship between the amount of UV degradation and the strength at break of PET exposed to UV at different period. The stress at break significantly decreased with the extent of exposure. This indicates that the formation of microcracks due to surface degradation leads to the initiation of failure (breakage) of PET under the least required tension applied. The decrease of stress at break also indicates the decrease of elongation ability of PET exposed to UV radiation.

Based on the sample preparation of UV degraded PET, when the time for accelerated weathering test for PET was prolonged, the progression of UV degradation was observed. UV degradation of PET was confirmed via:

1) The increase of intensity of absorption band of C=O for the formation of carboxylic acid group (-COOH) through the FT/IR analysis;
2) The observation of microcracks on PET surface through microscopic analyzation;
3) The decrease of tensile properties of UV degraded PET through the tensile test.

The samples prepared were loaded into the carbonizing reactor for reaction. Results are reported in the next section.

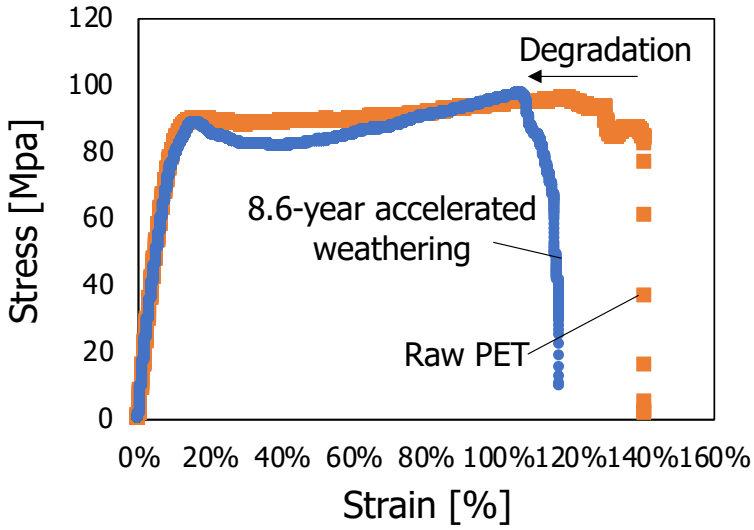

Figure 6-8: Stress-strain curves for raw PET and PET exposed to 8.6-year accelerated weathering.

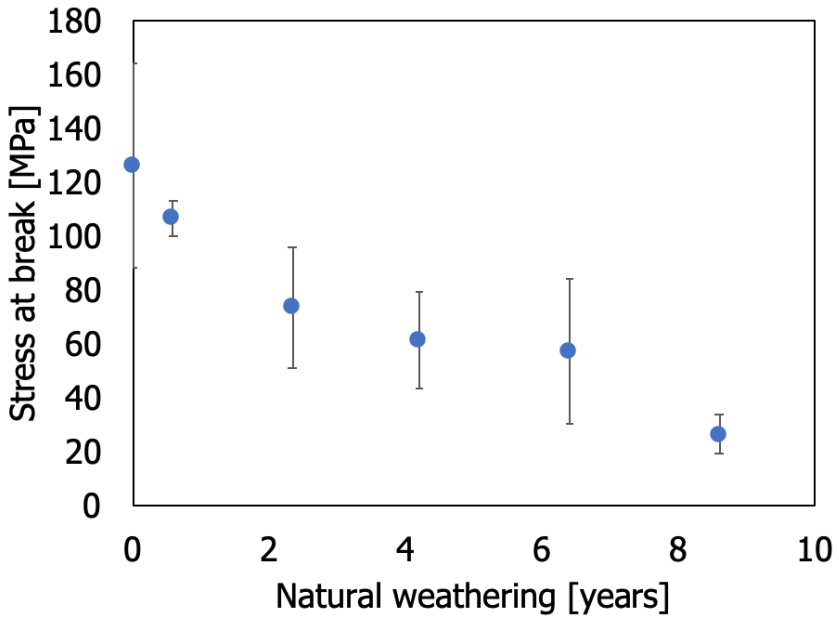

Figure 6-9: Relationship between the amount of UV degradation and the stress at break of PET.

6.2.5 Carbonization of UV degraded PET

6.2.5.1 Experimental procedures

Carbonization experiments were conducted based on methods described in Chapter 3. All experiments were conducted at 400-480°C and 120 min. Analyzation was also conducted using the methods described in Chapter 3, which include proximate analysis, ultimate analysis for char; and GC/TCD and GC/FID for gas.

6.2.5.2 Results and discussions

Product composition

Figure 6-10 shows the composition of products obtained from carbonization of PET exposed to different accelerated weathering tests. Note that wax was taken as the balance from char and gas due to the large amount of residual wax that was solidified in the pipes of the reactor. It can be seen that the average yield for char was 27.9 wt% (±1.4%), that for wax was 36.0 wt% (±2.1%) and that for gas was 36.1 wt% (±2.4%) for all products obtained from carbonization of PET exposed to different accelerated weathering tests. However, slight increase in the fixed-carbon yield can be seen, where increase from 18.2 wt% of carbonization of raw PET to 19.6 wt% for carbonization of PET exposed to 6.5-year acceleration was observed. Although not apparent, it can be deduced that the exposure to UV on PET surface contributes to the increase of fixed-carbon yield during PET carbonization. It can also be speculated that due to the chain scission and formation of carboxylic group by Norrish type II reaction caused by UV radiation, the tendency of C-C homolytic cleavage during thermal decomposition decreased. This results in the increase of frequency of C-O chain scisison in the carboxylic group of the main chain of the sample, thus increasing the fixation of carbon in the solid for char formation during carbonization reaction. In order to determine the statistical significance of assumption based on the results, a one-sample t-test was conducted to obtain the significance of difference in fixed-carbon yield due to UV degradation in PET. The null hypothesis is now given as: The fixed-carbon yield from carbonization of UV degraded PET is the same as the fixed-carbon yield from carbonization of PET without UV degradation, which is 18.2 wt% in UV0. Using a t-test for independent samples (1-tailed), the results are presented in **Table 6-1**.

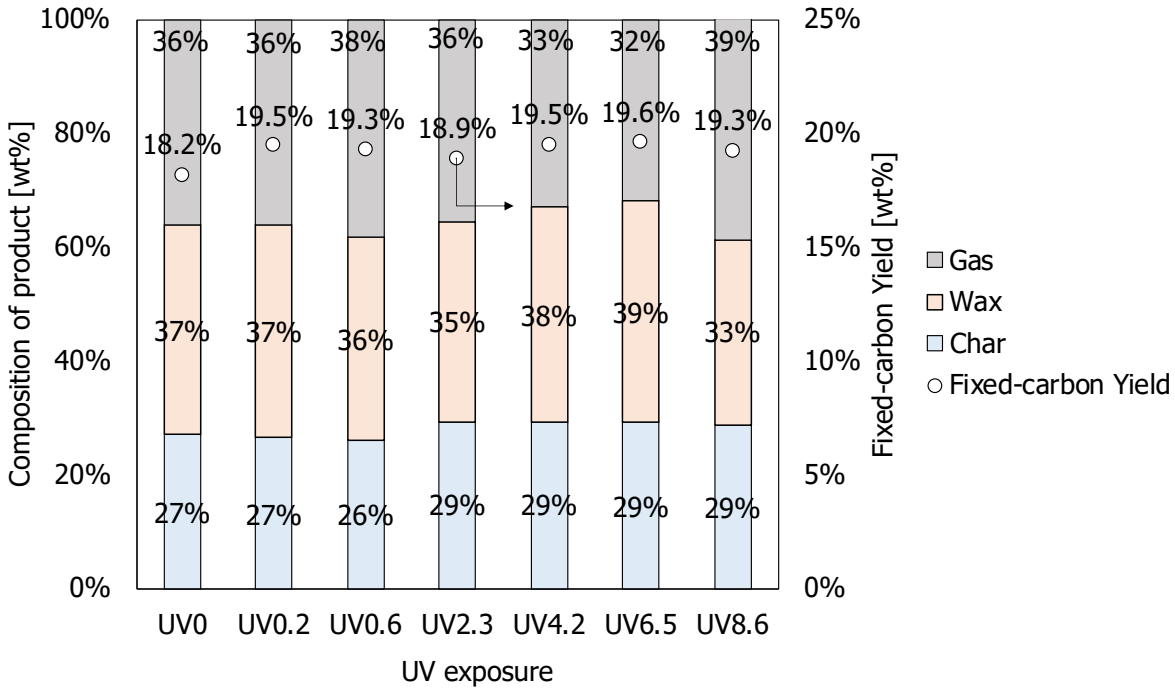

Figure 6-10: Composition of product obtained from carbonization of PET exposed to different accelerated weathering tests, where the following are denoted; UV0: 0 year, UV0.2: 0.2 year, UV0.6: 0.6 year, UV2.3: 2.3 years, UV6.5: 6.5 years, UV8.6: 8.6 years.

Table 6-1: Results of one sample t-test for the fixed-carbon yield.

	With UV exposure	Notes
Mean, M	0.194	
Variance	6.08E-06	
Observations, n	6	
Hypothesized mean	0.182	Fixed-carbon yield from UV0
df	5	
t Stat	11.538	
P(T<=t) one-tail	4.29E-05	$P < 0.05$
t Critical one-tail	2.015	t stat > t crit

Based on the statistical analysis, the null hypothesis was rejected based on t stat > t crit. Therefore, the following can be derived based on the results. The fixed-carbon yield of char from carbonization of PET exposed to UV degradation (M = 0.194, n = 6) had significant difference than that of carbonization of PET without UV exposure (M = 0.182). This difference was significant due to t(6) = 11.538, p = 4.29E-05 (one tail). There is enough evidence to conclude that there was statistically significant difference between the samples, in which it can be addressed that the fixed-carbon yield is relatively higher when PET is exposed to UV degradation. As a conclusion, during carbonization of UV degraded PET, higher fixed-carbon yield can be obtained.

Properties of Gaseous Product

Figures 6-11 and **6-12** show the composition of gaseous products and composition of hydrocarbons in gaseous product obtained from carbonization of PET exposed to different accelerated weathering tests, respectively.

For all experimental runs, CO_2 was the main gaseous compound at average 20.8 wt% (±2.0%), followed by CO at average 12.0 wt% (±1.5%) and hydrocarbons at average 3.3 wt% (±0.3%). Little to almost no hydrogen was detected. Due to the high CO and hydrocarbon concentration, the HHV of gas was calculated to be at average 8.4 MJ/kg (±0.4). On the other hand, the hydrocarbon composition from UV0 to UV0.6 showed good consistency in product. However, at prolonged accelerated weathering, ethylene and ethane yield increased while methane yield decreased. The increasing tendency was most evident for hydrocarbons collected at UV8.6, where ethane yield increased from 0.2 wt% to 0.6 wt%, and ethylene yield increased from 0.3 wt% to 1.0 wt%. As initially suggested, higher ethylene and/or ethane yield and lower methane yield was expected due to the decreased C-C homolytic cleavage during thermal decomposition of PET. This tendency was evident with the prolongation of accelerated weathering test, where ethylene and/or ethane yield was higher at UV8.6 compared to PET without or with less UV exposure. It is now speculated that accelerated weathering at 2.3 years and above leads to the higher production of ethylene and ethane. Statistical analysis was conducted to determine the accuracy of this statement.

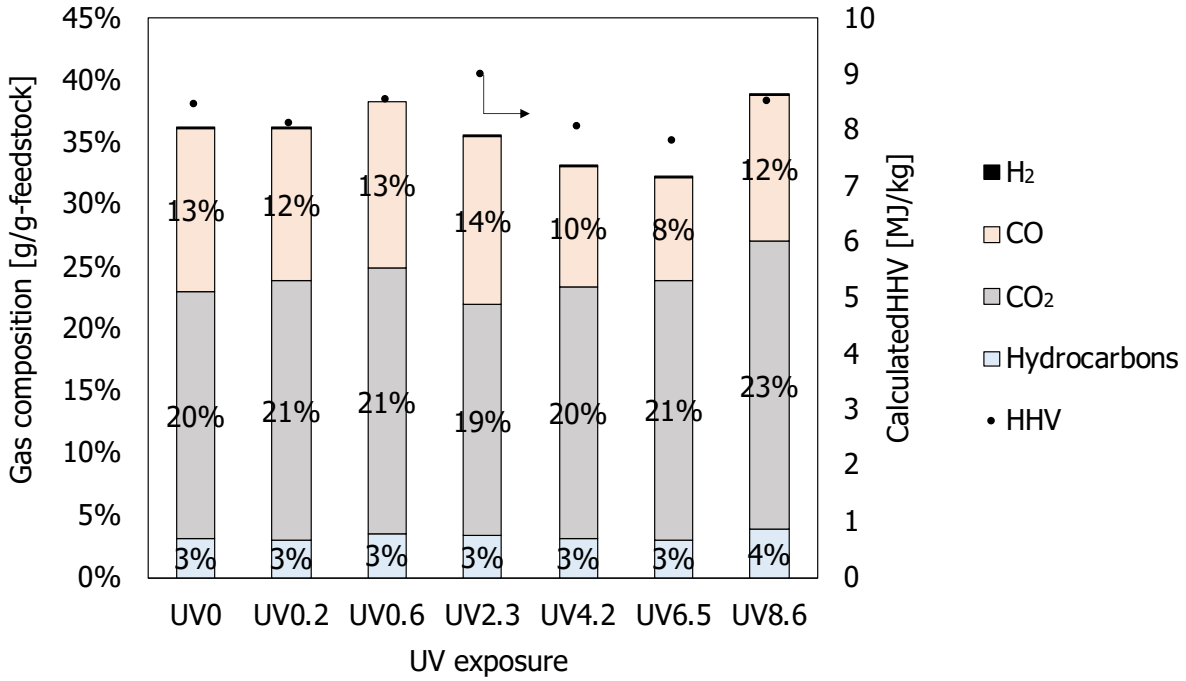

Figure 6-11: Composition of gaseous products obtained from carbonization of PET exposed to different accelerated weathering tests.

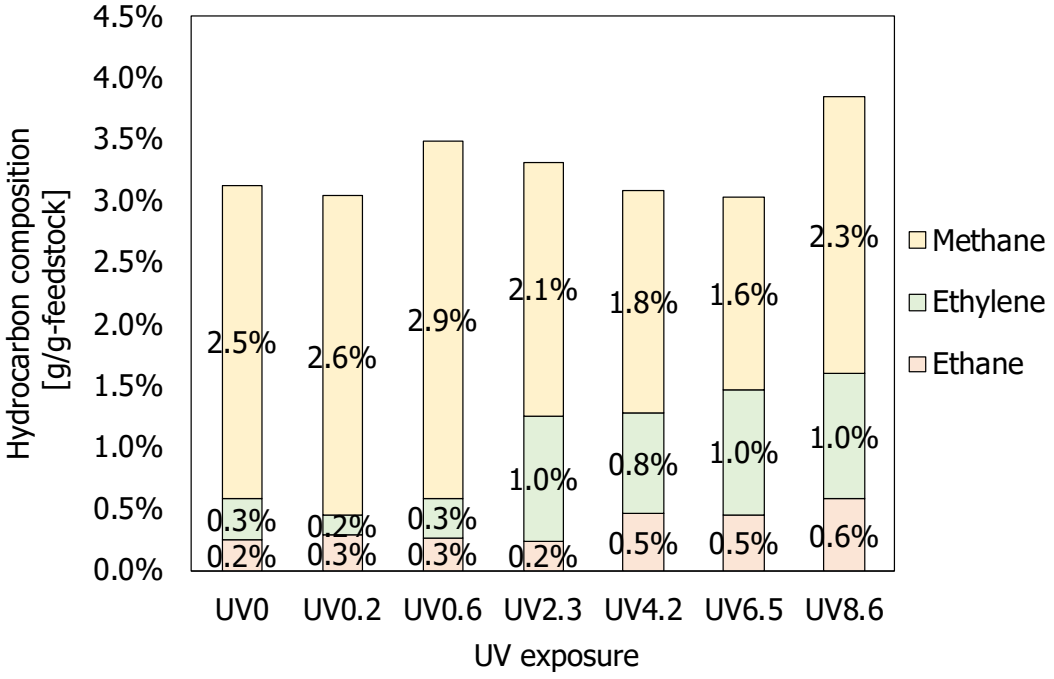

Figure 6-12: Hydrocarbon composition of gaseous products obtained from carbonization of PET exposed to different accelerated weathering tests.

In order to determine the statistical significance of the assumption that, accelerated weathering at 2.3 years and above leads to the higher production of ethylene and ethane, a one-sample t-test was conducted to obtain the significance of difference in ethylene and ethane production due to UV degradation in PET.

The null hypothesis is now given as: the total ethane and ethylene produced due to UV degradation of PET is the same as the total ethane and ethylene produced without UV degradation, which is 3.9 wt% in UV0. Using a t-test for independent samples (1-tailed), the results are presented in **Table 6-2**.

Table 6-2: Results of one sample t-test for total ethane and ethylene produced.

	With UV exposure	Notes
Mean, M	0.014	
Variance	2.62E-05	
Observations, n	4	
Hypothesized mean	0.005	Total ethane and ethylene from UV0 to UV0.6
df	5	
t Stat	9.191	
P(T<=t) one-tail	1.28E-04	$P < 0.05$
t Critical one-tail	2.571	t stat > t crit

Based on the statistical analysis, the null hypothesis was rejected based on t stat > t crit. Therefore, the following can be derived based on the results. The total ethane and ethylene produced from carbonization of PET exposed to UV degradation 2.3 years and above (M = 0.014, SD = 2.62E-05, n = 4) had significant difference than that of carbonization of PET without or with less UV exposure (M = 0.005). This difference was significant due to t(4) = 9.19, p = 1.28E-04 (one tail). There is enough evidence to conclude that there was statistically significant difference between the samples, in which it can be addressed that total ethane and ethylene produced was relatively higher when PET was exposed to 2.3 years and above of UV degradation. As a conclusion, UV degradation of PET for 2.3 years and above of PET produces higher ethylene and/or ethane yield.

Figure 6-13 shows the relationship between CO_2 and CO in unit mol/mol-feedstock obtained from PET carbonization. In most cases of PET carbonization, it is known that 1 mol of CO_2 is produced per 1 mol CO for PET (as discussed in Chapter 5). In the case of carbonization of PET exposed to UV degradation, it can be seen that CO_2 produced was slightly higher than CO produced in most cases. In addition, it can be seen that there was no significant correlation found between the CO and CO_2 of carbonization of UV degraded PET, due to p = 0.8291 (α = 0.05). This may be due to the reason that during the UV degradation of PET, carboxylic group was formed in the main chain of the polymer. The increase of carboxylic group led to the higher tendency of C-O scission in the main chain, thus leading to higher production of CO_2 and higher fixed-carbon yield in char.

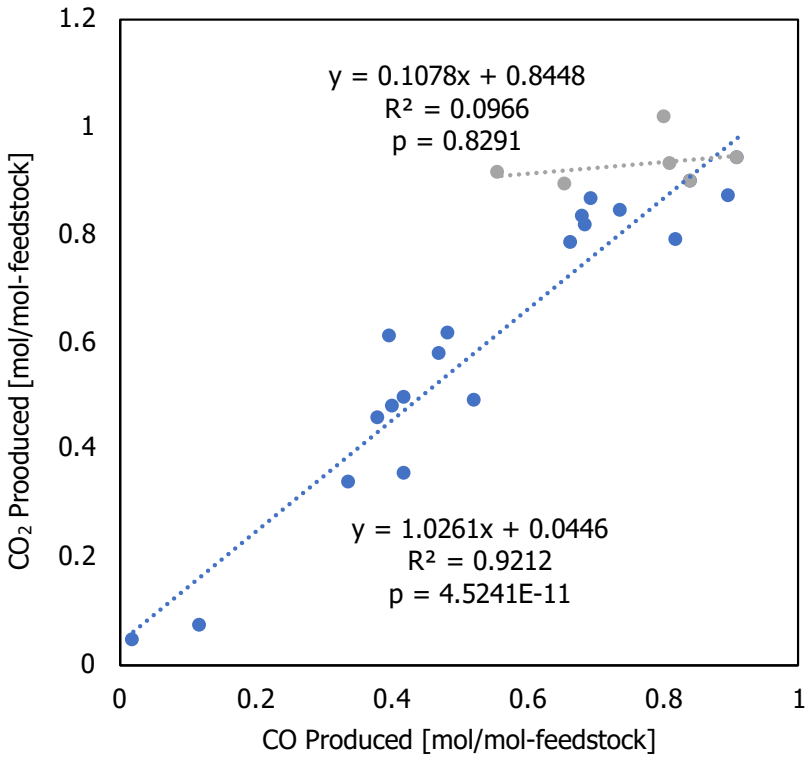

Figure 6-13: Relationship between CO_2 and CO obtained from carbonization of PET without exposure (denoted by blue markers) and PET with UV exposure (denoted by grey markers).

In order to determine the statistical significance of Figure 6-13, a Student's t-test was conducted on the two groups of data sets, they are, carbonization of PET without UV exposure (expressed as Control) and carbonization of PET with UV exposure (expressed as UV) as shown in **Figure 6-14**. Note that the y-axis is expressed as (CO_2 produced) – (CO produced).

The null hypothesis is now given as: the difference of CO_2 produced and CO produced in UV is the same as that in Control. Using a t-test for independent samples (1-tailed), the results are presented in **Table 6-3**.

Based on the statistical analysis, the null hypothesis was rejected based on t stat > t crit. Therefore, the following can be derived based on the results. The difference of CO_2 produced and CO produced in UV (M = 0.16, SD = 0.12, n = 6) had significant difference than that in Control (M = 0.06, SD = 0.08, n =20). This difference was significant due to t(6) = 1.975, p = 0.049 (one tail). There is enough evidence to conclude that there was statistically significant difference between the samples. On the other hand, it was discussed previously in Chapter 5, that 1 mol of CO_2 is produced per 1 mol CO for the case of Control. This implies that the difference of CO_2 produced and CO produced in Control is approximately equal to 0. Based on this, it can now be speculated that the difference of CO_2 produced and CO produced in UV is more than 0, which consequently means that the CO_2 produced is more than the CO produced in UV. Therefore, it can be addressed that CO_2 is relatively higher than CO produced during carbonization when PET is exposed to UV degradation.

As a conclusion, effects of UV degradation of PET on the product of carbonization were obtained as follows:

1) Increase in fixed-carbon yield was statistically significant when PET was exposed to UV degradation;
2) Increase of ethylene/ethane yield during carbonization was statistically significant for PET exposed to UV degradation for 2.3 years and above;
3) CO_2 yield was slightly higher than CO yield.

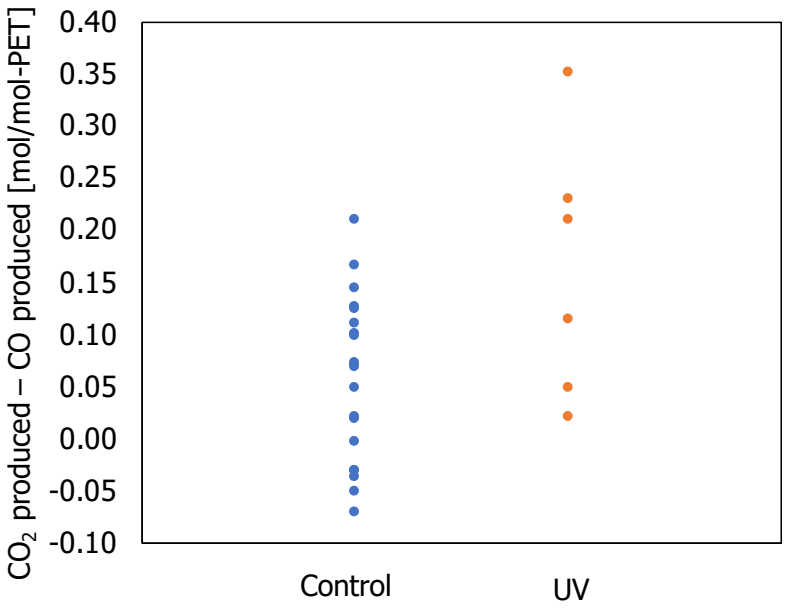

Figure 6-14: Comparison of carbonization of PET without UV exposure (expressed as control) and carbonization of PET with UV exposure (expressed as UV) using student's t-test.

Table 6-3: Results of t-test for independent samples for Control and UV.

	Control	UV	Notes
Mean, M	0.057	0.161	
Standard Deviation, SD	0.079	0.124	
Variance	0.006	0.015	
Observations, n	20	6	
df	6		
t Stat	1.975		
P(T<=t) one-tail	0.049		$P < 0.05$
t Critical one-tail	1.943		t stat > t crit

6.2.6 Conclusions: Effect of UV degraded PET on carbonized product

In the study of carbonization of UV degraded PET, sample preparation was conducted using the accelerated weathering test. The following is the summary based on the method for preparing UV degraded PET:

1) Microcracks were formed when PET was exposed to accelerated weathering. The observations of microcracks were evident during prolonged exposure to accelerated weathering.
2) Increase of absorption intensity of C=O stretching in the carboxylic acid group of PET structure was observed in the FT/IR spectra when PET was exposed to accelerated weathering. This is due to the formation of carboxylic acid group (-COOH) through Norrish II which consequently magnified the intensity of absorption band of C=O during the degradation of PET.
3) The stress at break of PET during tensile test significantly decreased with the extent of UV exposure.

Using the samples obtained from accelerated weathering tests, carbonization was conducted to determine the effects of UV degraded PET on carbonized product. The following is the summary based on current findings:

1) Although initial hypothesis suggested that higher char yield and lower wax yield were expected in the carbonization of UV degraded PET, results only showed that increase in fixed-carbon yield was statistically significant when PET was exposed to UV degradation.
2) Increase of ethylene/ethane yield was observed and was statistically significant for PET exposed to UV degradation for 2.3 years and longer, due to the decrease of C-C homolytic cleavage during thermal decomposition of PET.
3) Although not evident, it was observed that CO_2 yield was slightly higher than CO yield due to the increase of carboxylic end-group in the polymer structure.

Although a distinct difference in surface characteristics between PET with and without UV degradation was observed, the carbonized product showed otherwise. This is due to the singularity of the PET polymer, as discussed in Chapter 4, which produces consistent product composition and char characteristics during carbonization.

6.3 Effects of colored and multilayer PET on carbonized product

6.3.1 Background of colored and multilayer PET

Non-colored and lightly tinted blue PET bottles offer recyclers a high value in today's market. However, colored PET bottles such as green and red PET bottles, have limitations for their reuse and therefore, have much lower value as recycled materials. This is due to the problem in additives, that is, dyes which will contaminate the recycled PET materials and decrease polymer quality (Schloss, 2017). Dye pigments used in PET bottles are mainly organic dyes from phthalocyanine and anthraquinone families as shown in **Figure 6-15**. Phthalocyanine gives blue and green color to the resin while anthraquinone is the base for different dyes where color differs with different chemical group (Ambrogi et al., 2017). Pigments are applied in the form of discrete crystalline particles and are well dispersed in the resin (Hao and Iqbal, 1997). Due to the uniform dispersion of pigment in PET resin, removal of dye pigment from PET through mechanical separation is impossible.

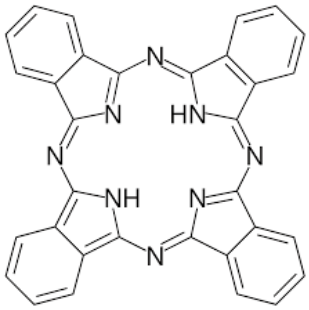

Phthalocyanine

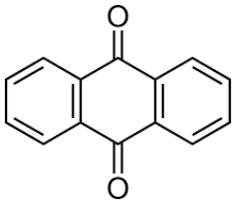

Anthraquinone

Figure 6-15: Chemical structure of phthalocyanine and anthraquinone.

On the other hand, multilayer bottles composed of combined multiple materials have been implemented to reduce oxygen permeability for the purpose of protecting beverages from oxidation and extending product shelf life (Morris, 2017). The combination of materials includes employing a core layer which is high in gas barrier properties, called oxygen barrier layer (from here on, denoted as OBL), sandwiched between PET layers. **Table 6-4** shows the summary of types of OBL generally used in PET bottle production.

Table 6-4: Major types of oxygen barrier used in multilayer PET bottles.

Type of Oxygen Barrier Layer	Description	REF
Metallized film with SiOx (Silicon oxide) coating	Inorganic barrier layer Often used in the form of PET/Metallized film/polyolefins*	Patterson and Utas (2002)
MXD6 Nylon	Organic barrier layer Encapsulated in the inner barrier between 5% and 10% of the bottle weight. Often used in Japan for monolayer, single-serve, green-tea packages in the form of PET/MXD6/PET*	GVM (2017)
Copolymer of ethylene and vinyl alcohol (EVOH)	Organic barrier layer Encapsulated in the inner barrier between 5% and 10% of the bottle weight. Often used in the form of plastic/EVOH/plastic*	Shifman (2012)

*Outer layer/Middle layer/Inner layer

Due to the multilayer structure of the bottles, mechanical recycling of the multilayer PET bottle becomes a challenge in the recycling industry (Beeva et al., 2015; Messin et al., 2017). It was reported that conventional float separation tank is ineffective in the removal of OBL (Rujnic-Sokele et al., 2008) and that intense mechanical separation is necessary to separate the layers (Kaiser et al., 2018). Therefore, in the recycling industry, multilayer bottles are widely considered as non-recyclable and are usually incinerated or landfilled.

Although both colored PET bottles and multilayer bottles have zero value in the recycling market, they have great potential in the synthesis of carbon-based adsorbents. It is of great interest to investigate the effects of additives, specifically dyes and OBL on the carbonized product. To date, there have been no reports on the effects of dyes and OBL in the PET feedstock on the product of carbonization. Additionally, the effects of added mass percentage of OBL in PET layers on the

carbonized product are also unknown. Studying these effects will give clarity to the compatibility of carbonization as a method to treat the non-recyclable colored and multilayer PET bottle.

This section discusses the yield and characterization of carbonized products obtained from carbonization of colored PET and carbonization of single PET with combination of OBL added at various mass percentage. The solid, liquid and gaseous products were obtained in the form of char, wax and gas. For char, surface analyzation and elemental analyzation were conducted to study its characteristics. For wax, liquid analysis and elemental analyzation were conducted, while for gaseous product, quantification of compounds was conducted. The effects of colored PET and OBL on the product yield and product characteristics were studied and discussed.

6.3.2 Preparation and characterization of feedstock

6.3.2.1 Preparation of samples

Samples were prepared from commercial 500 mL carbonated drink bottles, which were washed and dried overnight with their caps removed. The bottle layers were separated to give 3 different layers – thick outer layer (67.1 wt%), transparent middle layer (7.3 wt%) and thin inner layer (25.6 wt%) as shown in **Figure 6-16**.

Figure 6-16: Separated layers of commercial PET bottle sample.

6.3.2.2 Characterization of samples

Infrared spectroscopy by attenuated total reflection (ATR-FT/IR) analyzation and elemental analysis were conducted for each separated layer to determine the polymer characteristics of the commercial PET bottle samples. Analyzation methods are described in Chapter 3.

Based on the elemental analysis of separated layers of commercial PET bottle samples, elemental compositions of layers were obtained as shown in **Table 6-5**. Notice that N% obtained was relatively high in the middle layer.

Table 6-5: Elemental composition of separated layers of commercial PET bottle samples.

	Ultimate Analysis[a] [wt%]			
	C%	H%	N%	O%
Outer layer	62.1	4.1	0.2	33.6
Middle layer	65.9	7.1	11.0	16.0
Inner layer	62.0	4.0	0.2	33.8

[a]:Dry basis; Data obtained from CHN analysis had 0.3% error.

Figure 6-17 shows the FT/IR spectra of layers of commercial PET bottle samples. FT/IR spectra of outer layer and inner layer showed typical polyethylene terephthalate peaks: 1730 cm^{-1} refers to C=O stretching of carboxylic acid group, 1453 cm^{-1} and 1342 cm^{-1} indicate C-H bending and wagging of ethylene glycol segment, 1240 cm^{-1} shows C-O stretching of carboxylic acid, and 712 cm^{-1} is the interaction of benzene rings (Pereira et al., 2017). Therefore, this confirms that the outer layer and inner layer were made from PET polymer. Note that the FT/IR spectra did not show any indications of peak characterization from dye pigments. The reason for this might most possibly be that the concentration of colorant additives in the outer and inner layer were low enough to be undetected by the FT/IR analyzation as colorant additives are usually added at 1 wt% to 2 wt% of the total polymer weight (Sipe, 2016).

On the other hand, FT/IR spectra of middle layer showed typical polyamide peaks: 1635 cm^{-1} shows C=O stretching of amide I, 1541 cm^{-1} indicates N-H bending of amide II, 959 cm^{-1} is the C-C stretching, 755 cm^{-1} refers to N-H wagging and 712 cm^{-1} is the interaction of benzene rings (Charles et al., 2009; Zhu et al., 2016b). This explains the high N% obtained from the middle layer of the bottle. The polyamide peaks are often seen in typical nylon such as Nylon-6 and Nylon-66. However, the presence of benzene ring at 712 cm^{-1} in the polyamide structure identifies the polymer as MXD6 nylon (Harada et al., 1991). Additional verifications were conducted and reported in **Appendix G** and results confirmed that the middle layer of PET sample was MXD6 nylon layer. Therefore, this indicates that the OBL in the commercial PET bottle sample used in this study was MXD6 nylon.

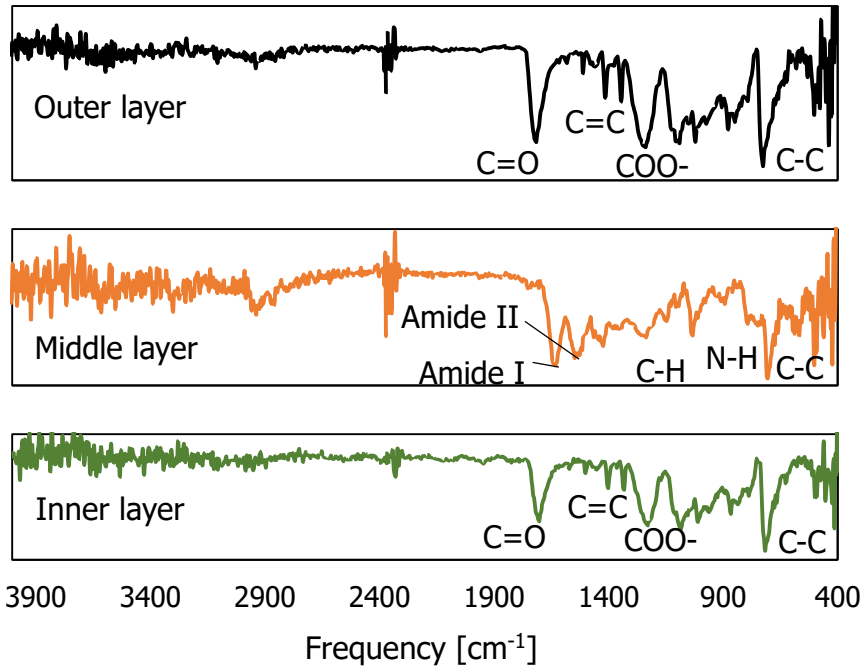

Figure 6-17: FT/IR spectra of layers of commercial PET bottle samples.

6.3.3 Carbonization of colored PET

6.3.3.1 Experimental procedures

Carbonization experiment of colored PET layer was conducted based on methods described in Chapter 3. Experiment condition was set to operate at 400-480°C and 120 min. Analyzation was also conducted using the methods described in Chapter 3, which includes proximate analysis and ultimate analysis for char; ultimate analysis for wax; and GC/TCD and GC/FID for gaseous product.

6.3.3.2 Results and discussions

Product Composition

The product distribution of carbonization of outer PET (colored PET) and inner PET (colored PET) were obtained and compared with the results of product distribution of carbonization of clear PET from Chapter 4 as shown in **Figure 6-18**. Note that wax was taken as the balance from char and gas due to the large amount of residual wax that was solidified in the pipes of the reactor. Char yield decreased from 28.4 wt% of clear PET to 21.4 wt% for outer PET and 22.5 wt% for inner PET. Wax yield was slightly higher for colored PET layers while no evident changes were observed for gas yield. On the other hand, evident decrease of fixed-carbon yield for the colored PET layers was observed compared with clear PET. The reason for the decrease of char yield and fixed-carbon yield may be due to the presence of colorant additives that is well-dispersed in the polymer structure. The colorant additives prevented and disrupted the formation of cross-link in char, while stimulated the release of volatile matter to form wax. Nevertheless, char yield and fixed-carbon yield of carbonization of PET with colorant additives are relatively high compared to carbonization of other plastic counterparts; that is, LDPE: y_{char} = 0 wt% (Batch, 550°C, 5°C/min; Marcilla et al., 2009), HDPE: y_{char} = 0 wt% (Batch, 550°C, 5°C/min; Marcilla et al., 2009), and PP: y_{char} = 13.3 wt% (Batch, 380°C, 3°C/min; Sakata et al., 1999).

Characteristics of wax

Results for elemental analysis of wax is presented in **Table 6-6**. Overall, wax obtained from carbonization showed no evident difference in wax properties for clear PET and PET with colored additives.

Properties of Gaseous Product

Figure 6-19 shows the composition of gaseous products obtained from carbonization of clear PET, outer PET layer and inner PET layer. Similar to previously discussed, CO_2 makes up the main gaseous compound, followed by CO and hydrocarbons. Little to almost no hydrogen was detected. Overall, gaseous products showed no evident difference in composition for clear PET and PET with colored additives.

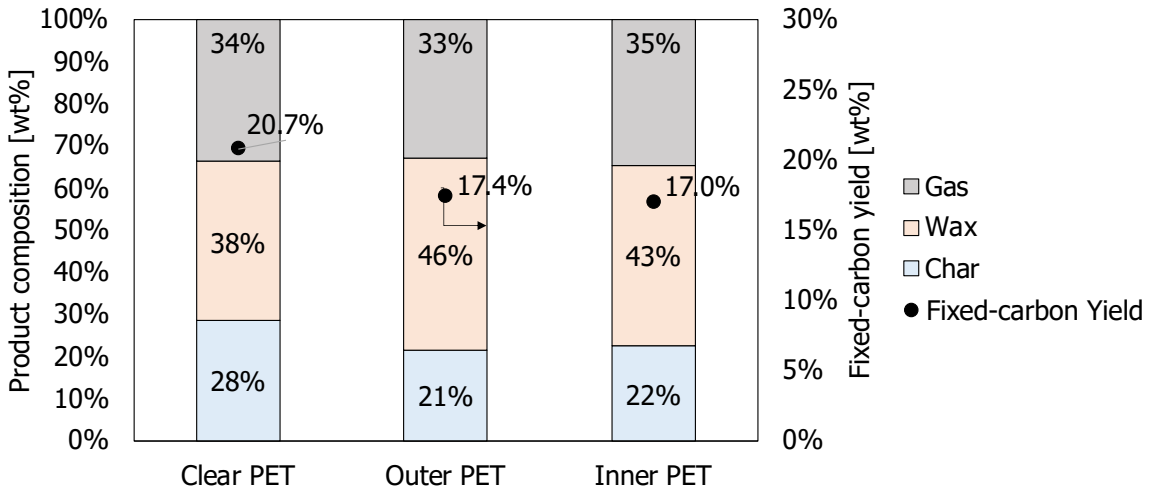

Figure 6-18: Comparison of product distribution and fixed-carbon yield obtained from carbonization of clear PET layer (from Chapter 4), outer PET and inner PET.

Table 6-6: Characteristics of wax obtained from carbonization of clear PET layer (from Chapter 4), outer PET layer and inner PET layer.

	Ultimate Analysis[a] [wt%]				HHV[a]
	C%	H%	N%	O%	[MJ/kg]
Clear PET	62.3	5.2	0.3	32.2	26.6
Outer PET	70.1	5.1	0.5	24.3	28.0
Inner PET	65.7	4.4	0.4	29.5	24.6

[a]:Dry basis; Data obtained from CHN analysis had 0.3% error.

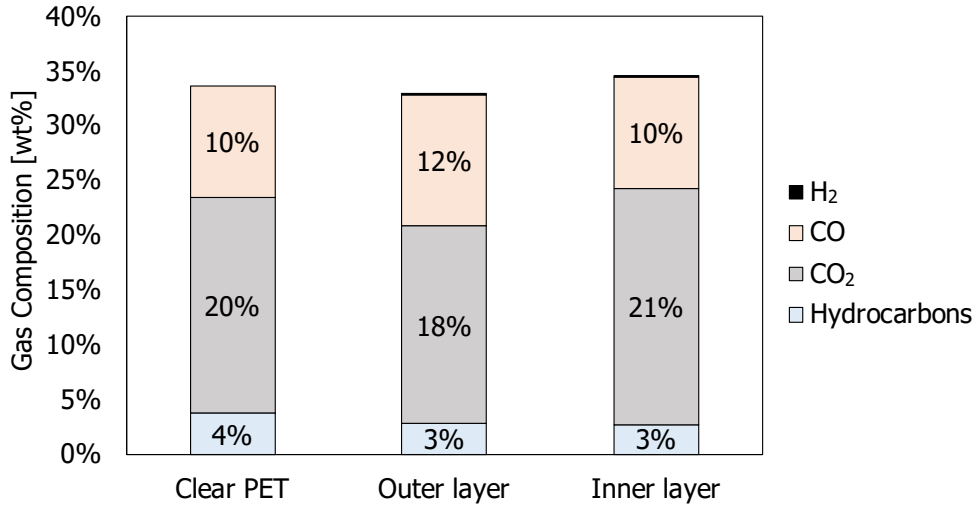

Figure 6-19: Comparison of gas composition obtained from carbonization of clear PET layer (from Chapter 4), outer PET and inner PET.

6.3.4 Carbonization of multilayer PET

6.3.4.1 Experimental procedures

Procedures for carbonization are described in detail in Chapter 3. The operating temperature was set constant to 400-480ºC and held for 120 min. Note that approximately 70 g outer layer (PET) with middle layer (OBL) added at mass percentage of 0, 2, 4, 6 and 8 wt% were packed for each experiment. Analyzation was conducted using the methods described in Chapter 3.

6.3.4.2 Results and discussion

Product composition

The product distribution obtained from carbonization of PET and mixture of PET and OBL of different added mass percentage is shown in **Figure 6-20**. From the results, char yield from carbonizing PET with 2 wt% of OBL slightly decreased compared with the char yield obtained from carbonizing single PET layer. However, minor positive correlation of char yield can be observed with increasing mass percentage of OBL. In the case of wax and gas composition, evident decrease of wax yield while increase of gas yield can be seen with increasing OBL mass percentage. Results indicate that, in the case of constant char yield, there was high possibility of cracking of wax to form gaseous product, which was dominant in the presence of OBL.

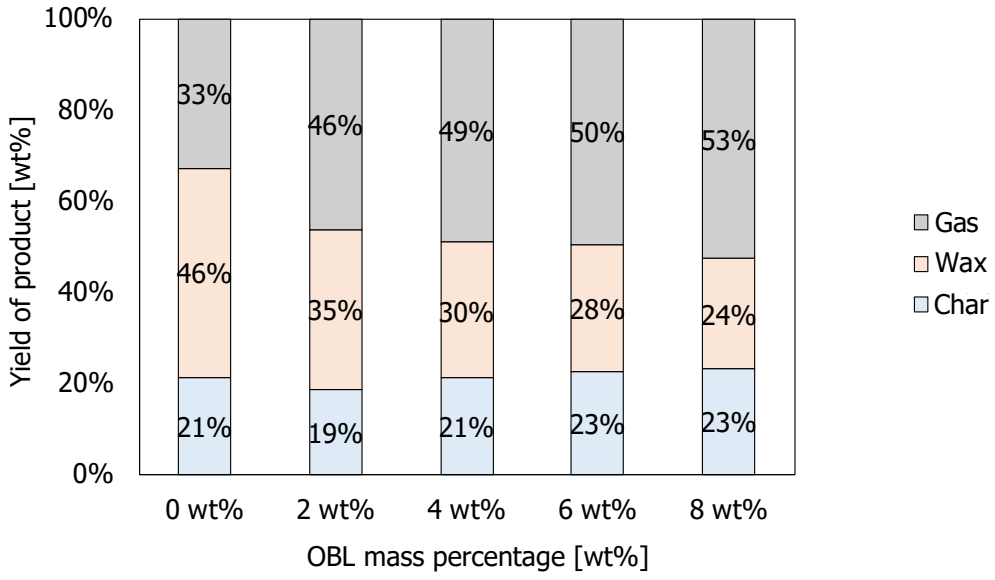

Figure 6-20: Product distribution obtained from carbonization of single PET layer and mixture of PET and OBL of different added mass percentage.

Characteristics of char

Figure 6-21 shows the FT/IR spectra of char obtained from carbonization of PET and mixture of PET and OBL of different added mass percentage. FT/IR spectra of char shows that char obtained from carbonization of single PET layer showed no remaining structure of PET. This indicates the complete carbonization of PET. However, for increased OBL mass percentage in the feedstock, large absorption peaks of N-H wagging at 755 cm^{-1} and benzene ring interaction at 712 cm^{-1} were observed. In addition, amide I and amide II peaks were observed for char at higher OBL mass percentage. This indicates that, compared to PET polymer, functional groups of MXD6 nylon have less tendency to volatilize into wax and gaseous product.

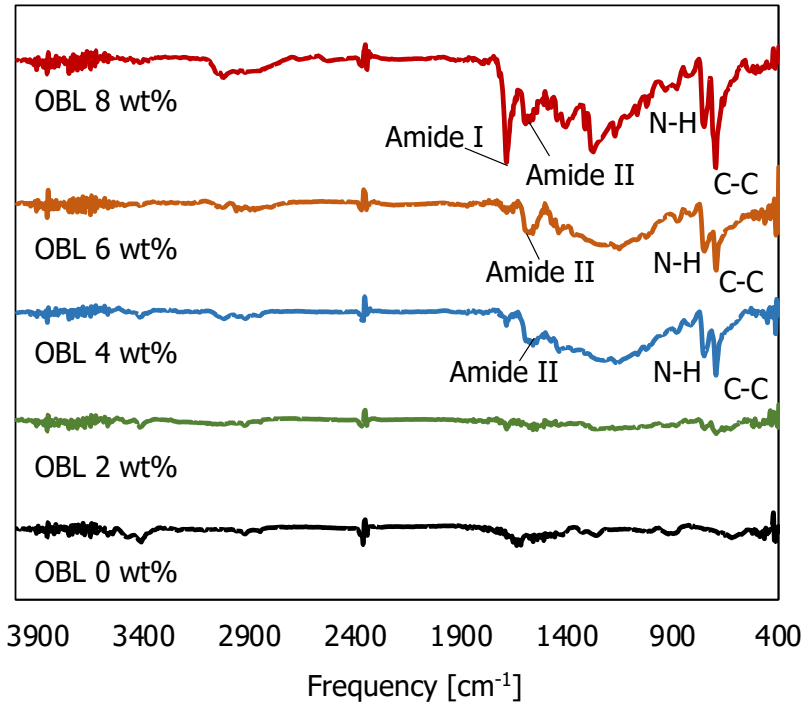

Figure 6-21: FT/IR spectra of char obtained from carbonization of PET and mixture of PET and OBL of different mass percentage.

Proximate and ultimate analysis were conducted for char whereas ultimate analysis and HHV measurements were conducted for wax, and the results are presented in **Table 6-7**. Based on the results obtained for char, volatile matter and fixed carbon contents were consistent for all runs. Fixed-carbon yield slightly increased with increasing OBL mass percentage. However, it was well noted that the amount of ash slightly increased with increasing OBL mass percentage. The leftover ash was collected for analysis using XRD to identify the component of ash.

Table 6-7: Characteristics of char obtained from carbonization of PET and mixture of PET and OBL of different added mass percentage.

OBL	Proximate Analysis[a] [wt%]			Fixed-carbon yield [wt%]	Ultimate Analysis[a] [wt%]			
	Ash	VM[b]	FC[c]		C%	H%	N%	O%
0 wt%	0.00	18.6	81.4	17.4	88.4	4.3	0.7	6.6
2 wt%	0.03	18.7	81.2	15.1	89.4	4.4	2.7	3.5
4 wt%	0.24	18.7	81.1	17.1	80.8	4.0	2.7	12.5
6 wt%	0.29	17.5	82.2	18.7	81.4	4.0	3.0	11.7
8 wt%	0.66	18.4	80.9	19.0	79.1	5.5	1.9	13.5

[a]: Dry basis; Data obtained from CHN analysis had 0.3% error

[b]: Volatile matter content

[c]: Fixed carbon content

Figure 6-22 shows the XRD pattern of leftover ash. Ash from combustion of single MXD6 nylon layer, labelled as "MXD6 layer" was obtained for comparison. Cobalt peaks in the form of cobalt oxide were observed in all the ash sample. The reason for this finding is that cobalt salt is usually blended with PET/MXD6 nylon to improve oxygen scavenging abilities of the packaging (Collette and Merrimack, 1991). Peaks for aluminum and silica were also detected which are most likely originated from the surface of alumina/silica crucible used in the proximate analyzation.

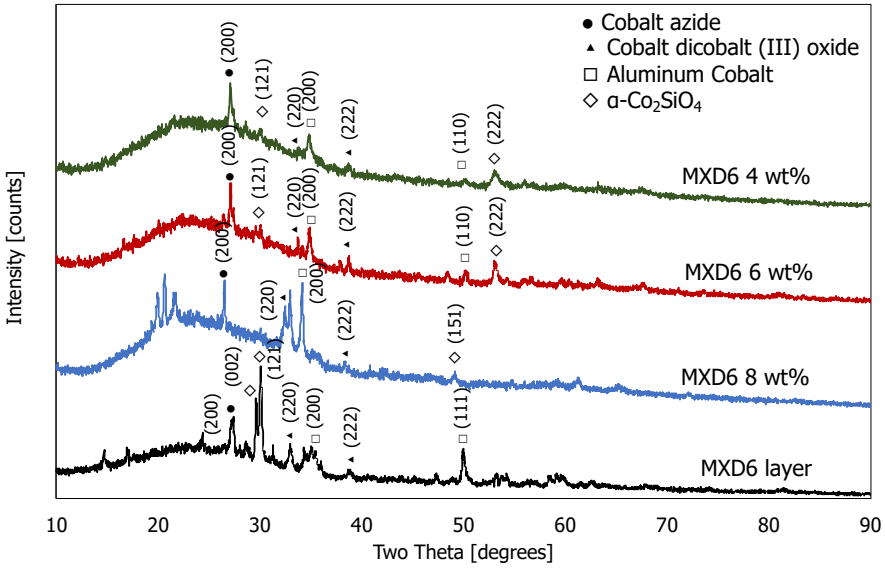

Figure 6-22: XRD pattern of leftover ash.

Characteristics of wax

Results for elemental analysis of wax is presented in **Table 6-8**. Wax from carbonization of PET with OBL showed slight decrease in O%, indicating the loss of oxygen in the wax phase to form CO_2 in the gas phase. This will be discussed later.

Table 6-8: Characteristics of wax obtained from carbonization of PET and mixture of PET and OBL of different mass fractions.

OBL	Ultimate Analysis[a] [wt%]				HHV[a]
	C%	H%	N%	O%	[MJ/kg]
0 wt%	70.1	5.1	0.5	24.3	28.0
2 wt%	70.4	5.2	1.7	22.7	29.6
4 wt%	72.2	5.3	2.0	20.6	29.7
6 wt%	73.4	5.5	2.2	19.0	29.3
8 wt%	71.5	5.4	1.6	21.5	28.1

[a]: Dry basis; Data obtained from CHN analysis had 0.3% error

Table 6-9 and **Figure 6-23** show the GC/MS analysis results of wax obtained from carbonization of single PET layer and PET with OBL of different mass percentage, with the relative peak area (%) given in the total chromatogram. The chemical compounds are grouped into carboxylic acid, aromatic ketone, aromatic hydrocarbon, phthalate ester and aromatic amine for ease of comparison. Based on the results, it is evident that benzoic acid was the main component of wax. With increasing OBL mass percentage, evident decrease in relative peak area of the carboxylic acid was observed. Compared to wax from carbonization of single PET layer, wax from carbonization of PET with OBL produced more aromatic hydrocarbons such as biphenyl and fluorene. Also, presence of OBL in the feedstock led to the detection of aromatic amine peaks such as pyridine and benzonitrile. Overall, increase in aromatic hydrocarbons and decrease in carboxylic acid were observed in wax obtained from carbonization of PET with OBL.

Table 6-9: GC/MS analysis results of the wax obtained from carbonization of single PET layer and PET with OBL of different added mass percentage.

Name of compounds	%Area				
OBL mass percentage	0 wt%	2 wt%	4 wt%	6 wt%	8 wt%
Carboxylic acid					
Acetic acid	0.32	0.78	0.28	0.25	0.00
Benzoic Acid	88.0	89.4	88.9	77.6	63.6
Benzoic acid, 3-methyl-	0.14	0.00	0.00	0.09	0.00
Benzoic acid, 4-methyl-	4.00	2.76	3.48	3.13	3.22
4-Ethylbenzoic acid	0.93	0.59	0.74	0.78	0.35
	93.4	93.5	93.4	81.8	67.2
Aromatic ketone					
Acetophenone	0.00	0.11	0.00	0.22	2.82
Benzeneacetaldehyde	0.00	0.00	0.00	0.00	0.88
Propiophenone	0.00	0.15	0.00	0.66	0.00
Butyrophenone	0.00	0.13	0.18	0.40	0.00
1-Butanone, 2-methyl-1-phenyl-	0.00	0.00	0.00	0.10	0.00
Benzaldehyde, 4-(1-methylethyl)-	0.12	0.00	0.00	0.00	0.46
	0.12	0.39	0.18	1.38	4.15
Aromatic hydrocarbon					
Biphenyl	2.08	3.25	2.88	10.3	14.6
1,1'-Biphenyl, 2-methyl-	0.10	0.00	0.00	0.25	0.00
Diphenylmethane	0.00	0.19	0.23	0.64	0.00
1,1'-Biphenyl, 3-methyl-	0.70	0.69	0.72	2.73	0.40
Bibenzyl	0.00	0.21	0.20	0.38	0.40
4-Ethylbiphenyl	0.25	0.00	0.00	0.27	0.26
Fluorene	0.00	0.40	0.45	1.02	0.62
9H-Fluorene, 9-methyl-	0.00	0.00	0.30	0.57	0.32
	3.13	4.74	4.78	16.13	16.60

Name of compounds	%Area				
OBL mass percentage	0 wt%	2 wt%	4 wt%	6 wt%	8 wt%
Phthalate ester					
Dimethyl phthalate	1.18	1.02	0.69	0.00	0.00
Diethyl phthalate	0.51	0.32	0.00	0.00	0.00
Dibutyl phthalate	1.66	0.00	0.00	0.00	0.00
	3.35	1.34	0.69	0.00	0.00
Aromatic amine					
Pyridine, 2-propyl-	0.00	0.00	0.14	0.12	0.00
Benzonitrile	0.00	0.00	0.00	0.04	10.46
Pyridine, 2-ethyl-5-methyl-	0.00	0.00	0.00	0.15	0.09
Pyridine, 3-ethyl-4-methyl-	0.00	0.00	0.00	0.05	0.05
Benzonitrile, 4-methyl-	0.00	0.00	0.00	0.05	0.63
4'-Benzamido-4-methylbenzanilide	0.00	0.00	0.00	0.00	0.18
Benzeneacetonitrile, α-methyl-	0.00	0.00	0.06	0.09	0.19
Butanenitrile, 2,3-bis(benzoyloxyimino)-	0.00	0.00	0.00	0.00	0.11
Benzamide	0.00	0.00	0.72	0.19	0.35
	0.00	0.00	0.92	0.69	12.06

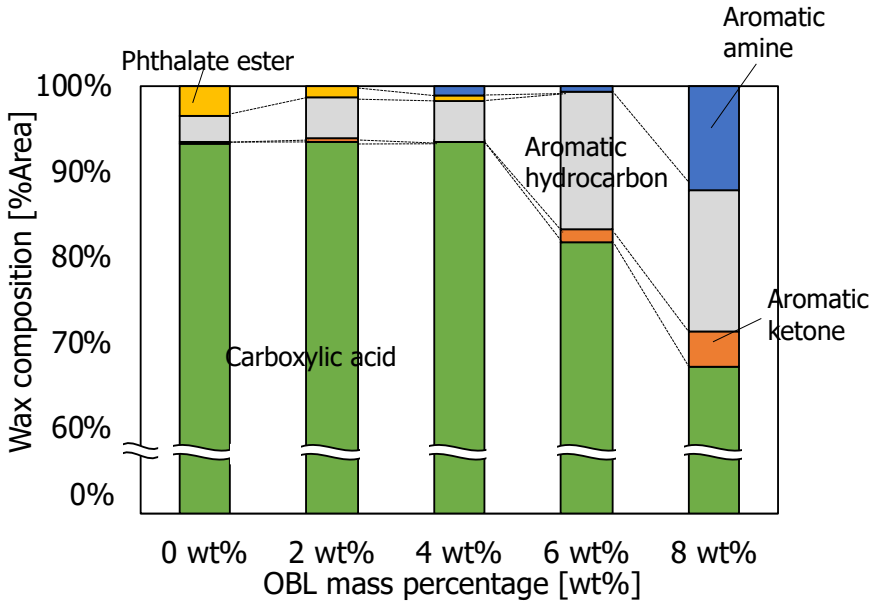

Figure 6-23: Graphical representation of the GC/MS analysis.

Composition of gaseous product

Figure 6-24 shows the overall gas composition and hydrocarbon composition of gaseous product obtained from all carbonization experiments. Similarly, the gaseous product was mainly consisted of CO_2, CO and hydrocarbons. However, the main difference was the increased CO_2 yield with increasing OBL mass percentage. As discussed in Chapter 5, 1 mol CO_2 was produced per 1 mol of CO when 1 mol PET was carbonized. However, in the presence of OBL, the total mol of CO_2 and mol CO produced for 1 PET monomer were obtained as follows: 1.7 mol-CO_2/mol-PET and 0.4 mol-CO/mol-PET for 2 OBL-wt%; 1.8 mol-CO_2/mol-PET and 0.4 mol-CO/mol-PET for 4 OBL-wt%; 1.9 mol-CO_2/mol-PET and 0.3 mol-CO/mol-PET for 6 OBL-wt%; 2.1 mol-CO_2/mol-PET and 0.2 mol-CO/mol-PET for 8 OBL-wt%; as compared to 0.8 mol-CO_2/mol-PET and 0.8 mol-CO/mol-PET for 0 OBL-wt%. Notice the total CO_2 produced was more than the maximum assumed CO_2 molecule. This indicates the possible decomposition of carboxylic acid during carbonization to form aromatic hydrocarbons in wax and CO_2 in gas. On the other hand, for hydrocarbons, the amount of methane decreased while ethane and ethylene increased in the presence of OBL, indicating lower conversion of short chain hydrocarbons from long chain hydrocarbons. Overall, higher CO_2 yield was obtained in the carbonization of PET and OBL mixture, indicating the decomposition of carboxylic acid in wax to form CO_2 in gas.

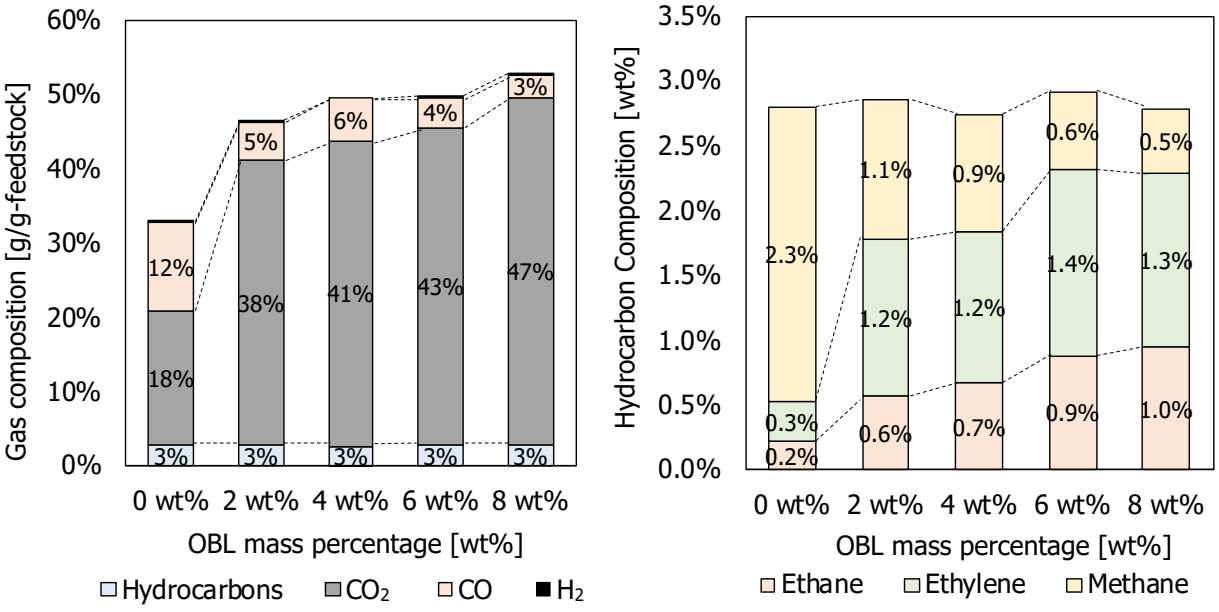

(a) Overall gas composition (b) Hydrocarbon composition

Figure 6-24: Overall gas composition and hydrocarbon composition of gaseous product obtained from carbonization.

6.3.5 Effect of cobalt oxide on carbonized product

The high yield of CO_2 from carbonization of PET with OBL compared to single PET layer could be explained by the presence of cobalt salt in the OBL. Cobalt salt was detected in the leftover ash by powder XRD analysis, in which identified as cobalt oxide, is known to be one of the most reactive metals that is comparable to iron and nickel compounds. Thingpen and Trebellas (1969) reported cobalt oxide as catalyst for the reaction of vapor carboxylic acid to form ketones at high temperatures around 400°C. It was assumed that the cobalt salt in OBL decomposed to cobalt oxide, which consequently led to the decomposition of carboxylic acid in the wax phase to form aromatic hydrocarbon and CO_2. In order to verify this assumption, additional investigation was conducted by carbonizing PET with cobalt oxide. Here, 1 wt% cobalt oxide was added in excess to the feedstock for the initial intention to completely decompose carboxylic acid and to produce high yield of aromatic hydrocarbons.

Figure 6-25 shows the comparison of product distribution and gas composition obtained from carbonization of single PET layer, PET with 8 wt% OBL and PET with 1 wt% cobalt oxide. PET with 8 wt% OBL was chosen as a comparison data to represent the actual fraction (7.9 wt%) of layers in commercial PET bottle sample. From the results, wax fraction decreased while gas fraction increased when 1 wt% cobalt oxide was added in the initial feedstock, in which the increase in aromatic hydrocarbons and decrease in carboxylic acids (based on GC/MS analysis) were observed in wax, while high gas yield was obtained. In the case of gas composition, results obtained were similar to findings from carbonization of PET with added OBL. The yield of CO_2 highly exceeded the predicted amount of total CO_2 in the presence of cobalt oxide, in which the mol of CO_2 and mol CO produced for 1 PET monomer was obtained as 1.6 mol-CO_2/mol-PET and 0.4 mol-CO/mol-PET. However, the decrease in wax and increase of CO_2 were not as evident as expected, and was lower than that in carbonization of PET with 8 wt% OBL as a consequence of lack of dispersion of the granular cobalt oxide in the initial feedstock. Nonetheless, the results verified that presence of cobalt oxide in the carbonization feedstock largely affects the composition of wax and gaseous product, in which cobalt oxide catalyzes the decomposition of carboxylic acid to form aromatic hydrocarbons in the wax and CO_2 in the gaseous product.

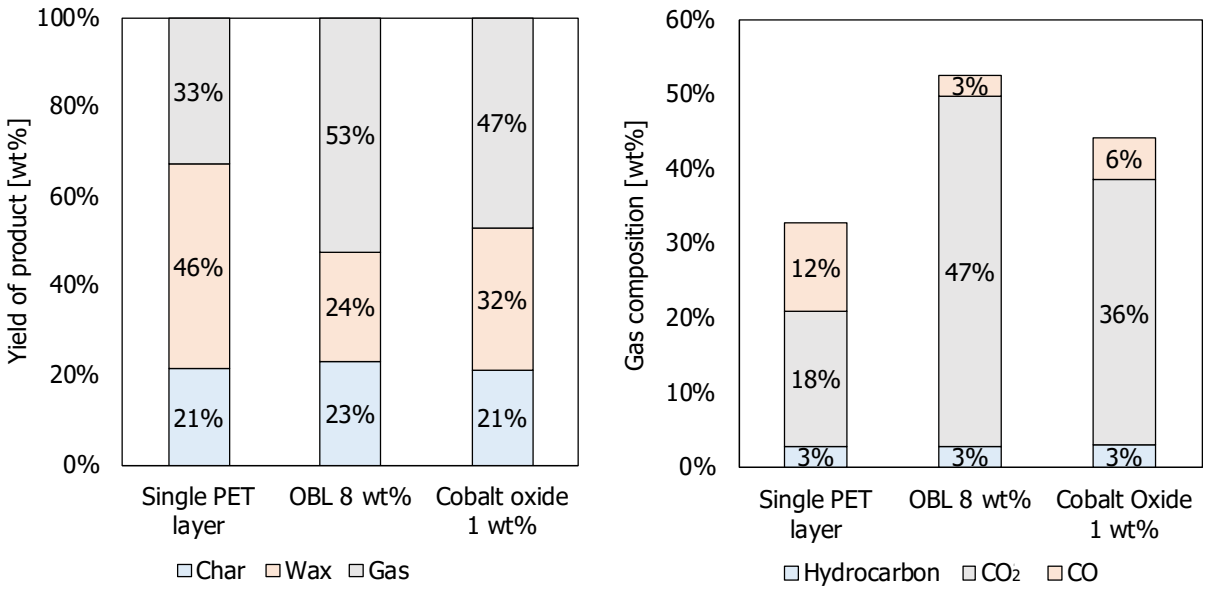

(a) Product distribution (b) Gas composition

Figure 6-25: Comparison of (a) product distribution and (b) gas composition obtained from carbonization of single PET layer, PET with 8 wt% OBL and PET with 1 wt% cobalt oxide.

6.3.6 Conclusions: Effects of colored and multilayer PET on carbonized product

In the study of carbonization of colored PET, sample feedstock from commercial PET bottle was used. The following is the summary based on current findings:

1) Results showed that char yield and fixed-carbon yield decreased compared to clear PET due to the presence of colorant additives which is well-dispersed in the polymer structure that prevented the formation of cross-link in char and stimulated the release of volatile matter to form wax.
2) Although decreased char yield and fixed-carbon yield were observed, the results obtained were relatively high compared to char yield and fixed-carbon yield from carbonization of other plastic counterparts.
3) Composition of wax and gaseous products were consistent and showed no large variance during the carbonization of colored PET bottle.

In the study of carbonization of multilayer PET, a comparison between carbonization of single layer PET and carbonization of PET with OBL added at different mass percentage was studied and the carbonized product was evaluated. MXD6 nylon was chosen as the OBL in this study. The following is the summary based on current findings:

1) Results obtained for char showed that OBL had no apparent effect in the process, in which char obtained from all experimental runs produced char with high carbon content.
2) Increase in OBL mass percentage led to decrease of wax yield and subsequent increase of gas yield.
3) Carbonization of PET with OBL produced more aromatic hydrocarbons such as biphenyl and fluorene in wax and more CO_2 in gaseous product.

Further investigation by adding cobalt oxide in the carbonization operation was conducted to study the effects of cobalt oxide on carbonized product. The following is the summary:

1) Cobalt compound in the OBL significantly affected the composition of wax and gaseous product.
2) It was speculated that cobalt oxide catalyzes the decomposition of carboxylic acid to aromatic hydrocarbons and CO_2.

6.4 Chapter summary

In this chapter, the effects of contaminants in non-recyclable PET on carbonized product were studied and presented. Colored PET, multilayer PET and PET exposed to UV degradation were chosen as the study target due to the non-recyclability of the materials. Carbonization of these non-recyclable PET was conducted under constant operating temperature and holding time, and the following summaries were obtained.

Firstly, the effects of UV degradation of feedstock on carbonization of PET were investigated by carbonizing PET, in which PET was exposed to different extent of UV degradation. UV degraded PET was prepared using the accelerated weathering method. Overall, carbonization of PET exposed to various extent of UV degradation produced char with high carbon content, thus indicating the suitability of method.

Next, the effects of carbonization of colored PET on carbonized product were investigated. Colored PET was prepared from commercial colored PET bottles which was dyed green. Results showed that char yield and fixed-carbon yield decreased compared to clear PET. The reasons may most likely be the presence of colorant additives which prevented the formation of cross-link in char and consequently stimulated the release of volatile matter to form wax.

Finally, the effects of carbonization of multilayer PET on carbonized product were studied and reported. The multilayer PET was obtained from commercial PET bottles and the oxygen barrier layer was identified as MXD6 nylon layer. Results showed that oxygen barrier layer had no apparent effect on the yield and characteristics of char. However, carbonization of PET with oxygen barrier layer produced more aromatic hydrocarbons such as biphenyl and fluorene in wax and more CO_2 in gaseous product, indicating possible decomposition reaction of volatile matter. Cobalt oxide was identified in the ash residue of char, indicating the presence of cobalt salt in the oxygen barrier layer which had led to the decomposition of volatile matter. In order to verify this assumption, further investigation was conducted by adding cobalt oxide in the carbonization operation. Results confirmed that cobalt oxide catalyzes the decomposition of volatile matter, carboxylic acid to aromatic hydrocarbons and CO_2.

Chapter 7: Gas adsorption study of activated char

7.1 Introduction

The production of activated carbon from solid waste is most advantageous in terms of low to zero cost of raw material. The valorization of solid waste is also beneficial in terms of providing a new usage to the solid waste and omitting the need for costly treatment of waste (Coelho et al., 2011; Singh et al., 2017; Wang et al., 2019). In this chapter, char from Chapter 4 was activated and the gas adsorption ability of product was studied in order to evaluate the capacity of carbon dioxide (CO_2) adsorption. The first half of the chapter reports a bench-scale static adsorption apparatus which was used to measure the CO_2 adsorption isotherm. The adsorption equilibrium data of CO_2 onto waste PET derived carbon adsorbent was presented and fitted to the Langmuir model. The second half of the chapter reports a bench-scale dynamic adsorption apparatus which was used to obtain the breakthrough curve of multiple gaseous compound. Based on the information from adsorption isotherm of CO_2, the breakthrough curve of CO_2 was correlated with LDF equation to obtain the adsorption kinetics of CO_2 onto PET derived carbon adsorbent with comparison to commercial activated carbon and zeolite. The experiments were carried out under controlled conditions according to the study scheme as shown in **Figure 7-1**.

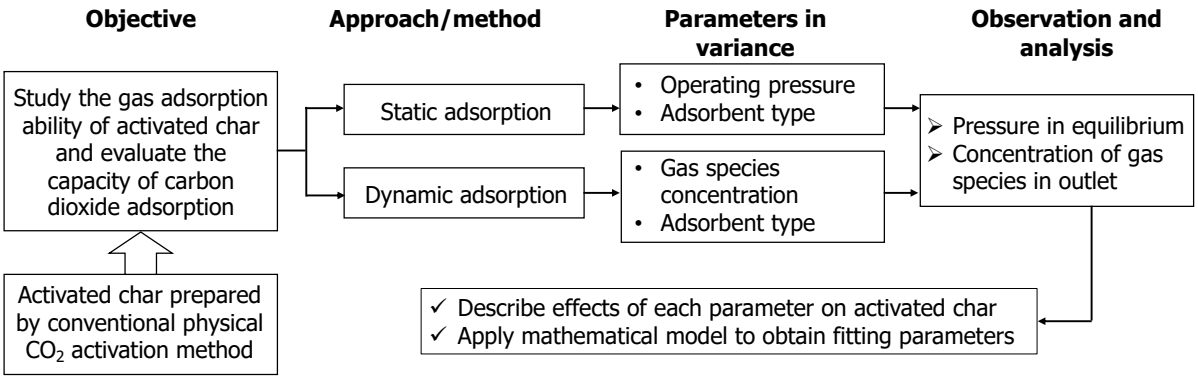

Figure 7-1: Study scheme of Chapter 7 to investigate the gas adsorption characteristics and gas adsorption capacity of activated char.

7.2 Activation of char and surface properties

7.2.1 Experimental procedures and materials

7.2.1.1 Activation of char

Char was prepared from carbonization at 400-480°C, 120 min in nitrogen atmosphere as described in Chapter 4. Activation was conducted using methods and conditions described in Chapter 3 to produce activated carbon (PET-AC). Commercial activated carbon (AC-GH2x) and zeolite (Zeolite 5A) were used as comparison. Characteristics of the commercial adsorbents are described in Chapter 3.

7.2.1.2 Analyzation of activated char

Characterization of PET-AC was conducted using ultimate analysis, scanning electron microscope for surface morphology, and BET/BJH analysis for specific surface area and pore size distribution.

7.2.2 Results and discussion

7.2.2.1 Physical characteristics of PET derived carbon adsorbent

A comparison of elemental composition of char obtained from PET carbonization as described in Chapter 4 and PET-AC obtained from char activation are presented in **Table 7-1**. Char contained high C% which consequently increased carbon active site for the oxidation reaction during CO_2 activation. The increase of carbon active site is essential for the reaction of carbon with CO_2 during activation for the formation of micropores and increase of surface area (Vallejos-Burgos et al., 2016; Oyarzún et al., 2020). After activation, slight decrease in carbon content and slight increase in oxygen was observed. This indicates that the burn-off of char occurred where carbon atoms from char were eliminated by CO_2 to expose micropores on surface. **Figure 7-2** shows the surface morphology of char obtained from PET carbonization and PET-AC obtained after activation of char. As seen in the magnification of char from PET carbonization, particle shape was irregular and distorted and that surface of char was smooth without any presence of pores on surface. After activation, evident change in PET-AC surface was observed, where rough surface of activated char and formation of fine pores on the surface are apparent. Fine pores of less than 1 μm can be seen dispersed on the surface of char in Figure 7-2(e).

Table 7-1: Comparison of elemental composition of char obtained from PET carbonization and PET-AC obtained after activation of char.

	Ultimate Analysis[a] [wt%]			
	C%	H%	N%	O%
Char	89.3	4.4	0.4	5.9
PET-AC	79.1	0.4	2.2	18.3

[a]:Dry basis; Data obtained from CHN analysis had 0.3% error.

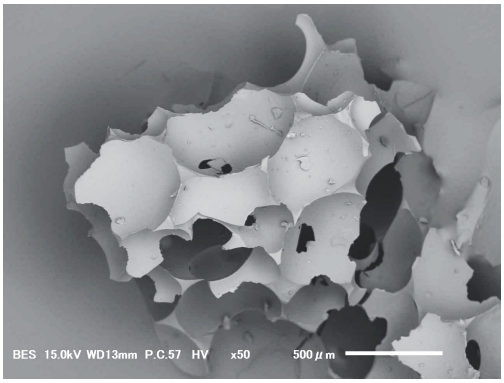

(a) Char surface (×50)

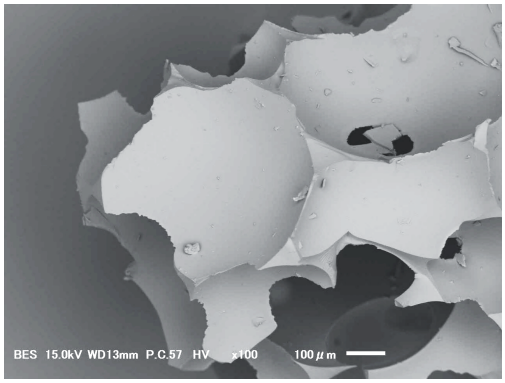

(b) Char surface at ×100

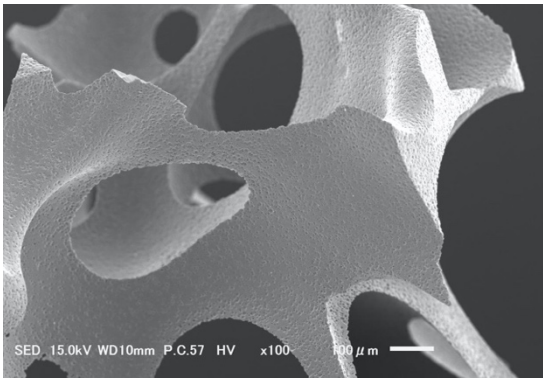

(c) PET-AC surface at ×100

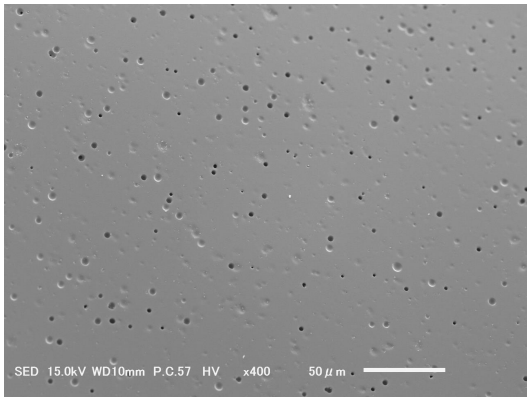

(d) PET-AC surface at ×400

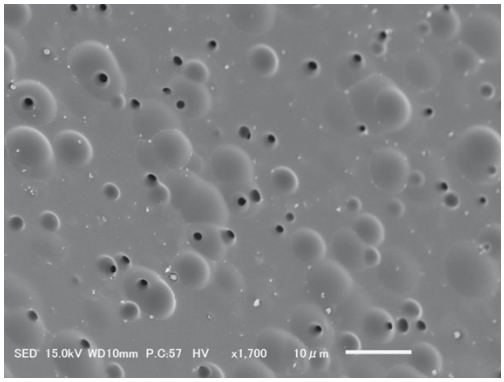

(e) PET-AC surface at ×1700

Figure 7-2: Surface magnification of (a), (b) char and (c)-(e) activated char, PET-AC.

7.2.2.2 BET/BJH characteristics of PET derived carbon adsorbent

The N_2 adsorption and desorption isotherms of PET-AC, commercial AC-GHx2 and Zeolite 5A were obtained as shown in **Figure 7-3** and the specific surface areas, total pore volumes and average pore sizes were calculated as shown in **Table 7-2**. Based on the results obtained, it can be seen that adsorbents considered herein have large surface area with pore diameter of the micropore range (<2 nm). However, it was observed that for the N_2 adsorption-desorption isotherm of PET-AC, the desorption curve did not follow the pathway of adsorption curve. This phenomenon can be explained by the structure of pores. Types of hysteresis loop are classified by the IUPAC and are given in **Figure 7-4**. Based on this classification, the isotherms obtained in PET-AC was identical to the hysteresis loops Type II and Type IV. Hysteresis loop Type II and Type IV are usually shown in solids with complex pore structures. The pore structures are generally described to have narrow branches connected to a pouch; and are usually referred to as ink-bottle-shaped pores for hysteresis loop Type II, and narrow slot-like pores for hysteresis loop Type IV. In both cases, the steep desorption curve is usually associated with pore-blocking due to the narrow necks of the pore structure (Thommes et al., 2015). Pore-blocking is the process in which a meniscus formed at the mouth of the neck recedes into the pore interior until the cavity is gradually emptied. Adsorbents with ink-bottle-pore structure are combinations of micropores and mesopores, where mesopores have access to the external surface through micropores. Based on the pore size distribution of PET-AC, although data was not obtained under 10Å due to limitation of instrument, it is evident that combinations of micropores and mesopores were present in the PET-AC structure, thus indicating the ink-bottle-pore or slit-like-pore structure of PET-AC.

7.2.3 Conclusions: Activation of char and surface properties

Based on the observation of surface morphology and analysis of N_2 adsorption/desorption isotherm of PET-AC, adsorbent with high BET surface area and small pore diameter was obtained by activating char from PET carbonization. This indicates the successful burn-off of char surface to produce activated carbon with pore diameter of the micropore range.

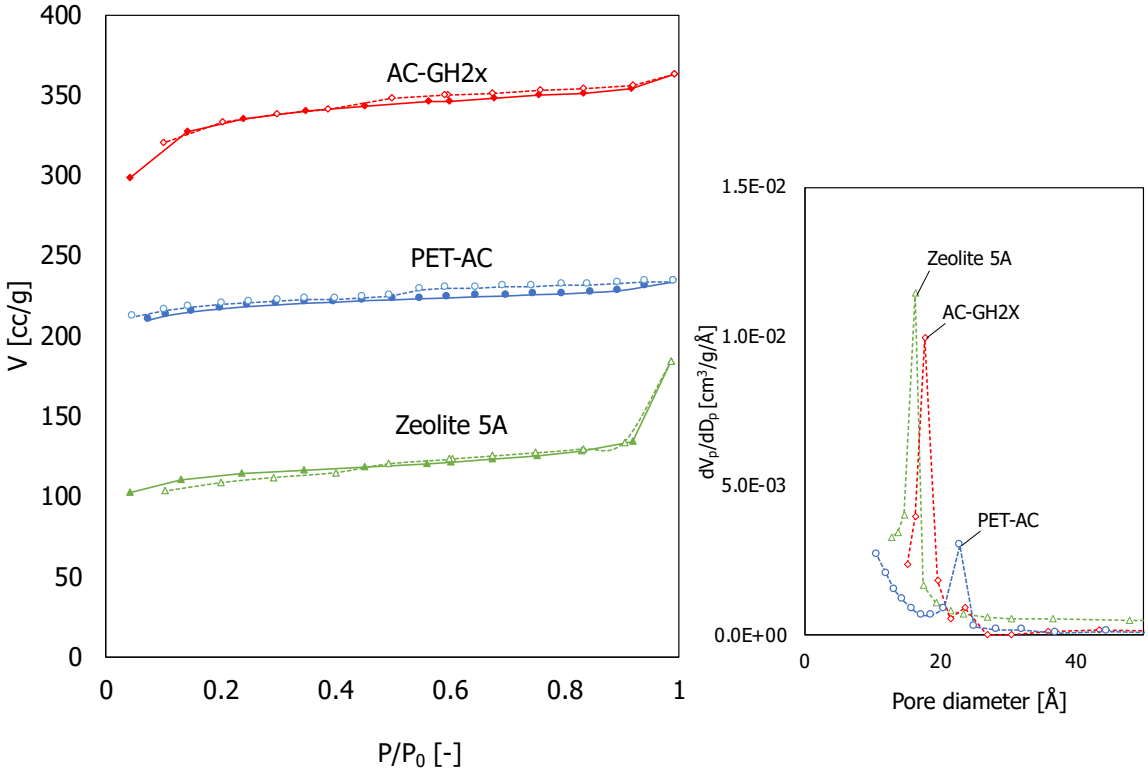

Figure 7-3: Adsorption isotherm and pore size distribution of PET-AC, AC-GH2x and zeolite 5A.

Table 7-2: Specific surface areas, total pore volumes and geometric mean radius of the adsorbents estimated from N_2 adsorption/desorption isotherm method.

		PET-AC	AC-GHx2	Zeolite 5A
BET surface area	[m^2/g]	616	1017	463
Total pore volume	[cc/g]	0.37	0.48	0.18
Geometric mean radius*	[nm]	1.00	1.36	1.20

*Taken at the 50% probability point of the cumulative lognormal size distribution.

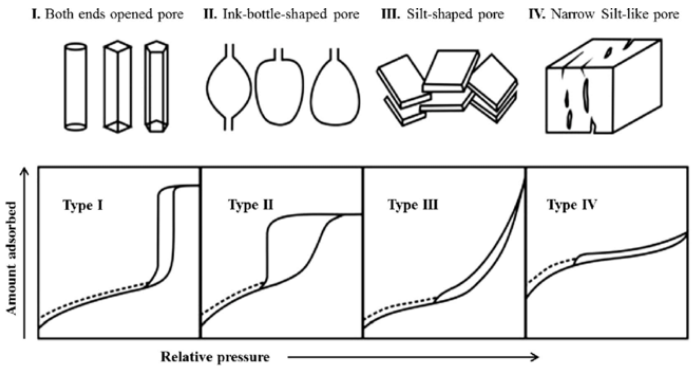

Figure 7-4: IUPAC classification of hysteresis loop corresponding to pore shapes. (Image adopted from Xiong et al., 2017)

7.3 Static adsorption study

7.3.1 Experimental set-up

Single gas component, binary gas component and multiple gas component adsorption isotherm measurements for static adsorption studies were conducted based on methods described in Chapter 3 using PET-AC, AC-GH2x and Zeolite 5A. For single gas component, the adsorption equilibrium capacity of N_2 and CO_2 were measured. For binary gas component, the adsorption equilibrium capacity of N_2 and CO_2 in mixture gas 20 CO_2-vol% (balance N_2) were measured. On the other hand, for multiple gas component, the adsorption equilibrium capacity of N_2, CO_2, CH_4 and CO in mixture gas 20 CO_2-vol%, 20 CH_4-vol% and 20 CO-vol% (balance N_2) were measured. Experiments were conducted at 20°C and 35°C in pressure range of 0.1 to 0.5 MPa. Note that pressure was measured in terms of gauge pressure. Note that all operations were conducted with constant holding time of 5 min, which is considered to be sufficient for adsorption of gas to achieve equilibrium.

7.3.2 Equations and expressions

7.3.2.1 Equilibrium adsorption capacity

The equilibrium adsorption capacity, q_e is defined as the ratio of amount of gas adsorbed to the mass of adsorbent given as

$$q_e = n/m \tag{7-1}$$

, where n is the amount of gas adsorbed in mol whereas m is the mass of adsorbent in the adsorbent tank in kg.

7.3.2.2 Henry coefficient

Henry coefficient states that the amount of gas adsorbed in the adsorbent is directly proportional to the amount of gas loaded into the system at low pressure region less than 1 MPa (Poursaeidesfahani et al., 2018). The linear function is given as

$$c_e = K_H c \tag{7-2}$$

, where K_H is the Henry coefficient whereas c_e is the amount of gas adsorbed in adsorbent at equilibrium and c is the total amount of gas loaded into the system. Note that the Henry coefficient is valid for single gas component adsorption isotherm measurements.

7.3.2.3 Langmuir Isotherm

In order to evaluate the adsorption equilibrium and predict the adsorption of gas from pure component isotherms (Ruthven, 1984), Langmuir isotherm is used to correlate the CO_2 adsorption of single gas component. The Langmuir isotherm is given as

$$q_e = \frac{q_m b P_e}{1 + b P_e} \tag{7-3}$$

, where P_e is the pressure in equilibrium, q_m is the maximum adsorbed amount per unit mass of adsorbent and b is the Langmuir isotherm equation parameter (MPa^{-1}).

For the prediction of adsorption of gas mixture from multiple component isotherms, a modified Langmuir isotherm is expressed as

$$q_{e,i} = \frac{y_i q_{m,i} b P_e}{1 + b P_e} \tag{7-4}$$

, where $q_{e,i}$ and $q_{m,i}$ are the equilibrium adsorption capacity and maximum adsorbed amount for gas species, i, respectively. y_i is the mole fraction of gas species i in the initial bulk (gas) phase.

7.3.2.4 Adsorption selectivity

Adsorption selectivity is often used to evaluate the efficiency of adsorbents for separation of gas components such as CO_2, CH_4 and CO from N_2 (Saha et al., 2010; Liu et al., 2016; Moura et al., 2018). Adsorption selectivity, $S_{A/B}$, is defined as,

$$S_{A/B} = \frac{x_A / x_B}{y_A / y_B} \tag{7-5}$$

, where x_A and x_B are the mole fractions of species A and B in the adsorbed phase, while y_A and y_B are the mole fractions of species A and B in the bulk (gas) phase. Note that species A is the stronger adsorbate whereas species B is the weaker adsorbate. Adsorption selectivity is plotted as a function of pressure or temperature. $S_{A/B} > 1$ indicates the selectivity of species A over species B whereas $S_{A/B} < 1$ indicates the selectivity of species B over species A. An ideal adsorbent with excellent gas separation properties is defined to possess the properties of increased selectivity with decreasing pressure and increasing temperature.

7.3.3 Results and discussion

7.3.3.1 Adsorption equilibrium of single gas component

Figure 7-5 shows the equilibrium adsorption capacity of pure CO_2 and N_2 using PET-AC, AC-GH2x and zeolite 5A with their corresponding Henry's plot during single gas component adsorption isotherm measurements at 20°C and 35°C.

It was observed that for all adsorbents, the amount of CO_2 adsorbed at equilibrium is more than the amount of N_2 adsorbed and that all adsorbents had strong affinity to CO_2 compared to N_2. In the case of PET-AC, it can be seen that CO_2 adsorption capacity decreased slightly from 2.66 mol/kg (20°C, 0.2 MPa) to 2.55 mol/kg (35°C, 0.2 MPa) when measurements were conducted at higher operating temperature. However, the decrease of CO_2 adsorption capacity at higher operating temperature is evident in AC-GH2x from 2.76 mol/kg (20°C, 0.2 MPa) to 2.10 mol/kg (35°C, 0.2 MPa); and most evident in zeolite 5A from 3.45 mol/kg (20°C, 0.2 MPa) to 0.99 mol/kg (35°C, 0.2 MPa). At low operating temperature of 20°C, equilibrium adsorption capacity of CO_2 in ascending order was PET-AC<AC-GH2x<zeolite 5A. However, at higher operating temperature of 35°C, equilibrium adsorption capacity in ascending order was zeolite 5A<AC-GH2x<PET-AC. On the other hand, the amount of CO_2 adsorbed was plotted against the amount of adsorbate loading to obtain Henry coefficient. Large Henry coefficient (≈ 1) indicates high adsorption capacity of adsorbent. In the case of PET-AC, it can be observed that Henry coefficient was approximately 0.45 for both 20°C and 35°C. In the case of AC-GH2x, Henry coefficient was 0.86 at 20°C, however, decreased to 0.36 at 35°C. Similarly, Henry coefficient of Zeolite 5A was 0.90 at 20°C, but sharply decreased to 0.23 at 35°C.

Based on the results obtained, it is evident that the adsorption properties of PET-AC were different from AC-GH2x and zeolite 5A, in which temperature had little effect on the adsorption of N_2 and CO_2 on PET-AC. This phenomenon will be explained in the later sub-sections, including analyzation of the isosteric heat of CO_2 adsorption, change of enthalpy during CO_2 adsorption and theories for the adsorption properties of PET-AC based on past studies.

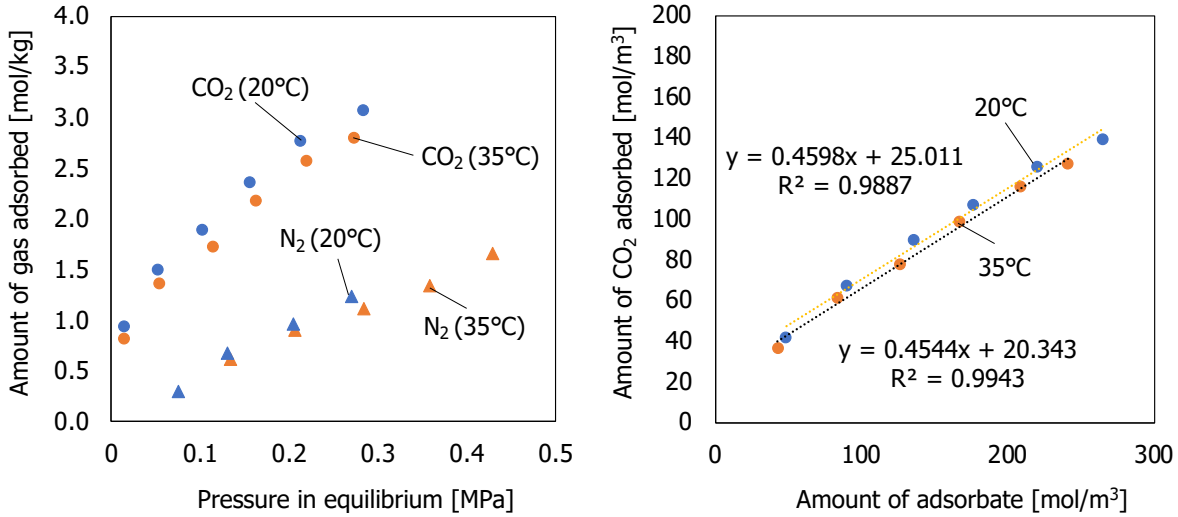

(a) PET-AC

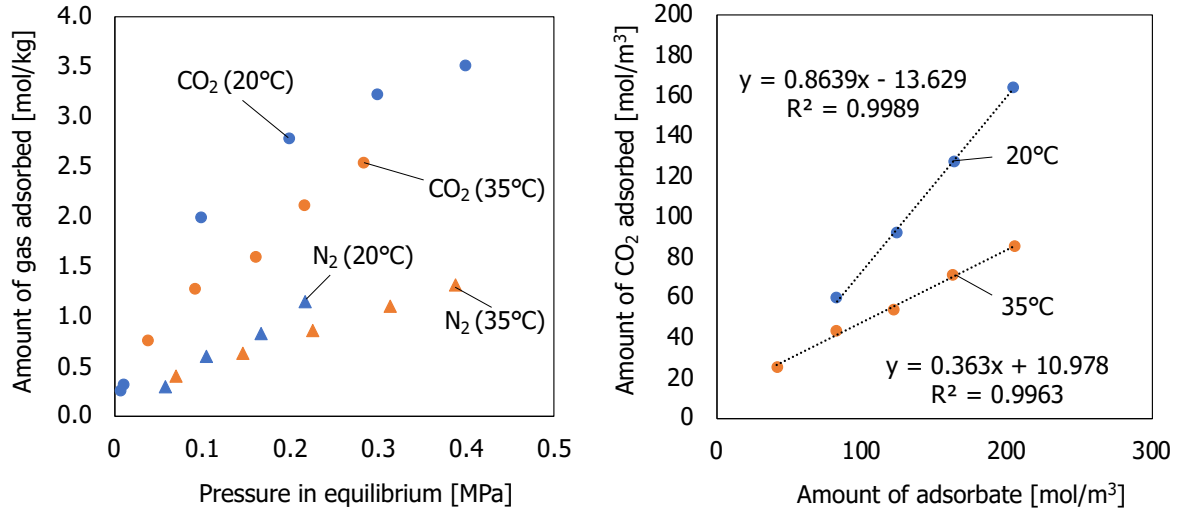

(b) AC-GH2x

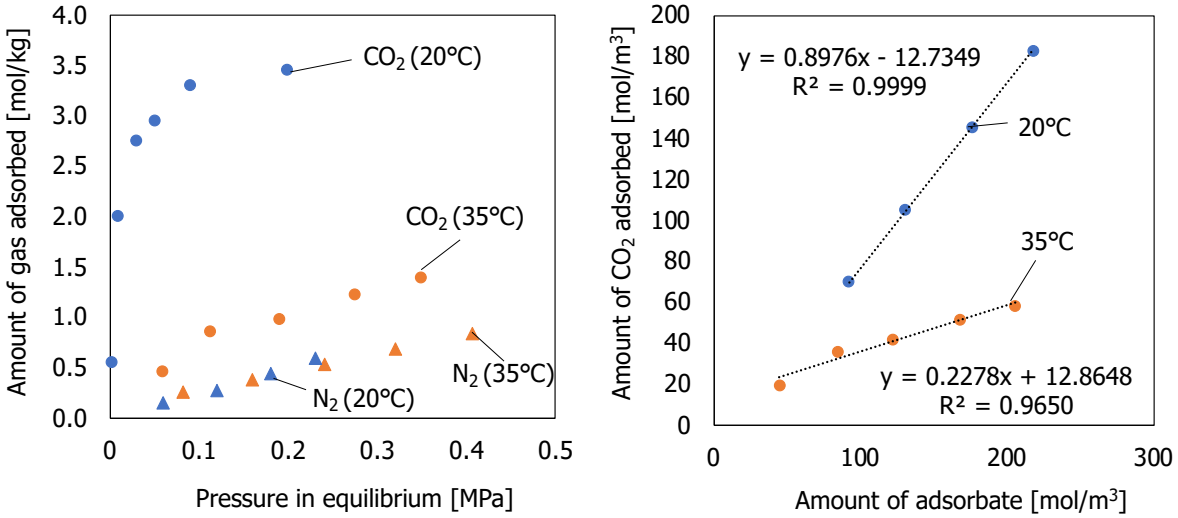

(c) Zeolite 5A

Figure 7-5: Amount of CO_2 and N_2 adsorbed and Henry's plot during single gas component adsorption isotherm measurements at 20°C and 35°C.

7.3.3.2 Adsorption equilibrium of binary gas component

Figure 7-6 shows the equilibrium adsorption capacity of CO_2 and N_2 from binary gas using PET-AC, AC-GH2x and zeolite 5A with their corresponding selectivity of gas components during binary gas component adsorption isotherm measurements at 35°C, 20 CO_2-vol% (N_2 balance). It should be noted that CO_2 adsorption was approximately 100% for all operations.

It was observed that for all adsorbents, the amount of CO_2 adsorbed at equilibrium increased with increasing pressure, indicating that all adsorbents had strong affinity to CO_2 compared to N_2. In the case of PET-AC, it can be seen that CO_2 adsorption capacity increased with increasing pressure, with fair amount of N_2 adsorbed. Similarly, AC-GH2x showed increasing adsorption capacity with increasing pressure, and also fair amount of N_2 adsorbed. Particularly, the amount of N_2 adsorbed was higher than the amount of CO_2 adsorbed at low pressure. The reason for this is that at low pressure, the total amount of CO_2 loading in the operation was low, thus, leading to the adsorption of N_2 in the vacant pores of PET-AC and AC-GH2x surface. With increasing pressure, the total amount of CO_2 loading increased, leading to the increased CO_2 adsorption on the adsorbent surface. For both PET-AC and AC-GH2x, the selectivity of CO_2 over N_2 increased with increasing pressure. It is also evident that selectivity of N_2 over CO_2 is close to zero due to the low affinity of N_2 in carbon adsorbents. On the other hand, zeolite 5A showed different tendency in which CO_2 is the main gas component adsorbed. Little to almost no N_2 was adsorbed in equilibrium. It was evident that zeolite 5A had high affinity to CO_2 compared to N_2 as seen in the high selectivity of more than 100 of the adsorbent. The reason for this is that zeolite 5A was specially designed to be highly selective to the adsorption of CO_2 due to the calcium cation attached to its framework (Harlick and Tezel, 2004; Mofarahi and Gholipour, 2014; Mendes et al., 2017). Therefore, although the BET surface area of zeolite 5A was relatively lower than PET-AC and AC-GH2x, the presence of cation in zeolite 5A resulted in strong interaction of quadruple moment between CO_2, thus, resulting in the high selectivity of CO_2 in binary mixture of CO_2 and N_2 gas. Nevertheless, PET-AC showed good CO_2 adsorption properties comparable to commercial adsorbents.

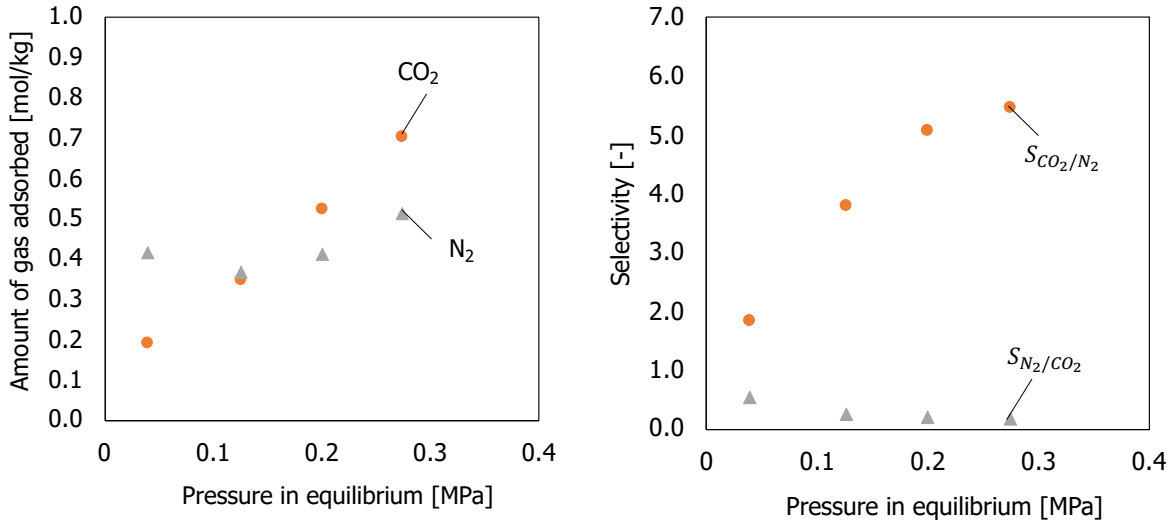

(a) PET-AC

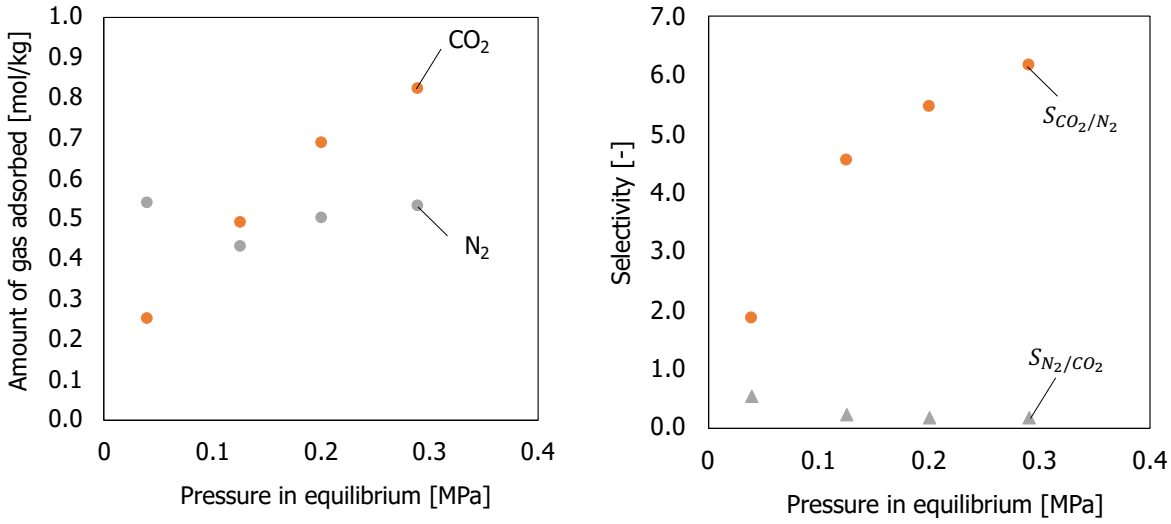

(b) AC-GH2x

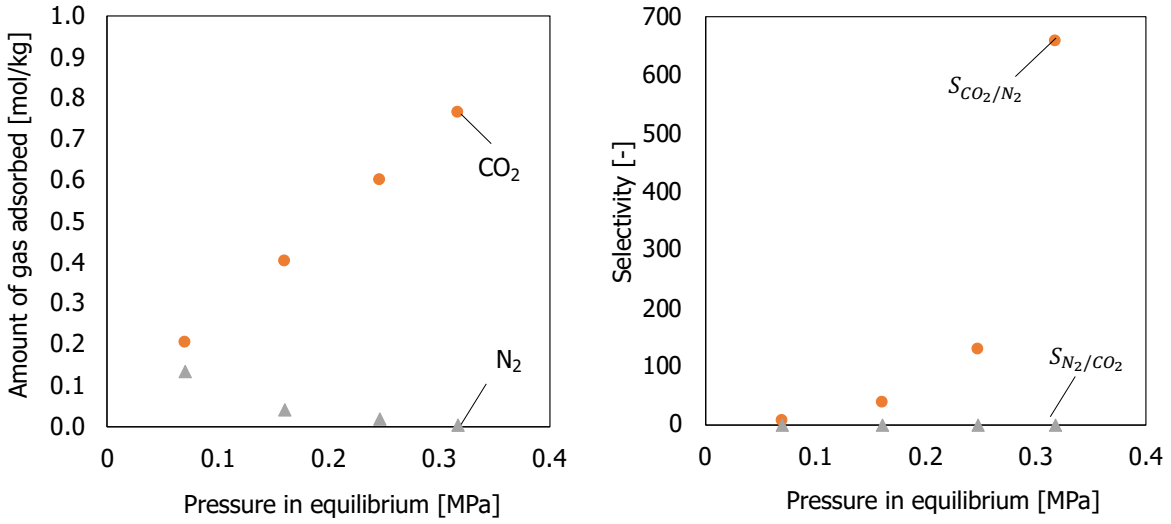

(c) Zeolite 5A

Figure 7-6: Amount of CO_2 and N_2 adsorbed and selectivity of gas components during binary gas component adsorption isotherm measurements at 35°C, 20 CO_2-vol% (N_2 balance).

7.3.3.3 Adsorption equilibrium of multiple gas component

Figure 7-7 shows the equilibrium adsorption capacity of CO_2, CO, CH_4 and N_2 using PET-AC, AC-GH2x and zeolite 5A with their corresponding selectivity of gas components during multiple gas component adsorption isotherm measurements at 35°C, 20 CO_2-vol%, 20 CO-vol%, 20 CH_4-vol% (N_2 balance).

It was observed that for PET-AC, the amount of all gas species adsorbed at equilibrium increased with increasing pressure. It was also noted that the amount of CH_4 adsorbed was similar to the total amount of CO_2 adsorbed. The selectivity of gas species shows that, adsorption of CO_2 was highly dominant over adsorption of N_2. On the other hand, for PET-AC, selectivity of CO_2 over CH_4, S_{CO_2/CH_4} and selectivity of CO_2 over CO, $S_{CO_2/CO}$ were approximately 1, indicating similar competitive adsorbent capability of these gases. In other words, PET-AC was unable to efficiently separate CO_2 from mixture gas of CO_2, CH_4 and CO in equilibrium state. In the case of AC-GH2x, the amount of CO_2, CO and CH_4 adsorbed at equilibrium increased with increasing pressure. However, it was observed that little to almost no amount of N_2 was adsorbed. For AC-GH2x, adsorption of CO_2 was dominant over adsorption of N_2. On the other hand, $S_{CO_2/CO}$ was approximately 1 at low pressure but increased with pressure, while S_{CO_2/CH_4} was approximately 1, indicating similar competitive adsorbent capability between CO_2 and CH_4, and lack of separation ability in equilibrium state. In the case of zeolite 5A, the amount of CO_2, CO and CH_4 adsorbed at equilibrium increased with pressure and little to almost no amount of N_2 was adsorbed. For zeolite 5A, adsorption of CO_2 was dominant over adsorption of N_2. In addition, the S_{CO_2/N_2} of zeolite 5A increased with pressure, indicating the strong affinity of CO_2 to zeolite 5A. S_{CO_2/CH_4} and $S_{CO_2/CO}$ were approximately 1 at low pressure, however, slightly increased with pressure. This indicates that separation of CO_2 from gas mixtures using zeolite 5A is most efficient at higher operating pressure.

Overall, although performance of PET-AC was inferior than the commercial AC-GH2x and zeolite 5A, it was observed that PET-AC exhibited good CO_2 adsorption capacity and selectivity, indicating the potential use of the adsorbent in gas separation.

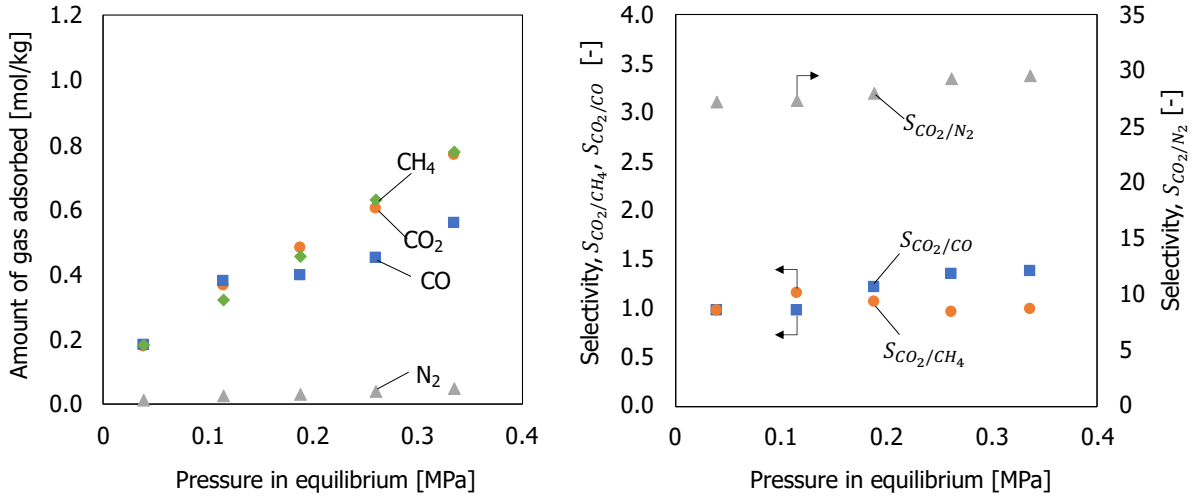

(a) PET-AC

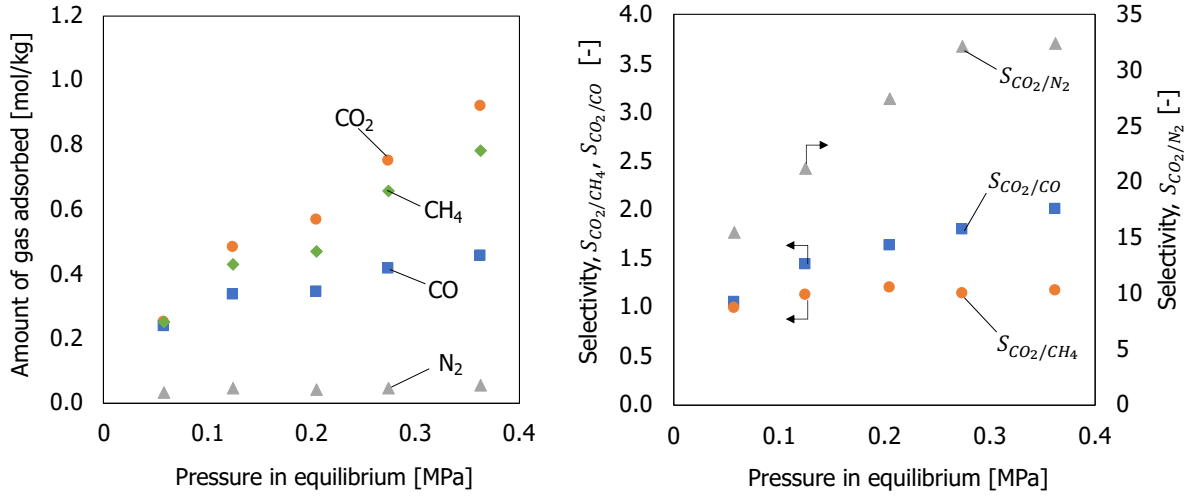

(b) AC-GH2x

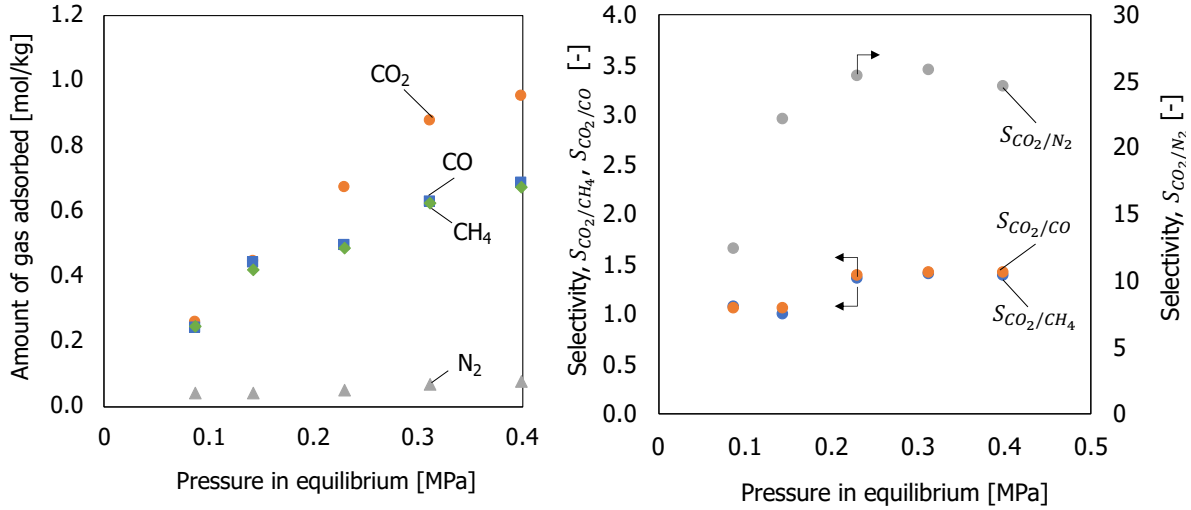

(c) Zeolite 5A

Figure 7-7: Amount of CO_2, CO, CH_4 and N_2 adsorbed and selectivity of the gas components during multiple gas component adsorption isotherm measurements at 35°C, 20 CO_2-vol%, 20 CO-vol%, 20 CH_4-vol% (N_2 balance).

7.3.3.4 Isosteric heat of adsorption

During the adsorption of gas, heat is generated which is defined as the isosteric heat of adsorption, expressed as (Sircar and Kumar, 1986)

$$q^0 = -\left(\frac{\partial H^0}{\partial n}\right)_T \tag{7-6}$$

, where q^0 is the isosteric heat of adsorption of pure gas during adsorbate loading, n and temperature, T. The variable H^0 is the total enthalpy of a closed adsorption system which contains the adsorbate at pressure, P and temperature, T. The isosteric heat of adsorption is also defined as the energy necessary to remove a target molecule from its average vibrational state to an infinite distance from the adsorbent surface (Kumar et al., 2019). Note that q^0 is independent of temperature. For an energetically homogenous adsorbent, q^0 is independent of adsorbate loading; whereas for an energetically heterogenous adsorbent, q^0 decreases with increasing adsorbate loading. In ideal gas where R is the gas constant, the isosteric heat of adsorption is given as

$$q^0 = +RT^2\left(\frac{\partial lnP}{\partial T}\right)_n \tag{7-7}$$

On the other hand, Henry's law, which is a function of temperature, can be expressed using the van't Hoff equation as

$$\left(\frac{\partial lnK_H}{\partial T}\right)_P = \frac{\Delta H^0}{RT^2} \tag{7-8}$$

$$lnK_H = -\frac{\Delta H^0}{R}\cdot\frac{1}{T} + \frac{\Delta S^0}{R} \tag{7-9}$$

, where ΔH^0 is the standard enthalpy, which is also the negative value of isosteric heat of adsorption ($q^0 = h_g - h_a = -\Delta H^0$, h_g: molar enthalpy of gas; h_a: molar enthalpy of adsorbed molecules) in the system, whereas ΔS^0 is the standard entropy. Plot of lnK_H versus $1/T$ gives a linear graph with slope $-\Delta H^0/R$ and intercept $\Delta S^0/R$. It should be noted that negative value of ΔH^0 (positive slope) indicates the exothermic process whereas positive value of ΔH^0 (negative slope) indicates the endothermic process. In the physical adsorption of gas phase on a solid adsorbent, ΔH^0 must always be negative due to the adsorption process which is exothermic (Thomas, 1961).

Due to the limitation of data in current study, only two available plots of different temperature (20°C and 35°C) were used for the plot of lnK_H versus $1/T$, for CO_2 adsorption as shown in **Figure 7-8**.

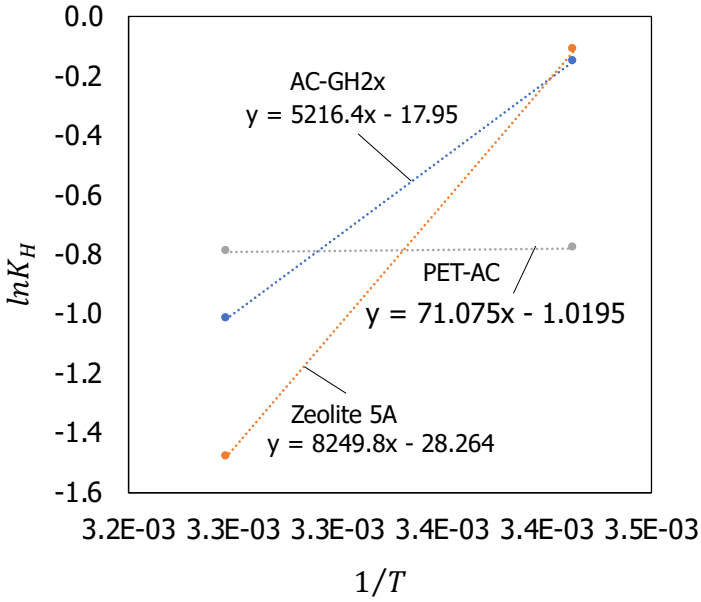

Figure 7-8: Isosteres for adsorption of CO_2 on PET-AC, AC-GH2x and zeolite 5A.

Based on the isosteres plot, it was observed that the slope for all adsorbents gave positive values, indicating the exothermic process of CO_2 adsorption. Based on the slopes, the standard enthalpy is calculated as: for PET-AC, $\Delta H^0 = 0.6\ kJ/mol$; for AC-GH2x, $\Delta H^0 = 43.4\ kJ/mol$; for zeolite 5A, $\Delta H^0 = 68.6\ kJ/mol$. The standard enthalpy of AC-GH2x and zeolite 5A were presented as proper values, however, the standard enthalpy of PET-AC was noticeably below acceptable value. The change in standard enthalpy describes the ordered arrangement of target molecules on the adsorbent active sites during adsorption. It is less likely that there was little difference between the molar enthalpy of gas and molar enthalpy of adsorbed molecules in PET-AC. Thus, the conventional expression of isosteric heat of adsorption, $q^0 = h_g - h_a = -\Delta H^0$ may not be valid in the case of CO_2 adsorption using PET-AC.

Another speculation is that upon adsorption of gas, PET-AC underwent deformation or swelling. Swelling is a phenomenon where physical changes occur due to adsorption of gas or liquid and often occurs in adsorbents with flexible framework consisting of cross-linked polymeric macromolecule that allows target molecule to penetrate into

the micropores (Xie, 2015). Cross-links are flexible which allows the bending and stretching upon exposure to external stress, leading to the swelling of adsorbent. Small molecules such as CO_2, CH_4 and H_2O can penetrate through the adsorbent and increase the distance between cross-linking points in the adsorbent structure, which leads to the deformation or swelling of adsorbents. Deformation or swelling of porous solid due to adsorption has been widely studied over the decades; for example, porous amorphous carbons (Rossi et al., 2009), coals (Ottiger et al., 2008), silica gel (Kawaguchi et al., 1986) and activated carbon (Harpalani and Schraufnagel, 1990). Ottiger et al. (2008) had reported the swelling of coal due to CO_2 adsorption, in which coal expanded by approximately 1% at 0.1 MPa. Although there are only very small changes in swelling, the local deformation can largely affect the adsorption kinetics. A study by Wang et al. (1998) had investigated the adsorption of tetrahydrofuran on coal to clarify the relationship between heat of adsorption and degree of swelling of coal. They reported that heat of adsorption was low when degree of swelling was large due to the expansion of cross-links in coal.

The simplest theory for adsorption induced length change was proposed by Bangham and Fakhoury (1931), given as

$$\frac{\Delta L}{L_0} = \lambda \cdot \Delta F \tag{7-10}$$

, in which ΔL is the change in length of adsorbent particle due to expansion or compression, L_0 is the original length of adsorbent particle at ambient pressure and temperature, ΔF is the change of surface energy of adsorbent due to adsorption and λ is the constant with relation to the material properties of adsorbent. The equation describes that change of surface energy, ΔF of the adsorbent during adsorption is directly proportional to the observed relative length change $\Delta L/L_0$.

Based on the expression given, the change in standard enthalpy of PET-AC during CO_2 adsorption can be expressed as

$$q^0 - \Delta F = h_g - h_a - \Delta F = -\Delta H^0 \tag{7-11}$$

, in which the change in standard enthalpy is the sum of isosteric heat of adsorption and the change of surface energy of adsorbent due to adsorption.

7.3.3.5 Comparison of CO_2 adsorption isotherm in single, binary and multiple gas component

In the characterization of adsorbents, adsorbents with only one type of adsorption site are generally defined as homogeneous adsorbents; whereas adsorbents with different types of binding sites are defined as heterogenous adsorbents. The binding sites are associated with adsorption energies of the adsorbent and binding site heterogeneity is commonly used to describe the adsorption properties of activated carbon (Kumar et al., 2010). Activated carbon obtained from physical or steam activation contains functional groups such as hydroxyl or carboxylic groups and possesses pore size heterogeneity. These properties can result to different levels of binding energy for a specified target molecule (Molina-Sabio et al., 1996). The Langmuir model can be used to model simple theoretical adsorption isotherms of adsorbents that contains one or two different types of binding sites. The Langmuir isotherm can also be used to describe the energetic heterogeneity by assuming that the adsorbent surface consists of a collection of locally homogeneous surfaces. The Langmuir isotherm model is generally modified as

$$\frac{1}{q_e} = \frac{1}{q_m} + \frac{1}{b \cdot q_m} \cdot \frac{1}{P_e} \tag{7-12}$$

Using this expression, q_m and b can be obtained through a linear regression analysis from the plot $1/q_e$ versus $1/P_e$. Although this equation can provide an easy solution for the design of batch adsorption systems, the expression oversimplifies the entire adsorption process, in which information on the number of binding sites, interactions between binding sites and target molecules, and heterogenous properties of adsorbents are not provided (Porkodi and Kumar, 2007; Kumar et al., 2019). Therefore, in order to obtain these information, the Langmuir isotherm model is now expressed using the equations

$$\frac{q_e}{P_e} = b_i \cdot q_m - b_i \cdot q_e \tag{7-13}$$

, in which the Scatchard plot (Scatchard, 1949), q_e/P_e versus q_e, is plotted. Here, b_i, which is obtained as the negative slope of the plot, refers to the binding energy of adsorbate to the adsorbent at different regions in the adsorption system.

Figure 7-9 shows the experimental and predicted adsorption isotherms based on the Langmuir isotherm model for PET-AC, AC-GH2x and zeolite 5A; and their respective Scatchard plots at 20°C and 35°C. It should be noted that the solid lines indicate the fitted parameters using Eq. (7-3) for pure CO_2 whereas dash lines indicate the modeled parameters based on Eq. (7-4) for 20% CO_2 in binary and multiple gas mixtures. It was observed that the Langmuir isotherm model was able to fit and predict data of all adsorbents with reasonable accuracy.

Based on the fitted results, it was observed that the Langmuir isotherm model fits well, leading to speculations about the homogeneity of the adsorbents. However, based on the Scatchard plots, the heterogeneity of the PET-AC, AC-GH2x and zeolite 5A was explicit. In the case of PET-AC, at least two distinct regions were observed. This indicates that, PET-AC contains at least two different types of adsorption sites with the corresponding binding energies, b_1 and b_2 at 20°C and 35°C, respectively. Similarly, at least two distinct regions were observed for AC-GH2x, indicating that AC-GH2x also contains at least two different types of adsorption sites with the corresponding binding energies, b_1 and b_2 at 20°C and 35°C, respectively. In the case of zeolite 5A, at least three distinct regions were observed for zeolite 5A, indicating that zeolite 5A contains at least three different types of adsorption sites with the corresponding binding energies, b_1, b_2 and b_3 at 20°C and 35°C, respectively. It should be well noted that the tendency and slope of regions were similar for both PET-AC and AC-GH2x but differs for zeolite 5A. One of the reasons may be the carbon materials of PET-AC and AC-GH2x, in which similar functional groups such as hydroxyl or carboxylic group are expected on the surface of carbon material. The microporous structures of PET-AC and AC-GH2x may also be one of the factors for the tendency.

Overall, it can be seen that PET-AC exhibited well adsorption performance and adsorption properties. The accuracy of the overall study can be further improved by obtaining the amount adsorbed at equilibrium over a wide range of initial concentrations of the adsorbate.

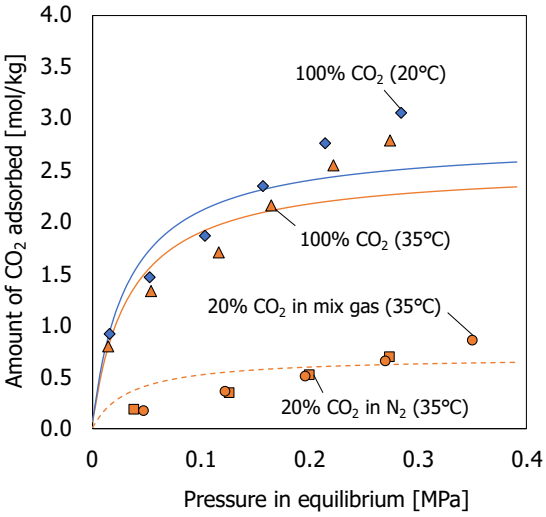

(a) Langmuir model for PET-AC

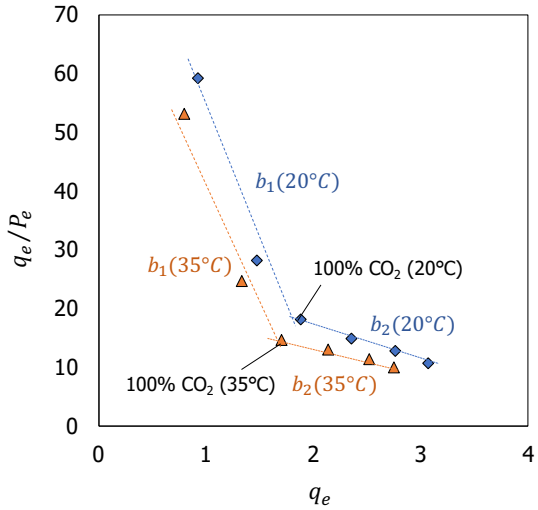

(b) Scatchard plot for PET-AC

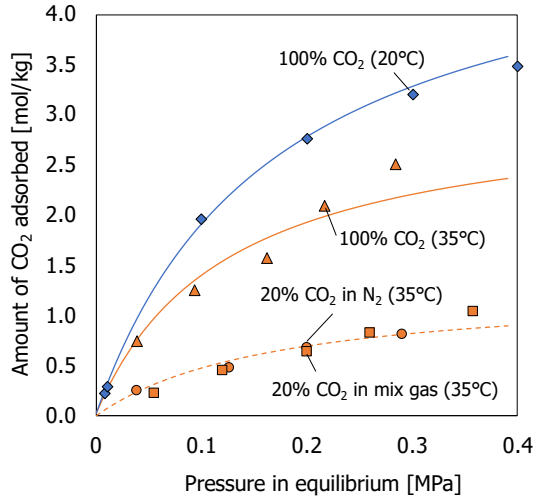

(c) Langmuir model for AC-GH2x

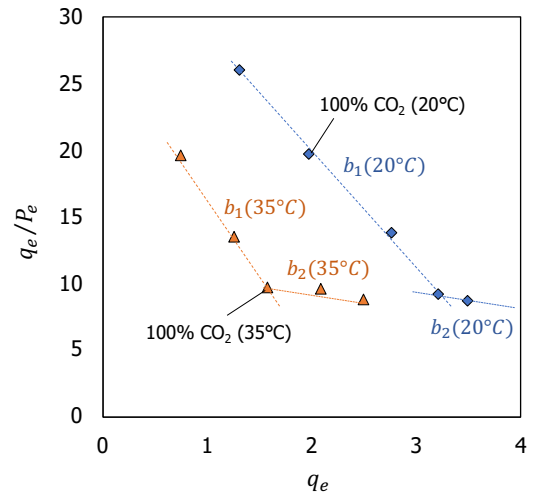

(d) Scatchard plot for AC-GH2x

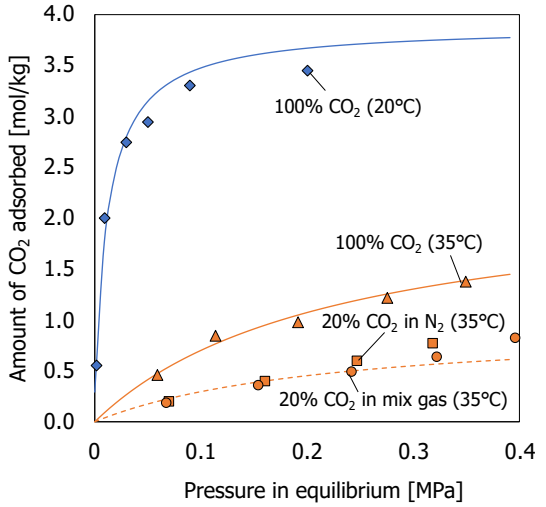

(e) Langmuir model for zeolite 5A

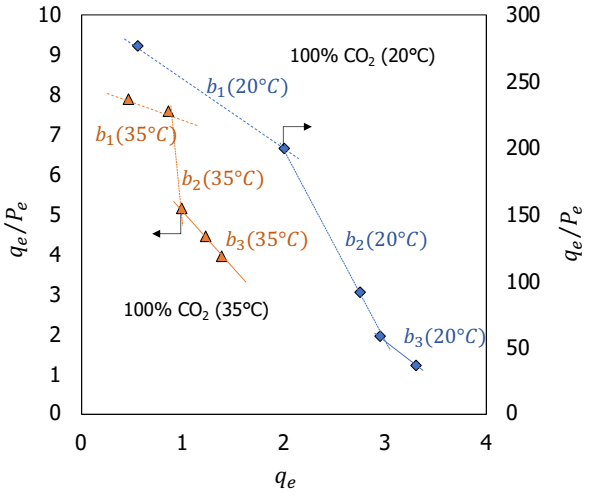

(f) Scatchard plot for zeolite 5A

Figure 7-9: Experimental and predicted adsorption isotherms based on the Langmuir isotherm model and Scatchard plots for PET-AC, AC-GH2x and zeolite 5A, respectively at 20°C and 35°C.

Table 7-3 summarizes the fitting parameters of Langmuir model for adsorption isotherm of pure CO_2 of PET-AC, AC-GH2x and zeolite 5A. Similar results were previously reported for activated carbon and carbon molecular sieves (Jayaraman et al., 2002; Campo et al., 2010; Park et al., 2018). In the case of zeolite 5A, the results obtained were similar to the results reported by Sarker et al. (2017) and Mofarahi and Gholipour (2014). It was well noted that for all cases, q_m decreased with increasing operating temperature. In addition, for all cases, modeled parameters based on Eq. (7-4) for 20% CO_2 was well fitted for both CO_2 adsorption isotherms of binary gas components and multiple gas components.

Overall, based on the comparison of CO_2 adsorption isotherm using single, binary and multiple gas components, it was well noted that operating temperature and operating pressure are important factors which determine the total amount of CO_2 adsorbed on the adsorbents. In the case of comparison of CO_2 adsorption isotherm of binary and multiple gas components, the presence of other gas components such as CO and CH_4 had little to almost no effects on the CO_2 adsorption capacity in equilibrium.

Table 7-3: Fitting parameters of Langmuir model for adsorption isotherm of pure CO_2.

Adsorbents	20°C		35°C	
	q_m [mol/kg]	b [MPa^{-1}]	q_m [mol/kg]	b [MPa^{-1}]
PET-AC	2.76	9.83	2.55	29.6
AC-GH2x	5.55	5.36	3.10	8.15
Zeolite 5A	3.89	84.6	2.28	4.47

7.3.3.6 Adsorption mechanism of PET-AC based on the adsorption equilibrium study

The selectivity of gas adsorption and diffusion of gases in adsorbents are highly affected by various factors such as the relative adsorbate molecule size, pore structure, high quadrupole moment, activation energy, etc (Didzinska, 2017). In the case of pore structure, the commonly assumed slit-shape of pores in carbon adsorbent can be divided into three categories (micropore, mesopore, and macropore) according to their widths or sizes. Micropores are defined as pores <2 nm in size, mesopores between 2 and 50 nm, and macropores >50 nm in size (Harpalani and Chen, 1997). For PET-AC, pores were estimated to have widths less than 1 nm based on the BET/BJH analysis, which is in the microporous range. On the other hand, the relative molecule size of adsorbate is also an important factor that affects the selectivity and diffusivity of gas in adsorbents. Micropore diffusivity of CO_2 is generally higher than CO, CH_4 and N_2 because micropore diffusivities of gases in carbon adsorbent, that is, PET-AC, increase strongly with decrease in gas kinetic diameters, in which their kinetic diameters have the relation: CO_2 (0.33 nm) < N_2 (0.364 nm) < CO (0.376 nm) < CH_4 (0.38 nm) (Matteucci et al., 2006; Ismail et al., 2015). Therefore, CO_2 can diffuse into microporous carbon adsorbent more easily than CO, CH_4 and N_2 (Radovic et al., 1997). Another factor that affects the selectivity of gas adsorption is the adsorption energy. Based on the findings presented by Cui et al. (2004), adsorption energies of CO_2, CH_4 and N_2 in micropores were calculated and they reported that adsorption energies are in the decreasing order of CO_2>CH_4>N_2, in which the adsorption energy of CO_2 is larger than adsorption energy of CH_4 in micropores; and much larger than adsorption energy of N_2 in pores at all size ranges. This indicates that CO_2 will most likely be first adsorbed by most pores competitively out of a gas mixture of CO_2, CH_4, and N_2 due to its larger adsorption affinity (energy). Therefore, it can be concluded that selectivity of gases are highly affected by both the adsorption affinity (energy) and kinetic diameter of gas molecules, in which a pore will preferably adsorb an adsorbate with large adsorption energy, and that the adsorbate gas with the smallest kinetic diameter has the greatest capability to enter most pores of various sizes.

The adsorption mechanism of single, binary and multiple gas components in PET-AC based on the adsorption equilibrium in this study was proposed as shown in **Figure 7-10**. As discussed in the previous section, structure of PET-AC was described to have ink-bottle-shaped pores as shown in Figure 7-10a, which are pores with narrow branches connected to a pouch. In the case of adsorption of pure N_2 in PET-AC (Figure 7-10b), results showed that adsorbed amount of N_2 increased with increasing pressure. Similar to the adsorption onto a homogeneous surface, the inert N_2 molecule fills the PET-AC surface gradually upon an increase in pressure to form a monomolecular layer (monolayer) at low pressure and until multimolecular layer (multilayer) is formed at higher pressure. It should be well noted that N_2 is difficult to penetrate through the narrow branches of the pores and saturates in the surface pores. In the case of adsorption of pure CO_2 in PET-AC (Figure 7-10c), results showed that total amount of CO_2 adsorbed was higher than the total amount of N_2 adsorbed due to the high microporous diffusivity of CO_2 and high affinity to the carbonaceous surface compared to N_2. In the case of adsorption of binary CO_2-N_2 in PET-AC (Figure 7-10d), results showed that the total amount of CO_2 adsorbed increased with increasing pressure whereas the total amount of N_2 remained constant throughout the operating pressures. The reason for this is that CO_2 is selectively adsorbed through the inner pores due to the high affinity with carbonaceous PET-AC surface whereas the adsorption of N_2 occurs on the vacant PET-AC surface to form monolayer. With increasing pressure, CO_2 selectively fills the inner pores and consequently, the surface pores. Note that in this assumption, CO_2 is the limiting factor whereas only N_2 is present as the excess component in the surrounding system. Finally, in the case of adsorption of multiple CO_2-CO-CH_4-N_2 in PET-AC (Figure 7-10e), results showed that the total amount of CO_2, CO and CH_4 adsorbed increased with increasing pressure whereas little to almost no N_2 was adsorbed. The reason for this is that, CO_2 is selectively adsorbed through the inner pores due to the high microporous diffusivity and affinity of CO_2 with carbonaceous PET-AC surface. With increasing pressure, CO_2 fills the inner pores whereas CO and CH_4 fills the surface pores, leaving N_2 as the excess component in the surrounding system. However, based on current findings, it is unclear whether CO and CH_4 have accessibility into the inner pores, which is largely dependent on the size and the accessibility of the bottle-neck pores.

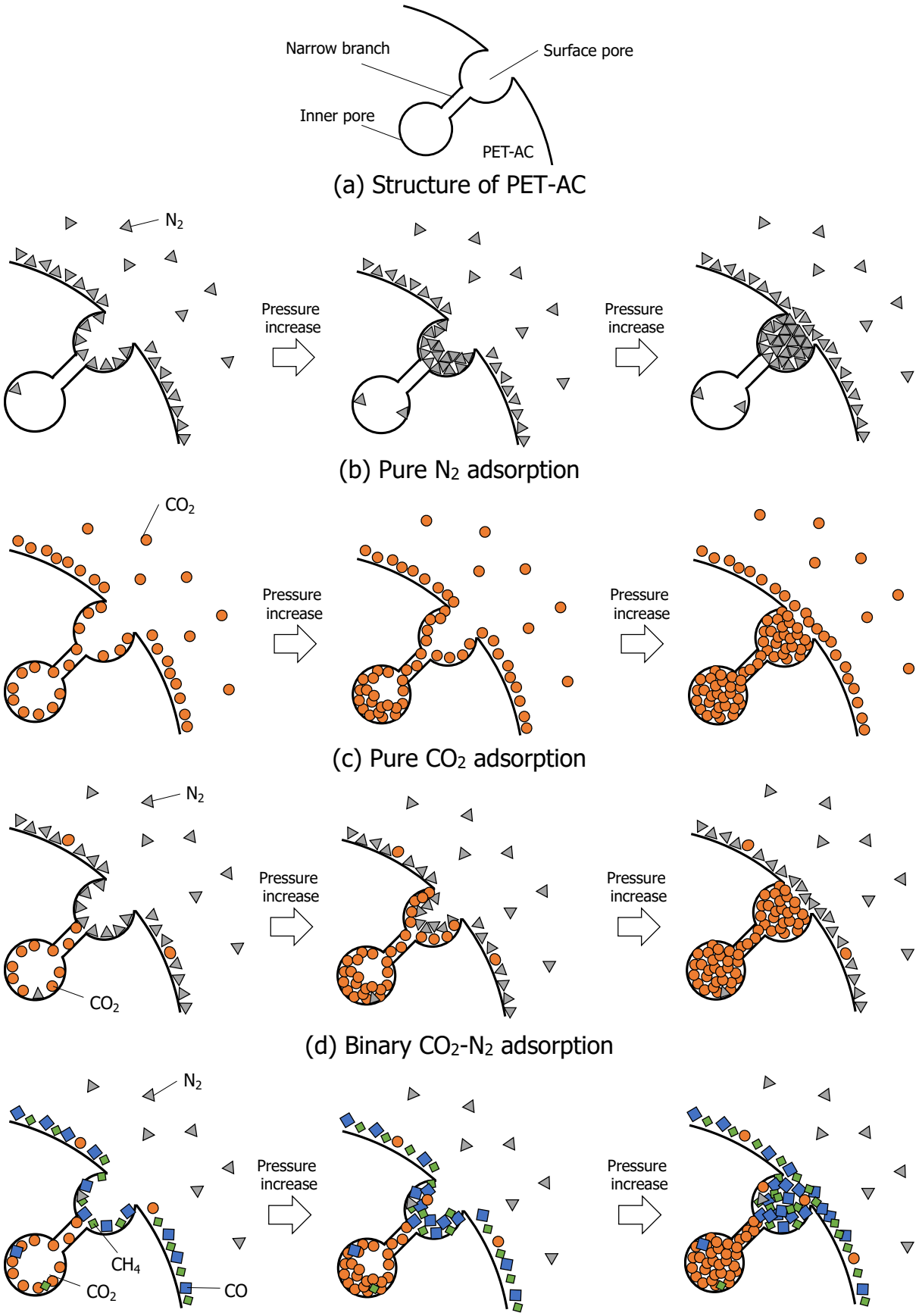

Figure 7-10: Adsorption mechanism of PET-AC proposed based on adsorption equilibrium.

7.3.4 Conclusions: Static adsorption study

Adsorption equilibrium study was conducted using single gas components, binary gas components and multiple gas components. Based on the adsorption equilibrium studies of single gas component, the following can be concluded: At 20°C, the equilibrium adsorption capacity of CO_2 was in the order of zeolite 5A > AC-GH2x > PET-AC. However, at higher operating temperature of 35°C, the equilibrium adsorption capacity of CO_2 was in the inverse order, which is PET-AC > AC-GH2x > zeolite 5A. Assessment of Henry coefficient also showed the slight effect of temperature change on equilibrium adsorption capacity of CO_2 in PET-AC compared to the other adsorbents. It was speculated that the microporous structure and the possible swelling of pores of PET-AC highly contributed to the equilibrium adsorption capacity of CO_2 despite temperature changes. Based on the adsorption equilibrium studies of binary gas component, the following can be concluded: all adsorbents tested had high selective properties of CO_2 adsorption to N_2 adsorption. However, of all adsorbents, zeolite 5A had the highest affinity of CO_2 to N_2. Overall, PET-AC showed gas separation properties comparable to AC-GH2x. Based on the adsorption equilibrium studies of multiple gas component of PET-AC, it can be concluded that the adsorption of CO_2 was dominant over adsorption of N_2 in PET-AC. However, selectivity of CO_2 over CH_4, and selectivity of CO_2 over CO were approximately 1, indicating the insufficient ability of PET-AC to efficiently separate CO_2 from mixture gas of CO_2, CH_4 and CO in equilibrium state.

Overall, the CO_2 adsorption capacity of PET-AC was surprisingly high at low operating pressure and high operating temperature; and was comparable to the adsorption capacity of commercial AC-GH2x. This also indicates that there is room for improvements for the adsorption capacity of activated char from PET. For one, steam activation, which is more frequently used in industry compared to CO_2 activation, provides higher reactivity on the carbon active sites, thus increasing the number of pores and depth of pore. Activating char using steam activation could most possibly further improve the adsorption capacity and needs to be studied in future works.

7.4 Dynamic adsorption study

7.4.1 Background of breakthrough curve

Breakthrough curve is a plot of the duration of test against the concentration of the adsorbate in the effluent stream of a gas mixture of air. Initially, when gas mixture enters the adsorbent bed, target gas species with high selectivity is adsorbed whereas gas species with low selectivity passes out of the bed free from the target species. This continues as long as the adsorbent bed has capacity to adsorb the target gas species. When saturation is approached, target gas species is detected in the effluent gas and its concentration increases until no further adsorption takes place and the composition of the effluent mixture is equal to the composition of the inlet mixture. **Figure 7-11** shows a typical breakthrough curve of gas adsorbed onto an adsorbent. Breakthrough point (t_b) is the time when the concentration reaches break point. Gas saturation point (t_d) is the time when the adsorbent surface is saturated with gas species. Note that t_d is taken when concentration ratio reaches 100%. A sharp breakthrough curve implies fast kinetics, whereas a distended breakthrough curve implies slow kinetics. In conventional industrial processes, the gas feed is switched to a fresh adsorbent bed when the breakthrough point is reached. The adsorption properties of adsorbents are mostly assessed through the gas breakthrough curve, where a prolonged breakthrough point and sharp breakthrough curve is ideal for gas adsorption processes.

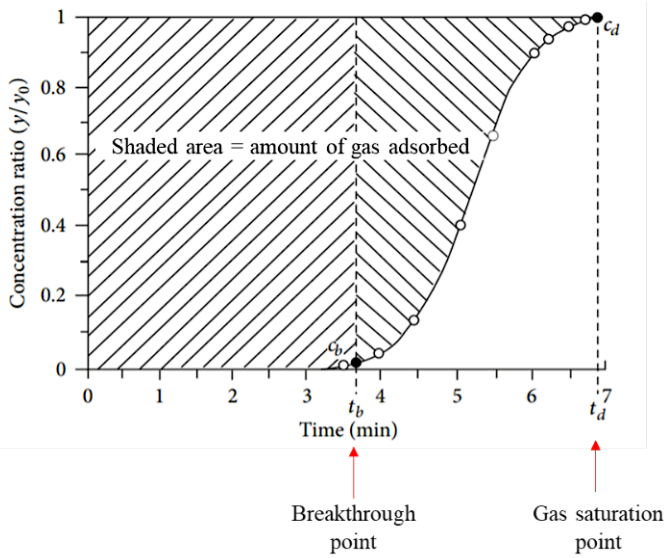

Figure 7-11: A typical breakthrough curve of gas adsorbed onto adsorbent (Adapted from Salam et al., 2013).

7.4.2 Experimental set-up

Binary gas component and multiple gas component adsorption isotherm measurements for dynamic adsorption studies were conducted based on methods described in Chapter 3 using PET-AC, AC-GH2x and zeolite 5A. For binary gas component, the breakthrough curve of N_2 and CO_2 in mixture gas 20 CO_2-vol% (balance N_2) were measured. On the other hand, for multiple gas component, the breakthrough curve of N_2, CO_2, CH_4 and CO in mixture gas 20 CO_2-vol%, 20 CH_4-vol%, and 20 CO-vol% (balance N_2) were measured. Experiments were conducted at 35°C.

7.4.3 Results and discussion

7.4.3.1 Breakthrough curve of binary gas component

Figure 7-12 shows the breakthrough curves of binary gas components for PET-AC, AC-GH2x and zeolite 5A under a span of 70 mins whereas **Table 7-4** shows the summary based on the breakthrough curves. For all cases, it was observed that N_2 reached breakthrough point in less than 5 min while reaching N_2 saturation point in less than 10 min, indicating the lack of holding ability of all adsorbents on N_2. It should be well noted that the concentration ratio of N_2 overshoots to 120% due to the adsorption of CO_2 in the feed, thus causing a decrease in the overall gas volume. With increasing run time, the overshoot of concentration ratio of N_2 decreased and converged to 100%. In the case of PET-AC, CO_2 reached breakthrough point in 24.5 min before reaching CO_2 saturation point in less than 47.5 min. For AC-GH2x and zeolite 5A, CO_2 reached breakthrough point in 22.5 min before reaching CO_2 saturation point in less than 42.5 min. It was well noted that the breakthrough curves of AC-GH2x and zeolite 5A had sharper steepness compared to the breakthrough curve of PET-AC, indicating faster mass transfer rate of CO_2 in both AC-GH2x and zeolite 5A compared to PET-AC. The reason for the slower CO_2 mass transfer rate of PET-AC compared to the commercial adsorbents may be due to the microporous structure of PET-AC, as explained by the hysteresis loop structure based on the BET/BJH analyzation. The narrow necks of the pore structure may have caused pore blockage of CO_2 into the micropores, leading to slower CO_2 diffusion into the pores. Overall, the total amount of CO_2 adsorbed was more than twice the total amount of N_2 adsorbed for all adsorbents.

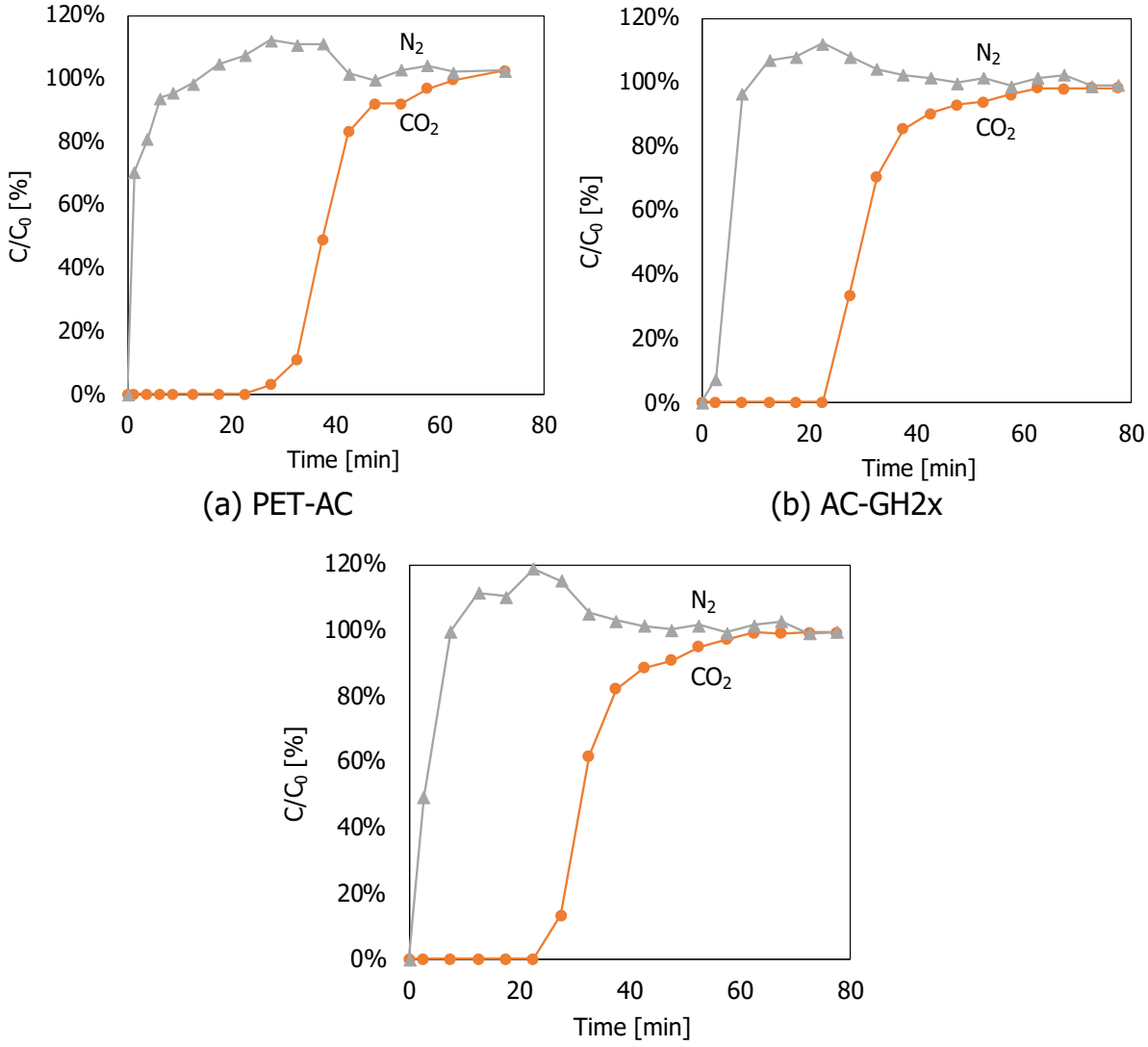

(a) PET-AC

(b) AC-GH2x

(c) Zeolite 5A

Figure 7-12: Breakthrough curves of binary gas components using PET-AC, AC-GH2x and zeolite 5A at 35°C, 20 CO_2-vol% (N_2 balance).

Table 7-4: Summary of breakthrough point, gas saturation point and amount of gas adsorbed.

	CO_2 breakthrough point, t_b [min]	CO_2 saturation point, t_d [min]	Amount of gas adsorbed, n_i [mol/kg]	
			N_2	CO_2
PET-AC	24.5	47.5	0.71	1.47
AC-GH2x	22.5	42.5	0.70	1.63
Zeolite 5A	22.5	42.5	0.56	1.27

7.4.3.2 Breakthrough curve of multiple gas component

Figure 7-13 shows the breakthrough curves of multiple gas components for PET-AC, AC-GH2x and zeolite 5A under a span of 70 mins whereas **Table 7-5** shows the summary based on the breakthrough curves. In the case of N_2, similar to the breakthrough curve of binary gas component, it was observed that N_2 reached breakthrough point in less than 2.5 min while reaching N_2 saturation point in less than 10 minutes for all adsorbents. In the case of CO, the breakthrough curve of CO also showed similar tendency as the breakthrough curve of N_2 for all adsorbents, in which CO reached breakthrough point in less than 2.5 min while reaching CO saturation point in less than 10 min. This indicates the lack of holding ability of all adsorbents on N_2 and CO. In the case of CH_4, PET-AC exhibited holding capability of CH_4 from the inlet stream, in which CH_4 was adsorbed from the stream before reaching breakthrough point in 9.5 min and CH_4 saturation point in less than 19.5 min. AC-GH2x showed slight holding capability of CH_4, in which breaking point and saturation point were 7.5 min and 12.5 min, respectively. Zeolite 5A had the least holding capability of CH_4, in which CH_4 reached breakthrough point and saturation point in less than 2.5 min and 10 min, respectively. In the case of CO_2, all adsorbents exhibited excellent holding capability of CO_2. The CO_2 breakthrough point and saturation point were 29.5 min and 54.5 min for PET-AC; 21.5 min and 40.5 min for AC-GH2x; and 20.5 min and 40.5 min for zeolite 5A, respectively. Compared to AC-GH2x and zeolite 5A, PET-AC showed the most time taken for CO_2 to reach saturation point. The reason may be the microporous structure of PET-AC, which hinders the effective mass transfer of gases in the pores of PET-AC. For all adsorbents, CO_2 was the most adsorbed gas from the gas stream, in which the amount of CO_2 adsorbed was 1.43 mol/kg for PET-AC, 1.59 mol/kg for AC-GH2x and 1.30 mol/kg for zeolite 5A.

As a summary, in the study of breakthrough curve of multiple gas components on different adsorbents, the holding capability of gases are as follows: $CO_2 >> CH_4 > CO > N_2$ for PET-AC; $CO_2 >> CH_4 > CO > N_2$ for AC-GH2x; $CO_2 >> CH_4 \cong CO > N_2$ for zeolite 5A.

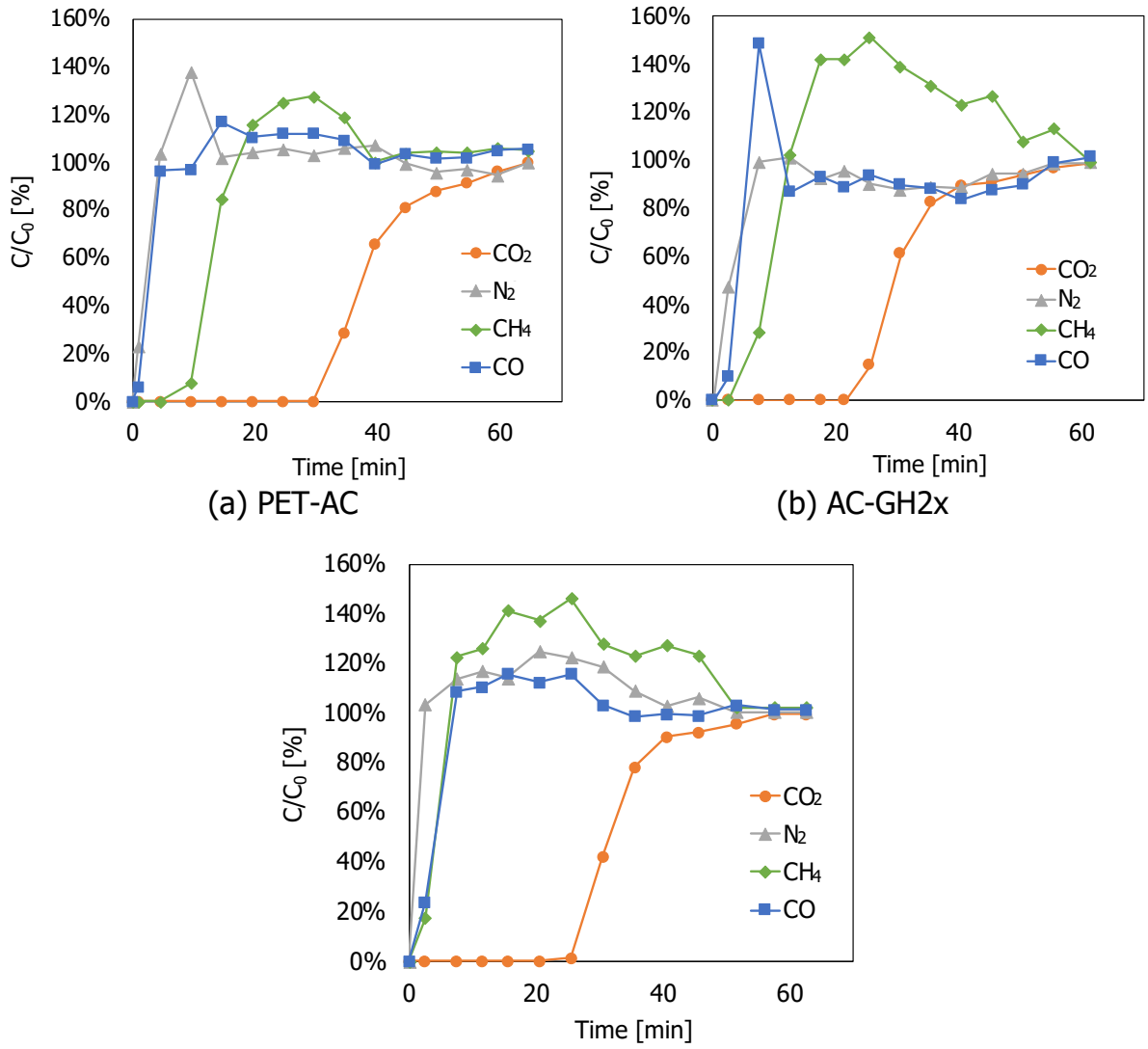

(a) PET-AC

(b) AC-GH2x

(c) Zeolite 5A

Figure 7-13: Breakthrough curves of multiple gas components using PET-AC, AC-GH2x and zeolite 5A at 35°C, 20 CO_2-vol%, 20 CO-vol%, 20 CH_4-vol% (N_2 balance).

Table 7-5: Summary of breakthrough point, gas saturation point and amount of gas adsorbed.

	CO_2 breakthrough point, t_b [min]	CO_2 saturation point, t_d [min]	Amount of gas adsorbed, n_i [mol/kg]			
			N_2	CO_2	CO	CH_4
PET-AC	29.5	54.5	0.16	1.43	0.08	0.44
AC-GH2x	21.5	40.5	0.28	1.59	0.18	0.43
Zeolite 5A	20.5	40.5	0.09	1.30	0.14	0.14

7.4.4 Conclusions: Dynamic adsorption study

In this section, dynamic adsorption study using PET-AC, AC-GH2x and PET-AC was conducted and the breakthrough curve of N_2 and CO_2 from binary gas components and that of N_2, CO_2, CO and CH_4 from multiple gas components were obtained.

From the results obtained from the breakthrough curve of binary gas components, all adsorbents showed lack of holding ability of N_2, as N_2 reached breakthrough point in less than 5 min and reaching N_2 saturation point in less than 10 min. In the case of CO_2, all adsorbents reached breakthrough point at similar time, indicating the high affinity of CO_2 in all adsorbents. It was also observed that the breakthrough curves of AC-GH2x and zeolite 5A have sharper steepness compared to the breakthrough curve of PET-AC, indicating faster mass transfer rate of CO_2 in the both AC-GH2x and zeolite 5A compared to PET-AC.

From the results obtained from the breakthrough curve of multiple gas components, holding capability of gas components are as follows: $CO_2 >> CH_4 > CO > N_2$ for PET-AC; $CO_2 >> CH_4 > CO > N_2$ for AC-GH2x; $CO_2 >> CH_4 \cong CO > N_2$ for zeolite 5A. PET-AC showed high holding ability of CO_2 compared to other two adsorbents. However, the overall amount of CO_2 adsorbed in the dynamic adsorption experiment was obtained as 1.43 mol/kg for PET-AC, 1.59 mol/kg for AC-GH2x and 1.30 mol/kg for zeolite 5A. It should be noted that the breakthrough curves of PET-AC could not be compared to the breakthrough curves of AC-GH2x and that of zeolite 5A due to the difference in the initial adsorbent loading. Therefore, further discussion based on the modelling of breakthrough curve was conducted in the next section in order to compare the CO_2 breakthrough point and CO_2 saturation point of PET-AC, AC-GH2x and zeolite 5A.

Overall, it is agreeable that PET-AC showed relatively high ability to separate gas and high potential to be applied in the PSA system. Although the selectivity of gas in equilibrium batch system was poor for PET-AC, by implementing the difference in gas species breakthrough point, it is highly possible to separate gas species easily and to obtain purified gas.

7.5 Model of breakthrough curve

7.5.1 Background of modelling

The modelling of breakthrough curves of dynamic adsorption study using mathematic models is essential to simulate the gas adsorption processes and to study the behavior of the adsorbents during adsorption-desorption cycles and to obtain kinetic parameters for optimization purposes. In this section, a classical method based on the linear driving force (LDF) approximation for the surface diffusion mechanism with constant diffusivity (Glueckauf and Coates, 1947) was used to predict the mass-transfer diffusivities and effective diffusivities of CO_2 on PET-AC, AC-GH2x and Zeolite 5A. The LDF-model was chosen in this study due to its simplicity and accuracy in predicting breakthrough curves. However, it should be well noted that the LDF-model is limited to predicting breakthrough curves in low concentration region (Chern and Chien, 2002).

7.5.2 Model for breakthrough curves

Modelling of breakthrough curves was conducted to predict the mass-transfer diffusivity and effective diffusivity of CO_2 on PET-AC, AC-GH2x and Zeolite 5A by fitting breakthrough curves from the measured adsorption isotherm. First, a fixed-bed packed with cross-sectional area of A_b is loaded with adsorbents with porosity of ε_b as shown in **Figure 7-14**.

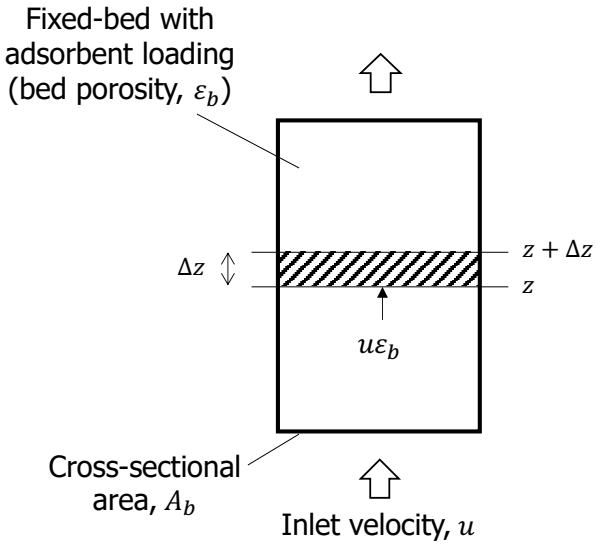

Figure 7-14: Schematic diagram of the fixed-bed adsorption used in this study.

The following assumptions were made:

(i) fluid flows through the bed at a constant interstitial velocity, u;
(ii) solute in the bulk fluid reaches instantaneous equilibrium;
(iii) there is no axial dispersion in the system;
(iv) the system is in isothermal condition; and
(v) equation of state for the adsorbed phase corresponds to the ideal gas law (Hartzog and Sircar, 1995; Seader and Henley, 1999; Chang et al., 2006; Poursaeidesfahani et al., 2019).

A mass balance on the solute for the flow of fluid through a differential adsorption bed length, dz, over a differential time duration, dt, is given as

$$\varepsilon_b u A_b c|_z = \varepsilon_b u A_b c|_{z+\Delta z} + \varepsilon_b A_b \Delta z \frac{\partial c}{\partial t} + (1-\varepsilon_b) A_b \Delta z \frac{\partial \bar{q}}{\partial t} \qquad (7\text{-}14)$$

, where the constant interstitial velocity is given as u; A_b is the cross-sectional area of bed; and ε_b is the void fraction of bed. By dividing by Δz and taking the limit as $\Delta z \rightarrow 0$ gives

$$\frac{\partial (uc)}{\partial z} + \frac{\partial c}{\partial t} + \frac{(1-\varepsilon_b)}{\varepsilon_b} \frac{\partial \bar{q}}{\partial t} = 0 \qquad (7\text{-}15)$$

, where the first term permits an axial variation in fluid velocity, the second term gives the concentration of solute in the bulk fluid and the third term accounts for the variation of adsorbate loading, $\bar{q}$ [mol/m^3] throughout the adsorbent particle.

The migration of adsorbate molecules from the gas phase into the adsorbent is described by Linear Driving Force (LDF-model). The LDF-model is reported to be a sufficient and efficient approximation for computing breakthrough curves (Sircar and Kumar, 1986; Ding and Alpay, 2000; Sircar and Hufton, 2000; Poursaeidesfahani et al., 2019). Based on the LDF-model, the mass transfer is given by

$$\frac{\partial \bar{q}}{\partial t} = k(q^* - \bar{q}) = kK(c - c^*) \qquad (7\text{-}16)$$

, where q^* is the adsorbate loading in equilibrium with the solute concentration, $\bar{q}$ is the average mol of adsorbate loading per unit volume of adsorbent, c is the concentration of adsorbate in bulk fluid; c^* is the concentration in equilibrium with average loading $\bar{q}$; k is the overall mass-transfer coefficient, which includes both

external and internal transport resistance (Snyder, 1992); and K is the adsorption equilibrium constant based on Eq. (7-2), where $K = K_H$.

For physical adsorption, the rate of adsorption is almost instantaneous after the adsorbate reaches the adsorbent surface. Thus, only external and internal mass-transfer resistances were considered (Seader and Henley, 1999). The relationship for the quantity kK, which is the overall mass-transfer coefficient, is given as the following formula for the additivity of resistances, where the overall mass-transfer resistance is the sum of external mass-transfer resistance and the internal mass-transfer resistance,

$$\frac{1}{kK} = \frac{1}{k_c a_v} + \frac{R_p^2}{15 D_e} \tag{7-17}$$

k_c is the external mass-transfer coefficient; a_v is the surface area to volume ratio, which is given as $3/R_p$ in the case of sphere with radius R_p; D_e is the effective diffusivity.

The external transport coefficient of particles in a fixed bed can be correlated by using Sherwood number, given as

$$Sh = 2 + 1.1 Re^{0.6} {Sc_i}^{1/3} \tag{7-18}$$

, where $Sh = k_c D_p / D_i$, Reynolds number, $Re = D_p G / \mu$, and Schmidt number, $Sc_i = \mu / D_i \rho$. Based on Sherwood number, the external mass-transfer coefficient k_c was estimated.

The analytical solution of a simplified form of Eq. (7-15) is modified as follows,

$$\frac{c}{c_F} \approx \frac{1}{2}\left[1 + erf\left(\sqrt{\tau} - \sqrt{\xi} + \frac{1}{8\sqrt{\tau}} + \frac{1}{8\sqrt{\xi}}\right)\right] \tag{7-19}$$

, where c_F is the final concentration of adsorbate in bulk fluid. ξ is the dimensionless distance coordinate, τ is the dimensionless time coordinate, both given as

$$\xi = \frac{kKz}{u} \cdot \frac{(1 - \varepsilon_b)}{\varepsilon_b} \tag{7-20}$$

$$\tau = k \cdot \left(t - \frac{z}{u}\right) \tag{7-21}$$

ξ and τ coordinates are transformations for z and t, which converts the equations to a simpler form of erf(x). The approximation given by Eq. (7-19) is known to be

acceptable and the error could be within 0.6% for ξ > 2.0. The equilibrium constant K for a given temperature can be correlated by experimental data as obtained from the previous sections. By fitting the experimental breakthrough curves to Eq. (7-19), the overall mass-transfer coefficient, k was estimated. Then by Eqs. (7-17) and (7-18), the effective diffusivity, D_e was evaluated.

7.5.3 Results and discussions

Figure 7-15 shows a comparison of breakthrough curves between experimental results and mathematical model of breakthrough curve for binary gas component and multiple gas component using PET-AC, AC-GH2x and zeolite 5A, respectively. It was observed that model predictions based on the simple LDF-models gave good approximation with experimental data, where the effective mass transfer coefficient, k was used as the fitting parameter.

From the results obtained, it can be seen that the simple LDF-model fits well with the experimental data for adsorption of CO_2 from binary gas components and multiple gas component using PET-AC, AC-GH2x and zeolite 5A. For comparison of dimensionless CO_2 breakthrough time, τ_b, the results in ascending order is as follows: 12 for PET-AC < 17 for AC-GH2x < 18 for zeolite 5A. The dimensionless CO_2 saturation time, τ_s, in ascending order is as follows: 36 for PET-AC < 41 for AC-GH2x < 53 for zeolite 5A. The slope of the breakthrough curve was steep for all adsorbents, indicating the small mass transfer resistance of the adsorbents.

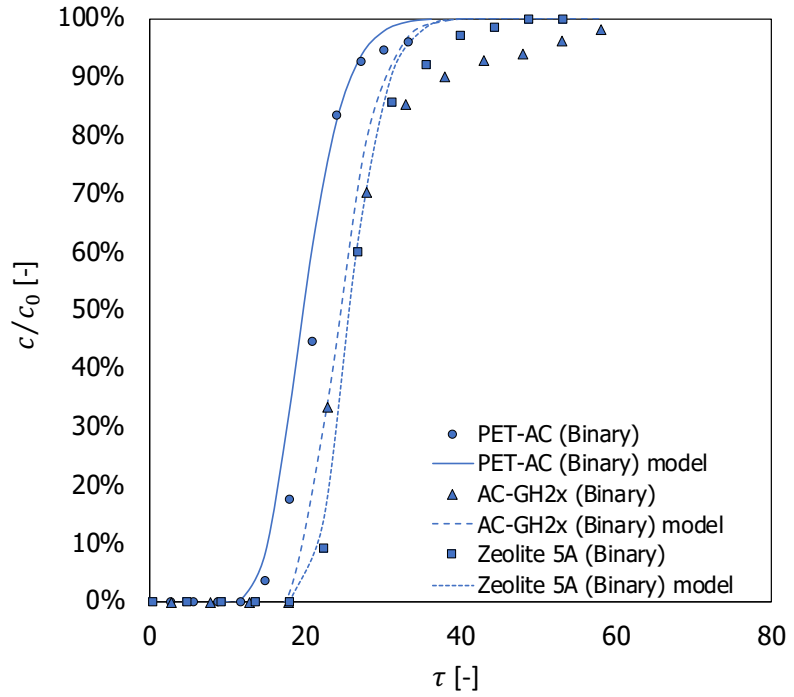

(a) Binary gas components

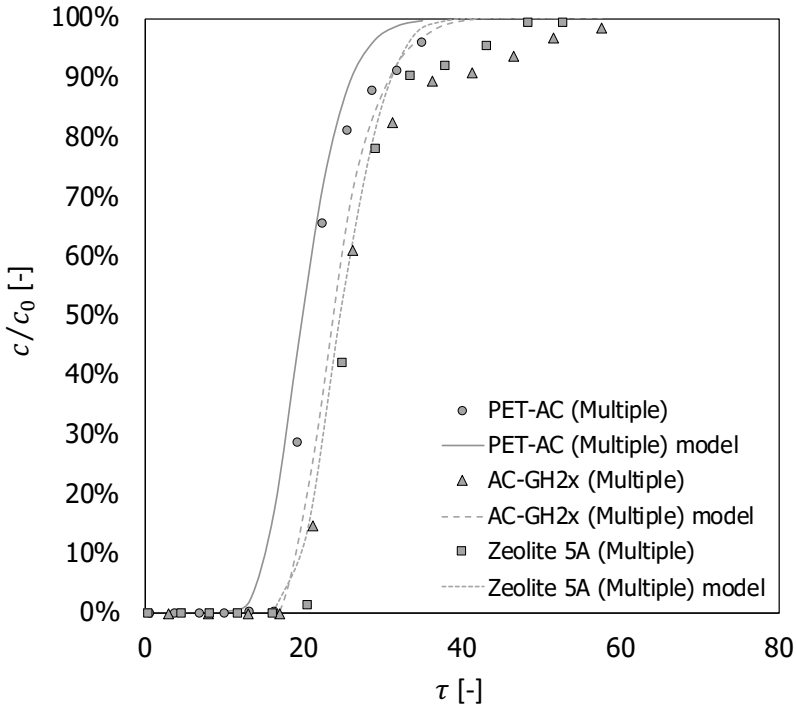

(b) Multiple gas components

Figure 7-15: Comparison of experimental results (filled markers) and mathematical model (solid/dashed lines) of breakthrough curves of PET-AC, AC-GH2x and zeolite 5A for (a) binary gas component and (b) multiple gas component at 35°C.

Table 7-6 shows the kinetic parameters of CO_2 on PET-AC, AC-GH2x and zeolite 5A obtained from the breakthrough curves. Based on the breakthrough curve obtained from experimental results and the calculation model, the overall mass-transfer coefficient, k was estimated as 1.02×10^{-2} s^{-1} for PET-AC, 1.69×10^{-2} s^{-1} for AC-GH2x, and 1.47×10^{-2} s^{-1} for zeolite 5A. On the other hand, the effective diffusivity was estimated as 3.77×10^{-10} m^2s^{-1} for PET-AC, 1.78×10^{-9} m^2s^{-1} for AC-GH2x, and 1.08×10^{-9} m^2s^{-1} for zeolite 5A. Although both k and D_e of AC-GH2x were higher than those of zeolite 5A, zeolite 5A had the longest holding time of CO_2 during adsorption. This is due to the presence of calcium cation attached to its framework, leading to the high selectivity to the adsorption of CO_2 regardless of resistance due to mass-transfer. In the case of PET-AC, the k and D_e obtained were smaller than the commercial adsorbents, due to CO_2 activation method used in this study. It is of great interest to study the adsorption capacity of activated char using steam activation in future works.

Table 7-7 shows the comparison of overall mass-transfer coefficient, k and effective diffusivity, D_e of CO_2 on different adsorbents obtained from this study and from previous reports, regardless of manufacturer and experimental method. The order-of-magnitude of the k and D_e for CO_2 obtained in this study was comparable to the results from previous work.

Overall, for all adsorbents, the internal mass-transfer resistance was larger than the external mass-transfer resistance. This indicates that internal mass-transfer resistance is the controlling factor during the physical adsorption of CO_2.

$$\frac{1}{kK} \cong \frac{R_p^2}{15D_e} \gg \frac{1}{k_c a_v} \tag{7-22}$$

Moreover, the overall mass-transfer coefficient obtained in this study was based on data at low superficial velocity. Referring to Eq. (7-22), the internal mass-transfer is the controlling factor. Therefore, the overall mass-transfer coefficient is similar for operations at both low velocity and high velocity. This indicates that the overall mass-transfer coefficient obtained in this study can also be used to predict the breakthrough curves for large superficial velocity, which is valuable information for the future design and scale up of a PSA unit.

Table 7-6: Kinetic parameters of CO_2 on PET-AC, AC-GH2x, zeolite 5A obtained from the breakthrough curves.

		PET-AC	AC-GH2x	Zeolite 5A
K	[-]	4.54×10^{-1}	3.63×10^{-1}	2.28×10^{-1}
k	[s^{-1}]	1.02×10^{-2}	1.69×10^{-2}	1.47×10^{-2}
D_e	[m^2s^{-1}]	3.77×10^{-10}	1.78×10^{-9}	1.08×10^{-9}

Table 7-7: Comparison of kinetic parameters of CO_2 on different adsorbents from different studies.

Adsorbents	Overall mass-transfer, k [s^{-1}]	Effective diffusivity, D_e [m^2s^{-1}]	REF
PET-AC	1.02×10^{-2}	3.77×10^{-10}	This study[b]
AC-GH2x	1.69×10^{-2}	1.78×10^{-9}	This study[b]
Zeolite 5A	1.47×10^{-2}	1.08×10^{-9}	This study[b]
Biochar	1.60×10^{-3}	3.20×10^{-9}	Plaza et al. (2016)[a]
AC	1.72×10^{-2} 1.68×10^{-2}	-	Singh and Kumar (2015)[a,b]
Biomass-based carbon adsorbent	-	4.00×10^{-8}	González et al. (2013)[a]
Carbon monoliths	2.50×10^{-2}	3.60×10^{-9}	Querejeta et al. (2017)[b]
Zeolite 5A	1.46×10^{-2}	1.00×10^{-8}	Yucel and Ruthven (1980)[a]
Zeolite 5A	1.48×10^{-2}	-	Plaza et al. (2016)[a]
Zeolite 5A	-	9.42×10^{-9}	Kim et al. (1995)[a]
Zeolite 5A	1.45×10^{-2} 1.48×10^{-2}	-	Singh and Kumar (2015)[a,b]

[a]25°C

[b]35°C

7.5.4 Conclusions: Model of breakthrough curve

The CO_2 breakthrough curves of dynamic adsorption studies of binary gas components and multiple gas components were modelled using the LDF-model in order to simulate the CO_2 adsorption process. The mass-transfer diffusivities and effective diffusivities of CO_2 of PET-AC, AC-GH2x and zeolite 5A were obtained and compared with the values of different adsorbents reported in past studies.

Results showed that model predictions based on the simple LDF-models gave good approximation with experimental data for all adsorbents in the case of binary and multiple gas component adsorption. Based on the comparison of breakthrough curves, the dimensionless CO_2 breakthrough time in ascending order was as follows: PET-AC < AC-GH2x < zeolite 5A. The dimensionless CO_2 saturation time followed the same order. Even though PET-AC exhibited the least CO_2 holding capability, difference between the compared adsorbents was not highly distinct, thus indicating the potential of PET-AC as adsorbent for the separation of CO_2 from flue gas. Finally, the overall mass-transfer coefficient and effective diffusivity of PET-AC was obtained as 1.02×10^{-2} s^{-1} and 3.77×10^{-10} m^2s^{-1}, respectively. Based on the kinetic parameters obtained, the internal mass-transfer resistance was the controlling factor for all adsorbents during the physical adsorption of CO_2 due to the large internal mass-transfer resistance compared to the external mass-transfer resistance.

7.6 Chapter summary

In this chapter, char obtained from carbonization of PET was activated using the conventional physical activation method. The surface characteristics and the adsorbent performance of the activated char, PET-AC, were evaluated. Adsorption isotherms of different gas components were measured via volumetric gas method using a static adsorption system whereas the breakthrough curves were obtained using a dynamic adsorption system. The results obtained were compared with commercial adsorbents, activated carbon AC-GH2x and zeolite 5A. A mathematical model was applied to the experimental results from dynamic adsorption system to compare the gas separation abilities of the adsorbents, and to obtain fitting parameters which is essential information for the design and scale up of PSA unit.

Char showed distinct surface changes upon activation, where formation of fine pores on the surface was observed. Adsorption isotherm and pore size distribution based on the BET/BJH method were obtained and results suggested pore-blocking phenomena of PET-AC, indicating the possible ink-bottle-pore structure of PET-AC. Static adsorption study showed the equilibrium adsorption capacity of CO_2 which was independent of temperature change. Results further suggested the possible swelling, or local deformation of PET-AC during adsorption of gas.

Overall, for CO_2 adsorption isotherms, results show that high CO_2 uptake of PET-AC. Binary gas component and multiple gas component breakthrough studies of PET-AC showed that PET-AC possessed excellent CO_2 holding ability, indicating the high affinity of CO_2 in PET-AC. Finally, the LDF-model was applied to the experimental results of dynamic adsorption studies and was able to predict the breakthrough curves of CO_2. Based on the fitting parameters from the breakthrough curve, the overall mass-transfer coefficient and effective diffusivity were obtained as 1.02×10^{-2} s^{-1} and 3.77×10^{-10} m^2s^{-1}, respectively. PET-AC exhibited satisfactory CO_2 adsorption performance that was comparable to commercial adsorbents, thus indicating the suitability of current method to be utilized in the gas adsorption process. The findings in this chapter is highly beneficial for the realization of low cost and high efficient operation of CO_2 capture from flue gas for negative carbon effect of greenhouse gas.

This page is intentionally left blank.

Chapter 8: Assessment of CO_2 emission and cost estimation

8.1 Introduction

In previous chapters, PET was experimentally carbonized and the effects of operating parameters for maximum char yield was determined, the mechanism of char formation was clarified, and the effects of contaminants in non-recyclable PET on char were studied and presented. The char obtained from PET carbonization was also activated and the gas adsorption ability of the activated char was studied. In order to study the feasibility of carbonization of PET in the realization of domestic circulation of waste PET in Japan as a model country, a simple economic assessment and CO_2 emission estimation based on the experimental data were conducted as shown in **Figure 8-1**. This chapter aims to conduct the life cycle assessments of different waste PET treatment methods and estimate the CO_2 emission reduction effects when carbonization is newly added to the treatment methods. Economic assessment and CO_2 emission estimation were conducted for 3 distinct cases for the treatment of PET bottles, including using a commercial scale carbonization facility and commercial scale PSA system. Boundary conditions such as the maximum numbers of carbonization and PSA facility that can be installed in the current situation of the recycling system were considered. Limitations such as maximum capacity of treatment were also included.

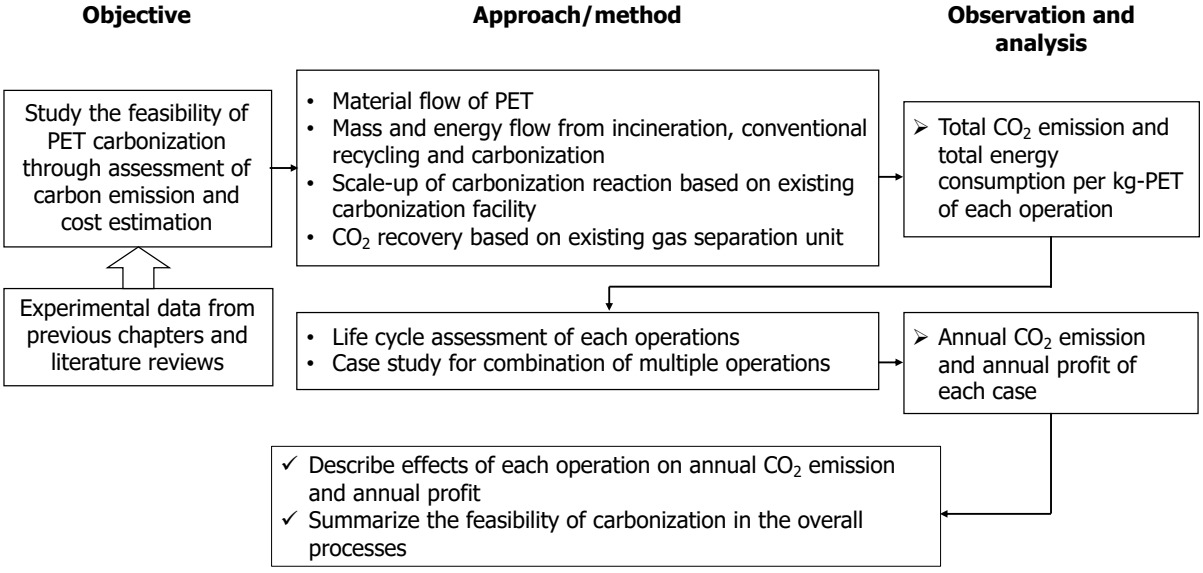

Figure 8-1: Study scheme of Chapter 8 to investigate the feasibility of carbonization in the overall treatment of PET based on the assessment of CO_2 emission and cost estimation.

8.2 CO_2 emission and cost estimation of various operations

8.2.1 Material flow of PET bottles in Japan

Figure 8-2 shows the material flow of PET bottles from collection to recycling in Japan which was reported in 2018. The total existing PET bottles in Japan was 626 kton/year. Total collection of bottles was reported as 529 kt/year. Out of the total bottles collected, 195 kton/year was treated overseas. The domestic recycling capacity in Japan was 334 kton/year, where PET bottles were recycled into new PET bottles, sheets, fibers and other plastic products. However, the total PET bottles that were not domestically recycled was 292 kton/year. These numbers will be used to estimate the daily PET bottles collection rate, PET bottles recycling rate in domestic recycling factories, and PET bottles which are not domestically recycled, as summarized in **Table 8-1**.

8.2.2 Collection and transport operations

In this assessment, the collection of PET bottles was based on the assumptions that: (1) waste PET bottles were pre-separated (labels and caps removed) by consumers before disposed at collection sites; (2) waste PET bottles were collected from sites and transferred to a temporary transport station before being sent to recycling/carbonization and incineration facilities (**Figure 8-3**); (3) distances travelled from a temporary transport station to recycling/carbonization and incineration facilities were constant; (4) storage and separation of bottles were conducted at the temporary transport station. The cost for collection and transport of PET bottles was calculated with similar methods as reported by Nakatani et al. (2010).

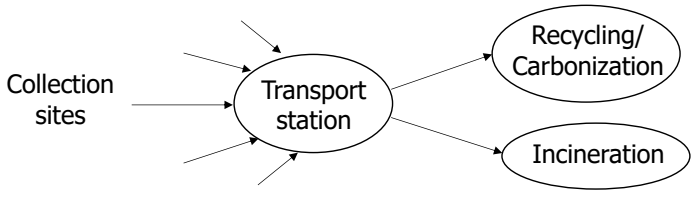

Figure 8-3: Transportation of waste PET from collection sites to transport station before sent to recycling or incineration facilities.

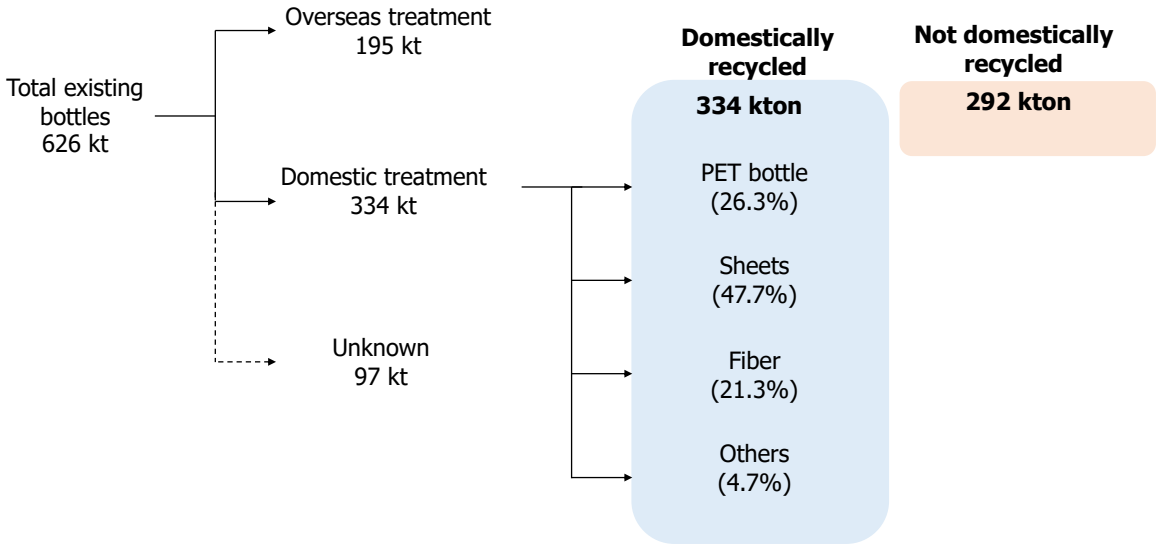

() is calculated by dividing total "Domestically recycled"
Not Domestically recycled = Total existing bottles – Domestically recycled

Figure 8-2: Material flow of PET bottles from collection to recycling in Japan.

Table 8-1: PET bottles collection rate, PET bottles recycling rate in domestic recycling factories, and PET bottles which are not domestically recycled.

	Numbers reported in 2018	Assumed daily numbers
	[kton/year]	[kton/day]
Bottles sold on the previous year	626	1.72
Total bottles collected	529	1.45
Domestic treatment*	334	0.92
PET bottles	(26.3%)	
Sheets	(47.7%)	
Fiber	(21.3%)	
Others	(4.7%)	
Not domestically recycled	195	0.53
Not domestically recycled and not collected or unknown	289	0.79

*Numbers may not represent the maximum capacity of domestic recycling capability

8.2.3 CO_2 emission and cost estimation from incineration with and without energy recovery

Complete combustion of 1 PET monomer under sufficient oxygen condition is:

$$C_{10}H_8O_4 + 10O_2 \rightarrow 10CO_2 + 4H_2O \quad (8\text{-}1)$$

Based on the reaction, complete combustion of 1 kg of PET produces 2.29 kg of CO_2. Therefore, CO_2 emission from PET incineration is 2.29 kg-CO_2/kg-PET. The power consumption per 1 kg waste PET without energy recovery using a conventional continuous stoker furnace was reported to be in average, approximately 0.0321 kWh/kg-PET in terms of electricity consumption and 0.000174 L/kg-PET in terms of heavy oil consumption. On the other hand, the power consumption per 1 kg waste PET with energy recovery was reported to be in average, approximately 0.0284 kWh/kg-PET in terms of electricity consumption and 0.000645 L/kg-PET in terms of heavy oil consumption (Nakatani et al., 2010).

On the other hand, the initial cost (15 years of operation) and operating cost (including labor and maintenance cost) of a conventional waste incineration facility was assumed as 7.87 yen/kg-PET and 19.96 yen/kg-PET, respectively (Tasaki et al., 2006) as shown in **Appendix H**. Note that the conventional stoker furnace has operating capacity of 600 t/day. For the average unit price of electricity, as reported by the Agency for Natural Resources and Energy, Japan in 2018 was 16.6 yen/kWh (METI, 2018), whereas the heavy oil price as reported by the Agency for Natural Resource and Energy, Japan in 2020 is 58 yen/L (METI, 2020).

The average electricity source of emission was based on the IDEA database (IDEA, 2020), and the average emission from heavy oil consumption was 0.736 kg-CO_2/L. Note that the avoided production of electricity in the case of incineration with energy recovery is credited as 0.607 kWh/kg-PET as public electricity (Nakatani et al., 2010).

8.2.4 CO_2 emission and cost estimation from conventional recycling

The estimation of power consumption and CO_2 emission for the recycling of waste PET bottles into PET pellet was conducted based on Nakatani et al. (2010). The recycling process from cleaning to shredding and molding for PET pellets were included as shown in **Table 8-2**. It is well noted that the yield of pellets from 1 kg of waste PET bottle was assumed as 0.923 kg-pellet/kg-PET for open-loop recycling (BtoF) and 0.850 kg-pellet/kg-PET for closed-loop recycling (BtoB). Note that pellet yield of BtoB is less than BtoF due to the requirement of higher quality PET pellet.

On the other hand, the initial cost (15 years of operation) and operating cost (including labor and maintenance cost) of pre-recycling facility was reported as 33.52 yen/kg-PET (The Council for PET Bottle Recycling, 2005). The initial cost (15 years of operation) and operating cost (including labor and maintenance cost) of a conventional PET recycling facility were assumed as 0.26 yen/kg-PET and 2.85 yen/kg-PET, respectively (Kato et al., 1997) as summarized in **Appendix H**. The cost (bid price) of collected bottles was reported as 33679 yen/ton-PET (JCPRA, 2018) in 2018.

Note that the avoided production of virgin PET pellet in the case of conventional recycling is credited as 0.923 kg-pellet/kg-PET for BtoF and 0.850 kg-pellet/kg-PET for BtoB. The cost of virgin PET pellet was reported as approximately 159.37 yen/kg-virgin PET (ARC, 2020). The CO_2 emission was based on IDEA data base (IDEA, 2020).

Table 8-2: List of inventories for conventional recycling

Process	Inventory	Inventory value
Baling	Fuel consumption[a]	Electricity: 0.0413 kWh/kg-PET
Crushing	Fuel consumption[a]	Electricity: 0.0526 kWh/kg-PET
Mechanical recycling	Fuel consumption[a]	Electricity: 0.357 kWh/kg-PET Heavy oil: 0.0535 L/kg-PET
Pelletizing	Fuel consumption[a]	Electricity: 0.308 kWh/kg-PET
BtoF	Yield ratio[b]	0.923 kg-pellet/kg-PET
BtoB	Yield ratio[c]	0.850 kg-pellet/kg-PET

[a]Nakatani et al., 2010; [b]Nakatani and Hirao, 2011; [c]Furusawa, 2019

8.2.5 CO_2 emission and cost estimation from carbonization reactor

Heat balance of PET carbonization reaction was conducted to estimate the amount of energy required in the reaction.

8.2.5.1 Heat balance calculation in lab-scale carbonization reaction

Figure 8-4 shows a heat balance diagram in the reactor adapted from Kodera and Kaiho (2016). Heat input was defined as the HHV of feedstock whereas heat output was defined as the HHV of products and heat loss from reactor. Heat of carbonization was defined as the difference between HHV of feedstock and HHV of products. Heat loss was defined as the transfer of heat from reactor surface to the atmosphere through convection and radiation. For ease of calculation, heat loss was calculated as the heat of convection and heat of radiation from the surface of thermal insulation jacket to the atmosphere.

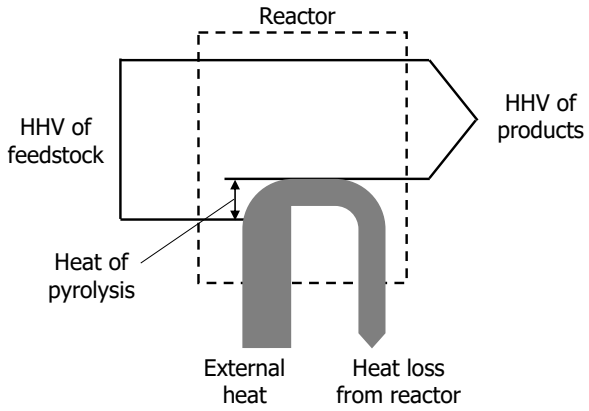

Figure 8-4: Heat balance diagram of reactor.

8.2.5.2 Heat of carbonization of PET

Using the stoichiometric approach, a general notation of pyrolysis of macromolecules was used as follows

$$CH_mO_n \rightarrow aH_2 + bCO + cCO_2 + dH_2O + eCH_4 + fC_2H_4 + gCH_pO_q + hCH_rO_t \quad (8\text{-}2)$$

In this equation, CH_mO_n as PET, CH_pO_q as char and CH_rO_t as wax, are the macromolecules which were expressed by unit compositional formula with one carbon atom. For example, in the case of PET with unit composition formula CH_mO_n, m is the ratio of the number of hydrogen atom to one carbon atom based on the elemental

composition of the macromolecules. Similarly, n was determined as the ratios of oxygen atom to one carbon atom. Note that all the empirical formulas were obtained through the ultimate analysis from Chapter 4 for raw PET, and char and wax obtained from carbonization at 400-480°C and 120 min, as summarized in **Table 8-3**. Based on the unit molecular weight obtained using the empirical formula, HHV from Chapter 4 is newly expressed in kJ/mol as shown in **Table 8-4**.

Table 8-3: Summary of empirical formulas and unit molecular weight.

	Ultimate Analysis[a] [wt%]			Empirical formula	Unit molecular weight [g/mol]
	C%	H%	O%		
Raw PET	62.0	4.0	34.0	$CH_{0.774}O_{0.411}$	19.350
Char	89.6	4.4	5.8	$CH_{0.589}O_{0.049}$	13.373
Wax	72.4	5.6	22.0	$CH_{0.929}O_{0.228}$	16.577

[a]: Dry basis; Note that Nitrogen content was excluded from the calculation.

Table 8-4: Calculation of HHV of PET, char, wax and gas in unit kJ/mol.

	HHV of product kJ/mol-product	Molar percent mol-product/mol-feedstock	HHV per 1 mol PET kJ/mol-feedstock
Raw PET	456.9	1.000	456.9
Char	477.3	0.413	197.1
Wax	457.9	0.395	180.9
Gas	351.8[b]	0.193	67.9

[b]: HHV of gas product was calculated based on the composition and heating values of hydrogen, methane, carbon monoxide, ethane and ethylene.

The heat of carbonization is calculated as

$$= \text{HHV (Product) kJ/mol-feedstock} - \text{HHV (PET) kJ/mol-feedstock} \quad (8\text{-}3)$$

$$= -11.0 \text{ kJ/mol-feedstock} < 0$$

The balance of HHV (Product) – HHV (PET) < 0 shows that the reaction is exothermic, which indicates the heat generation of feedstock during the carbonization reaction. Therefore, only external heat loss from the carbonization equipment needs to be taken into account during scale-up of the system.

8.2.5.3 Power consumption of continuous carbonization facility

In this section, an industrial scale carbonization facility was assumed in **Figure 8-5**. A continuous carbonization facility presented by CRIEPI (Shoji et al., 2015) was referred to in this study in order to estimate the amount of energy and power consumption needed to carbonize 1 kg-PET, industrially. The carbonization facility proposed here has an inner cylinder dimension of 800 mm in diameter and 6 m in length, which consists of a feeding system, conveyor belt, hot air supply inlet, exhaust outlet for volatile product and outlet for collection of char. The conveyor belt, which was assumed to be 5 m in length with motor power operating at 2.2 kW (52.8 kWh; ASG Plastic Recycling Machinery, 2013), is equipped with ceramic or alumina crucibles fixed on the bed. The reason for installing the conveyor belt with crucible over the conveyor is that PET undergoes melting process under heat exposure before carbonization. The melting process presents a challenge to transport the bulk material in the case of a conventional screw conveyor. Referring to the carbonization facility presented by CRIEPI, the carbonization facility here was assumed to have operating capacity of 4000 kg/day, hot air flow rate of 600 N-m^3/h and carbonization reactor temperature range of 400-500°C. Approximately 1 kg/h of wood pellet is needed in order to maintain the temperature range. The conveyor belt should be set to operate at a certain speed for the crucible to travel from the start of feeding to the discharge of product, which allows the retention time of 120 min in order to ensure the sufficient carbonization of PET. Note that the drying system was not considered in this assumption.

The initial cost (15 years of operation), operating cost (including labor and maintenance cost) and electricity cost (conveyor belt) of the carbonization facility were assumed as 9.11 yen/kg-PET, 33.30 yen/kg-PET and 0.22 yen/kg-PET, respectively as summarized in **Appendix H and I**. The cost (bid price) of collected bottles was not taken into account as the carbonization operation is a replacement for incineration.

On the other hand, the amount of CO_2 emitted and cost in order to maintain the heat in reactor from different heat source, namely wood pellet, electricity, waste plastic, and by-products from carbonization were estimated.

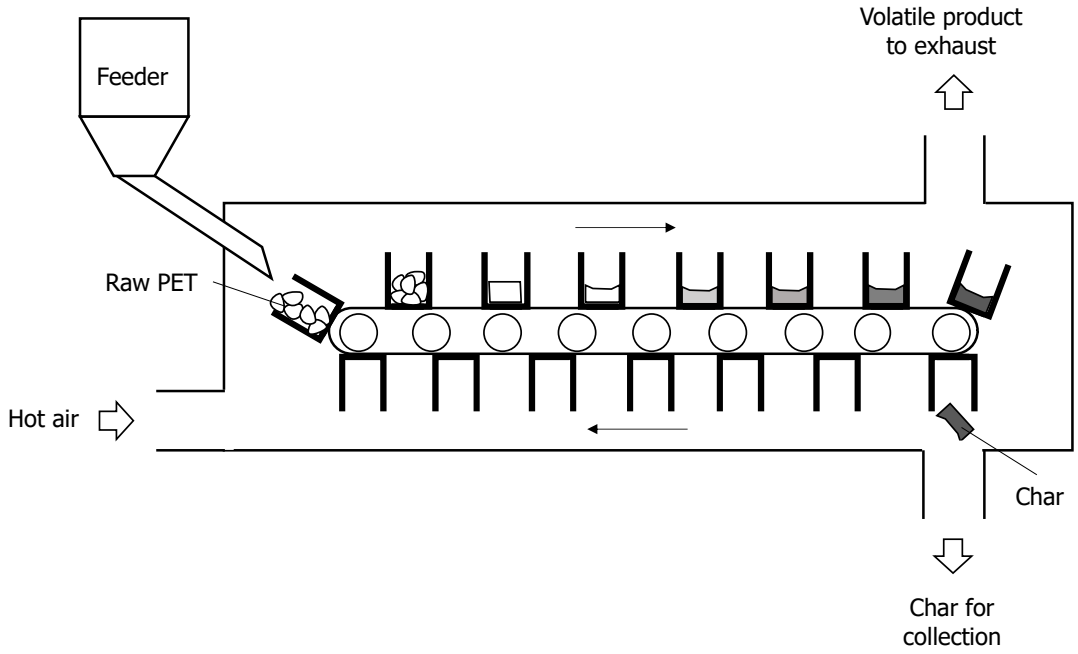

Figure 8-5: A proposal for PET carbonization facility for mass treatment.

Heat energy by wood pellet

Similar to the conventional carbonization facility, assuming the treatment of 4000 kg-PET/day, approximately 24 kg-pellet/day is needed to maintain the carbonization reactor temperature range. This is approximately equivalent to the power requirement of 0.0294 kWh/kg-PET, given that 1 kg pellet, which costs around 75 yen/kg, contains approximately 4.9 kWh, according to the Japan Wood Pellets Association. The amount of CO_2 emitted from 1 kg pellet is reported as 2.024 kg-CO_2/kg-pellet (Komata et al., 2010). Therefore, the amount of CO_2 emitted, including approximately 0.2 kg-CO_2/kg-PET emitted as gas product during PET carbonization and emission from conveyor belt, and cost for the carbonization reaction is

= (0.0121 + 0.20 + 0.0061) kg-CO_2/kg-PET

= 0.2182 kg-CO_2/kg-PET;

= 0.45 yen/kg-PET

Heat energy by electricity

Approximately 0.0294 kWh/kg-PET is needed to maintain the carbonization reactor temperature range. If the heat generation is supplied by electrical source, the amount of CO_2 emitted and cost from energy consumption is

= 0.463 kg-CO_2/kWh × 0.0294 kWh/kg-PET + (0.20 + 0.0061) kg-CO_2/kg-PET

= 0.2197 kg-CO_2/kg-PET;

= 16.6 yen/kWh × 0.0294 kWh/kg-PET

= 0.49 yen/kg-PET

Heat energy by waste plastic

It has been reported that 1 kg waste plastic (PE and PP) generates approximately 2.4 kWh (SANIX Inc.) while emitting approximately 2.75 kg-CO_2/kg-plastic (Ministry of the Environment, Japan). Therefore, approximately 0.01225 kg-plastic/kg-PET is needed to maintain the reactor temperature range. If the cost of waste plastic was assumed as 0 yen, the amount of CO_2 emitted and cost from energy consumption is

= 2.75 kg-CO_2/kg-plastic × 0.01225 kg-plastic/kg-PET + (0.20 + 0.0061) kg-CO_2/kg-PET

= 0.2398 kg-CO_2/kg-PET

Heat energy by by-products from carbonization

By-products from carbonization, wax and gas contain HHV of 26.62 MJ/kg and 9.18 MJ/kg, respectively. This is equivalent to 7.39 kWh/kg-wax and 2.55 kWh/kg-gas. Given that approximately 38 wt% wax and 34 wt% gas was emitted from PET carbonization, the energy balance is shown in **Figure 8-6**.

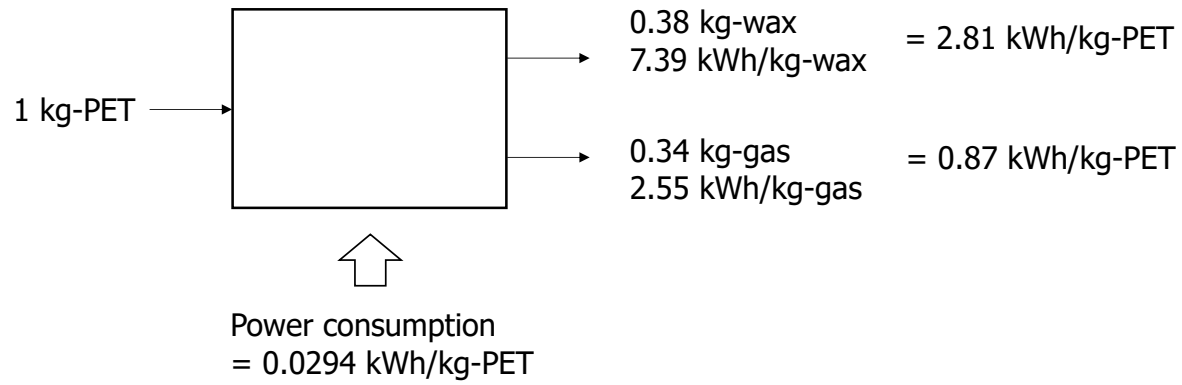

Figure 8-6: Mass and energy balance of wax and gas from PET carbonization.

On the other hand, the CO_2 emission from combustion of CO, CH_4, C_2H_4 and C_2H_6 was calculated as shown in **Table 8-5**. Note that the complete combustion reactions of the gases are given as follows:

$$CO + 0.5O_2 \rightarrow CO_2 \quad (8\text{-}4)$$

$$CH_4 + 2O_2 \rightarrow CO_2 + 2H_2O \quad (8\text{-}5)$$

$$C_2H_4 + 3O_2 \rightarrow 2CO_2 + 2H_2O \quad (8\text{-}6)$$

$$C_2H_6 + \frac{7}{2}O_2 \rightarrow 2CO_2 + 3H_2O \quad (8\text{-}7)$$

Approximately 2.81 kWh/kg-PET can be harvested from wax whereas 0.87 kWh/kg-PET can be harvested from gaseous product. It was well noted that, combustion of less than 4 wt% of the product gas alone is sufficient for the energy required for the carbonization of PET. Therefore, the process is considered to be self-sustainable, in addition to producing wax and the remaining combustible gas, which can be collected and utilized for other processes.

Table 8-5: Calculation for CO_2 emission from combustion of gas and wax.

Gas/wax species	Calorific value[a] [kWh/kg]	Mass of species [kg/kg-PET]	Energy [kWh/kg-PET]	Mass of CO_2 [kg-CO_2/kg-PET]
CO	2.807	0.102	0.2863	0.1602
CH_4	15.40	0.021	0.3234	0.0576
C_2H_4	15.34	0.013	0.1994	0.0405
C_2H_6	13.93	0.004	0.0557	0.0114
Wax			2.8082[b]	0.9391
		Total	3.6730	1.2088

[a]Perry et al. (1984); [b]This study

Note that the avoided production of carbon material in the case of PET carbonization is credited as 0.2867 kg/kg-PET. The cost and CO_2 emission of carbon material were reported as 28.76 yen/kg-biochar and 0.9603 kg-CO_2/kg-biochar (Heidari et al., 2019). On the other hand, by-products such as gas and wax are combusted for the avoided production of electricity which is credited as 0.368 kWh/kg-PET.

8.2.6 CO_2 recovery and cost estimation from carbon capture

A study by Shigaki et al. (2018) reports the CO_2 recovery rate and power consumption using pilot scale PSA tower using commercial Zeolite 13X. Note that the recovery rate and power consumption in their study were measured experimentally. 3 adsorbent tanks with height of 1.5 m were used. Total of 240 kg adsorbent was loaded into the adsorbent tanks. Initial feed gas was 22.5 CO_2-vol% (N_2 balance). CO_2 recovery rate was 4.69 t-CO_2/day with operating power consumption of 633.15 kWh/day. Other operating parameters are as follows: cycle time is 5 min/cycle, total cycles a day is 288 cycle/day, operating pressure at 0.151 MPa and operating temperature at 283 K.

Based on given information, the amount of CO_2 adsorbed per cycle can be calculated as follows,

$$\frac{4.69\ t\text{-}CO_2/day}{288\ cycle/day} = 16.2\ kg\text{-}CO_2/cycle$$

Therefore, the amount of CO_2 adsorbed per cycle per kg of Zeolite 13X can be calculated as,

$$\frac{16.2\ kg\text{-}CO_2/cycle}{240\ kg\text{-}adsorbent} = 0.0676\ kg\text{-}CO_2/kg\text{-}adsorbent = 1.54\ mol/kg$$

The total amount of CO_2 adsorbed per cycle per kg of Zeolite 13X based on the commercial scale of PSA system was 1.54 mol/kg at 0.151 MPa, 283 K operating at total of 288 cycle/day with operating power consumption of 135.00 kWh/day.

A summary of CO_2 adsorption capacity at equilibrium under 1 atm, 20-35°C and the total gas adsorbed using pilot PSA system for Zeolite 13X and PET-derived activated carbon is shown in **Table 8-6**. Based on the summary table, it can be seen that the total CO_2 adsorbed before reaching saturation point for 1 cycle breakthrough experiment using Zeolite 13X operated at lab-scale adsorbent system agrees well with the commercial scale adsorption amount reported by Shigaki et al. (2018).

Table 8-6: Summary of CO_2 adsorption properties for Zeolite 13X and PET-derived activated carbon.

	Adsorption condition for breakthrough curve	Total CO_2 adsorbed before reaching saturation point [mol/kg]	REF
Zeolite 13X	5 CO_2-vol% (He balance) at 30°C, 1 atm	1.49	Lopes et al., 2009
Zeolite 13X	20 CO_2-vol%, 60 CH_4-vol% (N_2 balance) at 20°C, 1 atm	1.57	Cavenati et al., 2006
PET activated carbon	20 CO_2-vol%, (N_2 balance) at 35°C, 0.1 MPa	1.47	This study

Following assumptions were made for the estimation: (1) the total amount of CO_2 adsorbed for 1 cycle during the PSA operation is approximately equivalent to the total CO_2 adsorbed before reaching saturation point of breakthrough curve at similar operating conditions (0.1 MPa and 308 K); (2) the power consumption is equivalent under similar operating conditions; (3) same dimension of commercial PSA system and adsorbent loading are assumed; (4) the adsorption efficiency is constant and the adsorbent is not subjected to degradation. By substituting Zeolite 13X with PET activated carbon, the CO_2 recovery rate is now calculated as

$$1.470\ mol\text{-}CO_2/kg \times 44\ kg/kmol \times 240\ kg \times 288\ cycle/day = 4471\ kg\text{-}CO_2/day$$

, while the CO_2 emission and cost from power consumption is calculated as

$$135.00\ kWh/day \times 0.463\ kg\text{-}CO_2/kWh = 62.505\ kg\text{-}CO_2/day$$

$$135.00\ kWh/day \times 16.6\ yen/kWh = 2241\ yen/day$$

The initial cost (15 years of operation) and operating cost (including labor and maintenance cost) of the PSA facility are 1826 yen/day and maintenance cost 66590 yen/day, respectively as summarized in **Appendix H**.

8.2.7 Landfill

Exhausted activated carbon is assumed to be landfilled as permanent storage in this study. Based on Nakatani et al. (2010), the power consumption per 1 kg waste for landfill was reported to be in average, approximately 0.0586 kWh/kg-PET in terms of electricity consumption and 0.000158 L/kg-PET in terms of heavy oil consumption.

On the other hand, it was assumed that the disposal unit price of non-regenerable activated carbon after multiple usage is 11243 yen/m^3 (Tsuchida et al., 2008). This is approximately 9.94 yen/kg, given that the bulk density of PET-derived activated carbon in this study was obtained as 1131 kg/m^3.

8.2.8 Conclusions: CO_2 emission and cost estimation of various operations

In this section, the total CO_2 emission and cost of operation per 1 kg PET from each operation were estimated and calculated. A summary of all the initial and maintenance cost of operations was presented in **Appendix H**. Note that the cost of operations did not include pre-treatment (drying) cost and post-treatment (pollutant removal) cost. A summary of the inventories of the overall operations was presented in **Appendix I**, which will be used for the life-cycle assessment study in the next section.

8.3 Life cycle assessment

8.3.1 Introduction

In order to determine the feasibility of carbonization as an additional treatment process for non-recyclable PET with comparison to other conventional operations, an evaluation based on the life cycle assessment (LCA) was studied in terms of CO_2 emission and net profit of operations. In this section, life cycle inventory (LCI) analysis was conducted based on the avoided burden approach. Avoided burden approach assumes that the recycled product (recovered energy) from the investigated system will replace the competing product (energy source). In this approach, the environmental burdens from the competing process are subtracted from those of the investigated system (Nakatani, 2014). The inventories of each operation were based on the previous section which are summarized in **Appendix I**.

8.3.2 Evaluated scenarios

The theoretical system boundaries for the case assessment in this study based on the avoided burden approach is shown in **Figure 8-7**. The scenarios that were evaluated in this study are given as follows: (i) waste PET bottles are recycled into recycled PET pellet through the mechanical recycling (Figure 8-7(a,b)); (ii) waste PET bottles are carbonized into char through carbonization (Figure 8-7(c)); (iii) incinerated without energy recovery; (iv) incinerated with energy recovery as electricity (power generation efficiency assumed as 10%); and (v) landfill of exhausted activated carbon.

For scenario (i), mechanical recycling of waste PET to PET pellet was assumed. In particular, mechanical BtoF (bottle-to-fiber) recycling and mechanical BtoB (bottle-to-bottle) recycling were assumed. For mechanical BtoF recycling, the yield of recycled PET pellet was assumed as 0.923 kg-pellet/kg-PET based on the calculations presented by Nakatani and Hirao (2010). On the other hand, for mechanical BtoB recycling, the yield of pellet which will be used to manufacture PET bottle was assumed to be 0.850 kg-pellet/kg-PET based on the information obtained from field survey (approximately 15 wt% disposal of PET; Furusawa, 2019; Kyoei Industry co. ltd, 2015). Note that the residue from recycling was assumed to be incinerated as the final disposal method. For the sales price of recycled pellet, the range price is usually set

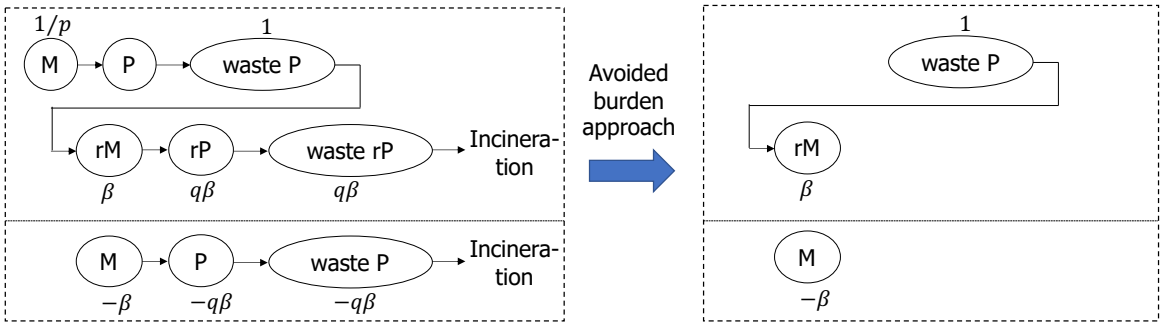

(a) Open-loop recycling (BtoF) of PET

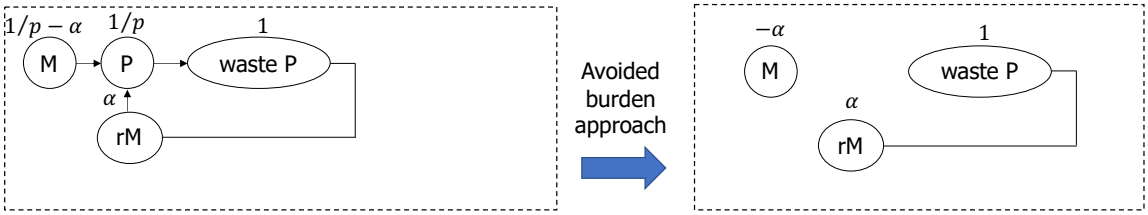

(b) Closed-loop recycling (BtoB) of PET

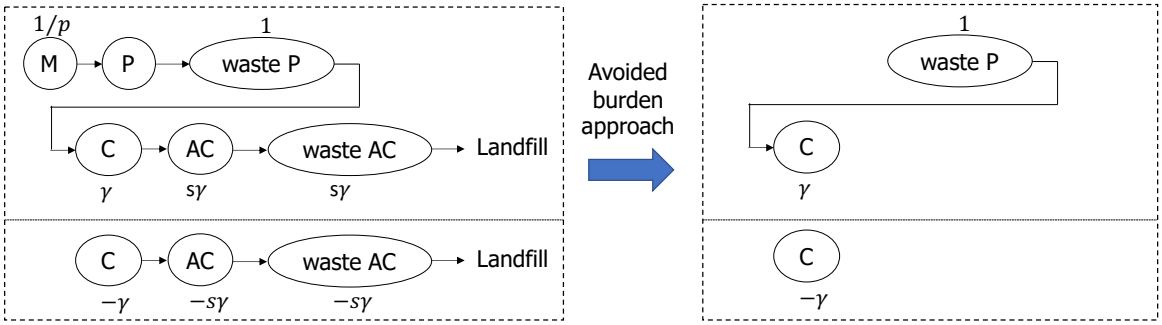

(c) Carbonization of PET

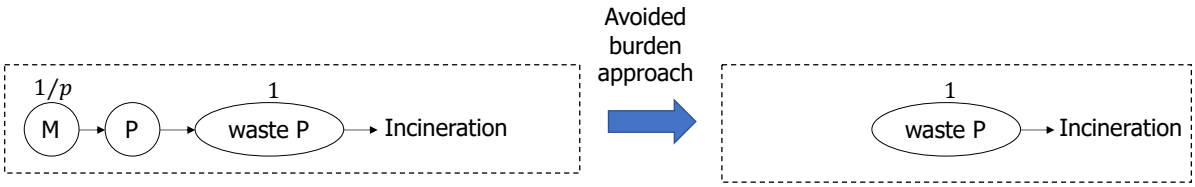

(d) Incineration of PET

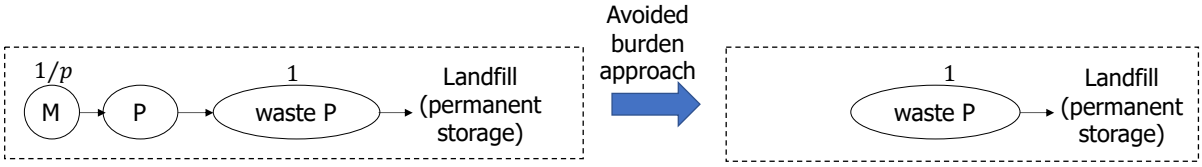

(e) Landfill of PET

Figure 8-7: Theoretical system boundaries for the case assessment of (a,b) material recycling, (c) carbonization, (d) incineration and (e) landfill based on the avoided burden approach. (M: Material; P: Product; rM: Recycled material; rP: Recycled product; C: Char; AC: Activated carbon; p: yield ratio of P; q: yield ratio of rP; s: yield ratio of AC; β: yield ratio of rM from material recycling (open-loop); α: yield ratio of rM from material recycling (closed-loop); γ: yield ratio of C from carbonization)

lower than the price of virgin pellet. In this assessment, the potential profit of virgin pellet is set in the range 60-100% of the price of virgin pellet (Furusawa, 2019).

For scenario (ii), waste PET bottles are carbonized into char using an industrial scale carbonization facility as presented in the previous section. In this scenario, the energy required for the carbonization process was supplied by 4 wt% of the product gas, which was obtained as the by-product. The residue by-product, including wax, was combusted for the avoided production of electricity.

Scenarios (iii)-(v) are the scenarios for final disposal. For scenarios (iii) and (iv), waste PET bottles are incinerated with and without energy recovery, respectively. For scenario (v), exhausted activated carbon, denoted as waste AC in Figure 8-6(c), was assumed to be landfilled for permanent storage.

All scenarios include transportation of waste PET from collection site to a temporary transport station, and transportation of waste PET to their consecutive treatment sites. Note that pre-recycling such as bottle sorting and baling were considered for the recycling scenario. **Figure 8-8** shows the simplified scenarios with their inventories.

Scenarios / Processes	Incineration (without energy recovery)	Incineration (with energy recovery)	Mechanical recycling	Carbonization	Landfill
Transportation	From collection site to incineration facility	From collection site to incineration facility	From collection site to recycling facility	From collection site to carbonization facility	From collection site to landfill site
Combustion	Combustion of collected PET	Combustion of collected PET	Combustion of PET residue	Combustion of by-product (wax and gas)	
Emission from process			Emission from production of recycled pellet	Emission from production of char	
Avoided production		Electricity generation	Production of virgin pellet	Production of carbon material Electricity generation	
Disposal					Disposal in landfill site without any treatment

Figure 8-8: Simplified scenarios for incineration (with and without energy recovery), mechanical recycling, carbonization and landfill with their consecutive inventories.

8.3.3 Results of LCA assessment

8.3.3.1 CO_2 emission of evaluated scenarios

Figure 8-9 shows the CO_2 emission of the scenarios for incineration (without energy recovery), incineration (with energy recovery), mechanical recycling, carbonization and landfill based on the avoided burden approach LCI analysis. Based on the results, combustion of PET and by-product from carbonization is the major factor for CO_2 emission. The landfill scenario emits the least CO_2, however, other environmental impacts such as groundwater pollution, air pollution with impact on climate through methane emission and potential health hazards were not considered in this assessment (Lisk, 1991).

The scenario for incineration without energy recovery generates the most CO_2 emission. This is the minimum amount of GHG emission for PET incineration due to the complete combustion of PET, which was assumed in this study. It is speculated that the total GHG emission will be higher than 2.346 kg-CO_2/kg-PET due to the possible production of gaseous products with higher Global Warming Potentials.

The scenario for incineration with energy recovery also generated high amount of CO_2 emission. The avoided production of electricity from energy recovery credited for the deduction of CO_2 emission. However, the credited amount of CO_2 emission was low due to the low HHV of waste PET. This result is in accordance with the result reported by Nakatani et al. (2010).

The scenario for mechanical recycling produced net CO_2 emission of -0.834 kg-CO_2/kg-PET for BtoF recycling and -0.546 kg-CO_2/kg-PET for BtoB recycling. Mechanical recycling which produced recycled pellets for the avoided production of virgin pellet highly credited to the decrease of CO_2 emission. In particular, combustion of residue from BtoB recycling (15 wt%) resulted in large CO_2 emission. Nevertheless, mechanical recycling is the only operation which resulted in negative CO_2 emission among the compared processes.

The scenario for carbonization with by-product as fuel resulted in net amount of 0.479 kg-CO_2/kg-PET for CO_2 emission. Carbonization produced char for the avoided production of carbon material which highly credited to the decrease of CO_2 emission. However, the combustion of by-products from carbonization such as combustible gas and wax for the avoided production of electricity resulted in large CO_2 emission. Nevertheless, carbonization of PET highly contributed to the decrease in net CO_2 emission compared to incineration of PET.

Overall, CO_2 emission of the evaluated scenarios is in the ascending order as follows: mechanical recycling (BtoF) < mechanical recycling (BtoB) < landfill < carbonization (by-product as fuel) < incineration (with energy recovery) < incineration (without energy recovery). Based on the results, the net CO_2 emission from mechanical recycling can further be decreased by replacing incineration of residue from recycling to carbonization as the disposal method. For the carbonization of PET with by-product as fuel, net CO_2 emission can be decreased by addition of CO_2 capture through PSA system in the operation. The combination of operations and CO_2 emission based on the life cycle assessment of operations will be discussed in later sections.

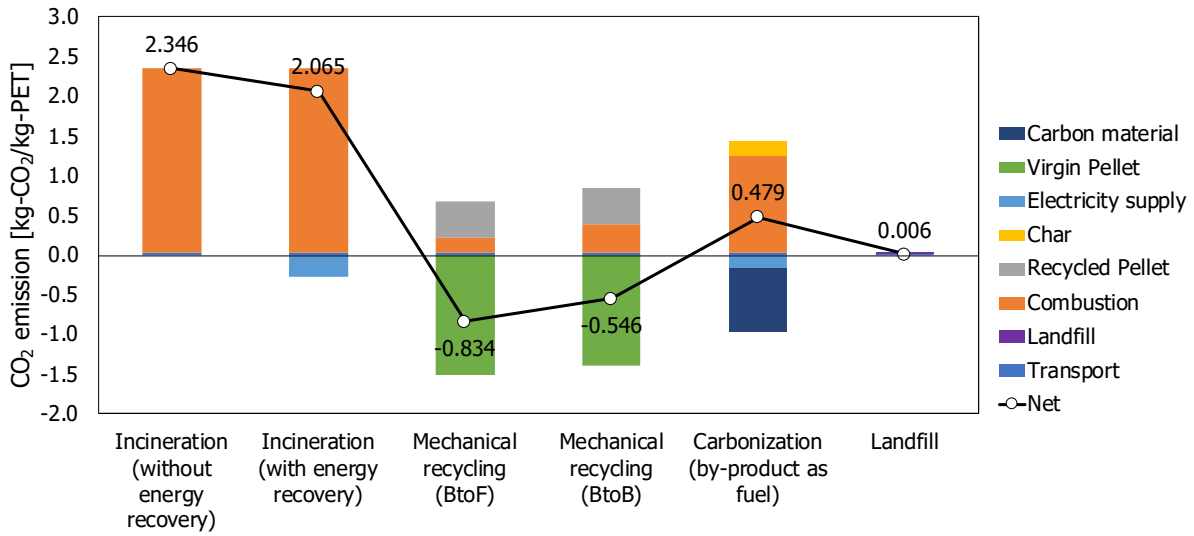

Figure 8-9: CO_2 emission of the evaluated scenarios based on the avoided burden approach LCI analysis.

8.3.3.2 Net profit of evaluated scenarios

Figure 8-10 shows the net profit of the scenarios for incineration (without energy recovery), incineration (with energy recovery), mechanical recycling (BtoF and BtoB), carbonization and landfill based on the avoided burden approach LCI analysis. Note that net profit was obtained by subtracting the potential profit by potential cost.

Based on the results, cost of facility is the major factor for potential cost in all operations. Mechanical recycling (BtoF and BtoB) is the only scenario with positive net profit due to the production of recycled pellet, which credited to the potential profit of operation. However, the fluctuation of recycled pellet sales price highly affects the net profit of mechanical recycling. In particular, in cases when recycled pellet price sales were only 60% of the virgin pellet price, the net profit of the BtoF and BtoB operations reached approximately zero to negative net profit. On the other hand, the scenario of carbonization presented the largest negative net profit among all compared operations. The major factor was due to the high cost of operation of the carbonization facility and low operating capacity. In addition, the profit of char sales is unknown, therefore was not included in this assumption. The positive net profit of mechanical recycling was used as a basis for the implementation of PSA operation for the carbon capture in the overall recycling system, which was presented in the next section.

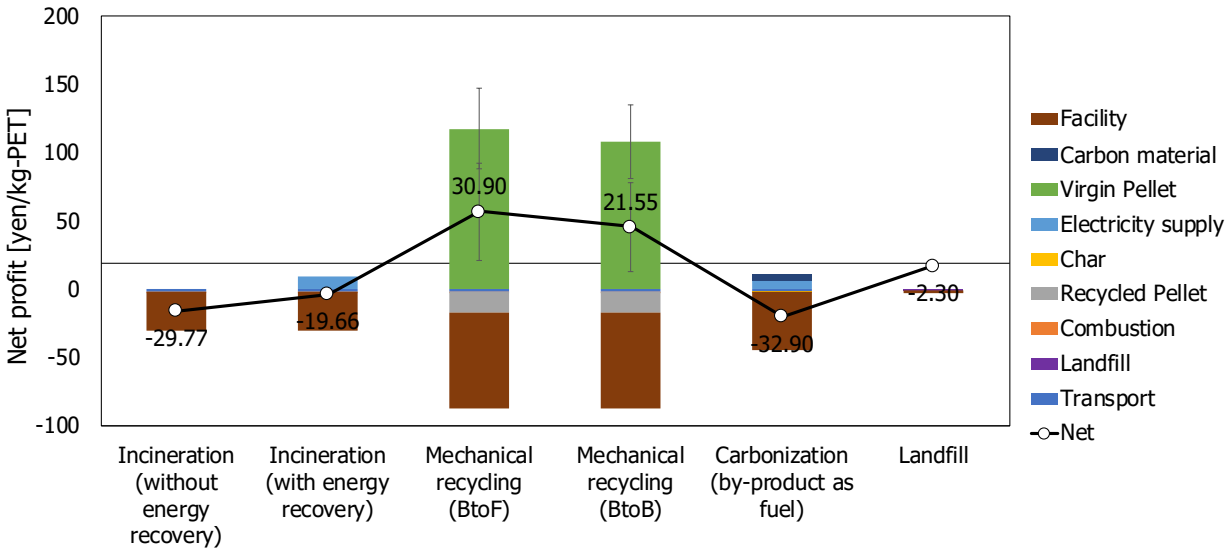

Figure 8-10: Net profit of the evaluated scenarios based on the avoided burden approach LCI analysis. (Net profit = Potential profit – cost of operation)

8.3.3.3 Comparison of the evaluated scenarios

In this section, a case comparison of the evaluated scenarios was conducted by combining multiple operations based on the maximum treatment capacity of waste PET of each operation. Carbon capture using the PSA facility was included as a feedback of the whole operation in terms of amount of carbon captured per unit cost of operation.

As seen in **Figure 8-11**, three different cases of PET bottle recycling and treatment were presented to determine the estimation of CO_2 emission and annual profit; they are, Case 1: Incineration of non-recycled PET bottles with energy recovery and conventional recycling of PET bottles; Case 2: Conventional recycling of PET bottles (BtoF) and carbonization of non-recycled PET bottles; and Case 3: Conventional recycling of PET bottles (BtoF), carbonization of non-recycled PET bottles and carbon capture using activated carbon produced from carbonization.

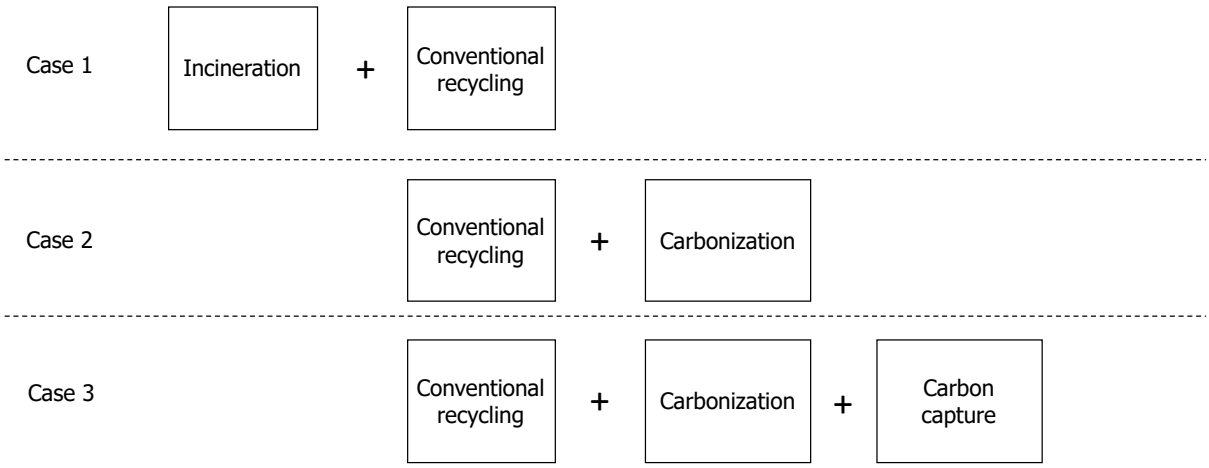

Figure 8-11: Estimation of CO_2 emission and reduction from different cases.

Boundary conditions such as the current total numbers of available recycling factories, the maximum possible installation of carbonization facility and the maximum operating capacities of facilities need to be considered. The current number of domestic recycling factories in Japan is 50 factories (JCPRA, 2018). It is notable that there are currently 50 domestic recycling factories that are operating at full capacity which are able to recycle 334 kton/year of PET bottles (refer to Table 8-1), yearly. This is equivalent to 6.68 kton/year per domestic recycling factories. Note that total bottles that are not

domestically recycled is 292 kton/year and that the cost (bid price) of recyclable bottle is 33679 yen/ton (JCPRA, 2018) for 2018. From here on, the number of domestic factories is expressed as N.

Case 1: Incineration (with energy recovery) + Conventional recycling

Carbon emitted was calculated as follows:

Carbon emitted from Recycling

= Total CO_2 emission(Recycling) × (N × Amount of bottles treated)

= -0.7783 kton-CO_2/kton-PET × 6.68 kton-PET/factories/year × N

= -5.20N kton-CO_2/year

Carbon emitted from Incineration

= Total CO_2 emission(Incineration) × [Total bottles collected − (N × Amount of bottles treated)]

= 2.065 kton-CO_2/kton-PET × (529 – 6.68N) kton-PET/year

= 1092.39 – 13.79N kton-CO_2/year (Total bottles < 529; $N \leq 79$)

Total carbon emitted

= Carbon emitted from Recycling + Carbon emitted from Incineration

= 1092.39 – 18.99N kton-CO_2/year

Annual net profit was calculated as follows:

Net profit from Recycling

= Net profit(Recycling) × (N × Amount of bottles treated)

= 18.00 million yen/kton-PET × 6.68 kton-PET/factories/year × N

= 120.24N million yen/year

Net profit from Incineration

= Net profit(Incineration)× [Total bottles collected − (N × Amount of bottles treated)]

= – 19.66 million yen/kton-PET × (529 − 6.68N) kton-PET/year

= – 10400.14 + 131.33N million yen/year (Total bottles < 529; $N \leq 79$)

Total net profit

= Net profit from Recycling + Net profit from Incineration

= – 10400.14 + 251.57N million yen/year

Case 2: Conventional recycling + Carbonization

Industrial scale carbonization facility proposed in the previous section was assumed in this assessment. Maximum operating capacity of the carbonization facility was given as 1.46 kton/year. Numbers of carbonization facility was set as 1 carbonization facility installed per 1 recycling factory. Note that the residue bottles that have exceeded the maximum treatment capacity will be incinerated with energy recovery. Also note that gaseous by-products from carbonization was considered as the heat source for carbonization in this assessment.

Carbon emitted was calculated as follows:

Carbon emitted from Recycling

= -5.20N kton-CO_2/year

Carbon emitted from carbonization

= {Total CO_2 emission(Carbonization) + Total CO_2 emission(Landfill)} × (N × Amount of bottles treated)

= (0.479 + 0.006) kton-CO_2/kton-PET × 1.46 kton-PET/factories/year × N

= 0.71N kton-CO_2/year

Carbon emitted from Incineration

= Total CO_2 emission(Incineration) × [Total bottles collected − (N × Amount of bottles treated)]

= 2.065 kton-CO_2/kton-PET × [529 − N × (6.68 + 1.46)] kton-PET/year

= 1092.39 – 16.81N kton-CO_2/year (Total bottles < 529; $N \leq 64$)

Total carbon emitted

= Carbon emitted from Recycling + Carbon emitted from Carbonization + Carbon emitted from Incineration

= 1092.39 – 21.30N kton-CO_2/year

Annual net profit was calculated as follows:

Net profit from Recycling

= 120.24N million yen/year

Net profit from Carbonization

= {Total net profit(Carbonization) + Total net profit(Landfill) } × (N × Amount of bottles treated)

= (– 32.90 – 2.3) million yen/kton-PET × (N × 1.46 kton-PET/factories/year)

= – 51.39N million yen/year

Net profit from Incineration

= [Total net profit(Incineration)] × [Total bottles collected − (N × Amount of bottles treated)]

= – 19.66 million yen/kton-PET × [529 − N × (6.68 + 1.46)]

= − 10400.14 + 160.03 N million yen/year (Total bottles < 529; $N \leq$ 64)

Total net profit

= Net profit from Recycling + Net profit from Carbonization + Net profit from Incineration

= – 10400.14 + 228.88N million yen/year ($N \leq 65$)

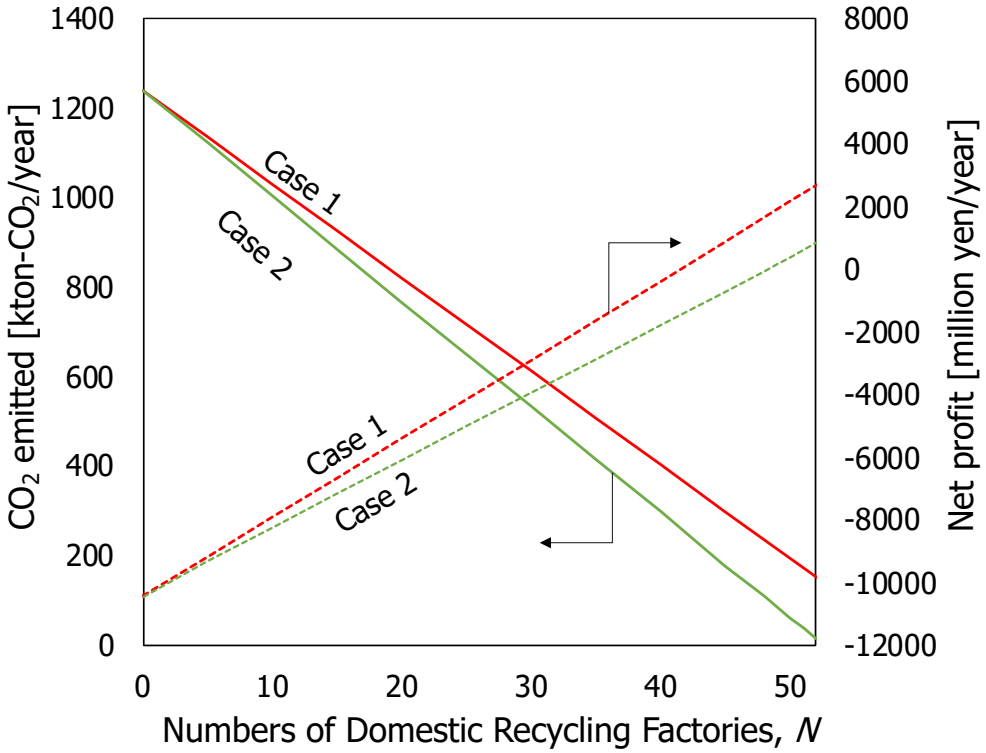

Figure 8-12: Comparison of CO_2 emitted and net profit of operation for Case 1 and Case 2, respectively.

Figure 8-12 shows the comparison of annual CO_2 emission and annual net profit of operation for Case 1 and Case 2, respectively. Note that positive net profit indicates the potential profit of the combined operations.

For Case 1, annual CO_2 emission decreased with increasing numbers of domestic recycling factories. This is due to the increased fraction of PET bottles treated through mechanical recycling, which produces recycled PET pellets to replace virgin pellets needed for manufacture of plastic products. The avoided production of virgin pellets and decrease in combustion of PET credited to the decrease of CO_2 emission. The net profit also increased with increasing numbers of domestic recycling factories due to the production of recycled PET pellets which replaces virgin PET pellets.

For Case 2, annual CO_2 emission was lower than that of Case 1. This is due to the carbonization process which produced char for the avoided production of carbon material, thus credited to the decrease of CO_2 emission. On the other hand, the net profit of Case 2 was lower than that of Case 1. This is due to the energy recovery in the form of electricity during incineration, which contributed to the higher potential profit in case 1 compared to case 2. It should be noted that actual annual profit of Case 2 may increase as the profit from char sales as carbon material was not considered in this estimation.

At current situation of 50 recycling factories, overall CO_2 emission decreased from 142 kton/year to 27 kton/year when 1 carbonization facility is installed to 1 recycling factories in the current situation, indicating a significant 81% cut in overall CO_2 emission.

Case 3: Conventional recycling + Carbonization + CO_2 recovery using PET derived AC

A conventional scale PSA system using PET derived activated carbon was assumed in this case. With reference to section 8.2.6, the CO_2 recovery and net profit (including initial cost and maintenance cost) per year for 1 PSA system under maximum operation were estimated as 1.63 kton/year/PSA system and 25.79 million yen/year/PSA system, respectively. Detailed calculations are summarized in **Appendix H**. It was assumed that PSA systems are installed only in positive net profit cases. Note that 1 carbonization facility is pre-installed per 1 recycling factories for all cases. Similar to previous cases, the residue bottles that have exceeded the maximum treatment capacity will be incinerated with energy recovery, and that gaseous by-product from carbonization was considered as the heat source for carbonization in this assessment. Numbers of PSA system were set as follows:

= Annual profit million yen/year ÷ 25.79 million yen/year/PSA system (Annual profit > 0)

Figure 8-13 shows the annual CO_2 emission and annual profit of operation for Case 3 with comparison to Case 2. Based on the results, the following was observed:

① PSA facility is installed at 46 domestic recycling factories and 46 carbonization facilities, in which the combined operation first reaches positive annual profit.

② With increasing numbers of PSA facilities, net CO_2 emission decreases.

③ Net CO_2 emission reaches zero carbon emission at 32 PSA facilities.

④ Under the constant operation of 32 PSA facilities, increased numbers of domestic recycling factories and carbonization facilities will result in increased potential profit of the combined operation.

⑤ Total of more than 51 domestic recycling factories and consequent carbonization facilities are needed for Case 2 in order to achieve zero emission, as compared to 49 domestic recycling factories, consequent carbonization facilities and 32 PSA facilities (point ③) needed for Case 3.

⑥ The blue shaded area indicates the cost needed to operate 32 PSA facilities in order to achieve zero/negative emission for the combined operation.

⑦ The green shaded area indicates the reduction of CO_2 emission under the operation of 32 PSA facilities for the combined operation.

On the other hand, total 15.17 kton/year of PET-derived activated carbon is needed in order to operate 32 PSA facilities, assuming that the PET derived activated carbon can be regenerated and reused for a span of 0.5 year. In the case of 49 recycling factories and 49 consecutive carbonization facilities, only 15.77 kton/year of PET derived activated carbon can be supplied (21 wt% fixed-carbon yield from carbonization and 80 wt% yield from activation), indicating the sufficient supply of carbon adsorbent without the need for compensation of adsorbent from other sources. Therefore, it is considered that the carbonization facility and PSA facilities are self-sufficient in terms of supply of carbon adsorbent.

Overall, evident decrease in CO_2 emission was observed when PSA facility and carbonization facility were included. Under the full operation of 32 PSA facilities, with the increased numbers of domestic recycling factories, potential profit can be generated, in addition to creating a negative emission of the systems using the combined operations. It should be well noted that the potential annual profit presented may increase in the actual case, due to the potential profit from recovered CO_2 sales as resource for chemical usage such as methanol production, which was not considered in this estimation.

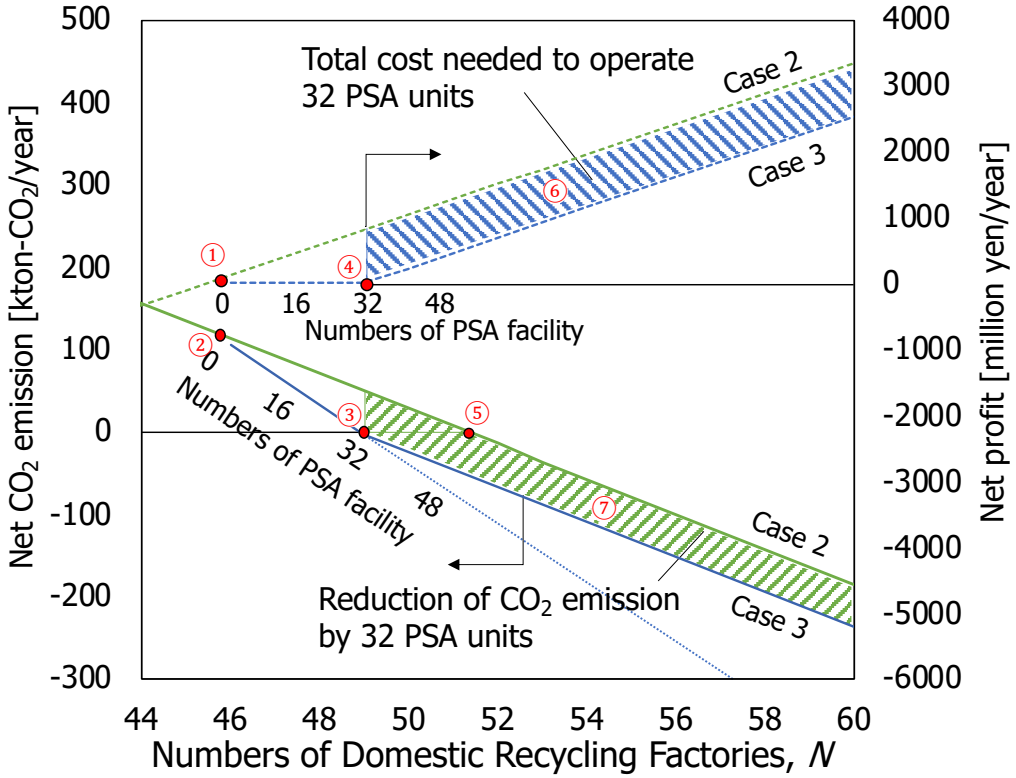

Figure 8-13: Annual CO_2 emission and annual profit of operation for Case 3.

8.3.4 Conclusions: Life cycle assessment

The CO_2 emission and net profit of operations were used as the inventories needed for the life cycle assessment study, in which the life cycle inventory analysis was conducted based on the avoided burden approach. Five distinct scenarios were evaluated, and results showed that mechanical recycling, in particular, the BtoF recycling, is the most effective approach to reduce CO_2 emission and generate profit among the compared scenarios. Although the carbonization scenario has reduced CO_2 emission compared to incineration scenarios, the running cost of operation was the highest among the compared scenarios. This is due to the high running cost of facility, which can be counter-measured by improving the operating capacity of the carbonization process.

The evaluated scenarios were compared, and results showed that replacement of incineration with carbonization resulted in significant cut in CO_2 emission due to the fixation of carbon in the form of char. This suggests that implementation of carbonization as a treatment of waste PET is highly effective in the reduction of CO_2 emission compared to the treatment of PET through incineration. On the other hand, implementation of PSA facilities based on the potential profit highly resulted in a significant reduction of CO_2 emission. Furthermore, maximum 32 numbers of PSA facilities under the operation of 49 recycling factories and 49 carbonization facilities are sufficient to mitigate the total CO_2 produced from the overall combined operation, leading to approximately zero carbon emission under full operating capacity. In other words, if 1 PSA facility is installed to 1 recycling factories and 1 consecutive carbonization facilities, operating capacity of PSA facility can be decreased to 65% in order to maintain the net zero CO_2 emission. This will help further decrease the labor cost and energy cost of the operation, which will lead to increase of potential profit of the system. Furthermore, the total usage of adsorbents needed for the operation of PSA facility can be decreased (<240 kg/6 months), thus leading to the increase in potential profit of activated char for other usage.

8.4 Additional assessment based on relating variables

8.4.1 Background

Up till this section, the economic assessment and CO_2 emission estimation were conducted for cases in which the carbonization process was conducted with specific conditions; namely, carbonization temperature of single PET feedstock at 400-480°C based on experimental data from Chapter 4, and adsorption performance of PET derived activated carbon obtained from CO_2 activation based on experimental data from Chapter 7. In this section, it is of great interest to probe into the relationship between the varying parameters; namely, carbonization at ranging temperatures based on experimental data from Chapter 4 and varying feedstock based on experimental data from Chapter 6; and their effects on the annual CO_2 emission and annual profit of operation for Case 2. Also, it is also of best interest to determine the extent of temperature effect on the annual CO_2 emission and annual profit for Case 3 with relation to gas adsorption properties of activated PET based on Chapter 7.

8.4.2 Assessment based on varying parameters

Varying temperature range: Effect on Case 2

The annual CO_2 emission and annual profit of operation for Case 2 in which carbonization of PET is conducted under the temperature ranges of low temperature (320-400°C), moderate temperature (360-440°C) and high temperature (400-480°C) were assumed based on the experimental results from Chapter 4. The following assumptions were made: (i) yield of activated carbon is based on the fixed-carbon yield of char, in particular, 8 wt% for low temperature (320-400°C), 16 wt% for moderate temperature (360-440°C) and 21 wt% for high temperature (400-480°C); (ii) performance of activated carbon produced from each temperature remains constant; and (iii) energy demand for the carbonization process remains constant regardless of varying temperature ranges. The results are shown in **Figure 8-14**. Note that Case 1 is presented in the figure as comparison of cases without carbonization.

The CO_2 emission of each case in the increasing order is as follows: Case 2 (400-480°C) < Case 2 (360-440°C) < Case 2 (320-400°C). It is well notable that the CO_2

emission of Case 2 (320-400°C) was similar to that of Case 1. This is due to the yield of char with high volatile matter when carbonization is conducted at low temperature range, thus leading to the high emission of CO_2 similar to incineration of PET. The CO_2 emission decreased with increasing temperature due to the yield of char with high fixed carbon content. However, it is not expected that the CO_2 emission will continue to decrease with increasing temperature (>480°C). This is due to the progress of decomposition reaction of char with increasing temperature, with reference to the decomposition profile of PET as shown in **Appendix C**. Therefore, it is speculated that Case 2 (400-480°C) presents the minimum net CO_2 emission from carbonization in the case of varying temperature range.

On the other hand, the annual profit of each case in the decreasing order is as follows: Case 2 (400-480°C) > Case 2 (360-440°C) > Case 2 (320-400°C). It is well noted that the annual profit of Case 1 is higher than all cases of Case 2 due to the relatively high amount of electricity generated from incineration with energy recovery. Case 2 (400-480°C) and Case 2 (360-440°C) showed no distinct difference due to the exemption of profit from sales of activated char. Note that the outcomes may differ if the profit from sales of activated char is included. On the other hand, Case 2 (320-400°C) presents the lowest profit due to the yield of char with low fixed-carbon yield and also to no generation of electricity due to low wax generation.

As a summary, decreasing the operating temperature lower than 400-480°C will lead to increased annual CO_2 emission and decreased annual profit, whereas increasing the operating temperature higher than 400-480°C will lead to expected decrease of char yield due to the decomposition reaction of char. As a conclusion, in the case of varying temperature range of carbonization, operating temperature in between 400-480°C should be the optimum temperature range for the carbonization of PET to obtain the appropriate char for activation (approximately 25 wt% volatile matter; Aworn et al., 2008), in addition to producing the lowest annual CO_2 emission and highest annual profit.

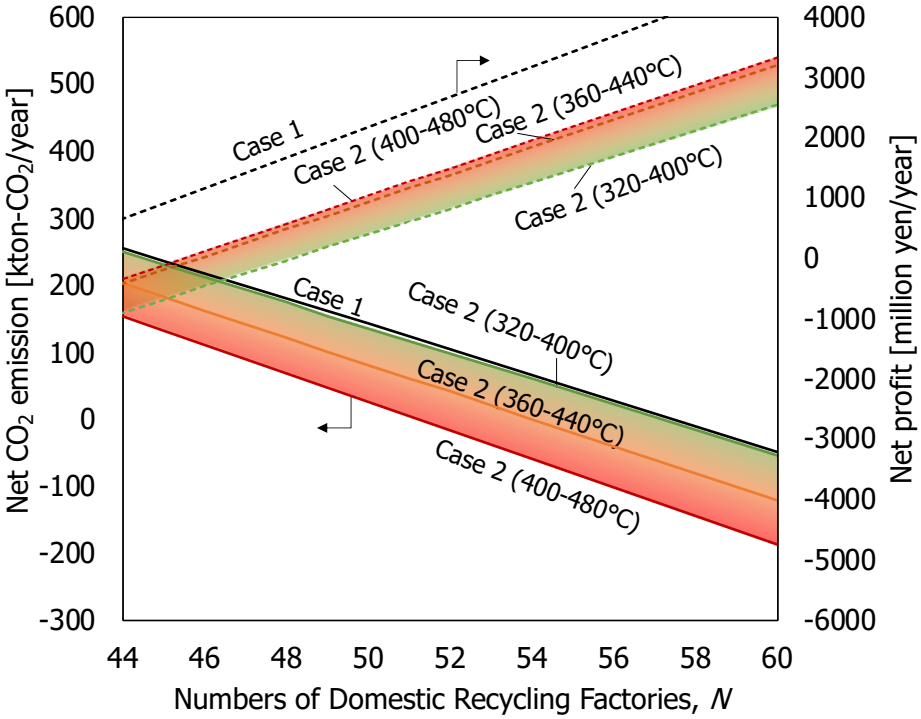

Figure 8-14: Annual CO_2 emission and annual profit of Case 2 in which carbonization of PET is conducted under varying temperatures.

Addition of cobalt oxide: Effect on Case 2

As mentioned in previous chapters, benzoic acid, which is the main component of wax, is a general sublime that clogs pipes and heat exchanger, thus resulting in serious problems in industrial scale operations (Shioya et al., 2005; Wan Ho, 2015; Anuar Sharuddin et al., 2017). In the assessment of annual CO_2 emission and annual profit in the previous section, the complication of reactor operation due to clogging of pipes and heat exchanger was not considered. However, it is highly speculated that clogging of pipes due to wax product will cause problems in the continuous operation of the carbonization facility, thus leading to increased cost for frequent need of equipment maintenance and decreased operating capacity. Therefore, in this section, countermeasure by introducing cobalt oxide, a catalyst that decomposes benzoic acid into CO_2 and other aromatic compounds which leads to the decreased production of wax, is taken into consideration to study the effects of presence of cobalt oxide in the carbonization of PET on the annual CO_2 emission and annual profit.

Here, cobalt oxide is considered as a catalyst for the decomposition of benzoic acid in wax, and the following were assumed: (i) cobalt oxide is added in the carbonization

operation at weight fraction 1 wt% to PET feedstock; (ii) yield of activated carbon is based on the fixed-carbon yield of char obtained at high temperature (400-480°C); (iii) performance of activated carbon remains constant; and (iv) energy demand for the carbonization process remains constant. The total energy and CO_2 emission from combustible gas and wax of PET carbonization in the presence of cobalt oxide are based on the experimental results from Chapter 6 as shown in **Table 8-7**. The annual CO_2 emission and annual profit of operation for Case 2 in which carbonization of PET is conducted in the presence of cobalt oxide are shown in **Figure 8-15**. Case 1 and Case 2 (400-480°C) are presented in the figure as comparison of cases without carbonization and with carbonization of single PET feedstock, respectively.

Table 8-7: Total energy and CO_2 emission from combustion of gas and wax.

Gas/wax species	Without cobalt oxide		With cobalt oxide	
	Energy [kWh/kg-PET]	Mass of CO_2 [kg-CO_2/kg-PET]	Energy [kWh/kg-PET]	Mass of CO_2 [kg-CO_2/kg-PET]
CO	0.2863	0.1602	0.0824	0.0462
CH_4	0.3234	0.0576	0.0752	0.0135
C_2H_4	0.1994	0.0405	0.1873	0.0423
C_2H_6	0.0557	0.0114	0.1458	0.0280
Wax	2.8082	0.9391	1.7874	0.8166
CO_2	-	0.1975	-	0.3555
Total	3.6730	1.4063	2.2781	1.3021

The CO_2 emission of each cases in the increasing order is as follows: Case 2 (Presence of cobalt oxide) ≅ Case 2 (400-480°C) < Case 1. It is well notable that the emission of Case 2 (Presence of cobalt oxide) was similar to that of Case 2 (400-480°C). This is due to the yield of char from carbonization of PET in the presence of cobalt oxide which was similar to that from carbonization of single PET. Although the yield of CO_2 is higher from carbonization of PET in the presence of cobalt oxide than that without cobalt oxide as reported in Chapter 6, combustion of gas and wax for the generation of electricity led to the overall CO_2 emitted from both operations equivalent, as seen in Table 8-7. On the other hand, the annual profit of each cases in the decreasing

order is as follows: Case 1 > Case 2 (400-480°C) > Case 2 (Presence of cobalt oxide). Similar to previously discussed, the annual profit of Case 1 is higher than all cases of Case 2 due to the relatively high amount of electricity generated from incineration with energy recovery. However, Case 2 (Presence of cobalt oxide) presents lower annual profit than that of Case 2 (400-480°C) as a result of low wax yield for the energy recovery in the form of electricity. As discussed in Chapter 6, the low wax yield during the carbonization of PET in the presence of cobalt oxide was due to the catalytic activity of cobalt oxide which progressed the decomposition of carboxylic acid to form aromatic hydrocarbons in wax and CO_2 in the gaseous product.

As a conclusion, addition of cobalt oxide is considered in the assessment and results showed that annual CO_2 emission had no distinct difference from that without cobalt oxide due to the combustion of gas and wax. However, decrease in annual profit will be a factor of concern due to the high cost of operation of carbonization. In addition, direct addition of cobalt oxide in the PET feedstock will lead to concerns regarding the cost of cobalt oxide supply and performance of activated carbon as gas adsorbent. Therefore, future study should consider addition of cobalt oxide in the carbonization operation as a coated layer in the inner surface of the fixed crucible of the reactor.

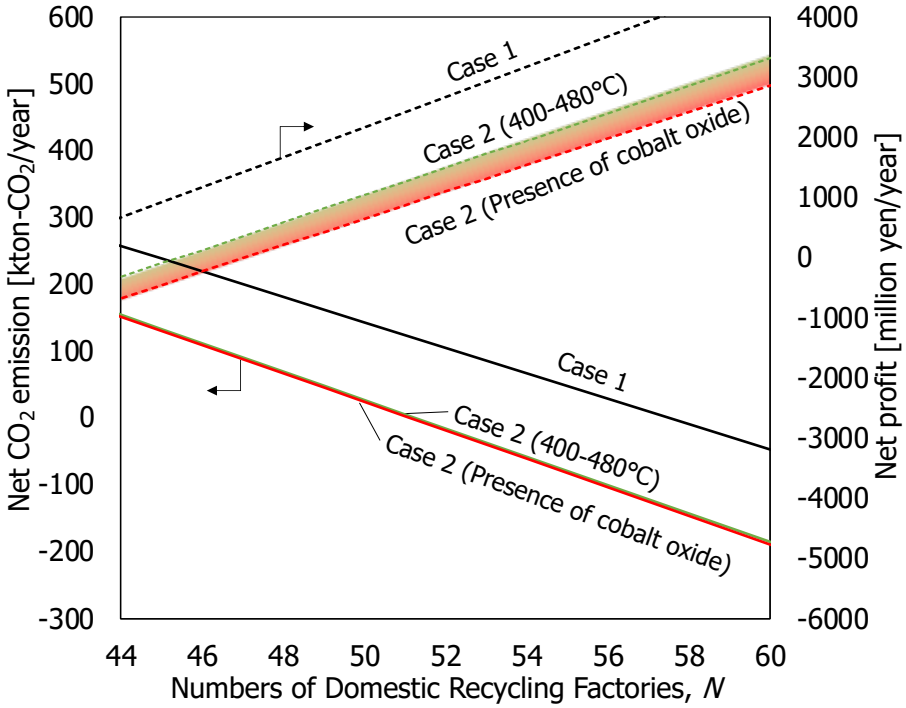

Figure 8-15: Annual CO_2 emission and annual profit of Case 2 in which carbonization of PET is conducted in the presence of cobalt oxide.

Varying temperature range: Effect on Case 3

The annual CO_2 emission and annual profit of operation for Case 3 in which carbonization of PET is conducted under different temperature ranges are shown in **Figure 8-16**, while **Table 8-8** shows the amount of supply and demand of PET-derived activated carbon for Case 3 under different temperature ranges. Note that the temperature ranges of the carbonization reactor are set as low temperature (320-400°C), moderate temperature (360-440°C) and high temperature (400-480°C) with the information based on the experimental results from Chapter 4, while the gas adsorption property of activated PET is based on Chapter 7.

Based on the results, for carbonization of PET at high temperature (400-480°C), a total of 49 domestic recycling factories and carbonization facilities were able to produce enough profit for the installments and operations of maximum 32 PSA facilities for approximately zero carbon emission; for carbonization of PET at moderate temperature (360-440°C), a total of 51 domestic recycling factories and carbonization facilities were able to produce enough profit for the installments and operations of maximum 45 PSA facilities for approximately zero carbon emission; for carbonization of PET at low temperature (320-400°C), a total of 54 domestic recycling factories and carbonization facilities were able to produce enough profit for the installments and operations of maximum 50 PSA facilities for approximately zero carbon emission. Overall, carbonization at 400-480°C requires the least cost for zero carbon emission (red shaded area) compared to carbonization at 360-440°C (orange shaded area) and carbonization at 320-400°C (green shaded area), with the least required numbers of domestic recycling factories, carbonization facilities and PSA facilities to achieve zero carbon emission. On the other hand, Case 3 with carbonization operated at 400-480°C is the only case in which the supply of PET-derived activated carbon meets the demand for carbon-based adsorbents needed to operate the PSA facilities.

In conclusion, carbonization temperature at 400-480°C is the optimum condition for producing the minimum carbon emission and maximum annual profit of operations, in addition to meeting the demand of PET-derived activated carbon needed for the operation of the PSA facilities.

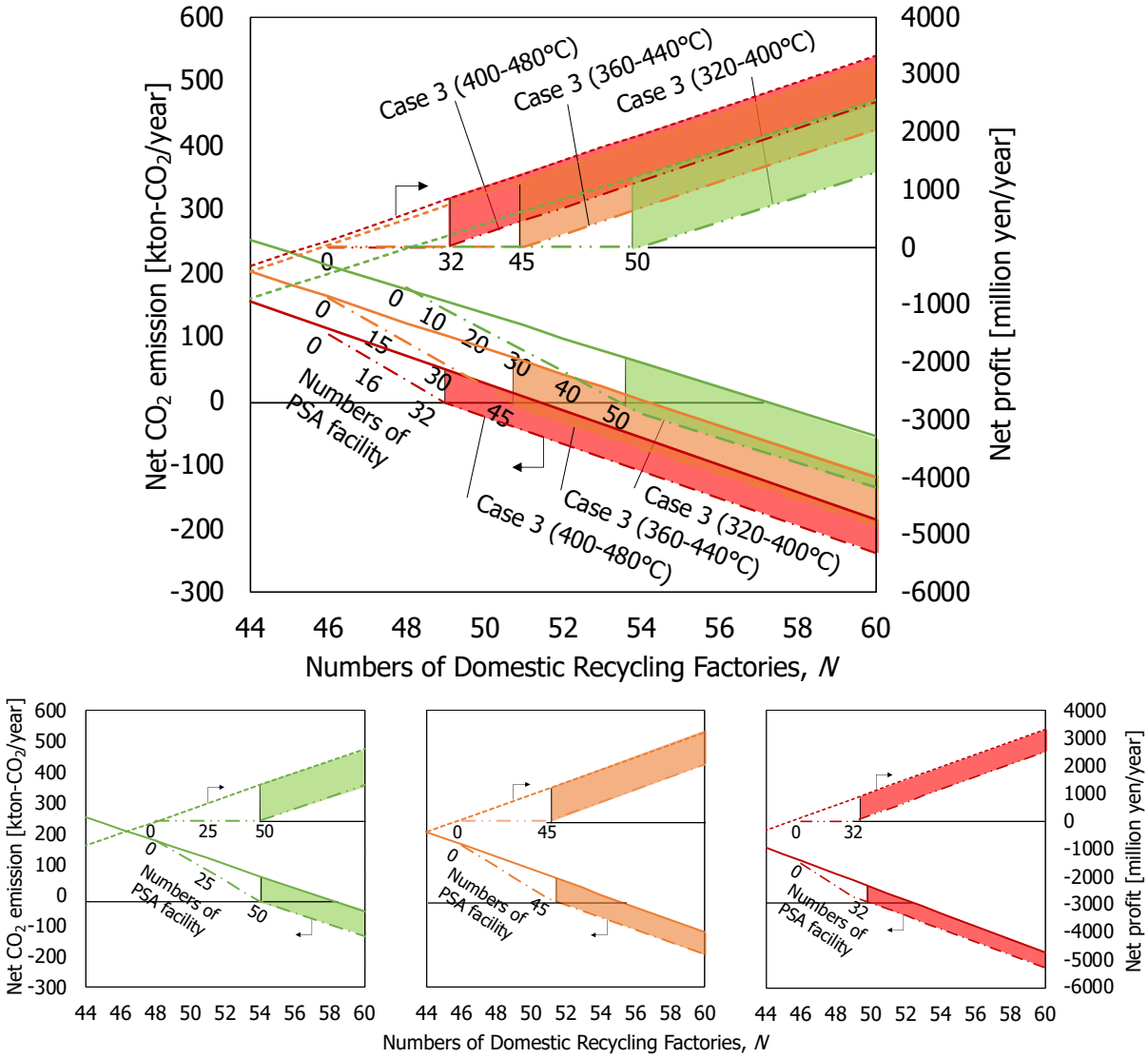

Figure 8-16: Annual CO_2 emission and annual profit of Case 3 in which carbonization of PET is conducted under varying temperatures. Bottom figure from right: Case 3 (320-400°C), Case 3 (360-440°C), Case 3 (400-480°C).

Table 8-8: Demand and supply of PET-derived activated carbon for Case 3.

Reactor temperature	Numbers of domestic recycling factories and carbonization facilities[a] [-]	Numbers of PSA facilities[a] [-]	Amount of PET-AC needed [kton/year]	Amount of PET-AC produced[b] [kton/year]
320-400°C	54	50	23.62	4.77
360-440°C	51	45	21.79	8.60
400-480°C	49	32	15.17	15.77

[a]: Taking the numbers of PSA facilities needed to reach zero carbon emission.

[b]: Taking y_{fc} = 8 wt% for 320-400°C, y_{fc} = 16 wt% for 360-440°C, y_{fc} = 21 wt% for 400-480°C; Burn-off during physical activation as 20 wt%.

8.4.3 Conclusions: Additional assessment based on relating variables

In this section, the CO_2 emission and net profit of operations was assessed based on varying parameters, in particular, temperature range and addition of cobalt oxide by referring to experimental data from previous chapters.

For the assessment based on temperature range, CO_2 emission decreased with increasing temperature due to the yield of char with high fixed carbon content while annual profit was higher at higher temperature range, which in this assessment, was at 400-480°C. However, it should be well noted that continual increase of CO_2 emission at increasing temperature is not expected due to the possibility of progression of decomposition reaction of char with increasing temperature.

For the assessment based on the addition of cobalt oxide, CO_2 emission showed no distinct changes in the case with and without the addition of cobalt oxide. Addition of cobalt oxide to the carbonization operation presented the lowest annual profit due to the low wax yield which consequently led to less energy recovery for electricity production. Nevertheless, the addition of cobalt oxide in the carbonization of PET will be profitable in terms of the ease of operation and the decreased labor cost for equipment maintenance due to the decrease of the wax yield.

Finally, the assessment of Case 3 was repeated in which carbonization of PET is conducted under different temperature ranges. Results showed that carbonization of PET at 400-480°C is the optimum temperature in which the operation presented the lowest carbon emission, highest annual profit and self-sufficient ability of the operation in terms of carbon adsorbent supply.

8.5 Chapter summary

In this chapter, a simple economic assessment and CO_2 emission estimation based on the experimental data were conducted and the feasibility of carbonization of PET in the realization of domestic circulation of waste PET in Japan was studied. In particular, the life cycle assessments of different waste PET treatment methods were conducted and the CO_2 emission reduction effects when carbonization is newly added to the treatment methods were estimated. Comparison of results showed that the replacement of incineration with carbonization led to significant cut in CO_2 emission, thus suggesting the feasibility of carbonization as an optional treatment of waste PET for the reduction of CO_2 emission.

Taking the real-life situation for instance, assume that PET from non-recyclable bottles and residues from recycling accounts for 15 wt% of the total amount of PET bottles collected yearly in Japan, which estimates around 86 kton/year. Given that a carbonization facility is able to treat 4 t/day, approximately 60 carbonization facilities are needed to treat all existing non-recyclable PET. This means that installation of 1 to 2 carbonization facility per prefecture (of total 47 prefectures in Japan) is sufficient to treat all non-recyclable PET while reducing a massive 91% of carbon emission, which is from 204 kton-CO_2/year due to incineration to 19 kton/year as a result of carbonization. This accounts for approximately 0.015% cut in annual emission of CO_2 in Japan (1254 million ton in 2016; EDGAR, 2017).

Overall, the results in this chapter showed that carbonization is a process with potential of replacing conventional waste PET treatment and improving the domestic recycling of PET, leading to the decrease of marine pollution and possible health problems. Implementation of carbonization also expands the possibility of installing PSA facility in the recycling section, leading to the reduction of CO_2 emission and extension of CO_2 utilization from waste PET.

This page is intentionally left blank.

Chapter 9: Conclusions and recommendations

9.1 Conclusions

This research has the ultimate objective of the realization of domestic circulation for PET recycling through the improvement of material value of non-recyclable PET. Japan was chosen as the research location due to the high collection rate but low domestic recycling rate and high dependency on overseas exportation. This dissertation investigated the potential contribution of the carbonization of PET in the process of waste PET management. In particular, utilization of char obtained from carbonization of PET as activated char.

Experimental procedures were initialized to study the fundamental effects of operating parameters on the carbonization of PET. Commercial clear PET was chosen as the model feedstock and a laboratory scale batch reactor was used. Results demonstrated that feedstock size and shape had no evident effects on the product composition and char characteristics due to the singularity of the polymer in feedstock. This is highly beneficial for the treatment of PET with physical irregularities. Carbonization of PET at 400-480°C produced char with high carbon content. FT/IR analyzation revealed that char did not retain any of the structural properties of PET, which has never been reported by any forms of scientific article so far. These properties were used to determine the progression of carbonization reaction, in which complete carbonization of PET was described to produce char with high fixed-carbon content ($\%fC$ > 70%) and no remaining PET structure. Wax was mainly consisted of benzoic acid whereas gaseous product was mainly consisted of carbon dioxide and carbon monoxide. Presence of water in the reaction led to the progression of hydrolysis reaction of PET, which produced char with low carbon content.

Second, the mechanism of char formation during PET carbonization was studied in order to better understand the carbonization reaction. The van Krevelen diagram was applied to identify the reaction pathways of phase changes during PET carbonization and results revealed that PET underwent decarbonylation to produce char with high carbon content; and decarboxylation to form wax with high oxygen and hydrogen content. The analysis of cross-linking behavior confirmed that the release of CO due

to decarbonylation to form char while the release of CO_2 due to decarboxylation to form aromatic compounds in wax. The findings highly contributed to mending the research gaps and provided clarification to the mechanism of formation of char.

Next, the effects of carbonization of non-recyclable PET in the state closest to the "real-world" feedstock on the product composition was studied. One of the "real-world" feedstocks, which is the presence of water in PET was studied in the preliminary stage and results concluded that water is not desirable in the carbonization reaction due to the hydrolysis of PET. Other "real-world" feedstocks, that is, UV degraded PET, colored PET and multilayer PET were chosen as the study target in this research due to the inapplicability of current recycling technologies to treat these materials. For UV degraded PET, samples were prepared based on the accelerated weathering test and its physical properties were analyzed to observe the progression of UV degradation. Carbonization results showed slight increase in fixed-carbon yield when PET was exposed to UV degradation. This indicates the benefits and applicability of carbonization on non-recyclable UV degraded PET. For colored PET, sample was prepared from one type of commercial colored PET bottles which was dyed to green color. Carbonization of the colored PET showed a decrease in fixed-carbon yield compared with clear PET due to the presence of colorant additives which hindered the formation of char. For multilayer PET, samples were prepared from commercial PET bottles and the oxygen barrier layer was identified as MXD6 nylon. Carbonization of the multilayer PET showed no apparent change in char yield and fixed-carbon yield. However, increasing the amount of oxygen barrier layer resulted in a significant decrease in wax yield and increase in gas yield. It was speculated that cobalt salt, as identified by XRD analysis, is the main factor for the decrease of wax yield and increase of gas yield. Additional experiment was conducted to clarify this speculation, in which 1 wt% cobalt oxide was added to the carbonization of PET. The findings revealed that the presence of cobalt oxide indeed decreased the wax yield and increased the gas yield. It was speculated that the decomposition of wax into gaseous product occurred in the presence of cobalt oxide. This indicates the possibility of applying cobalt oxide as a catalyst for the decomposition of wax in the industrial scale of PET carbonization to prevent the clogging of pipes due to wax.

The gas adsorption ability of activated char was studied in order to evaluate the capacity of CO_2 adsorption. Char was activated using physical activation method. The CO_2 adsorption isotherm showed satisfactory CO_2 uptake. Findings also revealed the possible deformation or swelling of the activated char, due to the flexible nature of the PET polymer. The swelling of activated char may be one of the factors as to why temperature change had little to no effects on the adsorption of CO_2. The CO_2 breakthrough curve of multiple gaseous compounds revealed that activated char exhibited excellent CO_2 holding ability and capability to separate CO_2 from a stream of different gaseous component. An additional study was conducted to model the CO_2 breakthrough curve using a classic LDF-model. Results showed that the LDF-model was able to give good approximation with the experimental data.

Finally, in order to determine the feasibility of PET carbonization in the realization of domestic circulation of waste PET in Japan, energy consumption and CO_2 emission were assessed. Results concluded that replacement of incineration with carbonization resulted in drastic cut in annual CO_2 emission.

Overall, the main significance and contributions of this thesis include:

1) **Disclosing the importance of the reconsideration of the limitations and restrictions of current technologies.** In this study, the limitations and disadvantages of current conventional methods for treatment of waste PET were reconsidered. Some may argue that the current technologies for material recycling and/or chemical recycling of waste PET bottle and waste PET material are sufficient and adequate to meet the conditions necessary for the proper management of waste PET. However, preliminary review stated otherwise due to the incapability of domestic waste PET treatment. Furthermore, globalization had catalyzed the export of waste PET to developing countries, which had resulted in the accumulation of waste PET in terrestrial and marine environment. This research had stated the importance of reviewing the limitations of current technologies, and the necessity of continuous improvement of technologies.

2) **Demonstrating the importance of revisiting past research.** In this study, carbonization of PET was focused as the research topic. The thermal degradation of PET had been studied and widely reported in the past 20 years. Pyrolysis or thermal degradation of PET advanced to different technologies such as catalytic pyrolysis and co-pyrolysis of polymers. Carbonization or thermal degradation of PET was considered as a sophisticated technique for the past few years. However, revisiting of PET carbonization and intensifying the findings resulted in the clarification of characteristics of char. The research comes to a breakthrough in successfully clarifying the mechanism of char formation based on the phase change and relationship between characteristics of product. The findings have potentially led to mending of research gaps, in addition to the contribution of the better understanding of char formation of polymer during carbonization.

3) **Exhibiting the importance of using feedstock in the state closest to the "real-world".** Three different samples were chosen as the main feedstock in the state closest to the "real-world". The carbonization of samples with different properties such as physical degradation and additives showed results that did not match with the initial intuition – that is, the consistent product composition and char characteristics were speculated due to the singularity of polymer. Interestingly, the study has brought positive outcomes such as increase in fixed-carbon yield with respect to increased UV exposure, indicating the applicability of carbonization; and decrease of wax yield and increase of gas yield due to the presence of cobalt salt in the feedstock, which is beneficial in the design and scaling up of current method.

9.2 Recommendations for future work

1) **Studying the effects of various non-recyclable PET on carbonized product.** In the study of effects of contaminants in non-recyclable PET on carbonized product (Chapter 6), UV degraded PET, colored PET and multilayer PET were chosen as the non-recyclable PET, in which all of the samples were obtained from commercial PET bottle. It is of interest to study other non-recyclable PET such as carpeted material, clothing and fabric made of recycled PET, cushion material made from recycled PET, etc. It is highly speculated that the results will be consistent with current findings due to the singularity of material. However, the assumption should be verified in future studies.

2) **Effect of dispersion of cobalt oxide during PET carbonization.** In the study of effects of cobalt oxide on carbonization of feedstock (Chapter 6), granular cobalt oxide was added into the initial feedstock for the carbonization operation. Results showed that the decrease in wax and increase in gaseous product were not as evident as the results in carbonization of PET with 8 wt% oxygen barrier layer. One of the assumptions was due to the lack of dispersion of the granular cobalt oxide in the initial feedstock compared to oxygen barrier layer. Therefore, it is of great interest to study the effects of PET carbonization on the carbonized product when cobalt oxide is dispersed in the initial feedstock.

3) **Clarifying the relationship between heat of adsorption and degree of swelling of activated char.** In the gas adsorption study of activated char (Chapter 7), it was observed that temperature change had little to almost no effect on the CO_2 adsorption properties on activated char. The isosteric heat of adsorption of activated char was analyzed and results showed that the standard enthalpy of activated char was noticeably small compared to the commercial adsorbents. Assumptions were made in which the swelling or deformation of activated char had contributed to the difference in change in standard enthalpy. The change in pore size of activated char during gas adsorption should be determined and the relationships between the heat of adsorption and degree of swelling of activated char should be verified in future studies.

4) **Optimization of the PSA adsorption process.** In the study of assessment of CO_2 emission and cost estimation from carbon capture (Chapter 8), the assessment of PSA adsorption process was conducted based on assumptions and limited experimental data. The improvement of the PSA adsorption process needs to be considered, including the process optimization through coupling of two-stage PSA/VSA and consideration of multiple combinations of different adsorption/desorption cycles in order to further improve the estimation of CO_2 emission and cost reduction.

References

Aaron and Tsouris, 2005: Aaron, D., Tsouris, C. 2005. Separation of CO_2 from flue gas: A review. *Separation Science and Technology*. **40**. 321–348.

Al-Azzawi, 2015: Al-Azzawi, F. 2015. Degradation Studies on Recycled Polyethylene Terephthalate. London Metropolitan University.

Al-Salem and Lettieri, 2010: Al-Salem, SM., Lettieri, P. 2010. Kinetic Study of High Density Polyethylene (HDPE) Pyrolysis. *Chemical Engineering Research and Design.* **88**(12). 1599–1606.

Al-Salem et al., 2009: Al-Salem, SM., Lettieri, P., Baeyens, J. 2009. Recycling and Recovery Routes of Plastic Solid Waste (PSW): A Review. *Waste Management.* **29**(10). 2625–2643.

Al-Salem et al., 2017: Al-Salem, SM., Antelava, A., Constantinou, A., Manos, G., Dutta A. 2017. A Review on Thermal and Catalytic Pyrolysis of Plastic Solid Waste (PSW). *Journal of Environmental Management.* **197**(1408). 177–98.

Alkhatib et al., 2011: Alkhatib, MF., Muyibi, SA., Amode, JO. 2011. Optimization of Activated Carbon Production from Empty Fruit Bunch Fibers in One-Step Steam Pyrolysis for Cadmium Removal from Aqueous Solution. *Environmentalist.* **31**(4). 349–357.

Alongi et al., 2013: Alongi, J., Camino, G., Malucelli, G., 2013. Heating rate effect on char yield from cotton, poly(ethylene terephthalate) and blend fabrics. *Carbohydrate Polymers*. **92**. 1327-1334.

Ambrogi et al., 2017: Ambrogi, V., Carfagna, C., Cerruti, P., Marturano, V. 2017. Additives in Polymers. In book: Modification of Polymer Properties, Chapter: 4. Publisher: William Andrew Publishing. 87-108.

American Chemistry Council, Inc., 2020: American Chemistry Council, Inc. 2020. America's Plastics Makers. https://www.plasticsmakeitpossible.com/whats-new-cool/recycled-t-shirt-vending-machine-at-new-york-fashion-week/

Antal and Gronli, 2003: Antal, M.J., Grønli, M. 2003. The art, science, and technology of charcoal production. *Industrial and Engineering Chemistry Research*. **42**(8). 1619-1640.

Antal et al., 2000: Antal, MJ., Allen, SG., Dai, X., Shimizu, B., Tam, MS., Grønli, M. 2000. Attainment of the theoretical yield of carbon from biomass. *Industrial & Engineering Chemistry Research*. **39**. 4024–4031.

Anuar Sharuddin et al., 2016: Anuar Sharuddin, SD., Abnisa, F., Wan Daud, WMA., Aroua, MK. 2016. A review on pyrolysis of plastic wastes. *Energy Conversation Management*. **115**. 308–26.

Anuar Sharuddin et al., 2017: Anuar Sharuddin, SD., Abnisa, F., Wan Daud, WMA., Aroua, MK. 2017. Energy Recovery from Pyrolysis of Plastic Waste: Study on Non-Recycled Plastics (NRP) Data as the Real Measure of Plastic Waste. *Energy Conversion and Management.* **148**. 925–934.

ARC, 2020: ARC. 2020. リサイクル が進む PET 樹脂は循環経済を実現するか. 株式会社　旭リサーチセンター. ARC リポート（RS-1043）1-56.

Aresta and Dibenedetto, 2010: Aresta, M., Dibenedetto, A. 2010. Industrial utilization of carbon dioxide (CO_2). In: Maroto-Valer, M.M. (Ed.), Developments and Innovation in Carbon Dioxide (CO_2) Capture and Storage Technology: Volume 2: Carbon Dioxide (CO_2) Storage and Utilisation, Vol. 2. Woodhead Publishing Limited, Great Abington.

ASG Plastic Recycling Machinery, 2013: PET Bottle Washing Line by ASG Plastic Recycling Machinery. URL: https://www.petbottlewashingline.com/500-kgh-pet-washing-line/

ASTM, 1970: American Society for Testing and Materials. 1970. ASTM D 271-46, Standard Methods of Laboratory Sampling and Analysis of Coal and Coke, ASTM D271 (Industrial Standardization) ASTM International, Philadelphia, PA.

ASTM, 2000: ASTM D-5033-90. 2000. Standard guide for development of ASTM standards relating to recycling and use of recycled plastics. American Society for Testing and Materials.

ASTM, 2005: ASTM D 4329-05. 2005. Standard Practice for Fluorescent UV exposure of Plastics. American Society for Testing and Materials.

Avery-Gomm et al., 2019: Avery-Gomm, S., Walker, T.R., Mallory, M.L., Provencher, J.F. 2019. There is nothing convenient about plastic pollution. Rejoinder to Stafford and Jones "Viewpoint – Ocean plastic pollution: A convenient but distracting truth?" *Marine Policy.* **106**. 103552.

Awaja and Dumitru, 2005: Awaja, F., Dumitru, P. 2005. Recycling of PET. *European Polymer Journal.* **41**(7). 1453–1477.

Aworn et al. (2008): Aworn, A., Thiravetyan, P., Nakbanpote, W. 2008. Preparation and characteristics of agricultural waste activated carbon by physical activation having micro- and mesopores. *Journal of Analytical and Applied Pyrolysis*. **82**. 279-285.

Bacon and Tang, 1964: Bacon, R., Tang, MM. 1964. Carbonization of cellulose fibers-II. Physical property study. *Carbon*. **2**. 221–225.

Bakir et al., 2012: Bakir, A., Rowland, SJ., Thompson, RC. 2012 Competitive sorption of persistent organic pollutants onto microplastics in the marine environment. *Marine Pollution Bulletin.* **64**. 2782–2789.

Bangham and Fakhoury, 1931: Bangham, M.R., Fakhoury, N. 1931. The translation motion of molecules in the adsorbed phase on solids. *Journal of Chemical Society.* 1324-1333.

Beeva et al., 2015: Beeva, DA., Borisov, VA., Mikitaev, AK., Ligidov, MK., Beev, AA., Barokova, EB. 2015. Controlling the Barrier Properties of Polyethylene Terephthalate. A review. *International Polymer Science and Technology.* **3**. 46-51.

Berge et al., 2011: Berge, ND., Ro, KS., Mao, J., Flora, JRV., Chappell, MA., Bae, S. 2011. Hydrothermal Carbonization of Municipal Waste Streams. *Environmental Science and Technology.* **45**(13). 5696–5703.

BKS Plastics Ltd., 2020: BKS Plastics Ltd. 2020. Heavy weight plastic forks. Retrieved on 28 April 2020. URL: http://www.bksplastics.co.uk/plastic-cutlery/plastic-forks/190mm-plus-range-fork-5-2g.

Blazsó et al., 2002: Blazsó, M., Czégény, Z., Coma, C. 2002. Pyrolysis and debromination of flame retarded polymers of electronic scrap studied by analytical pyrolysis. *Journal of Analytical and Applied Pyrolysis.* **64**. 249–261.

Borenstein, 2018: Borenstein, S. 2018. Science Says: Amount of straws, plastic pollution is huge, Article on 21 April 2018, Retrieved on 28 April 2020. URL: https://phys.org/news/2018-04-science-amount-straws-plastic-pollution.html.

Brems et al., 2011: Brems, A., Baeyens, J., Vandecasteele, C., Dewil, R., 2011. Polymeric Cracking of Waste Polyethylene Terephthalate to Chemicals and Energy. *Journal of the Air & Waste Management Association*. **61**. 721–731.

Brooks et al., 2018: Brooks, Amy L., Shunli Wang, and Jenna R. Jambeck. 2018. The Chinese Import Ban and Its Impact on Global Plastic Waste Trade. *Science Advances.* 4(6). 1–8.

Bruhn et al., 2016: Bruhn, T., Naims, H., Olfe-Kräutleinn, B. 2016. Separating the debate on CO_2 utilisation from carbon capture and storage. Environmental Science & Policy. **60**. 38–43.

Bui et al., 2018: Bui, M., Adjiman, C.S., Bardow, A., Anthony, E.J., Boston, A., Brown, S., Fennell, P.S., Fuss, S., Galindo, A., Hackett, L.A., Hallett, J.P., Herzog, H.J., Jackson, G., Kemper, J., Krevor, S., Maitland, G.C., Matuszewski, M., Metcalfe, I.S., Petit, C., Puxty, G., Reimer, J., Reiner, D.M., Rubin, E.S., Scott, S.A., Shah, N., Smit, B., Trusler, J.P.M., Webley, P., Wilcox, J., Dowell, N.M. 2018. Carbon Capture and Storage (CCS): The Way Forward. *Energy and Environmental Science.* **11**(5). 1062–1176.

Campo et al., 2010: Campo, M.C., Magalhães, F.D., Mendes, A. 2010. Comparative study between a CMS membrane and a CMS adsorbent: Part I-Morphology, adsorption equilibrium and kinetics. *Journal of Membrane Science.* **346**. 15–25.

Cavenati et al., 2006: Cavenati, S., Grande, C.A., Rodrigues, A.E. 2006. Separation of CH_4 / CO_2 / N_2 Mixtures by Layered Pressure Swing Adsorption for Upgrade of Natural Gas. *Chemical Engineering Science.* **61**(12). 3893–3906.

Cepeliogullar and Putun, 2013: Cepeliogullar, O., Putun, A.E. Utilization of two different types of plastic wastes from daily and industrial life. In: Ozdemir, C., Sahinkaya, S., Kalipci, E., Oden, MK. ICOEST Cappadocia 2013. Turkey: ICOEST Cappadocia; 2013. 1–13.

CGER/NIESS, 2018: Center for Global Environmental Research, National Institute for Environmental Studies. 2018. Monitoring Network for Ultraviolet Radiation. URL: http://db.cger.nies.go.jp/gem/en/uv/data.html.

Chaiwat et al., 2008: Chaiwat, W., Hasegawa, I., Kori, J., Mae, K. 2008. Examination of degree of cross-linking for cellulose precursors pretreated with acid/hot water at low temperature. *Industrial & Engineering Chemistry Research.* **47**. 5948–5956.

Chaiwat et al., 2009: Chaiwat, W., Hasegawa, I., Tani, T., Sunagawa, K., Mae, K. 2009. Analysis of Cross-Linking Behavior during Pyrolysis of Cellulose for Elucidating Reaction Pathway. *Energy Fuels*. **2**. 5765-5772.

Chanda and Roy, 2006: Chanda, M., Roy, S.K. 2006. Plastics technology handbook. CRC Press. 1–6. ISBN 978-0-8493-7039-7.

Chang et al., 2006: Chang, H., Yuan, X.G., Tian, H., Zeng, A.W. 2006. Experiment and prediction of breakthrough curves for packed bed adsorption of water vapor on cornmeal. *Chemical Engineering and Processing: Process Intensification*. **45**. 747–754.

Charles et al., 2009: Charles, J., Ramkumaar, G.R., Azhagiri, S., Gunasekaran, S. 2009. FTIR and Thermal Studies on Nylon-66 and 30% Glass Fibre Reinforced Nylon-66. *Journal of Chemistry*. **6**. 23–33.

Chen et al., 2020: Chen, S., Liu, Z., Jiang, S., Hou, H. 2020. Carbonization: A feasible route for reutilization of plastic wastes. *Science of the Total Environment.* **710**. 136-250.

Chern and Chien, 2002: Chern, J.M., Chien, Y.W. 2002. Adsorption of Nitrophenol onto Activated Carbon: Isotherms and Breakthrough Curves. *Water Research.* **36**(3). 647–655.

Chilton et al., 2010: Chilton, T., Burnley, S., Nesaratnam, S. 2010. A Life Cycle Assessment of the Closed-Loop Recycling and Thermal Recovery of Post-Consumer PET. *Resources, Conservation and Recycling.* **54**(12). 1241–1249.

Chirayil et al., 2019: Chirayil, C.J., Mishra, RK., Thomas, S. 2019. Materials Recovery, Direct Reuse and Incineration of PET Bottles. Elsevier Inc.

Chouikhi et al., 2020: Chouikhi, N., Brandani, F., Pullumbi, P., Perre, P., Puel, F. 2020. Biomethane Production by Adsorption Technology: New Cycle Development, Adsorbent Selection and Process Optimization. *Adsorption*.

Çit et al., 2007: Çit, I., Sinağ, A., Tekeş, AT., Acar, P., Misirlioğlu, Z., Canel, M. 2007. Effect of polymers on lignite pyrolysis. *Journal of Analytical and Applied Pyrolysis.* **80**. 195–202.

Çit et al., 2010: Çit, İ., Sınağ, A., Yumak, T., Uçar, S., Mısırlıoğlu, Z., Canel, M. 2010. Comparative pyrolysis of polyolefins (PP and LDPE) and PET. *Polymer Bulletin.* **64**(8). 817–834.

Coelho et al., 2011: Coelho, T.M., Castro, R., Gobbo, J.A. 2011. PET containers in Brazil: Opportunities and challenges of a logistics model for post-consumer waste recycling. *Resources, Conservation & Recycling*. **55**. 291–299.

Collette and Merrimack, 1991: Collette, W.N., Merrimack, N.H. 1991. Recyclable multilayer plastic preform and container blown thereform. United States Patent, US5077111A.

Cui et al., 2004: Cui, X., Bustic, R.M., Dipple, G. 2004. Selective transport of CO_2, CH_4 and N_2 in coals: insights from modeling of experimental gas adsorption data. *Fuel*. **83**. 293-303.

Dasgupta and Sathiyamoorthy, 2013: Dasgupta, K., Sathiyamoorthy, D. 2013. Disordered carbon – its preparation, structure and characterization. *Materials Science and Technology.* **19**. 995-1002.

Davis and Sims, 1983: Davis, A, Sims, D. 1983. Weathering of Polymers. Applied Science Publishers Ltd, England.

De Castro et al., 2018: De Castro, C.S., Viau, L.N., Andrade, J.T., Mendonça, T.A.P., Gonçalves, M. 2018. Mesoporous activated carbon from polyethyleneterephthalate (PET) waste: Pollutant adsorption in aqueous solution. *New Journal of Chemistry.* **42**(17). 14612–14619.

Delgado et al., 2015: Delgado, J.A., Agueda, V.I., Uguina, M.A., Sotelo, J.L., Brea, P. 2015. Hydrogen Recovery from Off-Gases with Nitrogen-Rich Impurity by Pressure Swing Adsorption Using CaX and 5A Zeolites. *Adsorption.* **21**(1–2). 107–123.

Diaz-Silvarrey et al., 2018: Diaz-Silvarrey, L.S., McMahon, A., Phan, A.N. 2018. Benzoic Acid Recovery via Waste Poly(Ethylene Terephthalate) (PET) Catalytic Pyrolysis Using Sulphated Zirconia Catalyst. *Journal of Analytical and Applied Pyrolysis* **134**. 621–631.

Didzinska, 2017: Didzinska, A. 2017. Adsorption Properties of Hard Coals with Regards to Gases Present in the Mine Atmosphere. *Journal of Earth Science*. **28**(1). 124-130.

Dimitrov et al., 2013: Dimitrov, N., Kratofil Krehula, L., Ptiček Siročić, A., Hrnjak-Murgić, Z. 2013. Analysis of recycled PET bottles products by pyrolysis-gas chromatography. *Polymer Degradation and Stability.* **98**(5). 972–979.

Ding and Alpay, 2000: Ding, Y., Alpay, E. 2000. Equilibria and kinetics of CO_2 adsorption on hydrotalcite adsorbent. *Chemical Engineering Science.* **55**. 3461–3474.

Ding et al., 2020: Ding, K., Xiong, Q., Zhong, Z., Zhong, D., Zhang, Y. 2020. CFD Simulation of Combustible Solid Waste Pyrolysis in a Fluidized Bed Reactor. *Powder Technology.* **362**. 177–187.

Djahed et al., 2016: Djahed, B., Shahsavani, E., Khalili Naji, F., Mahvi, A.H. 2016. A novel and inexpensive method for producing activated carbon from waste polyethylene terephthalate bottles and using it to remove methylene blue dye from aqueous solution. *Desalination and Water Treatment.* **57**(21). 9871–9880.

DOL, 1993a: United States Department of Labor. 1993. 1910 Subpart Z - Occupational Safety and Health Standards. Accessed May 2019.

DOL, 1993b: United States Department of Labor. 1993. 1910.1028 App A - Substance safety data sheet, Benzene. Accessed May 2019.

EDGAR, 2017: Emission Database for Global Atmospheric Research. 2017. Accessed October 2020. URL: https://edgar.jrc.ec.europa.eu/

Ehlers et al., 1969: Ehlers, G.F.L., Fisch, K.R., Powell, W.R. 1969. Thermal degradation of polymers with phenylene units in the chain. III. Polyarylates. *Journal of Polymer Science Part A: Polymer Chemistry.* **7**. 2969–2981.

El Essawy et al., 2017: El Essawy, N.A., Ali, S.M., Farag, H.A., Konsowa, A.H., Elnouby, M., Hamad, H.A. 2017. Green synthesis of graphene from recycled PET bottle wastes for use in the adsorption of dyes in aqueous solution. *Ecotoxicology and Environmental Safety.* **145**. 57–68.

Encinar and González, 2008: Encinar, J.M., González, J.F. 2008. Pyrolysis of Synthetic Polymers and Plastic Wastes. Kinetic Study. *Fuel Processing Technology.* **89**(7). 678–686.

EPA, 2011: United States Environmental Protection Agency. 2011. Municipal Solid Waste Generation, Recycling, and Disposal in the United States Tables and Figures for 2010. Retrieved on 28 April 2020. URL: http://www.epa.gov/osw/nonhaz/municipal/pubs/2010_MSW_Tables_and_Figures_508.pdf

EPA, 2012: United States Environmental Protection Agency. 2012. Channel Processes: Suspended Sediment Transport. In Water: Science & Technology. Retrieved on 28 April 2020. URL: http://water.epa.gov/scitech/datait/tools/warsss/suspend.cfm

Eriksson and Finnveden, 2009: Eriksson, O., Finnveden, G. 2009. Plastic waste as a fuel – CO_2-neutral or not? *Energy & Environmental Science*. **2**. 907-914.

Fakhrhoseini and Dastanian, 2013: Fakhrhoseini, SM. Dastanian, M. 2013. Predicting Pyrolysis Products of PE, PP, and PET Using NRTL Activity Coefficient Model. *Journal of Chemistry*.

Fechine et al., 2004: Fechine, G.J.M., Rabello, M.S., Souto Maior, R.M., Catalani, L.H. 2004. Surface Characterization of Photodegraded Poly(Ethylene Terephthalate). The Effect of Ultraviolet Absorbers. *Polymer.* **45**(7). 2303–2308.

Fogler, 2010: Fogler, HS. 2010. Elements of Chemical Reaction Engineering, fourth ed. Pearson Education Inc., New Jersey.

FUJITEX Co., Ltd.: FUJITEX Co., Ltd. URL: www.fjtex.co.jp

Furfari, 2016: Furfari, A. 2016. Opportunities for the European Plastics Recyclers in the new EU Plastic Strategy. ISWA Circular Economy: the Role of Biowaste and Plastics, Brussels.

Furusawa, 2019: Furusawa, E. (2019, March 22). Personal interviews.

Geyer et al., 2016: Geyer, B., Lorenz, G., Kandelbauer, A. 2016. Recycling of Poly(Ethylene Terephthalate) – A Review Focusing on Chemical Methods. *Express Polymer Letters.* **10**(7). 559–586.

GCCSI, 2016: Global CCS Institute. 2016. Saga City Waste Incineration Plant, Global CCS Institute. Accessed July 2017. URL: www.globalccsinstitute.com/files/content/page/122975/ files/Saga%20City%20Waste%20Incineration%20Plant_0. pdf

GCCSI, 2017a: Global CCS Institute. 2017. Large-scale CCS projects, Global CCS Institute. accessed July 2017. URL: http://www.globalccsinstitute.com/projects/large-scale- ccs-projects,.

GCCSI, 2017b: Global CCS Institute. 2017. Projects Database: CO_2 utilization, Global CCS Institute. Accessed July 2017. URL: https://www.globalccsinstitute.com/projects/ co2-utilisation-projects

Giannotta et al., 1994: Giannotta, G., Po, G., Cardi, N. 1994. Processing effects on poly(ethylene terephthalate) from bottle scraps. *Polymer Engineering & Science.* **34**. 12-19.

Glueckauf and Coates, 1947: Glueckauf, E., Coates, J.E. 1947. Chemical Engineers' Handbook, Perry R.H. and Chilton, C.H. 7th Ed., New York, McGraw-Hill.

González et al., 2013: González, A.S., Plaza, M.G., Rubiera, F., Pevida, C. 2013. Sustainable biomass-based carbon adsorbents for post-combustion CO_2 capture. *Chemical Engineering Journal*. **230**. 456–465.

Grause et al., 2004: Grause, G., Kaminsky, W., Fahrbach, G. 2004. Hydrolysis of poly(ethylene terephthalate) in a fluidised bed reactor. *Polymer Degradation and Stability*. **85**(1). 571-575.

Grimaud and Rouge, 2014: Grimaud, A., Rouge, L. 2014. Carbon sequestration, economic policies and growth. *Resource and Energy Economics*. **36**. 307–331.

GVM, 2017: Gesellschaft für Verpackungsmarktforschung. 2017. Flexible Plastic Packaging Market in Germany and in Europe. Mainz, Germany.

Hahladakis et al., 2020: Hahladakis, J.N, Iacovidou, E., Gerassimidou, S. 2020. *Plastic waste in a circular economy. Plastic Waste and Recycling*. Academic Press. 481–512.

Hao and Iqbal, 1997: Hao, Z., Iqbal, A. 1997. Some aspects of organic pigments. *Chemical Society Reviews*. **26**, 203-213.

Harada et al., 1991: Harada, M., Hayashi, T., Mishima, H., Shimazaki, H. 1991. Polyamide resin composition and film therefrom. United States Patent, US5268219A.

Harlick and Tezel, 2004: Harlick, P.J.E., Tezel, F.H. 2004. An experimental adsorbent screening study for CO_2 removal from N_2. *Microporous and Mesoporous Materials.* **76**. 71-79.

Harpalani and Chen, 1997: Harpalani, S., Chen, G. 1997. Influence of gas production induced volumetric strain on permeability of coal. *Geotechnical and Geological Engineering.* **15**. 303-325.

Harpalani and Schraufnagel, 1990: Harpalani, S., Schraufnagel, R.A. 1990. Shrinkage of coal matrix with release of gas and its impact on permeability of coal. *Fuel.* **69**. 551–556.

Hartzog and Sircar, 1995: Hartzog, D.G., Sircar, S. 1995. Sensitivity of PSA process performance to input variables. *Adsorption.* **1**. 133–151.

Haykiri-Acma et al., 2005: Haykiri-Acma, H., Yaman, S., Kucukbayrak, S. 2005. Gasification of biomass chars in steam–nitrogen mixture. *Energy Conversion Management*. **47**(7-8). 1004-1013.

Heidari et al., 2019: Heidari, A., Khaki, E., Younesi, H., Lu, H.R. 2019. Evaluation of fast and slow pyrolysis methods for bio-oil and activated carbon production

from eucalyptus waste using a life cycle assessment approach. *Journal of Cleaner Production*. **241**. 118394.

Heidenreich, 2016: Heidenreich, S. 2016. Chapter 3 – Biomass Pretreatment, in: Heidenreich, S., Muller, M., Foscolo, PU., Advanced Biomass Gasification. Academic Press: Cambridge, 11-17.

Ho et al., 2008: Ho, M.T., Allinson, G.W., Wiley, D.E. 2008. Reducing the cost of CO_2 capture from flue gases using pressure swing adsorption. *Industrial & Engineering Chemistry*. **47**. 4883–4890.

Hoornweg et al., 2005: Hoornweg, D., Lam, P., Chaudhry, M. 2005. Waste management in China: Issues and recommendations. The World Bank Urban Development Working Papers. **9**. World Bank, Washington DC.

Huang et al., 2018: Huang, J.B., Zeng, G.S., Li, X.S., Cheng, X.C., Tong, H. 2018. Theoretical studies on bond dissociation enthalpies for model compounds of typical plastic polymers. *IOP Conference Series: Earth and Environmental Science*. **167**. 1-7.

Huang et al., 2020: Huang, Q., Chen, G., Wang, Y., Chen, S., Xu, L., Wang, R. 2020. Modelling the Global Impact of China's Ban on Plastic Waste Imports. *Resources, Conservation and Recycling.* **154**. 104607.

Hujuri et al., 2010: Hujuri, U., Ghoshal, A.K., Gumma, S. 2010. Temperature-dependent pyrolytic product evolution profile for low density polyethylene from gas chromatographic study. *Waste Management*. **30**. 814–820.

IDEA, 2020: LCI データベース IDEA version 2.3 (2019/12/27) 国立研究開発法人 産業技術総合研究所 安全科学研究部門 IDEA ラボ 一般社団法人サステナブル経営推進機構"

Ioakeimidis et al., 2016: Ioakeimidis, C., Fotopoulou, K.N., Karapanagioti, H.K., Geraga, M., Zeri, C., Papathanassiou, E., Galgani, F., Papatheodorou, G. 2016.

The degradation potential of PET bottles in the marine environment: An ATR-FTIR based approach. *Scientific Reports.* **6**. 1–8.

Ioannidou and Zabaniotou, 2007: Ioannidou, O., Zabaniotou, A. 2007. Agricultural Residues as Precursors for Activated Carbon Production-A Review. *Renewable and Sustainable Energy Reviews.* **11**(9). 1966–2005.

Islam et al., 2018: Islam, MS., Uddin, J., Alshehri, K. 2018. Plastic Waste and Carbon Footprint Generation Due to the Consumption of Bottled Waters in Saudi Arabia. *Research & Development in Material Science.* **5**. 3–5.

Ismail et al., 2015: Ismail, A.F., Khulbe, K., K., Matsuura, T. 2015. *Gas Separation Membranes: Polymeric and Inorganic*, Springer, ISBN 3319010956.

Jalilian, 2017: Jalilian, M. 2017. Impact of MXD6 on the structure and properties of mechanically recycled PET blends. Master Thesis, The University of Toledo.

Japan-China Environment Service Center, 2017: Japan-China Environment Service Center. 2017. Weekly China Environment Regulation and Business Report. **37**.

Japan LP Gas Association, 2019: Accessed on 31 October 2020. URL: https://www.j-lpgas.gr.jp/stat/index.html

Japan Wood Pellets Association. URL: https://w-pellet.org/pellet-2/1-7/

Jayaraman et al., 2002: Jayaraman, A., Chiao, A.S., Padin, J., Yang, R.T., Munson, C.L. 2002. Kinetic separation of methane/carbon dioxide by molecular sieve carbons. *Separation Science and Technology.* **37**. 2505–2528.

JCPRA, 2018: The Japan Containers and Packaging Recycling Association. 2018. Classification Standard of PET bottles. Revised on 2018. URL: https://www.jcpra.or.jp/tabid/100/index.php.

Kaiser et al., 2018: Kaiser, K., Schmid, M., Schlummer, M. 2018. Recycling of Polymer-Based Multilayer Packaging: A Review. *Recycling.* **3**(1). 1-26.

Kaminsky and Kim, 1999: Kaminsky, W., Kim, J.S. 1999. Pyrolysis of mixed plastics into aromatics. *Journal of Analytical and Applied Pyrolysis.* **51**. 127–134.

Kaminsky et al., 2004: Kaminsky, W., Predel, M., Sadiki, A. 2004. Feedstock recycling of polymers by pyrolysis in a fluidised bed. *Polymer Degradation and Stability*. **85**. 1045–1050.

Karbalaei et al., 2018: Karbalaei, S., Hanachi, P., Walker, T.R., Cole, M., 2018. Occurrence, sources, human health impacts and mitigation of microplastic pollution. *Environmental Science and Pollution Research.* **25**(36). 36046–63.

Kato, 1997: 加藤悟. 1997. 廃棄物処理・リサイクルシステムにおける環境政策の評価に関する研究. *UTokyo Repository*.

Kaur et al., 2019a: Kaur, B., Gupta, R.K., Bhunia, H. 2019. Chemically activated nanoporous carbon adsorbents from waste plastic for CO_2 capture: Breakthrough adsorption study. *Microporous Mesoporous Material.* **282**. 146–158.

Kaur et al., 2019b: Kaur, B., Singh, J., Gupta, R.K., Bhunia, H., 2019. Porous carbons derived from polyethylene terephthalate (PET) waste for CO_2 capture studies. *Journal of Environmental Management*. **242**. 68–80.

Kawaguchi et al., 1986: Kawaguchi T., Iura, J., Taneda, N., Hishikura, H., Kokubu, Y. 1986. Structural changes of monolithic silica gel during the gel-to-glass transition. *Journal of Non-Crystalline Solids.* **82**. 50-56.

Kim et al., 1995: Kim, W.G., Yang, J., Han, S., Cho, C., Lee, C.H., Lee, H. 1995. Experimental and theoretical study on H_2/CO_2 separation by a five-step one-column PSA process. *Korean Journal of Chemical Engineering*. **12**. 503–511.

Knox, 2019: Knox, A. 2019. How much coffee cup waste do you create, Article on 29 April 2019. Retrieved on 28 April 2020. URL: https://reusaboo.com/how-much-coffee-cup-waste-do-you-create.

Ko et al., 2014: Ko, K.H., Rawal, A., Sahajwalla, V. 2014. Analysis of Thermal Degradation Kinetics and Carbon Structure Changes of Co-Pyrolysis between Macadamia Nut Shell and PET Using Thermogravimetric Analysis and 13C Solid State Nuclear Magnetic Resonance. *Energy Conversion and Management.* **86**. 154–164.

Kodera and Kaiho, 2016: Kodera, Y., Kaiho, M., 2016. Model Calculation of Heat Balance of Wood Pyrolysis. *Journal of the Japan Institute of Energy.* **95**(10). 881–889.

Kojima, 2018: 小島道一. 2018. リサイクルと世界経済:貿易と環境保護は両立できるか. 中公新書. 53-61.

Komata et al., 2010: Komata H., Orihashi, K., Ishikawa, Y., Hitoe, K., Hattori, N. 2010. Life cycle impact assessment of wood pellets made in Hokkaido. *木質学会誌*, **56**(3). 139-148.

Kovarskaya et al., 1975: Kovarskaya, B.M., Blumelfield, A.B., Levantovskaya, I.I. 1975. Thermal stability of heterochain polymers. Moscow, Khimiya, 147-257.

Kumagai et al., 2013: Kumagai, S., Morohoshi, Y., Grause, G., Kameda, T., Yoshioka, T. 2013. A Novel Approach for Determining the Proportions of Pyrolysis and Hydrolysis in the Degradation of Poly(Ethylene Terephthalate) in ^{18}O-Labeled Steam. *Chemistry Letters.* **42**(3). 212–214.

Kumagai et al., 2014: Kumagai, S, Grause, G., Kameda, T., Yoshioka, T. 2014. Simultaneous Recovery of Benzene-Rich Oil and Metals by Steam Pyrolysis of Metal-Poly(Ethylene Terephthalate) Composite Waste. *Environmental Science and Technology.* **48**(6). 3430–3437.

Kumagai et al., 2015: Kumagai, S., Hasegawa, I., Grause, G., Kameda, T., Yoshioka, T. 2015. Thermal Decomposition of Individual and Mixed Plastics in the Presence of CaO or $Ca(OH)_2$. *Journal of Analytical and Applied Pyrolysis.* **113**. 584–590.

Kumar et al., 2010: Kumar, K.V., Monteiro de Castro, M.C., Martinez-Escandell, M., Molina-Sabio, M., Rodriguez-Reinoso, F. 2010. Adsorption on heterogeneous surfaces: site energy distribution functions from Fritz–Schlüender isotherms. *ChemPhysChem*. **11**. 2555 —2560.

Kumar et al., 2011: Kumar, S., Panda, A.K., Singh, R.K. 2011. A Review on Tertiary Recycling of High-Density Polyethylene to Fuel. *Resources, Conservation and Recycling,* **55**(11). 893–910.

Kumar et al., 2019: Kumar, K.V., Gadipelli, S., Wood, B., Ramisetty, K.A., Stewart, A.A., Howard, C.A., Brett, D.J.L., Rodriguez-Reinoso, F. 2019. Characterization of the adsorption site energies and heterogeneous surface of porous materials. *Journal of Materials Chemistry A*. **17**. 1-74.

Kuroda et al., 2018: Kuroda, S., Nagaishi, T., Kameyama, M., Koido, K., Seo, Y., Dowaki, K. 2018. Hydroxyl aluminium silicate clay for biohydrogen purification by pressure swing adsorption: Physical properties, adsorption isotherm, multicomponent breakthrough curve modelling, and cycle simulation. *International Journal of Hydrogen Energy.* **43**. 16573–16588.

Kyoei Industry co. ltd, 2015: 協栄産業株式会社（栃木県）. 2015. ボトル to ボトルで資源循環. *環境ビジネス.* **16**. 141-150.

Lam et al., 2019: Lam, S.S., Su, M.H., Nam, W.L., Thoo, D.S., Ng, C.M., Liew, R.K., Yek, P.N.Y., Ma, N.L., Vo, D.V.N. 2019. Microwave Pyrolysis with Steam Activation in Producing Activated Carbon for Removal of Herbicides in Agricultural Surface Water. *Industrial and Engineering Chemistry Research.* **58**(2). 695–703.

Lamberti et al., 2020: Lamberti, F.M., Román-Ramírez, L.A., Wood, J. 2020. Recycling of Bioplastics: Routes and Benefits. *Journal of Polymers and the Environment.*

Levchik, 2000: Levchik, S. 2000. Chapter 6 – Char Formation, in: Grand, A.F., Wilkie, CA., Fire Retardancy of Polymeric Materials. Marcel Dekker, Inc., New York, 172-207.

Li et al., 2011: Li, J.R., Ma, Y., McCarthy, M.C., Sculley, J., Yu, J., Jeong, H.K., Balbuena, P.B., Zhou, H.C. 2011. Carbon dioxide capture-related gas adsorption and separation in metal-organic frameworks. *Coordination Chemistry Reviews*. **255**. 1791–1823.

Li et al., 2016a: Li, Q., Song, R., Liu, X., Liu, G., Sun, Y., 2016. Monitoring of carbon dioxide geological utilization and storage in China: a review. In: Acid Gas Extraction for Disposal and Related Topics. Wiley-Scrivener, New York, 331–358.

Li et al., 2016b: Li, Q., Wei, Y.N., Chen, Z.A., 2016b. Water-CCUS nexus: Challenges and opportunities of China's coal chemical industry. *Clean Technologies & Environmental Policy.* **18**. 775–786.

Lisk, 1991: Lisk, D.J. 1991. Environmental effects of landfills. *Science of the Total Environment*. **100**. 415-468.

Liu et al., 2016: Liu, X.Q., He, X., Qiu, N.X., Yang, X., Tian, Z.Y., Li, M.J., Xue, Y. 2016. Molecular Simulation of CH_4, CO_2, H_2O and N_2 Molecules Adsorption on Heterogeneous Surface Models of Coal. *Applied Surface Science.* **389**. 894–905.

Liu et al., 2020: Liu, B., Yu, X., Shi, W., Shen, Y., Zhang, D., Tang, Z. 2020. Two-Stage VSA/PSA for Capturing Carbon Dioxide (CO_2) and Producing Hydrogen (H_2) from Steam-Methane Reforming Gas. *International Journal of Hydrogen Energy.* **45**(46). 24870–24882.

Lopes et al., 2009: Lopes, F.V.S., Grande, C.A., Ribeiro, A.M., Loureiro, J.M., Evaggelos, O., Nikolakis, V., Rodrigues, A.E. 2009. Adsorption of H_2, CO_2, CH_4, CO, N_2 and H_2O in Activated Carbon and Zeolite for Hydrogen Production. *Separation Science and Technology.* **44**(5). 1045–1073.

López et al., 2011: López, A., Marco, I., Caballero, B.M., Laresgoiti, M.F., Adrados, A. 2011. Influence of Time and Temperature on Pyrolysis of Plastic Wastes in a Semi-Batch Reactor. *Chemical Engineering Journal.* **173**(1). 62–71.

Lu et al., 2013: Lu, J., Behtash, S., Faheem, M., Heyden, A., 2013. Microkinetic modeling of the decarboxylation and decarbonylation of propanoic acid over Pd(1 1 1) model surfaces based on parameters obtained from first principles. Journal of Catalysis. **305**. 56–66.

Ludlow-Palafox and Chase, 2001: Ludlow-Palafox, C., Chase, H.A., 2001. Microwave-induced pyrolysis of plastic waste. *Industrial & Engineering Chemistry Research*. **40**. 4749-4756.

Mainichishinbun, 2019: Mainichishinbun. Request for Incineration of Plastic waste including industrial waste. **14**. 16 May 2019.

Malpass, 2010: Malpass, D. 2010. Introduction to Industrial Polyethylene: Properties, Catalysts, and Processes. John Wiley and Sons. 1-9.

Marcilla et al., 2009: Marcilla, A. Beltrán, M.I., Navarro, R. 2009. Thermal and catalytic pyrolysis of polyethylene over HZSM5 and HUSY zeolites in a batch reactor under dynamic conditions. *Applied Catalysis B: Environmental*. **86**(1–2). 78-86.

Marongiu et al., 2003: Marongiu, A., Faravelli, T., Bozzano, G., Dente, M., Ranzi, E. 2003. Thermal degradation of poly(vinyl chloride). *Journal of Analytical and Applied Pyrolysis.* **70**. 519–553.

Mascia, 1974: Mascia. 1974. The Role of Additives in Plastics, Edward Arnold Publishers Ltd, London.

Matteucci et al., 2006: Matteucci, S., Yampolskii, Y., Freeman, B.D., Pinnau, I. 2006. Transport of gases and vapors in glassy and rubbery polymers. In: Yampolskii, Y., Freeman, B.D., Pinnau, I., *Materials Science of Membranes for Gas and Vapor Separation*, 1-47, John Wiley & Sons, ISBN 0470029048.

McBeath et al., 2011: McBeath, A.V., Smernik, R.J., Schneider, M.P.W., Schmidt, M.W.I., Plant, E.L. 2011. Determination of the aromaticity and the degree of aromatic condensation of a thermosequence of wood charcoal using NMR. *Organic Geochemistry*. **42**. 1194–1202.

Mehl et al., 2004: Mehl, M., Marongiu, A., Faravelli, T., Bozzano, G., Dente, M., Ranzi, E. 2004. A kinetic modeling study of the thermal degradation of halogenated polymers. *Journal of Analytical and Applied Pyrolysis.* **72**. 253–272.

Mendes et al., 2017: Mendes, P.A.P., Ribeiro, A.M., Gleichmann, K., Ferreira, A.F.P., Rofrigues, A.E. 2017. Separation of CO_2/N_2 on binderless 5A zeolite, *Journal of CO_2 Utilization.* **20**, 224–233.

Mendoza-Carrasco et al., 2016: Mendoza-Carrasco, R., Cuerda-Correa, E.M., Alexandre-Franco, M.F., Fernandez-Gonzalez, C., Gomez-Serrano, V. 2016. Preparation of high-quality activated carbon from polyethyleneterephthalate (PET) bottle waste. Its use in the removal of pollutants in aqueous solution. *Journal of Environmental Management*. **181**. 522-535.

Messin et al., 2017: Messin, T., Follain, N., Guinault, A., Miquelard-Garnier, G., Sollogoub, C., Delpouve, N., Gaucher, V., Marais, S. 2017. Confinement effect in PC/MXD6 multilayer films: Impact of the microlayered structure on water and gas barrier properties. *Journal of Membrane Science.* **525**. 135-145.

METI, 2016: 経済産業省　資源エネルギー庁. 2016. 特定排出者の事業活動に従う温室効果ガスの排出量の算定に関する省令. Accessed on 31 October 2020. URL: https://www.env.go.jp/council/16pol-ear/y164-04/mat04.pdf

METI, 2018: 経済産業省　資源エネルギー庁. 2020.電気料金について. Accessed on 31 October 2020. URL: https://www.enecho.meti.go.jp/category/electricity_and_gas/electric/fee/

METI, 2020: 経済産業省　資源エネルギー庁. 2020. 石油製品価格調査. Accessed on 31 October 2020. URL: https://www.enecho.meti.go.jp/statistics/petroleum_and_lpgas/pl007/results.html

Ministry of Ecology and Environment, 2018: Ministry of Ecology and Environment. Administrative Catalogue of Waste Importation. Revised on 2018, April 19.

Ministry of the Environment, Japan: Ministry of the Environment, Japan. URL: https://www.env.go.jp/earth/ondanka/ghgmrv/committee/h27/material/Waste_27.pdf

Mofarahi and Gholipour, 2014: Mofarahi, M., Gholipour F. 2014. Gas adsorption separation of CO_2/CH_4 system using zeolite 5A. *Microporous and Mesoporous Materials.* **200**. 1-10.

Mok and Antal, 1983: Mok, W.S.L, Antal, M.J. 1983. Effects of Pressure on Biomass Pyrolysis. I. Cellulose Pyrolysis Products. *Thermochimica Acta.* **68**(2–3). 155–164.

Molina-Sabio et al., 1996: Molina-Sabio, M., Gonzalez, M.T., Rodriguez-Reinoso, F., Sepúlveda-Escribano, A. 1996. Effect of steam and carbon dioxide activation in the micropore size distribution of activated carbon. *Carbon*. **34**. 505-509.

Morita and Hayashi, 2018: Morita, Y., Hayashi, S. 2018. Proposals to Strengthen Japan's Domestic Measures and Regional Cooperation on Stable and Environmentally Sound Plastic Scrap Recycling: Response to China's Ban on Imports of Plastic Scrap. *The Institute for Global Environmental Strategies*. **41**. 1-14.

Morris, 2017: Morris, B.A. 2017. The Science and Technology of Flexible Packaging, William Andrew Publication, Elsevier, Oxford, United Kingdom.

Moura et al., 2018: Moura, P.A.S., Vilarrasa-Garcia, E., Maia, D.A.S., Bastos-Neto, M., Ania, C.O., Parra, J.B., Azevedo, D.C.S. 2018. Assessing the Potential of Nanoporous Carbon Adsorbents from Polyethylene Terephthalate (PET) to Separate CO_2 from Flue Gas. *Adsorption.* **24**(3). 279–291.

Murata et al., 2004: Murata, K., Sato, K., Sakata, Y. 2004. Effect of Pressure on Thermal Degradation of Polyethylene. *Journal of Analytical and Applied Pyrolysis.* **71**(2). 569–589.

Nagaoka et al., 2010: Nagaoka, K., Yoshida, N., Kaneko, T. 2010. 消費電力量あたりゴミ処理量を指標とした清掃工場の性能水準変化に関する分析. *Japan Society of Material Cycles and Waste Management conference proceedings.*

Nakatani et al., 2010: Nakatani, J., Fujii, M., Moriguchi, Y. 2010. Life-cycle assessment of domestic and transboundary recycling of post-consumer PET bottles. *The International Journal of Life Cycle Assessment*. **15**. 590-597.

Nakatani and Hirao, 2011: Nakatani J., Hirao, M. 2011. Multicriteria Design of Plastic Recycling Based on Quality Information and Environmental Impacts. *Journal of Industrial Ecology*. **15**(2). 228-244.

Nakatani et al., 2013: Nakatani, J., Okuno, A., Minoru, F., Hirao, M. 2013. Life-Cycle Assessment of Material Recycling Based on Market Substitutability: A Case Study of PET Bottle Recycling. *Journal of Life Cycle Assessment, Japan.* **7**(1). 96–107.

Nakatani, 2014: Nakatani, J. 2014. Life Cycle Inventory Analysis of Recycling: Mathematical and Graphical Frameworks. *Sustainability*. **6**. 6158-6169.

NAPCOR, 2018: National Association for PET Container. 2018. Report on Postconsumer PET Container Recycling Activity in 2017. National Association for PET Container Resources and the Association of Plastic Recyclers, USA, Canada and Mexico.

Naustdalslid, 2014: Naustdalslid, J. 2014. Circular economy in China – The environmental dimension of the harmonious society. *International Journal of Sustainable Development & World Ecology*. **21**. 303-313.

Ocean Conservancy, 2019: Ocean Conservancy. 2019. International Coastal Cleanup 2019 Report. 28 September 2019. Retrieved 27 April 2020.

Oehlmann et al., 2009: Oehlmann, J., Schulte-Oehlmann, U., Kloas, W., Jagnytsch, O., Lutz, I., Kusk, K.O., Wollenberger, L., Santos, E.M., Paull, G.C., Van Look, K.J., Tyler, C.R. 2009. A critical analysis of the biological impacts of plasticizers on

wildlife. *Philosophical Transactions of the Royal Society B: Biological Sciences*. **364**. 2047–2062.

Onwudili et al., 2009: Onwudili, J.A., Insura, N., Williams, P.T. 2009. Composition of products from the pyrolysis of polyethylene and polystyrene in a closed batch reactor: effects of temperature and residence time. *Journal of Analytical and Applied Pyrolysis.* **86**. 293-303.

Ottiger et al., 2008: Ottiger, S., Pini, R., Storti, G., Mazzotti, M. 2008. Competitive adsorption equilibria of CO_2 and CH_4 on a dry coal. *Adsorption*. **14**. 539-556.

Oyarzún et al., 2020: Oyarzún, A.M., García-Carmona, X., Radovic, L.R. 2020. Kinetics of oxygen transfer reactions on the graphene surface. Part ii. H_2O vs. CO_2. *Carbon.* **164**. 85–99.

Pappas and Winslow, 1981: Pappas, S.P., Winslow, F.H. 1981. Photodegradation and Photostabilization of Caotings, American Chemical Society, *ACS Symposia Series*. **151**. USA.

Park et al., 2018: Park, Y., Moon, D.K., Park, D., Mofarahi, M., Lee, C.H. 2018. Adsorption Equilibria and Kinetics of CO_2, CO, and N_2 on Carbon Molecular Sieve. *Separation and Purification Technology.* **212**. 952–964.

Parker, 2018: Parker, L. 2018. China's ban on trash imports shifts waste crisis to Southeast Asia. National Geographical (Accessed 9 October 19). URL: https://www.nationalgeographic.com/environment/2018/11/china-ban-plastic-trash-imports-shifts-waste-crisis-southeast-asia-malaysia/

Patil et al., 2014: Patil, Sandip V., Laxmi Gayatri Sorokhaibam, Vinay M. Bhandari, D. J. Killedar, and Vivek V. Ranade. 2014. Investigating Role of Sulphur Specific Carbon Adsorbents in Deep Desulphurization. *Journal of Environmental Chemical Engineering.* **2**(3). 1495–1505.

Patterson and Utas, 2002: Patterson, A., Utas, J. 2002. Barrier Material. Russian Patent No. 218456, MPK B 32 B 27/06, B 32 B 33/00, A 61 M 25/01.

Pawlak et al., 2000: Pawlak, A., Pluta, M., Morawiec, J., Galeski, A., Pracella, M. 2000. Characterization of Scrap Poly(Ethylene Terephthalate). *European Polymer Journal.* **36**(9). 1875–1884.

Pearce et al., 1983: Pearce, E., Bulking, B., Yeen, M. 1983. Fourier Transform IR Spectroscopy for the Study of Polymer Degradation – Thermal and Thermooxidative Degradation of Polyethylene Terephthalate. *Polymer Characterization.* **33**. 571-593.

Pereira et al., 2017: Pereira, A.P., Silva, M.H., Junior, E.P., Paula, A.S., Tommasini, F.J. 2017. Processing and Characterization of PET Composites Reinforced With Geopolymer Concrete Waste. *Journal of Materials Research.* **20**. 411-420.

Perry et al., 1984: Perry, R.H., Green, D. W., Maloney, J.O. 1984. *Perry's Chemical engineers' handbook*. New York: McGraw-Hill.

Peters et al., 2011: Peters, M., Ko¨hler, B., Kuckshinrichs, W., Leitner, W., Markewitz, P., Mu¨ller, TE. *ChemSusChem*. **4**. 1216–1240.

Plasticseurope, 2019: Plasticseurope. 2019. Plastics—the Facts 2019. An analysis of European plastics production, demand and waste data. 2018.

Plaza et al., 2016: Plaza, M.G., Durán, I., Querejeta, N., Rubiera, F., Pevida, C. 2016. Experimental and Simulation Study of Adsorption in Postcombustion Conditions Using a Microporous Biochar. 1. CO_2 and N_2 Adsorption. *Industrial & Engineering Chemistry Research*. **55**. 3097–3112.

Porkodi and Kumar, 2007: Porkodi K., Kumar, K.V. 2007. Equilibrium, kinetics and mechanism modeling and simulation of basic and acid dyes sorption onto jute fiber carbon: Eosin yellow, malachite green and crystal violet single component systems. *Journal of Hazardous Materials*. **143**. 311-327.

Poursaeidesfahani et al., 2019: Poursaeidesfahani, A., Andres-Garcia, E., de Lange, M., Torres-Knoop, A., Rigutto, M., Nair, N., Kapteijn, F., Gascon, J., Dubbeldam, D., Vlugt, T.J.H. 2019. Prediction of adsorption isotherms from breakthrough curves. *Microporous and Mesoporous Materials*. **277**. 237–244.

Prata et al., 2019: Prata, J.C., Patrício Silva, A.L., da Costa, J.P., Mouneyrac, C., Walker, T.R., Duarte, A.C., Rocha-Santos, T. 2019. Solutions and integrated strategies for the control and mitigation of plastic and microplastic pollution. *International Journal of Environmental Research and Public Health.* **16**. 1–19.

Qi et al., 2016: Qi, J., Zhao, J., Li, W., Peng, X., Wu, B., Wang, H. 2016. The Circular Economy – Oriented Practice in the Petrochemical Industry. Development of Circular Economy in China, Springer, 169-182.

Querejeta et al., 2017: Querejeta, N., Plaza, M.G., Rubiera, F., Pevida, C., Avery, T., Tennisson, S.R. 2017. Carbon Monoliths in Adsorption-based Post-combustion CO_2 Capture. *Energy Procedia.* **114**. 2341–2352.

Radovic et al., 1997: Radovic, L.R., Menon, V.C., Leon, C.A., Kyotani, T., Danner, R.P., Anderson, S., Hatcher, P.G. 1997. On the porous structure of coals: evidence for an interconnected but constricted micropore system and implications for coalbed methane recovery. *Adsorption.* **3**. 221–232.

Rai and Singh, 2018: Rai, P., Singh, K.P. 2018. Valorization of Poly(ethylene) terephthalate (PET) wastes into magnetic carbon for adsorption of antibiotic from water: Characterization and application. *Journal of Environmental Management.* **207**. 249–261.

Ranby and Rabek, 1975: Ranby, B., Rabek, J.F. 1975. Photodegradation, Photo-oxidation and Photostabilisation of Polymers: Principles and Applications, John Wiley and Sons Ltd.

Rehan et al., 2017: Rehan, M., Miandad, R., Barakat, M.A., Ismail, I.M.I., Almeelbi, T., Gardy, J., Hassanpour, A., Khan, M.Z., Demirbas, A., Nizami, A.S. 2017. Effect of Zeolite Catalysts on Pyrolysis Liquid Oil. *International Biodeterioration and Biodegradation.* **119**. 162–175.

Rodden, 2010: Rodden, G. 2010. It's The Only One With Coffee, *PPI: Pulp & Paper International*. **52**(11). 19-21.

Rossi et al., 2009: Rossi, M.P., Gogotsi, Y., Kornev, K.G. 2009. Deformation of carbon nanotubes by exposure to water vapor. *Langmuir*. **25**. 2804–2810.

Rujnic-Sokele et al., 2008: Rujnic-Sokele, M., Sercer, M., Pilipovic, A. 2008. PET bottles recycling waste – Utilization and properties. *12th International Research/Expert Conference "Trends in the Development of Machinery and Associated Technology".* 605-608.

Ruthven, 1984: Ruthven, D.M. 1984. Principles of Adsorption and Adsorption Processes, John Wiley & Sons, New York.

Saha et al., 2008: Saha, B., Karthik Reddy, P., Ghoshal, A.K. Hybrid genetic algorithm to find the best model and the globally optimized overall kinetics parameters for thermal decomposition of plastics. *Chemical Engineering Journal.* **138**. 20–29.

Saha et al., 2010: Saha, D., Bao, Z. Jia, F., Deng, S. 2010. Adsorption of CO_2, CH_4, N_2O, and N_2 on MOF-5, MOF-177, and Zeolite 5A *Environmental Science and Technology.* **44**(5). 1820–26.

Saima et al., 2013: Saima H., Mogi, Y., Haraoka, T. 2013. Development of PSA Technology for the Separation of Carbon Dioxide from Blast Furnace Gas. *JFE Steel Giho*. **32**. 44-49.

Sakata et al., 1999: Sakata, Y., Uddin, M.A., Muto, A. 1999. Degradation of polyethylene and polypropylene into fuel oil by using solid acid and non-acid catalysts. *Journal of Analytical and Applied Pyrolysis*. **51**(1–2). 135-155.

Salam et al., 2013: Salam, M. A., Sufian, S., Lwin, Y., Murugesan, T. 2013. Hydrogen storage of a Fixed Bed of Nanocrystalline Mixed Oxide. *ISRN Nanomaterials.* **2013**. 1-10.

SANIX Inc.: URL: https://sanix.jp/biz/evr_resource/recycle_1.php#situation

Santillan-Jimenez and Crocker, 2012: Santillan-Jimenez, E., Crocker, M. 2012. Catalytic deoxygenation of fatty acids and their derivatives to hydrocarbon fuels

via decarboxylation/decarbonylation. *Journal of Chemical Technology & Biotechnology*. **87**. 1041–1050.

Sarker et al., 2017: Sarker, A.I., Aroonwilas, A., Veawab, A. 2017. Equilibrium and Kinetic Behaviour of CO2Adsorption onto Zeolites, Carbon Molecular Sieve and Activated Carbons. *Energy Procedia*. **114**. 2450–2459.

Scatchard, 1949: Scatchard, G. 1949. The attractions of proteins for small molecules and ions. *Annals of the New York Academy of Sciences.* **51**. 660-672.

Scheirs and Duane, 2003: Scheirs, J., Duane, P., 2003. Modern Styrenic Polymers: Polystyrenes and Styrenic Copolymers. John Wiley & Sons. 3. ISBN 978-0-471-49752-3.

Schimmelpfennig and Glaser, 2001: Schimmelpfennig, S., Glaser, B. 2011. One Step Forward toward Characterization: Some Important Material Properties to Distinguish Biochars. *Journal of Environmental Quality*. **41**.

Schloss, 2017: Schloss, F. 2017. Amber PET bottles: recycling challenges and opportunities. *Packaging Sustainability, Recycling, Materials.* Published: October 04, 2017. URL: https://www.plasticstoday.com/packaging/amber-pet-bottles-recycling-challenges-and-opportunities/183258147357587.

Schnitzer and Hoffman, 1965: Schnitzer, M., Hoffman, I., 1965. Thermogravimetry of soil humic compounds. Geochimica et Cosmochimica Acta. **29**. 859–870.

Scott et al., 1990: Scott, D.S., Czernik, S.R., Piskorz, J., Radlein, D.A.G. 1990. Fast Pyrolysis of Plastic Wastes. *Energy and Fuels.* **4**(4). 407–411.

Seader and Henley, 1999: Seader, D., Henley, E.J. 1999. Separation process principles. *Choice Review Online.* **36**. 581-587.

Shen et al., 2012: Shen, C., Liu, Z., Li P., Yu, J. 2012. Two-Stage VPS/A Process for CO_2 Capture from Flue Gas Using Activated Carbon Beads. *Industrial & Engineering Chemistry.* **51**. 5011–5021.

Shifman, 2012: Shifman, Y. 2012. A multilayer flat or sleeve shell or film for foodstuff. Russian Patent No. 2446692, MPK A 22 C 13/00.

Shigaki et al., 2018: Shigaki, N., Mogi, Y., Haraoka, T., Sumi, I. 2018. Reduction of Electric Power Consumption in CO_2-PSA with Zeolite 13X Adsorbent. *Energies* **11**(4). 1–21.

Shioya et al., 2005: Shioya, M., Kawanishi, T., Shiratori, N., Wakao, H., Sugiyama, E., Ibe, H. 2005. Development of waste plastics liquefaction technology, feedstock recycling in Japan. In: Muller-Hagedorn M, Bockhorn H, editors. Feedstock recycling of plastics, Germany. 19–42.

Shoji et al., 2015: Shoji, T., Sakuragi, K., Taki, M., Otaka, M., 2015. Evaluation of effects of operating conditions to properties of carbonized fuel by using 4t/d carbonization facility. *CRIEPI Energy Engineering Research Laboratory*. **14012**, 1-17.

Singh and Kumar, 2015: Singh, V.K., Kumar, E.A. 2015. Comparative Studies on CO_2 Adsorption Kinetics by Solid Adsorbents. *Energy Procedia*. **90**. 316–325.

Singh et al., 2017: Singh, N., Hui, D., Singh, R., Ahuja, I.P.S., Feo, L., Fraternali, F. 2017. Recycling of plastic solid waste: A state of art review and future applications. *Composites Part B: Engineering*. **115**. 409–422.

Sipe, 2016: Sipe, M. 2016. Understanding the science of color. *Plastic Technology.* Published in 26 August 2016. URL: https://www.ptonline.com/articles/understanding-the-science-of-color

Sircar and Hufton, 2000: Sircar, S., Hufton, J.R. 2000. Why does the linear driving force model for adsorption kinetics work? *Adsorption.* **6**. 137–147.

Sircar and Kumar, 1986: Sircar, S., Kumar, R., 1986. Column Dynamics for Adsorption of Bulk Binary Gas Mixtures on Activated Carbon. Separation Science and Technology. **21**. 919–939.

Skreiberg et al., 2018: Skreiberg, Ø., Wang, L., Bach, Q.V., Grønli, M. 2018. Carbonization Pressure Influence on Fixed Carbon Yield. *Chemical Engineering Transactions.* **65**. 7–12.

Slaughter et al., 2011: Slaughter, E., Gersberg, R.M., Watanabe, K., Rudolph, J., Stransky, C., Novotny, T.E. 2011. Toxicity of Cigarette Butts, and Their Chemical Components, to Marine and Freshwater Fish. *Tobacco Control.* **20**. 25–29.

Snyder, 1992: Snyder, L.R. 1992. Theory of chromatography. *Journal of Chromatography Library*. **51**. A1–A68.

Sogancioglu et al., 2017: Sogancioglu, M., Ahmetli, G., Yel, E. 2017. A Comparative Study on Waste Plastics Pyrolysis Liquid Products Quantity and Energy Recovery Potential. *Energy Procedia.* **118**. 221–226.

Stankevičius et al., 2013: Stankevičius, V., Paukštys, V., Bliudžius, R., Šadauskiene, J., Turskis, Z., Samajauskas, R. 2013. Convection in Mineral Wool Used as Insulation for Buildings. *Journal of Civil Engineering and Management.* **19**(2). 296–304.

Takahasi et al., 2013: 高橋 史武, 鈴木 慎也, 上田 康平, 吉田 飛雄士, 菅田 尚之, 松藤 康司, 回収ペットボトルの 16 分別詳細調査－心理的トリガーとしてのキャップ外しの重要性. *廃棄物資源循環学会研究発表会講演集*. 2013. **24** 巻. 第 24 回廃棄物資源循環学会研究発表会. 公開日: 2014/01/21.

Tang and Bacon, 1964: Tang, M.M., Bacon, R. 1964. Carbonization of cellulose fibers-I. Low temperature pyrolysis. *Carbon*. **2**. 211–220.

Terazono and Oguchi, 2019: 寺園 淳, 小口 正弘. 2019. 廃プラスチックと雑品スクラップの国内資源循環に向けた課題. *環境経済・政策研究*. **12** 巻 2 号. 84-88.

Terazono et al., 2011: 寺園 淳, 林 廣和, 吉田 綾, 中谷 隼, 森口 祐一.2011 使用済み PET ボトルの国内外マテリアルフローと中国におけるプラスチックリサイクル, 廃棄物資源循環学会誌. **22** 巻 2 号. 125-139.

Tasaki et al., 2006: 田崎 智宏, 橋本 征二, 森口 祐一, 小林 健一, 入佐 孝一. 2006. 廃棄物処理施設のライフサイクルコストの調査・研究. *第 17 回廃棄物学会研究発表会*. A3-4.

The Containers and Packaging Recycling Law, 2019: Based on interviews with The Containers and Packaging Recycling Law (16 May 2019).

The Council for PET Bottle Recycling, 2005: PET ボトルリサイクル推進協議会. 2005. PET ボトルの分別収集コストに関する調査中間報告書の概要 PET ボトルリサイクル推進協議会. Accessed on 31 October 2020. URL: https://www.maff.go.jp/j/study/other/recycle/pdf/5_3.pdf

The Council for PET bottle recycling, 2019: The Council for PET bottle recycling. 2019. PET bottle recollection rate. Accessed on 27 May 2019. URL: http://www.petbottle-rec.gr.jp/data/transition.

The Edge Malaysia, 2019: The Edge Malaysia. Malaysia – the world's top dump site for plastic waste. Accessed on 21 May 2019. URL: https://www.theedgemarkets.com/article/malaysia-worlds-top-dump-site-plastic-waste.

The ImpEE Project, 2006: The ImpEE Project. 2006. Energy balance in recycling one PET bottle. *The Cambridge-MIT Institute*. 1-4. URL: http://www-g.eng.cam.ac.uk/impee/topics/RecyclePlastics/files/RecyclingEnergyBalance.pdf.

Thingpen and Trebellas, 1969: Thingpen, H.H., Trebellas, J.C. 1969. Method for preparing unsymmetrical ketones by cobalt catalyzed decarboxylation of acids. United States Patent, US3660491A.

Thomas, 1961: Thomas, J.M. 1961. The Existence of Endothermic Adsorption. *Journal of Chemical Education*. **38**. 138-139.

Thommes et al., 2015: Thommes, M., Kaneko, K., Neinmark, A.V., Olivier, J.P., Rodriguez-Reinoso, F., Rouquerol, J., Sing, K.S.W. 2015. Physisorption of gases, with special reference to the evaluation of surface area and pore size distribution (IUPAC Technical Report). *Pure Applied Chemistry*. **87**. 1051-1069.

Thompson et al., 2004: Thompson, R.C., Olson, Y., Mitchell, R.P., Davis, A., Rowland, S.J., John, A.W.G., McGonigle, D., Russell, A.E. 2004. Lost at Sea: Where Is All the Plastic? *Science.* **304**(5672). 838.

Tripathi, 2001: Tripathi, D. 2001. Practical guide to polypropylene. Shrewsbury: RAPRA Technology. ISBN 978-1859572825.

Tsuchida et al., 2008: 土田大輔, 中山裕文, 島岡隆行, 2008. 安定型最終処分場の分類による削減された最終処分費用と環境修復費用の推定. *廃棄物学会論文誌*. **19**(2). 120-130.

UNFCCC, 2016: United Nations Framework Convention on Climate Change. 2016. Historic Paris Agreement on climate change: 195 nations set path to keep temperature rise well below 2°C. Retrieved on July 2017. URL: http://newsroom.unfccc.int/unfccc-newsroom/finale-cop21/

Vallejos-Burgos et al., 2016: Vallejos-Burgos, F., Díaz-Pérez, N., Silva-Villalobos, Á., Jiménez, R., García, X., Radovic, L.R. 2016. On the structural and reactivity differences between biomass- and coal-derived chars. *Carbon.* **109**. 253–263.

van Krevelen, 1950: van Krevelen, D.W. 1950. Graphical-statistical method for the study of structure and reaction processes of coal. *Fuel*. **29**. 269-284.

van Krevelen, 1975: van Krevelen, D.W. 1975. Some basic aspects of flame resistance of polymeric materials. *Polymer*. **16**. 615-620.

van Krevelen, 1984: van Krevelen, D.W. 1984. Organic geochemistry-old and new. *Organic Geochemistry.* **6**. 1–10.

Velis, 2014: Velis, CA. 2014. Global recycling markets – plastic waste: A story for one player – China. ISWA Global Waste Management Task Force, September 2014.

Venkatachalam et al., 2012: Venkatachalam, S., Shilpa, G., Jayprakash, V., Prashant, R., Rao, K., Anil, K. 2012. Degradation and Recyclability of Poly(Ethylene Terephthalate). *Polyester*. InTech, Croatia.

Vivero et al., 2005: Vivero, L., Barriocanal, C., Álvarez, R., Díez, M.A. 2005. Effects of Plastic Wastes on Coal Pyrolysis Behaviour and the Structure of Semicokes. *Journal of Analytical and Applied Pyrolysis.* **74**(1–2). 327–336.

Vouvoudi and Dimitris, 2019: Vouvoudi, E.C., Dimitris, S.A. 2019. Pyrolytic Degradation of Common Polymers Present in Packaging Materials. *Journal of Thermal Analysis and Calorimetry.* **138**(4). 2683–2689.

Wagner et al., 2014: Wagner, M., Scherer, C., Alvarez-Muñoz, D., Brennholt, N., Bourrain, X., Buchinger, S., Fries, E., Grosbois, C., Klasmeier, J., Marti, T., Rodriguez-Mozaz, S., Urbatzka, R., Vethaak, AD., Winther-Nielsen, M., Reifferscheid, G. 2014. Microplastics in Freshwater Ecosystems: What We Know and What We Need to Know. *Environmental Sciences Europe.* **26**(1). 1–12.

Wan Ho, 2015: Wan Ho, M. Waste plastics into fuel oil? *UK: Institute of Science in Society*. 2015.

Wang et al., 1998: Wang, N., Sasaki, M., Yoshida, T., Kotanigawa, T. 1998. Characterization of Different Possible Solvent-Coal Interaction Mechanisms by the Relationship between the Volumetric Swelling of Coals and Heat Release in Swelling Solvent. *Energy & Fuels*. **12**. 531-535.

Wang et al., 2011: Wang, L., Trninic, M., Skreiberg, O., Gronli, M., Considine, R., Antal, M.J. 2011. Is Elevated Pressure Required to Achieve a High Fixed-Carbon Yield of Charcoal from Biomass? Part 1: Round-Robin Results for Three Different Corncob Materials. *Energy and Fuels.* **25**(7). 3251–3265.

Wang et al., 2019: Wang, W., Themelis, N.J., Sun, K., Bourtsalas, A.C., Huang, Q., Zhang, Y., Wu, Z. 2019. Current influence of China's ban on plastic waste imports. *Waste Disposal & Sustainable Energy*.

Wang et al., 2020: Wang, C., Zhao, L., Lim, M.K., Chen, W.Q., Sutherland, J.W. 2020. Structure of the Global Plastic Waste Trade Network and the Impact of China's Import Ban. *Resources, Conservation and Recycling.* **153**. 104591.

Warhurst et al., 1997: Warhurst, M.A., McConnachie, G.L., Pollard, S.J.T. 1997. Characterisation and Applications of Activated Carbon Produced from Moringa Oleifera Seed Husks by Single-Step Steam Pyrolysis. *Water Research.* **31**(4). 759–766.

Welle, 2011: Welle, F. 2011. Twenty Years of PET Bottle to Bottle Recycling - An Overview. *Resources, Conservation and Recycling.* **55**(11). 865–875.

Wen et al., 2019: Wen, Y., Kierzek, K., Chen, X., Gong, J., Liu, J., Niu, R., Mijowska, E., Tang, T. 2019. Mass production of hierarchically porous carbon nanosheets by carbonizing "real-world" mixed waste plastics toward excellent-performance supercapacitors. *Waste Management.* **87**. 691–700.

Westerhout et al., 1997: Westerhout, R.W.J., Waanders, J., Kuipers, J.A.M., van Swaaij, W.P.M. 1997. Kinetics of the low-temperature pyrolysis of polyethene, polypropene, and polystyrene modelling, experimental determination and comparison with literature models and data. *Industrial & Engineering Chemistry Research*. **36**. 1955-1964.

Wiedemeier et al., 2015: Wiedemeier, D.B., Abiven, S., Hockaday, W.C., Keiluweit, M., Kleber, M., Masiello, C.A., McBeath, A.V., Nico, P.S., Pyle, L.A., Schneider, M.P.W., Smernik, R.J., Wiesenberg, G.L.B., Schmidt, M.W.I. 2015. Aromaticity and degree of aromatic condensation of char. *Organic Geochemistry*. **78**. 135–143.

Wilk et al., 2019: Wilk, M., Magdziarz, A., Jayaraman, K., Szymańska-Chargot, M., Gökalp, I. 2019. Hydrothermal Carbonization Characteristics of Sewage Sludge

and Lignocellulosic Biomass. A Comparative Study. *Biomass and Bioenergy.* **120**. 166–175.

Williams and Slaney, 2007: Williams, P.T., Slaney, E. 2007. Analysis of products from the pyrolysis and liquefaction of single plastics and waste plastic mixtures. *Optics Communications.* **51**. 754–769.

Wright et al., 2013: Wright, S.L., Thompson, R.C., Galloway, T.S. 2013. The physical impacts of microplastics on marine organisms: a review. *Environment Pollution*. **178**. 483–492.

WWF, 2018: World Wildlife Foundation, 2018. The lifecycle of plastics. Article published on 19 Jun 2018. Retrieved on 28 April 2020. URL: https://www.wwf.org.au/news/blogs/the-lifecycle-of-plastics#gs.4oy9y0

Xie, 2015: Xie, K.C. 2015. Structure and Reactivity of Coal. Springer-Verlag.

Xiong et al., 2017: Xiong, F., Jiang, Z., Amooie, M.A., Soltanian, M. 2017. Pore structure of transitional shales in the Ordos Basin, NW China: Effects of composition on gas storage capacity. *Fuel*. **206**. 504-515.

Xu et al., 2013: Xu, D., Xiao, P., Zhang, J., Li, G., Xiao, G., Webley, PA., Zhai, Y. 2013. Effects of Water Vapour on CO_2 Capture with Vacuum Swing Adsorption Using Activated Carbon. *Chemical Engineering Journal.* **230**. 64–72.

Yang et al., 2000: Yang, M., Tsukame, T., Saitoh, H., Shibasaki, Y. 2000. Investigation of the thermal degradation mechanisms of poly(styrene-co-methacrylonitrile)s by flash pyrolysis and TG-FTIR measurements. *Polymer Degradation and Stability*. **67**. 479–489.

Yoshioka et al., 2004: Yoshioka, T., Kitagawa, E., Mizoguchi, T., Okuwaki, A. 2004. High Selective Conversion of Poly(Ethylene Terephthalate) into Oil Using $Ca(OH)_2$. *Chemistry Letters.* **33**(3). 282–283.

Yucel and Ruthven, 1980: Yucel, H., Ruthven, D.M. 1980. Diffusion of CO_2 in 4A and 5A zeolite crystals. *Journal of Colloid and Interface Science*. **74**. 186–195.

Zhang et al., 2014: Zhang, T., Walawender, W.P., Fan, L.T., Fan, M., Daugaard, D., Brown, R.C. 2014. Preparation of activated carbon from forest and agricultural residues through CO_2 activation. *Chemical Engineering Journal.* **105**. 53–59.

Zhang et al., 2019: Zhang, B., Song, C., Liu, C., Min, J., Azadmanjiri, J., Ni, Y., Niu, R., Gong, J., Zhao, Q., Tang, T. 2019. Molten salts promoting the "controlled carbonization" of waste polyesters into hierarchically porous carbon for high-performance solar steam evaporation. *Journal of Materials Chemistry A.* **7**. 22912–22923.

Zhao et al., 2018a: Zhao, P., Xie, J., Gu, F., Sharmin, N., Hall, P., Fu, J., 2018. Separation of mixed waste plastics via magnetic levitation. *Waste Management* **76**. 46-54.

Zhao et al., 2018b: Zhao, L., Kaiser, R., Xu, B., Ablikim, U., Ahmed, M., Joshi, D., Veber, G., Fischer, F., Mebel, A. 2018. Pyrene synthesis in circumstellar envelopes and its role in the formation of 2D nanostructures. *Nature Astronomy*. **2**. 413-419.

Zhou et al., 2015: Zhou, H., Wu, C., Onwudili, J.A., Meng, A., Zhang, Y., Williams, P.T. 2015. Polycyclic Aromatic Hydrocarbons (PAH) Formation from the Pyrolysis of Different Municipal Solid Waste Fractions. *Waste Management.* **36**. 136–146.

Zhou et al., 2020: Zhou, X., Deng, J., Yang, R., Zhou, D., Fang, C., He, X., Wang, D., Lei, W., Hu, J., Li, Y. 2020. Facile Preparation and Characterization of Fibrous Carbon Nanomaterial from Waste Polyethylene Terephthalate. *Waste Management.* **107**. 172–81.

Zhu et al., 2016a: Zhu, Y., Romain, C., Williams, C.K. 2016. Sustainable Polymers from Renewable Resources. *Nature.* **540**(7633). 354–362.

Zhu et al., 2016b: Zhu, Y., Zhang, Z.C., Guan, X.M. 2016. The nonisothermal crystallization behavior of polyamide-6,6/mobile crystalline material hybrid composites prepared by in situ polymerization. *Journal of Thermoplastic Composite Materials.* **29**(5). 638-655.

Zhuo and Levendis, 2014: Zhuo, C., Levendis, Y.A. 2014. Upcycling Waste Plastics into Carbon Nanomaterials: A Review. *Journal of Applied Polymer Science.* **131**(4). 1–14.

Appendix A. – Rank of bale

Most local municipal collectors and some private entities establish consignment with the Japan Containers and Packaging Recycling Association to ensure regular collection of PET bottles from the storage sites. The PET bottles collected from municipalities will be characterized based on the Classification Standard before being handed over to specified recyclers through the association. Classification Standard of PET bottle is established by The Council for PET Bottle Recycling for the purpose of encouraging the progression of PET bottle recycling by local government and private entities. A segment of Classification Standard of PET bottle (translated from Japanese) is shown in **Figure A-1**. The classification is based on visual inspection, inspection by measurement and others such as the presence of foreign contents. The standard gives information on the bale condition in terms of overall cleanliness, ease of bale transport and recycle capability. In terms of inspection by measurement, the standard gives information on estimated total number of bottles with cap, labels, liquid contents and foreign objects. Points are allocated to each section and based on the total points allocated, the bales are then rated as Rank A, Rank B and Rank D, respectively. It is noted that colored PET bottles are rated as Rank D, despite the cleanliness of its insides. Examples of bale with respective ranks are shown in **Figure A-2**.

Classification standard

Overall results						
Visual Inspection	Classification			Point allocation		
Bale condition				A	B	D
1. Degree of appearance	A. No dirt	B. Some dirt	D. Mostly dirty	8	4	1
2. Stability of bale load	A. No collapse	B. Some collapse	D. Not stable	6	3	1
3. Dismantling of bale	A. Possible by hand	B. Possible with equipment	D. Not possible with equipment	4	2	1
Measurement Inspection	Numbers	Weigh [g]	Weigh [%]	Point allocation		
Factors affecting recycling				A	B	D
4. Bottles with cap				8	4	1
5. Bottles with labels				8	4	1
6. Bottles with liquid contents				8	4	1
7. Bottles with tape/paint				8	4	1
8. Bottles with foreign contents				8	4	1

Factors affecting recycling	Rank A		Rank B		Rank D	
4. Bottles with cap	Under 1%	8	Under 20%	4	More than 20%	1
5. Bottles with labels	Under 10%	8	Under 30%	4	More than 30%	1
6. Bottles with liquid contents	Under 0.5%	8	Under 1.5%	4	More than 1.5%	1
7. Bottles with tape/paint	Not detected	8	Under 0.05%	4	More than 0.05%	1
8. Bottles with foreign contents	Not detected	8	Under 0.05%	4	More than 0.05%	1

Figure A-1: A segment from Classification Standard of PET bottle.
(The Japan Containers and Packaging Recycling Association, 2018)
(translated from Japanese)

Rank A Rank B Rank D

Figure A-2: PET bottle bale characterized based on the Classification Standard (The Council for PET bottle recycling, 2019).

Appendix B. – Derivation of equation for average intensity of exposure

Figure B-1 shows the cross-section of PET bottle placed at surface distance, a from source of UV.

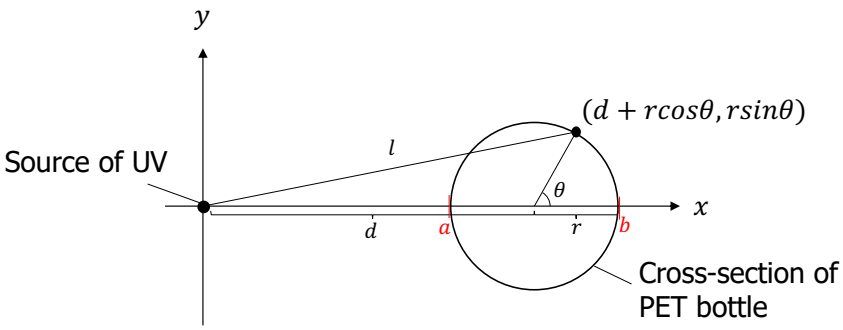

Figure B-1: Cross-section of PET bottle from source of UV.

The intensity of exposure by UVA-365 lamp ($18.2\ W/m^2$ at 0.05 m) was given as

$$Intensity\ of\ light\ source, I = \frac{0.0455}{l^2} \tag{B-1}$$

, where l is the distance of surface of exposure from light source. Based on the figure, the distance of surface of exposure is given as

$$\begin{aligned} l^2 &= (d + rcos\theta)^2 + (rsin\theta)^2 \\ &= d^2 + r^2 + 2drcos\theta \end{aligned} \tag{B-2}$$

Using Eqs. (B-1) and (B-2), the average intensity of exposure becomes

$$\begin{aligned} I_{avg} &= \frac{\int_0^{2\pi} I\, d\theta}{\int_0^{2\pi} d\theta} \\ &= \frac{\int_0^{2\pi} \frac{0.0455}{d^2 + r^2 + 2drcos\theta}\, d\theta}{2\pi} \\ &= \frac{0.0455}{2\pi} \int_0^{2\pi} \frac{1}{(d^2 + r^2) + 2drcos\theta}\, d\theta \end{aligned} \tag{B-3}$$

Due to the identical area under the graph, Eq. (B-3) is now expressed as

$$I_{avg} = \frac{0.0455}{\pi} \int_0^{\pi} \frac{1}{(d^2 + r^2) + 2drcos\theta}\, d\theta \tag{B-4}$$

Eq. (B-4) is solved using the Weierstrass substitution as shown as follows,

$$J = \int_0^{\pi} \frac{1}{A + Bcos\theta}\, d\theta \tag{B-5}$$

Let $t = tan\ \frac{\theta}{2}$, where $\theta: 0 \to \pi$ becomes $t: 0 \to +\infty$ $\cdots$ (B-6).

Differential of Eq. (B-6) to give

$$dt = \frac{1}{cos^2\frac{\theta}{2}} \cdot \frac{d\theta}{2}$$

Using the following identity: $1 + tan^2\theta = \frac{1}{cos^2\theta}$,

$$dt = \left(1 + tan^2\frac{\theta}{2}\right) \cdot \frac{d\theta}{2}$$

$$dt = (1 + t^2) \cdot \frac{d\theta}{2}$$

$$\therefore d\theta = \frac{2dt}{1 + t^2} \tag{B-7}$$

Next, converting $cos\theta$ using the following identity:

$cos2\theta = 2cos^2\theta - 1$ and $1 + tan^2\theta = \frac{1}{cos^2\theta}$,

$$cos\theta = cos2 \cdot \frac{\theta}{2}$$

$$= 2cos^2\frac{\theta}{2} - 1$$

$$= 2\frac{1}{1 + tan^2\frac{\theta}{2}} - 1$$

$$= \frac{2}{1 + t^2} - 1$$

$$\therefore cos\theta = \frac{1 - t^2}{1 + t^2} \tag{B-8}$$

Based on the Eqs. (B-5), (B-6), (B-7), and (B-8)

$$J = \int_0^{\infty} \frac{1}{A + B \cdot \frac{1 - t^2}{1 + t^2}} \cdot \frac{2}{1 + t^2}\, dt$$

$$J = \int_0^{\infty} \frac{2}{A(1 + t^2) + B(1 - t^2)}\, dt$$

$$J = \int_0^{\infty} \frac{2}{A + B + (A - B)t^2}\, dt$$

$$J = \int_0^{\infty} \frac{\frac{2}{A+B}}{1 + \left(\frac{A-B}{A+B}\right) t^2}\, dt \qquad \text{(B-9)}$$

Let $tan\phi = \sqrt{\frac{A-B}{A+B}}\, t$, where $t: 0 \to +\infty$ becomes $\phi: 0 \to \frac{\pi}{2} \cdots$ (B-10)

Modifying Eq. (B-10) as follows,

$$t = \sqrt{\frac{A+B}{A-B}}\, tan\phi$$

$$dt = \sqrt{\frac{A+B}{A-B}} \cdot \frac{1}{cos^2\phi} \cdot d\phi \qquad \text{(B-11)}$$

Substitute Eqs. (B-10) and (B-11) into Eq. (B-9)

$$J = \int_0^{\frac{\pi}{2}} \frac{\frac{2}{A+B}}{1 + \left(\frac{A-B}{A+B}\right)\left(\sqrt{\frac{A+B}{A-B}}\, tan\phi\right)^2} \cdot \sqrt{\frac{A+B}{A-B}} \cdot \frac{1}{cos^2\phi} \cdot d\phi$$

$$= \int_0^{\frac{\pi}{2}} \frac{2}{A+B} \cdot \sqrt{\frac{A+B}{A-B}} \cdot \frac{1}{1 + tan^2\phi} \cdot \frac{1}{cos^2\phi} \cdot d\phi$$

$$= \int_0^{\frac{\pi}{2}} \frac{2}{\sqrt{(A+B)(A-B)}}\, d\phi$$

$$= \frac{2}{\sqrt{A^2 - B^2}} \cdot \frac{\pi}{2}$$

$$\therefore \int_0^{\pi} \frac{1}{A + Bcos\theta}\, d\theta = \frac{\pi}{\sqrt{A^2 - B^2}} \qquad \text{(B-12)}$$

Based on the derived integral, the average intensity of exposure is now solved as

$$I_{avg} = \frac{0.0455}{\pi} \int_0^{\pi} \frac{1}{(d^2 + r^2) + 2drcos\theta}\, d\theta$$

$$= \frac{0.0455}{\pi} \cdot \frac{\pi}{\sqrt{(d^2 + r^2)^2 - (2dr)^2}} \qquad \text{(B-13)}$$

$$= \frac{0.0455}{d^2 - r^2} \qquad (d > r)$$

Appendix C. – Decomposition profile of PET

Figure C-1 shows the decomposition profile of PET based on Alongi et al. (2013). As shown in the figure, rapid decomposition of PET occurs between 400-500°C.

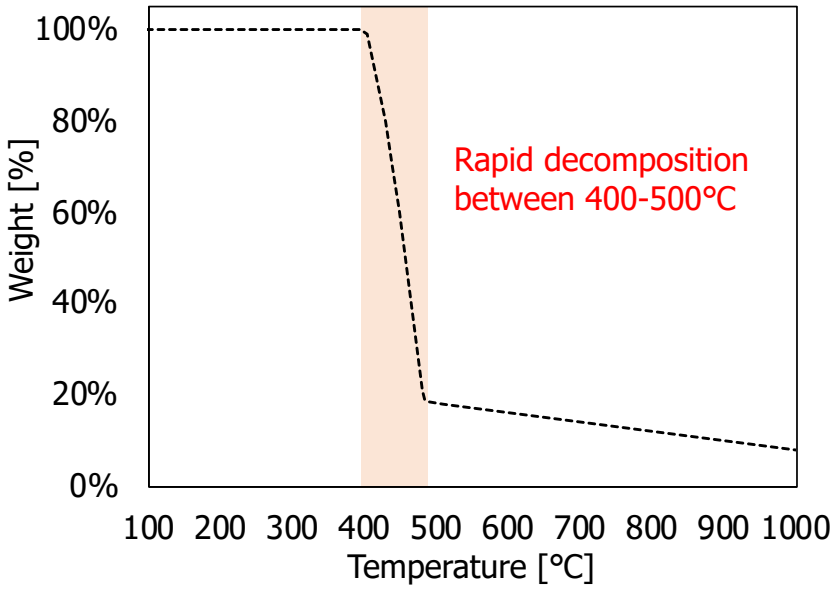

Figure C-1: Decomposition profile of PET.

Appendix D. – Temperature distribution of reactor in equilibrium

Figure D-1 shows the temperature distribution of reactor in equilibrium when the center of reactor reaches target temperature, while **Table D-1** shows the list of equations fitted to the temperature distribution of reactor in equilibrium and the calculated average temperatures of each operating condition.

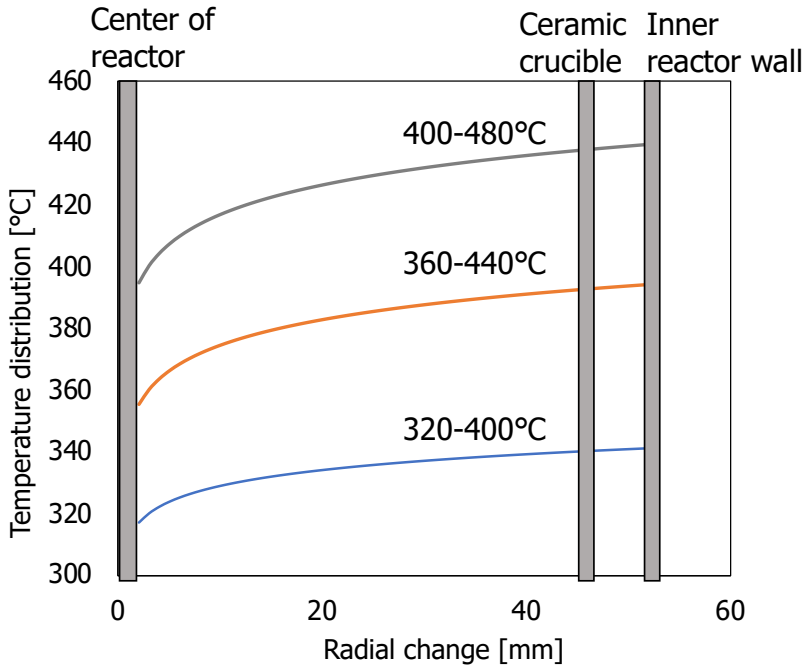

Figure D-1: Temperature distribution of reactor in equilibrium.

Table D-1: List of equations fitted to the temperature distribution of reactor in equilibrium and calculated average temperatures of each temperature setting.

Temperature setting	Equation of temperature distribution in equilibrium	Average temperature*
400-480°C	$T = 13.77\ln(r) + 384.87$	432°C
360-440°C	$T = 11.93\ln(r) + 346.89$	388°C
320-400°C	$T = 7.344\ln(r) + 311.93$	337°C

*The average value of function by integration

The average value of function by integration was calculated using the method as shown below. A cross-section of the reactor is given in Figure D-2, where R_1 is the center of the autoclave reactor, where as R_2 is the inner wall of the autoclave reactor.

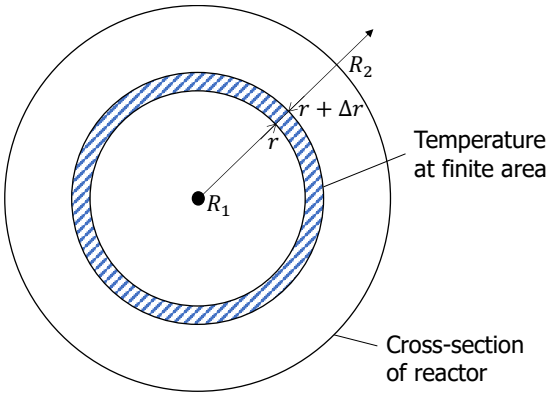

Figure D-2: Cross-section of reactor.

The temperature distribution of reactor was given as $T(r)$, which was obtained from the experiment. Therefore, the average temperature of the reactor was calculated as

$$Average\ temperature = \frac{\int_{R_1}^{R_2} T(r) \times 2\pi r\ dr}{\int_{R_1}^{R_2} 2\pi r\ dr} \tag{D-1}$$

Note that the solution of integral is given as

$$\int (ax \ln x + bx)\ dx = \frac{2ax^2 \ln x - ax^2 + 2bx^2}{4} \tag{D-2}$$

Appendix E. – Reproducibility of carbonization experiment

An additional study was conducted with aims to determine the reproducibility of data in this section. Carbonization experiment was conducted at constant temperature and holding time using carbonated drink bottle (Asahi Soft Drinks Co., Ltd.; Label A) prepared with minimal treatment. The experiment was repeated 3 times with the same conditions, labelled as Rep 1, Rep 2 and Rep 3, respectively.

The composition of product and fixed-carbon yield of char after carbonization are shown in **Figure E-1**. Char was obtained in the range of 27.9-28.8%; wax was obtained in the range of 37.1-40.6%; gas was obtained in the range of 31.5-34.0%. On the other hand, the fixed-carbon yield of char was obtained in the range of 19.7-20.9%.

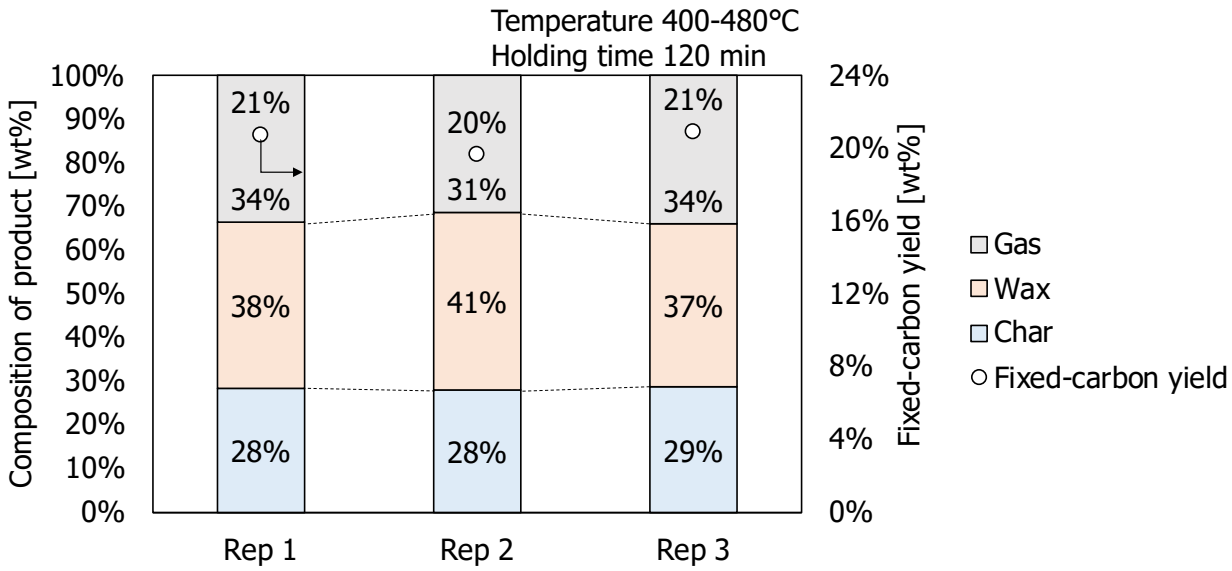

Figure E-1: Composition of product and fixed-carbon yield of char after carbonization of PET from the same starting feedstock type and feedstock treatment.

A simple statistical analysis based on the analysis of variance, ANOVA was conducted to assess the relative size of variance among group means (Between Group) compared to the average variance within groups (Within Group). Here, Rep 1-3 are the group of comparison, whereas char yield and volatile matter content were chosen as the data within the compared group, as shown in **Table E-1**.

The statement in this test is now given as follow:

H_o: Mean of groups are equal to one another

H_a: There is at least one inequality among the groups

The null hypothesis is not rejected when F value < F crit (α = 0.05).

All groups were compared (labels Rep 1-3), and the critical F value, 0.468 was smaller than the critical F value, 9.552, thus retaining the null hypothesis. Therefore, with high level of confidence it can be concluded that the product composition of carbonized product and the characteristics of char showed good consistency in the reproducibility test. This indicates that the experimental results can be reproduced with high level of consistency.

Table E-1: Descriptive statistics of char yield and volatile matter of char for the same starting feedstocks.

Label	Char	VM[a]
Rep 1	28.4%	27.0%
Rep 2	27.9%	29.5%
Rep 3	28.8%	27.5%
Mean	28.4%	28.0%
Variance	2.13E-05	1.83E-04

[a]: Dry basis;

VM: Volatile matter content

One-way ANOVA Analysis of Variance for same feedstock (between Rep 1-3)

Source of Variation	SS	df	MS	F	P-value	F crit
Between Groups	1.03E-04	2	5.15E-05	0.467820	0.665517	9.552094
Within Groups	3.30E-04	3	1.10E-04			
Total	4.33E-04	5				

Appendix F. – Statistical analysis

F.1. Statistical analysis of effects of feedstock variance on carbonized product based on analysis of variance (ANOVA)

The one-way ANOVA is normally used to compare more than two group means in order to assess the relative size of variance among group means (Between Group) compared to the average variance within groups (Within Group). Here, labels A-E are the group of comparison, whereas char yield, volatile matter content and carbon content were chosen as the data within the compared group, as shown in **Table F-1**.

The statement in this test is now given as follows:

H_o: Mean of groups are equal to one another

H_a: There is at least one inequality among the groups

The null hypothesis is not rejected when F value < F crit (α = 0.05).

For comparison of bottle makers (labels A, B and C), the critical F value was 5.143 in the F table when α = 0.05. The observed F value was 1.44E-04, which was smaller than the critical F value, thus failing to reject the null hypothesis. Therefore, this indicates that there is no statistically significant difference between the carbonized product of PET from different bottle makers. Similarly, for comparison of treatment method (labels A, D and E), the observed F value was 4.84E-05, which was smaller than the critical F value, 5.143, thus retaining the null hypothesis. Therefore, this indicates that there is also no statistically significant difference between the carbonized product of PET from different shapes and sizes. Finally, all groups were compared (labels A-E), and the critical F value, 8.16E-05 was smaller than the critical F value, 3.478, thus retaining the null hypothesis. Therefore, with high level of confidence it can be concluded that the product composition of carbonized product and the characteristics of char showed good consistency regardless of the starting feedstock state.

Table F-1: Descriptive statistics of char yield, volatile matter of char and carbon content of char for feedstocks with label A-E.

Label	Char	VM[a]	%C[a]
A	28.4%	27.0%	89.3%
B	27.9%	29.5%	87.3%
C	27.1%	26.8%	89.5%
D	29.6%	29.0%	85.4%
E	28.5%	27.7%	87.9%
Mean	28.3%	28.0%	87.9%
Variance	8.23E-05	1.48E-04	2.85E-04

[a]: Dry basis; Data obtained from CHN analysis had 0.3% error

VM: Volatile matter content

One-way ANOVA Analysis of Variance for bottle makers (between A, B and C)

Source of Variation	SS	df	MS	F	P-value	F crit
Between Groups	3.58E-05	2	1.79E-05	0.000144	0.999856	5.143253
Within Groups	0.743358	6	0.123893			
Total	0.743393	8				

One-way ANOVA Analysis of Variance for treatment method (between A, D and E)

Source of Variation	SS	df	MS	F	P-value	F crit
Between Groups	1.13E-05	2	5.67E-06	4.84E-05	0.999952	5.143253
Within Groups	0.701811	6	0.116968			
Total	0.701822	8				

One-way ANOVA Analysis of Variance for all labels (between A-E)

Source of Variation	SS	df	MS	F	P-value	F crit
Between Groups	3.89E-05	4	9.73E-06	8.16E-05	1	3.47805
Within Groups	1.191853	10	0.119185			
Total	1.191892	19				

F.2. Statistical analysis of relationship between CO_2 produced and CO produced based on the linear regression analysis

Linear regression analysis was conducted to determine the statistical significance of relationship between the variables, CO_2 produced and CO produced. When α = 0.05, the decision rule is given as follows: if p-value is less than 0.05, then the null hypothesis "H_0: Coefficient is 0" can be rejected and that the correlation between the variables is statistically significant.

Taking "CO_2 produced" as "Y" and "CO produced" as "X", the estimated regression equation was obtained as

$$Y = 0.0363 + 1.0373\ X, \qquad R^2 = 0.9138$$
$$(1.293) \quad (12.458)$$

, where the number in the parentheses represents the t-value, and the p value were obtained as 0.123, 5.66E-10 respectively. It can now be concluded that: for the intercept (=0.0363), the p value > 0.05, thus indicating the acceptance of null hypothesis which states that the coefficient is 0; for the gradient (=1.0373), the p value < 0.05, thus indicating the reject of null hypothesis and conclude that the coefficient is not 0. The coefficient of determination, R^2 indicates that the linear regression is well fitted. An alternative analysis was conducted for the obtained data using the fitted regression model Y = X to obtain R^2 = 0.8464, which further proves that the data was well fitted with the linear relationship of CO_2 produced = CO produced. As a summary, based on the linear regression analysis, there is significant relationship between the CO_2 produced and the CO produced, given as CO_2 produced ≅ CO produced.

F.3. Statistical analysis of relationship between C=O/C=O_0 and $X_{cross\text{-}link}$ based on the linear regression analysis

Linear regression analysis was conducted to determine the statistical significance of relationship between the variables, C=O/C=O_0 and $X_{cross\text{-}link}$. Similarly, when α=0.05, the decision rule is given as follows: if p-value is less than 0.05, then the null hypothesis "H_0: Coefficient is 0" can be rejected and that the correlation between the variables is statistically significant.

Taking "$C=O/C=O_0$" as "Y" and "$X_{cross\text{-}link}$" as "X", the estimated regression equation was obtained as

$$Y = 0.9944 - 1.1042\ X, \qquad R^2 = 0.7734$$
$$(9.446) \quad (-6.399)$$

, where the number in the parentheses represents the t-value, and the p value were obtained as 6.60E-07, 3.40E-05 respectively. It can now be concluded that: for the intercept (=0.09944), the p value < 0.05, thus indicating the reject of null hypothesis and conclude that the coefficient is not 0; for the gradient (=-1.1042), the p value < 0.05, thus also indicating the reject of null hypothesis and that the coefficient is not 0. The coefficient of determination, R^2 indicates that the linear regression is well fitted. An alternative analysis was conducted for the obtained data using the fitted regression model Y = 1 – X to obtain $R^2 = 0.6426$, which further proves that the data was well fitted with the linear relationship of $C=O/C=O_0 = 1 - 1 \times X_{cross\text{-}link}$. As a summary, based on the linear regression analysis, there is significant relationship between the $C=O/C=O_0$ and the degree of decarbonylation, given as $C=O/C=O_0 \cong 1 - X_{cross\text{-}link}$.

F.4. Statistical analysis of relationship between X_c and $X_{cross\text{-}link(CO)}$; and X_w and $X_{cross\text{-}link(CO_2)}$ based on the linear regression analysis

Linear regression analysis was conducted for both cases to determine the statistical significance of relationship between the variables. Firstly, for the relationship between $X_{cross\text{-}link(CO)}$ and X_c, when $\alpha = 0.05$, the decision rule is given as follows: if p-value is less than 0.05, then the null hypothesis "H_0: Coefficient is 0" can be rejected and that the correlation between the variables is statistically significant.

Taking "X_c" as "Y" and "$X_{cross\text{-}link(CO)}$" as "X", the estimated regression equation was obtained as

$$Y = 0.0169 + 1.0199\ X, \qquad R^2 = 0.7665$$
$$(0.641) \quad (6.532)$$

, where the number in the parentheses represents the t-value, and the p value were obtained as 0.532, 1.91E-10 respectively. It can now be concluded that: for the intercept (=0.0169), the p value > 0.05, thus indicating the acceptance of null hypothesis which states that the coefficient is 0; for the gradient (=1.0199), the p

value < 0.05, thus indicating the reject of null hypothesis and conclude that the coefficient is not 0. An alternative analysis was conducted for the obtained data using the fitted regression model Y = X to obtain R^2 = 0.6844, which further indicates that the linear regression was well fitted with the relationship of $X_c = X_{cross\text{-}link(CO)}$. As a summary, based on the linear regression analysis, there is significant relationship between the X_c and the $X_{cross\text{-}link(CO)}$, given as $X_c \cong X_{cross\text{-}link(CO)}$.

Next, for the relationship between $X_{cross\text{-}link(CO_2)}$ and X_w, when α = 0.05, the decision rule is given as follows: if p-value is less than 0.05, then the null hypothesis "H_0: Coefficient is 0" can be rejected and that the correlation between the variables is statistically significant.

Taking "X_w" as "Y" and "$X_{cross\text{-}link(CO_2)}$" as "X", the estimated regression equation was obtained as

$$Y = 0.0336 + 0.9334\ X, \qquad R^2 = 0.7504$$
$$(0.811) \quad (6.252)$$

, where the number in the parentheses represents the t-value, and the p value were obtained as 0.432, 2.96E-05 respectively. It can now be concluded that: for the intercept (=0.0336), the p value > 0.05, thus indicating the acceptance of null hypothesis which states that the coefficient is 0; for the gradient (=0.9334), the p value < 0.05, thus indicating the reject of null hypothesis and conclude that the coefficient is not 0. An alternative analysis was conducted for the obtained data using the fitted regression model Y = X to obtain R^2 = 0.7145, which further indicates that the linear regression was well fitted with the relationship of $X_w = X_{cross\text{-}link(CO_2)}$. As a summary, based on the linear regression analysis, there is significant relationship between the X_w and the $X_{cross\text{-}link(CO_2)}$, given as $X_w \cong X_{cross\text{-}link(CO_2)}$.

Appendix G. – Verification of oxygen barrier layer

Analysis and comparison with raw MXD6 nylon sample were conducted to further confirm whether the middle layer was indeed MXD6 nylon layer. MXD6 nylon sample (Injection molding) was obtained from Standard Test Piece, Japan. Elemental analysis using CHN/O/S elemental analyzer (CE-440F; Sci Globe, Japan) was conducted. Results are shown in **Table G-1**.

Table G-1: Elemental composition of middle layer, sample from Standard Test Piece and the ideal elemental composition of MXD6 nylon based on the chemical composition.

	Ultimate Analysis [wt%]			
	C%	H%	N%	R%*
Middle layer	65.92	7.13	10.98	15.96
MXD6 nylon from Standard Test Piece	35.87	4.02	5.96	54.15
Ideal CHN composition of MXD6 nylon from calculation**	68.29	7.32	11.38	13.01

*R is denoted for residue. For organics, oxygen is generally the residue from elemental composition. For inorganics, mixture of oxygen and metal are the residue.

**Chemical composition of MXD6 nylon: $C_{14}H_{18}N_2O_2$

From the results, it was observed that the R% was high for the MXD6 nylon sample obtained from Standard Test Piece, Japan. Based on their website (standard-testpiece.com), it was stated that some polymers such as nylon 66 produced through injection molding contains 30-50 wt% reinforcing agents. Reinforcing agents used are generally glass fiber, a type of silica (SiO_2). The assumption here now is that the MXD6 nylon sample obtained from Standard Test Piece, Japan contains some inorganic reinforcing agents which causes the high composition of R% in elemental analysis.

Supposing that unknown compound with mass fraction x is contained in the MXD6 nylon sample from Standard Test Piece, a simple calculation is made based on the results from CHN analyzation as:

	C	H	N	O	R	R+O	Total
MXD6 + Unknown	35.87	4.02	5.96			54.15	100
Unknown					x		x
MXD6 nylon	35.87	4.02	5.96	54.15-x			100-x
Pure MXD6 nylon	68.19	7.64	11.33	12.83			100

When the mass fraction of unknown compound x is 47.4%, C%, H%, N% and O% composition is obtained as 68.19%, 7.64%, 11.33% and 12.83%, respectively. These values are close to the ideal CHN composition of MXD6 nylon from calculation.

Using the same method, suppose that unknown compound with mass fraction y is contained in the middle layer,

	C	H	N	O	R	R+O	Total
Middle layer + Unknown	65.92	7.13	10.98			15.96	100
Unknown					y		y
Middle layer	65.92	7.13	10.98	15.96-y			100-y
Pure Middle layer	68.32	7.39	11.38	12.91			100

When the mass fraction of unknown compound y is 3.5%, C%, H%, N% and O% composition is obtained as 68.32%, 7.39%, 11.38% and 12.91%, respectively. These values are also close to the ideal CHN composition of MXD6 nylon from calculation. Note that for comparison, the ideal CHN composition of MXD6 nylon, Nylon-6 and Nylon-66 are shown in the **Table G-2** below.

Table G-2: Ideal CHN composition of MXD6 nylon, Nylon-6 and Nylon-66 based on their chemical compositions.

	C%	H%	N%	O%
MXD6 nylon	68.29	7.32	11.38	13.01
Nylon-6	63.72	9.73	12.39	14.16
Nylon-66	63.72	9.73	12.39	14.16

Chemical composition of MXD6 nylon: $C_{14}H_{18}N_2O_2$; Nylon-6: $C_6H_{11}N_1O_1$; Nylon-66: $C_{12}H_{22}N_2O_2$

Based on these calculations, it highly states that both MXD6 nylon sample from Standard Test Piece and OBL from middle layer of the PET sample are MXD6 nylon due to the elemental compositions proximate to the ideal CHN composition of MXD6 nylon. In addition, it can be seen that 47.4 wt% of unknown compound was found in the MXD6 nylon sample from Standard Test Piece. The unknown compound could most likely be reinforcing agents such as glass fiber. On the other hand, the middle layer contains approximately 3.5 wt% of unknown compound. The unknown compound can most likely be cobalt oxide, as detected from the XRD analyzation.

Figure G-1 shows the comparison of FT/IR spectra between MXD6 nylon sample from Standard Test Piece and middle layer from PET sample. From the results shown, it can be seen that FT/IR peaks were evident and identical around 1635 cm^{-1} (C=O stretching of amide I), 1541 cm^{-1} (N-H bending of amide II), 959 cm^{-1} (C-C stretching), 755 cm^{-1} (N-H wagging) and 712 cm^{-1} (interaction of benzene rings).

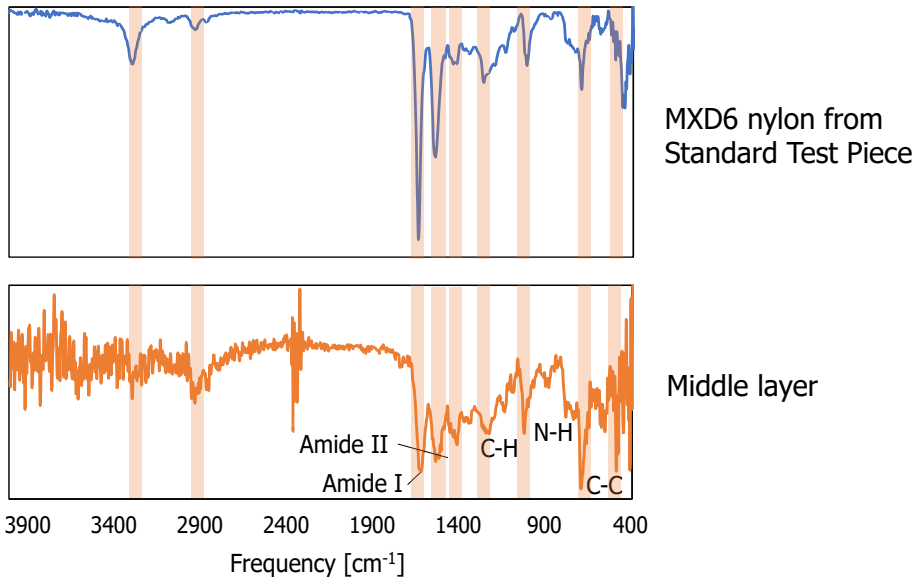

Figure G-1: FT/IR spectra of MXD6 nylon sample from Standard Test Piece and compared with middle layer.

On the other hand, researches on MXD6 nylon was reviewed and the FT/IR analysis were obtained and shown in **Figure G-2**. From the results shown, it can be seen that FT/IR peaks were evident and identical approximately around 1635 cm^{-1} (C=O stretching of amide I), 1541 cm^{-1} (N-H bending of amide II), 959 cm^{-1} (C-C stretching), 755 cm^{-1} (N-H wagging) and 712 cm^{-1} (interaction of benzene rings). This finally confirms that OBL used in this study is indeed MXD6 nylon.

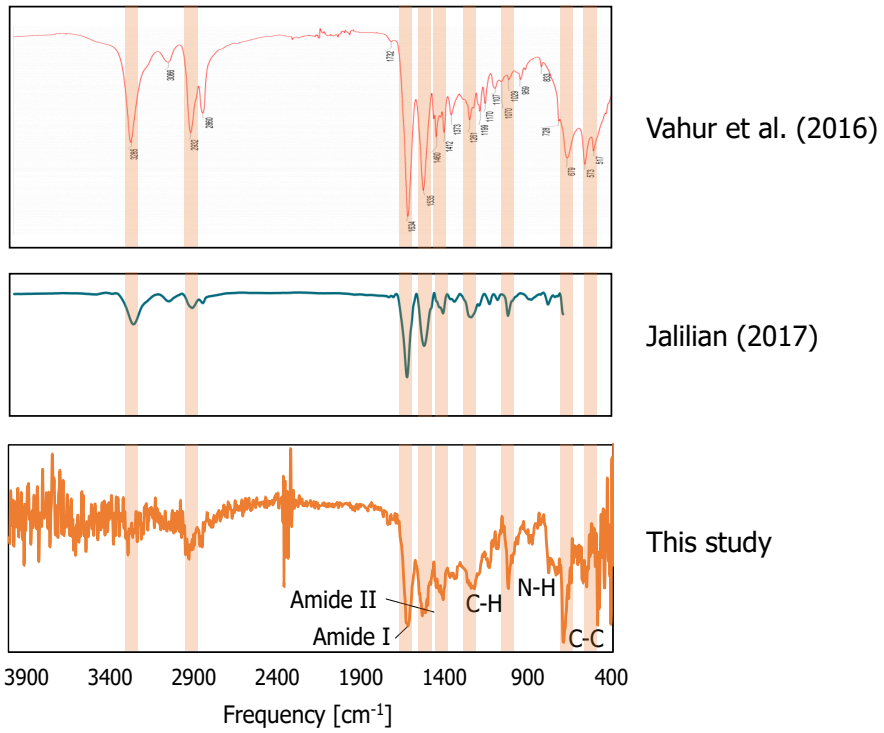

Figure G-2: FT/IR spectra of MXD6 nylon from previous researches and compared with this study.

Appendix H. – Initial and maintenance cost of operations

H.1. Incineration facility

Table H-1: Summary of operation and maintenance costs for a conventional waste incineration facility (Tasaki et al., 2006).

	Units	Average cost
Facility construction cost	million yen	25868
Operating years	year	15
Operating capacity	t/day	600
Maintenance cost	yen/t	19961
Labor cost (2 person)		(34.9%)
Repair cost		(28.1%)
Others		(37.0%)

Total cost of facility: (1) Initial cost for 15 years of operation = 25868 million yen ÷ 15 year ÷ 365 day/year ÷ 600000 kg-PET/day = 7.87 yen/kg-PET; (2) Cost of operation = 19.96 yen/kg-PET; (1)+(2) = 27.83 yen/kg-PET.

H.2. Recycling facility

Table H-2: Summary of operation and maintenance costs for a conventional PET recycling facility (Kato, 1997).

	Units	Average cost
Facility construction cost	million yen	100
Operating years	year	15
Operating capacity	t/day	70
Maintenance cost	yen/t	2854
Labor cost (3 person)		(36.0%)
Repair cost		(22.0%)
Others		(42.0%)

Total cost of facility: (1) Initial cost for 15 years of operation = 100 million yen ÷ 15 year ÷ 365 day/year ÷ 70000 kg-PET/day = 0.26 yen/kg-PET; (2) Cost of operation = 2.85 yen/kg-PET; (1)+(2) = 3.11 yen/kg-PET.

H.3. Carbonization facility

Table H-3: Summary of operation and maintenance costs for an assumed carbonization facility.

	Units	Average cost
Facility construction cost	million yen	200
Operating years	year	15
Operating capacity	t/day	4
Maintenance cost		33295
Labor cost (2 person)	yen/t	(36.0%)
Repair cost and others*		(64.0%)

*Assume similar fraction of repair and other maintenance cost as a recycling facility

Total cost of facility: (1) Initial cost for 15 years of operation = 200 million yen ÷ 15 year ÷ 365 day/year ÷ 4000 kg-PET/day = 9.13 yen/kg-PET; (2) Cost of operation = 33.30 yen/kg-PET; (1)+(2) = 42.43 yen/kg-PET.

H.4. PSA facility

Table H-4: Summary of operation and maintenance costs for an assumed PSA facility.

	Units	Average cost
Facility construction cost	million yen	10
Operating years	year	15
Operating capacity	t-CO_2/day	4.5
Maintenance cost		66590
Labor cost (1 person)	yen/day	(36.0%)
Repair cost and others*		(64.0%)

*Assume similar fraction of repair and other maintenance cost as a recycling facility

CO_2 recovery (from page 193) = 4.471 t-CO_2/day x 365 days/year = 1632 t-CO_2/year = 1.63 kt-CO_2/year; Total cost of operation: (1) Electricity cost (from page 193) = 2241 yen/day x 365 day/year = 0.82 million yen/year; (2) Initial cost for 15 years of operation = 10 million yen ÷ 15 year = 0.66 million yen/year; (3) Cost of operation = 66590 yen/day x 365 day/year = 24.31 million yen/year; (1)+(2)+(3) = 25.79 million yen/year.

Appendix I. – List of inventories

Table I-1: Summary of inventories for CO_2 emission and cost estimation of various operations.

Process	Inventory	Inventory value	Cited literature
PET collection (from collection site to temporary transport station)	Fuel consumption	Light oil: 0.73 L/t km	Nakatani et al. (2010)
	Transport distance	20 km	
	Cost	Light oil: 91.6 yen/L	METI (2020)
	CO_2 emission	Light oil: 2.619 kg-CO_2/L	METI (2016)
Baling, crushing and sorting	Fuel consumption	Electricity: 0.0939 kWh/kg-PET	Nakatani et al. (2010)
	Cost	Electricity: 16.6 yen/kWh	METI (2018)
		Facility: 33.52 yen/kg	The Council for PET Bottle Recycling (2005)
	CO_2 emission	Electricity: Refer to IDEA database	IDEA (2020)
Transportation (from transport station)	Fuel consumption	Light oil: 0.0460 L/t km	Nakatani et al. (2010)
	Transport distance	10 km (assumed same for all operations)	
	Cost	Light oil: 91.6 yen/L	METI (2020)
	CO_2 emission	Light oil: 2.619 kg-CO_2/L	METI (2016)
Incineration (without energy recovery)	Fuel consumption	Electricity: 0.0321 kWh/kg-PET Heavy oil: 0.000174 L/kg-PET	Nakatani et al. (2010)
	Cost	Electricity: 16.6 yen/kWh	METI (2018)
		Heavy oil: 58 yen/L	METI (2020)

Process	Inventory	Inventory value	Cited literature
		Facility: 27.83 yen/kg-PET	Tasaki et al. (2006)
	CO_2 emission	Electricity: Refer to IDEA database	IDEA (2020)
		Heavy oil: 2.710 kg-CO_2/L	METI (2016)
		Waste PET: 2.2917 kg-CO_2/kg-PET	*Calculated in this study
Incineration (with energy recovery)	Fuel consumption	Electricity: 0.0284 kWh/kg-PET Heavy oil: 0.000645 L/kg-PET	Nakatani et al. (2010)
	Cost	Electricity: 16.6 yen/kWh	METI (2018)
		Heavy oil: 58 yen/L	METI (2020)
		Facility: 27.83 yen/kg-PET	Tasaki et al. (2006)
	CO_2 emission	Electricity: Refer to IDEA database	IDEA (2020)
		Heavy oil: 2.710 kg-CO_2/L	METI (2016)
		Waste PET: 2.2917 kg-CO_2/kg-PET	*Calculated in this study
	Avoided production	Electricity: 0.607 kWh/kg-PET	Nakatani et al. (2010)
Mechanical recycling (flake and pellet)	Fuel consumption	Electricity: 0.681 kWh/kg-PET Heavy oil: 0.0535 L/kg-PET	Nakatani et al. (2010)
	Cost	Electricity: 16.6 yen/kWh	METI (2018)
		Heavy oil: 58 yen/L	METI (2020)
		Facility: 3.11 yen/kg-PET	Kato (1997)
		Bid price: 33.679 yen/kg-PET	JCPRA (2018)
	CO_2 emission	Electricity: Refer to IDEA database	IDEA (2020)
		Heavy oil: 2.710 kg-CO_2/L	METI (2016)

Process	Inventory	Inventory value	Cited literature
	Avoided production	Virgin PET pellet: 0.923 kg-pellet/kg-PET (BtoF)	Nakatani and Hirao (2011)
		Virgin PET pellet: 0.850 kg-pellet (BtoB)	Furusawa, 2019
Carbonization	Fuel consumption	Electricity: 0.0132 kWh/kg-PET	ASG Plastic Recycling Machinery (2013)
	Cost	Electricity: 16.6 yen/kWh	METI (2018)
		Facility: 42.43 yen/kg-PET	*Assumed in this study
	CO_2 emission	Electricity: Refer to IDEA database	IDEA (2020)
		CO_2 produced: 0.1884 kg-CO_2/kg-PET	*This study
	Avoided production	Raw materials for activated carbon production: 0.3 kg-char/kg-PET Electricity (by-products): 0.368 kWh/kg-PET	*This study
Landfill	Fuel consumption	Electricity: 0.0586 kWh/kg-PET	Nakatani et al. (2010)
		Light oil: 0.000158 L/kg-PET	
	Cost	Disposal unit price: 11243 yen/m^3	Tsuchida et al. (2008)
	CO_2 emission	Electricity: Refer to IDEA database	IDEA (2020)
		Light oil: 2.619 kg-CO_2/L	METI (2016)
PSA system	Fuel consumption	Electricity: 135.00 kWh/day	Shigaki et al. (2018)

Process	Inventory	Inventory value	Cited literature
	Cost	Electricity: 16.6 yen/kWh	METI (2018)
		Facility: 66590 yen/day	Saima et al. (2013)
	CO_2 emission	Electricity: Refer to IDEA database	IDEA (2020)
Virgin PET from fossil fuel	Cost	Global import cost: 159.37 yen/kg-virgin PET (pre-COVID)	ARC (2020)
	CO_2 emission	Total (including transport): Refer to IDEA database	IDEA (2020)
Raw materials for activated carbon production	Fuel consumption	Electricity: 1.7326 kWh/kg-biochar	Heidari et al. (2019)
	Cost	Electricity: 16.6 yen/kWh	METI (2018)
	CO_2 emission	Electricity: Refer to IDEA database	IDEA (2020)
		CO_2 produced: 2.289 kg-CO_2/kg-biochar (assume 30 wt% yield of AC)	Heidari et al. (2019); IDEA (2020)

Appendix J. – Safety note

It should be noted that for all runs of the carbonization experiment, benzene and toluene were detected using the GC/FID. Based on the substance safety data sheet of benzene (DOL, 1993a), the maximum time-weighted average (TWA) exposure limit is 1 ppm for 8-hour working day and the maximum short-term exposure limit (STEL) is 5 ppm for any 15-minute period. On the other hand, for toluene (DOL, 1993b), the maximum TWA exposure limit is 200 ppm for 8-hour working day and the maximum STEL is 500 ppm for any 10-minute period. The concentrations of these compounds were quantified through benzene and toluene standards, where 0.01 mg/L, 0.1 mg/L, 1 mg/L and 10 mg/L of benzene and toluene diluted with dichloromethane were used. Note that dichloromethane was not detected in the FID detector. Through the calibrated curve, the detected benzene and toluene in this work were confirmed to be under 0.01 mg/L, which is 3.0 ppm for benzene and 2.6 ppm for toluene at 20°C and 1 atm. This is under the maximum short-term exposure limit of benzene, and well under the safety exposure limit of toluene. However, safety measures were taken during the experimental operation such as installing active carbon as adsorbents in the instrument outlet, ventilation of working space and usage of safety gas mask during gas sampling to ensure minimum exposure to the toxic gases.